Modelling of Multistage Hydraulic Fracture Operations in Unconventional Resources – The Application of Geomechanics and Field Data to the Optimization of Fracture Spacing and Production

by

Natalia Skomorowski

A thesis

presented to the University of Waterloo

in fulfillment of the

thesis requirement for the degree of

Master of Science

in

Earth Sciences

Waterloo, Ontario, Canada, 2016

Author's Declaration

I hereby declare that I am the sole author of this thesis. This is a true copy of the thesis, including any required final revisions, as accepted by the examiners.

I understand that my thesis may be made electronically available to the public.

Abstract

Massive multistage hydraulic fracturing using horizontal wells has been an integral part of the natural resource industry in Canada. The process uses long horizontal wells divided into many stages to access large volumes of oil and gas bearing formations. Each well is divided into fracture stages. Fluids are pumped down into each stage of the well to generate a fracture which increases the porosity and permeability of the formation to allow economic resource extraction.

The *in situ* geomechanical stresses of the formation do not remain static during the fracturing of the rock. Each fracture creates a volume change within the formation which in turn leads to alteration of the stress and strain conditions within the rock mass. There is the possibility that the alteration of stress conditions will have an effect on the initiation and propagation of subsequent stages of the multi-stage hydraulic fracture operation. This phenomenon is known as 'stress shadowing'. Stress shadowing occurs when the minimum compressive stress in the formation is increased due to the fracturing of the rock. Increasing the minimum compressive horizontal stress can have several effects, including the rotation or diversion of fracture propagation, stages that do not initiate, thinner fractures, and reduced porosity and permeability within the fracture stage.

Currently, many hydraulic fracture operations do not invest in advanced mathematical models of geomechanics. Some pressure monitoring is carried out during operations, but the data are inadequate to warrant advanced numerical methods to predict stress change and its effects. This thesis presents a semi-analytical solution for the stresses around an ellipsoid (the Eshelby Solution) for use in predicting fracture geometry and stress shadow effects. The program is quick to use and can be linked to field data.

A study of field data from the Montney Formation is presented. The algorithm developed in this thesis is used to evaluate stress changes within the Montney Formation and the outputs are compared to the stress changes seen in the hydraulic fracture pressure data.

Acknowledgements

Need to acknowledge Dr. Maurice B. Dusseault, Dr. Robert Gracie, Dr. Giovanni Cascante, and Dr. Walter Illman for being an exemplary supervisory committee. Thank you for walking me through all the math, theory, and programming needed to write this thesis. Thank you to Caralyn Bennett and Dr. Michael Morgan of GLJ Petroleum Consultants for funding my research and giving me the opportunity to see the practical side of my thesis through many hikes and field schools. Your boundless enthusiasm was very much appreciated and enjoyed. Thank you to the Natural Sciences and Engineering Council (NSERC) of Canada for making this thesis possible through financial assistance. And finally a very special thank you to my family, friends, and cats who gave me endless moral support during my degree.

Dedication

This thesis is dedicated to all the people who have helped me through my education. Thank you to all the teachers, mentors, advisors, friends, and family who were very encouraging and wonderful while I completed my studies.

Table of Contents

List of Figures

List of Tables

Nomenclature

A	[m^2]	Cross sectional fracture area normal to σ_h
BHTP	[MPa]	Bottom Hole Treatment Pressure
c	[m]	Fracture half length
C^*_{ijkl}	[MPa]	Stiffness tensor of inclusion
c_c	[m]	Critical crack length
C_{ijkl}	[MPa]	Stiffness tensor
c_r	[m]	Radius of hole
D	[-]	Medium domain
dc	[m]	Change in fracture length
D_{ijkl}	[-]	Exterior elastic field tensor
E	[MPa]	Young's modulus
E'	[MPa]	Plain strain Young's modulus
E_{el}	[Joules/m^3]	Total strain energy due to inhomogeneity
E^F	[Joules/m^3]	Energy dissipated by a fracture
E_{int}	[Joules/m^3]	Interaction energy of elastic fields
E^T	[Joules/m^3]	Total strain energy increase
G	[MPa]	Shear modulus
G_F	[MPa.$m^{1/2}$]	Strain energy release rate
H	[m]	Fracture height
ISIP	[MPa]	Instantaneous Shut in Pressure
K	[MPa]	Bulk modulus
k	[-]	Stress concentration factor
K_I	[MPa.$m^{1/2}$]	Stress intensity factor
K_{IC}	[MPa.$m^{1/2}$]	Critical stress intensity factor
p_b	[MPa]	Breakdown pressure
p_c	[MPa]	Closure pressure
p_f	[MPa]	Fracture pressure
p_{head}	[MPa]	Head loss
p_n	[MPa]	Net pressure
$p_{net\text{-}frac}$	[MPa]	Net pressure at tip
$p_{net\text{-}tip}$	[MPa]	Pressure difference to close tip of fracture
$p_{surface}$	[MPa]	Pressure measured at the surface
p_{tip}	[MPa]	Pressure to force propagation at tip of fracture
p_v	[MPa]	Viscous pressure
Q	[m^3/s]	Flow rate
r	[m]	Radius of curvature

R_{tip}	[m]	Radius of fracture tip
S_{ijkl}	[-]	Eshelby tensor
T_0	[MPa]	Tensile strength of the rock
u	[m]	Displacement
U_s	[Joules/m^3]	Strain energy
U_γ	[Joules/m^2]	Surface energy
V_F	[m^3]	Volume of fluid in a fracture
V_I	[m^3]	Injected volume
V_L	[m^3]	Volume of fluid lost into the formation
V_p	[m^3]	Volume pumped into formation
V_S	[m^3]	Stimulated volume
x_1	[m]	Semi axis of ellipsoid in x direction
x_2	[m]	Semi axis of ellipsoid in y direction
x_3	[m]	Semi axis of ellipsoid in z direction
Y	[-]	Geometric factor
α	[-]	Biot co-efficient
γ	[Joules/m^2]	Fracture energy
δ_{ij}	[-]	Kronecker delta
$\Delta p_{perf+pipe}$	[MPa]	Change in pressure across the perforation
$\Delta\varphi$	[-]	Change in porosity
ϵ	[-]	Strain
ϵ^*	[-]	Eigenstrain
$\epsilon_{ij}\infty$	[-]	Remote strain
ϵ^p_{kl}	[-]	Initial eigenstrain
ϵ^T	[-]	Total volumetric strain
λ	[MPa]	Lamé's first parameter
μ	[Pa.s]	Viscosity
ν	[-]	Poisson's ratio
ρ	[gm/cc]	Bulk density
σ	[MPa]	Stress
σ'	[MPa]	Effective stress
σ_1	[MPa]	Maximum principal stress
σ_2	[MPa]	Middle principal stress
σ_3	[MPa]	Minimum principal stress
σ^a	[MPa]	Applied stress
σ^A_{ij}	[MPa]	Components of *in situ* stress field
σ_h	[MPa]	Minimum horizontal stress
σ_H	[MPa]	Maximum horizontal stress
$\sigma_{ij}\infty$	[MPa]	Remote homogeneous stress

σ_v	[MPa]	Vertical stress
φ	[m]	Radius of curvature of tip of hole
φ	[%]	Effective porosity
ψ	[-]	Function
Ω	[-]	Inclusion subdomain
Φ	[-]	Function

Chapter 1 Introduction

1.1 Hydraulic Fracturing in Canada

Hydraulic fracturing in Canada in unconventional reservoirs has taken place for over 30 years but it has only been within the last decade or so that horizontal wells and other advanced completion techniques have allowed the extraction of oil and gas from tight gas sands and shale reservoirs across the country to develop into a major industry. It is estimated that there are approximately $30x10^{12}$ cubic metres (m^3) of gas reserves in Canadian shale basins (ALL Consulting 2012) which could represent a significant contribution to the Canadian economy in the coming years. Shale plays, including the Montney, Horn River, Bakken, Duvernay and Utica, are all currently either being developed or being explored for development opportunities. There are several more potential plays in Canada in addition to the ones listed above. A map of known plays as of February 2013 is shown below in Figure 1-1.

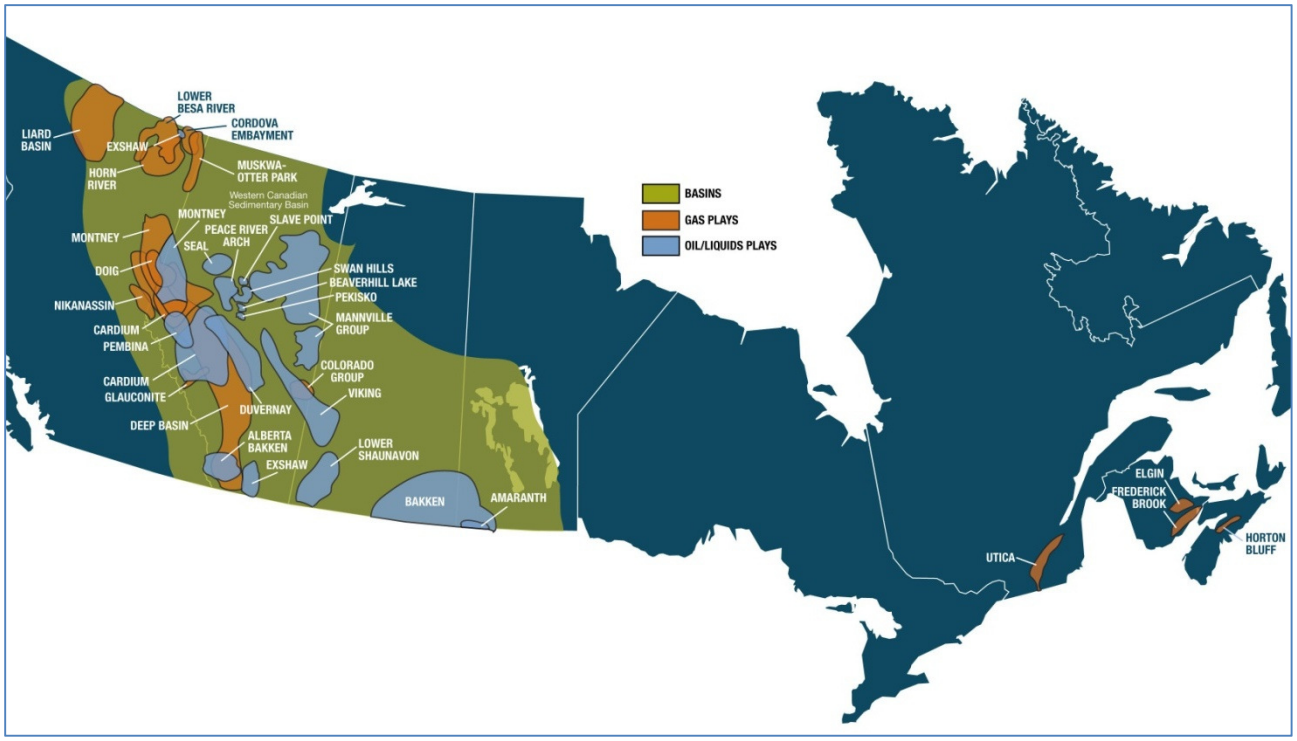

Figure 1-1 Map of Canadian Shale Plays as of February 2013 [reproduced from www.pacwestcp.com]

Canada stands to substantially benefit from the exploitation of unconventional resources. The benefit to the economy would be even greater if an in-depth understanding of the governing geomechanical processes of hydraulic fracture in shales were applied to fracture modelling and production forecasting. Currently, simplistic and rapidly executing programs are used to create a basic production forecast for multi-well, multi-stage production based on factors such as fracture spacing, type of proppant, type of fracturing fluid, injection pressures, etc. However, there is a general lack of fracture planning programs based on software which incorporates the effects of geomechanics and changing stress values during the hydraulic fracture process. The effects of geomechanics on stimulation success and therefore production are not negligible and should be considered when planning a hydraulic fracture job. It is possible that more representative models which incorporate geomechanics, even at a basic level, could give more accurate production prediction and therefore lead to a greater economic benefit.

1.2 Characteristics of Unconventional Resources

Shale gas is the most common of the unconventional natural gas resources in Canada. In general, unconventional shale plays are defined by their permeability and porosity, which are substantially lower than in conventional reservoirs.

There is no established formal definition of unconventional gas resources in the petroleum industry. It is generally agreed that the term ‘unconventional resource’ is used for oil and gas plays where the permeability, porosity, and fluid trapping mechanisms are different from those found in conventional carbonate and sandstone reservoirs. Unlike in a conventional play where the porosity and permeability are high enough to allow flow of the resource without aggressive well stimulation, within an unconventional reservoir the fluids are more tightly trapped within the smaller pore spaces within the formation and do not flow freely unless aggressive stimulation is implemented. The natural gas resources found in shale gas strata, coalbeds, sediments with gas hydrates, and tight gas sands all fall under this definition.

Figure 1-2 shows one definition based on permeability values for unconventional resources (in red) versus conventional resources (in green). Figure 1-3 shows typical porosity values of different shale gas plays in North America.

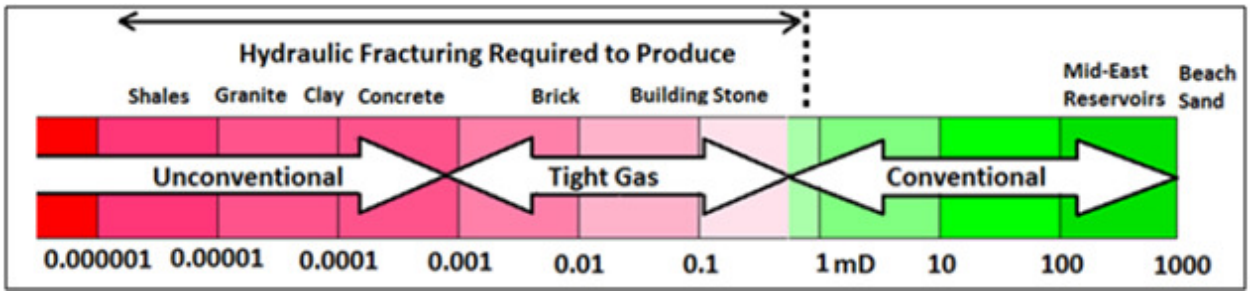

Figure 1-2 Permeability Values for Unconventional Resources and Conventional Resources (King 2010)

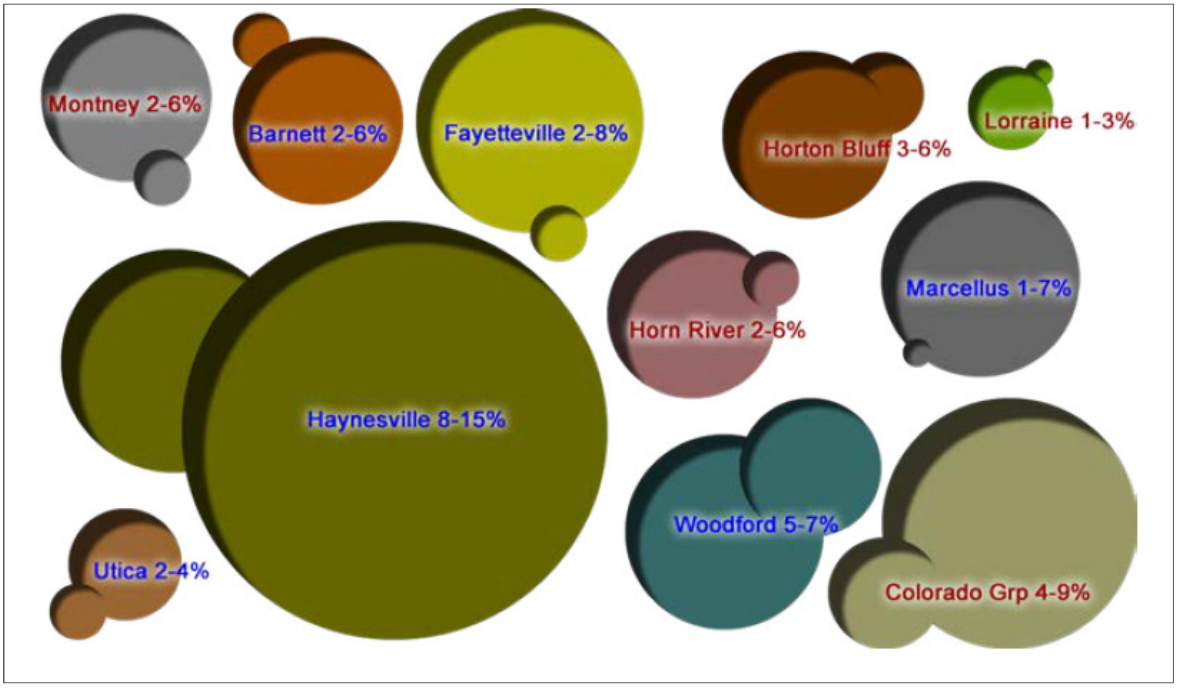

Figure 1-3 Porosity in North American Shale Plays (ALL Consulting 2012)

The grain size of the rock in an unconventional shale formation will generally be small enough to be considered to be shale, though the rock may or may not have a clay-dominated mineralogy. Shales with higher clay content, especially if there is some smectite present, behave in a more ductile fashion and are subject to risks of swelling when exposed to water. Fracture jobs should, in principle, account for

ductility when designing a fracture program. Figure 1.4 shows a range of mineralogy and grain size for American and Canadian unconventional reservoirs.

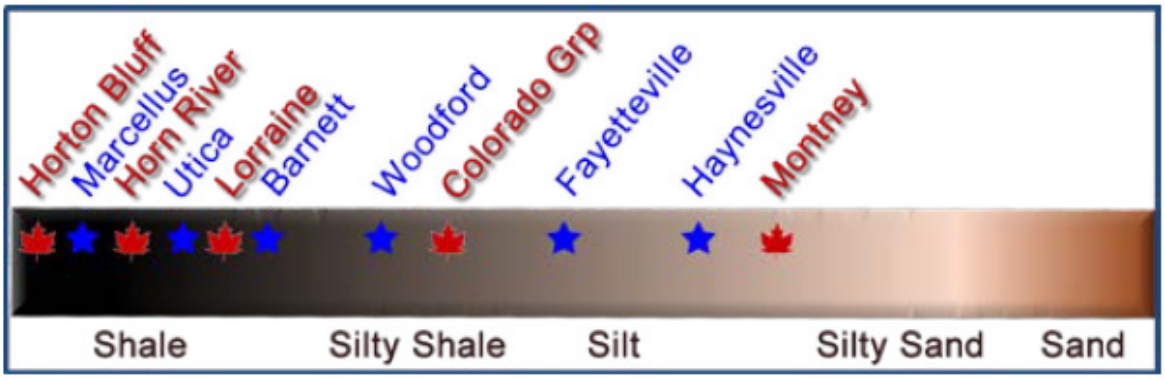

Figure 1-4 Mineralogy and Grain Size of North American Shale Plays (ALL Consulting 2012)

No reservoirs will have the same *in situ* properties over the scale of the play, and it is common for a single shale play to differ significantly from one area to another on a variety of scales. Current and maximum burial depth, thickness, pressure history and current pressure, geomechanical properties, and natural fabric will all affect the rock formation's behaviour. The mechanical properties of particular interest to the design of hydraulic fracturing stimulation will be expanded upon in Chapter 3.

Many unconventional resources possess planes of weaknesses in the forms of bedding planes, joints, and faults. Because features such as bedding planes and joints can be preferential flow paths in their natural state or when stimulated, the fabric of the rock will influence production of the resource. An understanding of the natural fracture system and its effects on fracture stimulation performance is of value to the planning of a hydraulic fracture operation.

Unless the vertical extent of the resource is large, vertical wells and traditional stimulation methods involving small-volume hydraulic fracturing may not permit economic exploitation of shale gas reservoirs. Wells that are drilled horizontally for considerable distances (1 – 3 km) with many stages (10-50) of hydraulic fracture stimulation along the well axis to increase the porosity and permeability of the rock are needed to effectively exploit most shale gas reservoirs.

1.3 Hydraulic Fracturing of Unconventional Reservoirs

Hydraulic fracturing is the process in which pressurized fluid is used to create cracks within the rock in order to increase the permeability of the formation. The opening of natural joints through hydraulic fracture stimulation generates new pathways that allow fluids to flow more quickly to the well and from a larger volume of the reservoir. Horizontal wells are used to give a long contact length and to access more of the formation from a single well pad. They are usually 1-3 km long and are completed with multiple fracture stages to increase the fractured volume of the reservoir rock. An example of a horizontal well with multiple fracture stages is presented in Figure 1-5

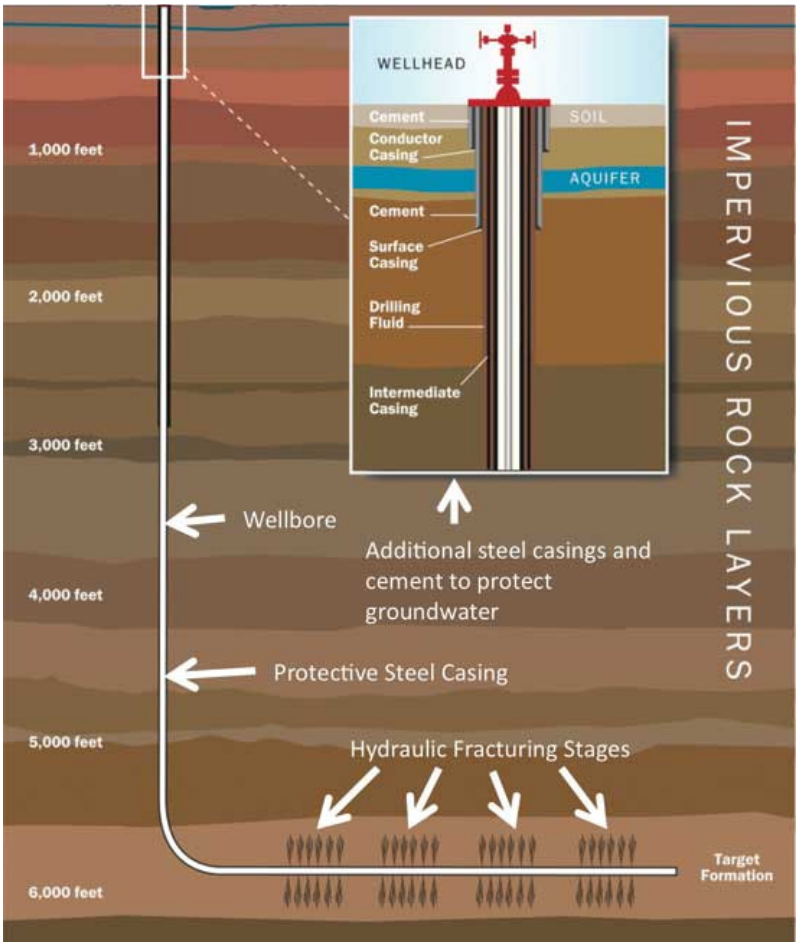

Figure 1-5 A Representation of a Multistage Horizontal Hydraulically Fractured Well (Suchy and Newelll 2012)

The horizontal well allows a greater volume of the reservoir to be accessed than what could be done with a typical vertical well. Horizontal well technology has significantly increased the number of hydraulic fracture operations around the world as it has made many unconventional plays into viable economic prospects. There are several different technologies which are used to implement hydraulic fracture stimulation in a horizontal well. Chapter 2 will expand on the technology and testing used to plan, operate and analyze a hydraulic fracture operation.

The geomechanics aspects involved in reservoir development cover a wide range of topics including wellbore stability, pore pressure prediction, compaction and subsidence, sand production, and hydraulic fracture design. These engineering issues are all linked to the mechanical properties of the rock mass and the stress state of the formation. For example, a major geomechanical effect during hydraulic fracturing is a change in the stress state of the formation because of increase in volume from the injected fluids (generation of fracture aperture plus poroelastic effects). This will be explored further in Chapter 3.

1.4 Modelling Unconventional Reservoirs

Understanding the processes that occur during hydraulic fracturing can aid in planning more effective multi-stage multi-well fracturing operations. Unconventional gas reservoirs provide a particular challenge when it comes to correctly modelling the thermal, hydrogeological, and geomechanical processes involved in hydraulic fracture well stimulation.

Modelling methods can be broken down into four main categories (Jing and Hudson 2002) which are as follows:

- Method A – design based on previous experience
- Method B – design based on simplified models
- Method C – design based on modelling which attempts to include the most important mechanisms
- Method D – design based on an all-encompassing model

Within these methods, there are two levels of 'mapping'. Mapping refers to the use of either direct physical processes (1:1 mapping) or representations or estimations of the physical processes (not 1:1).

Each method can attempt to directly include a mechanism thought to be present in the physical system by relations such as explicit stress-strain laws (1:1), or it can use systems that are not direct such as rock mass classification and database comparison (not 1:1) (Jing and Hudson 2002). Figure 1.6 below shows a general flowchart of the modelling process which can use various methods to achieve a model's goals.

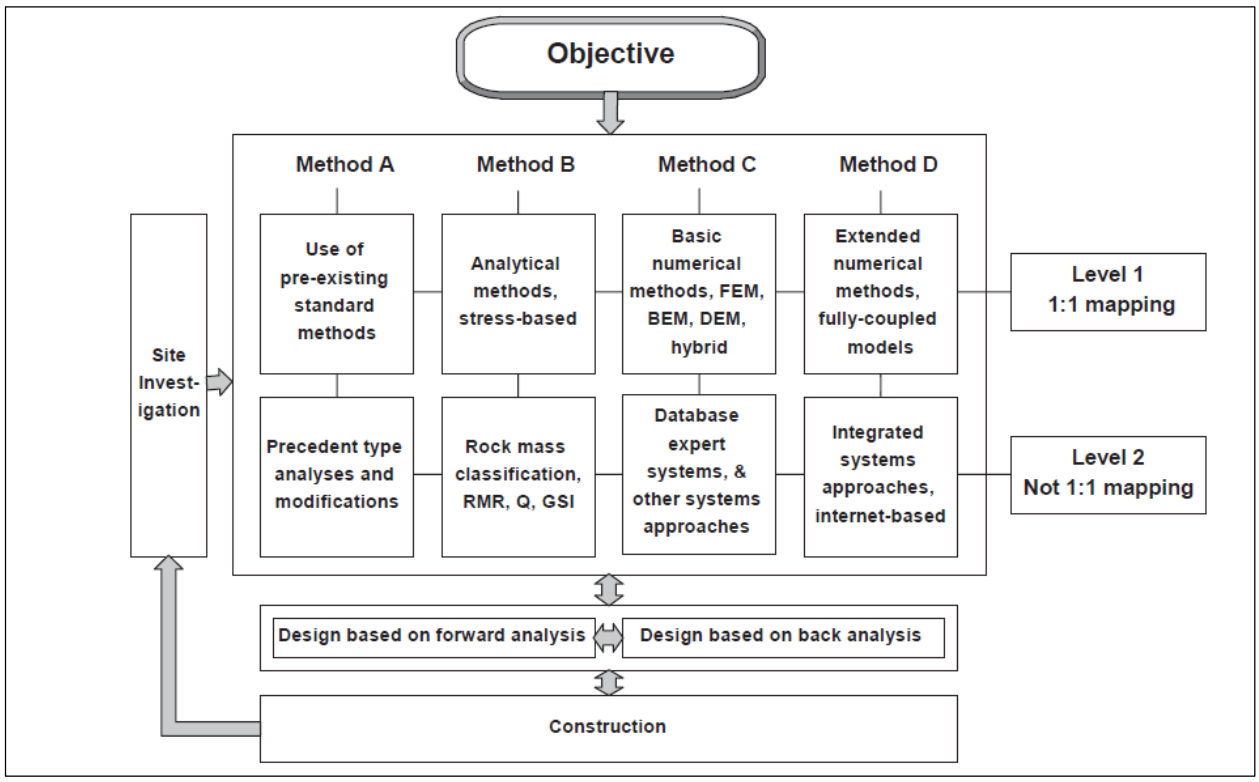

Figure 1-6 Modelling Process Flowchart (Jing and Hudson 2002)

Many hydraulic fracture stimulation designs are based on modelling methods that fall within categories A, B, and occasionally C (Jing and Hudson 2002). The majority of the models can be in either mapping level within methods A or B. Fracture jobs are generally planned using software that simplifies the subsurface environment and fracture physics into a model that can be solved quickly to give a general idea of ultimate production amounts. In many cases the software was designed for conventional reservoirs and does not incorporate geomechanical effects created through the use of horizontal wells and multiple fracture stages (Hack et al. 2006). These programs often rely on a combination of pre-existing standard

methods, some form of rock mass classification and type curve analysis, limited analytical methods, and very basic numerical models (Hack et al. 2006). It is not usual to see a fracture job planned solely with numerical methods or extended fully coupled models.

More numerically and physically complex methods are usually not used due to the high demand for quick planning and rapid modelling of large scope projects. The selection of input parameters for the models can be complicated and is often completed based on limited data. It can be difficult to justify advanced reservoir and fracture modelling if the model inputs are not sufficiently representative of the *in situ* conditions or simply not available. However, if data are available, numerical and analytical models can benefit hydraulic fracture design.

Thus far, the standard industry software has been effective enough to predict production results but with the rise in use of multiple horizontal wells in unconventional strata with increasingly higher numbers of stages, it is reasonable to assume that the simple models are largely limited or insufficient to estimate production response. There is the possibility that more complex models that incorporate geomechanics and other physically relevant aspects properties of unconventional reservoirs, such as better fabric models and better desorption-diffusion models, could provide more accurate prediction of production and could be worth the time and cost associated with multiphysics modelling.

1.4.1 Analytical Models

There are many scientific articles and publications describing advanced complex modelling for multistage hydraulic fracture operations. Many of them rely on similar numerical and analytical methods to produce results. Analytical methods are simplified representations of the problem assuming, for example, axisymmetric or two-dimensional geometry, linear elastic rock behaviour, homogeneous and isotropic rock mass properties, constant permeability over time, and so on. In naturally fractured unconventional reservoirs, factors such as geological heterogeneity, complexity of mechanisms and evolution of properties such as permeability are important enough to make these simple analytical models of questionable value for commercially oriented design purposes. However, analytical models used in a

parametric study or to attempt to understand a response in a real situation can give insight into the mechanisms, thus providing value to engineering design activities.

In analytic models, the hydraulic fracture is generally represented by a two dimensional crack in an infinite homogeneous elastic medium. One of the classic solutions for a two-dimensional fracture in an elastic medium is the Perkins-Kern-Nordgren (PKN) approach developed by Perkins and Kern in 1961 (Perkins & Kern, 1961) with modifications completed by Nordgren in 1972 (Nordgren 1972). The other commonly used solution is known as the Kristianovitch-Geertsma-de Klerk (KGD) model developed by Khristianovitch and Zheltov in 1955 (Khristianovitch amd Zheltov 1955) and expanded on by Geertsma and de Klerk in 1969 (Geertsma and Klerk 1969). The PKN and KGD models are shown in Figure 1-7 and Figure 1-8 respectively.

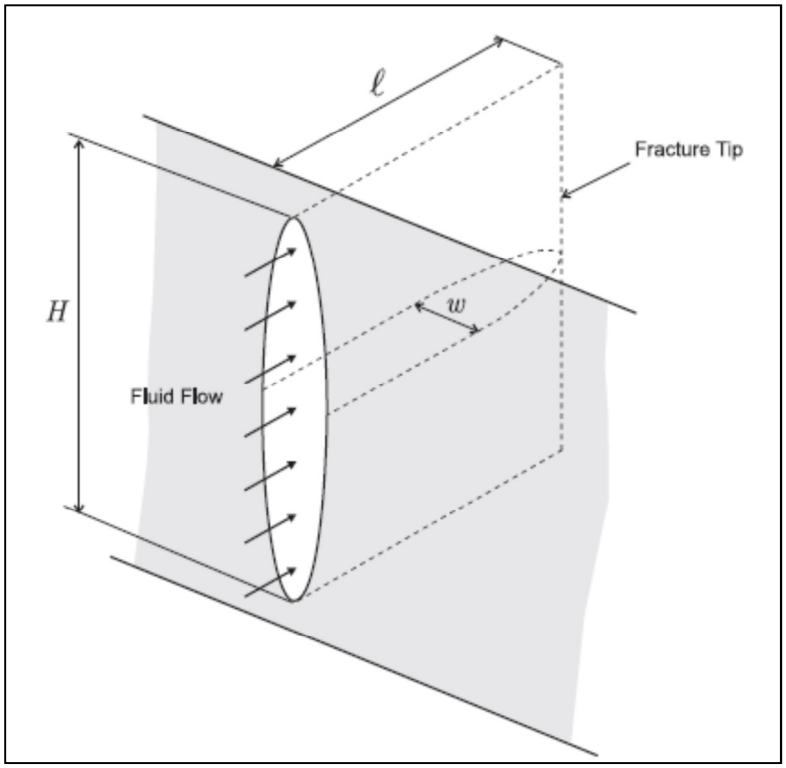

Figure 1-7 PKN Fracture Geometry (Adachi et al. 2007)

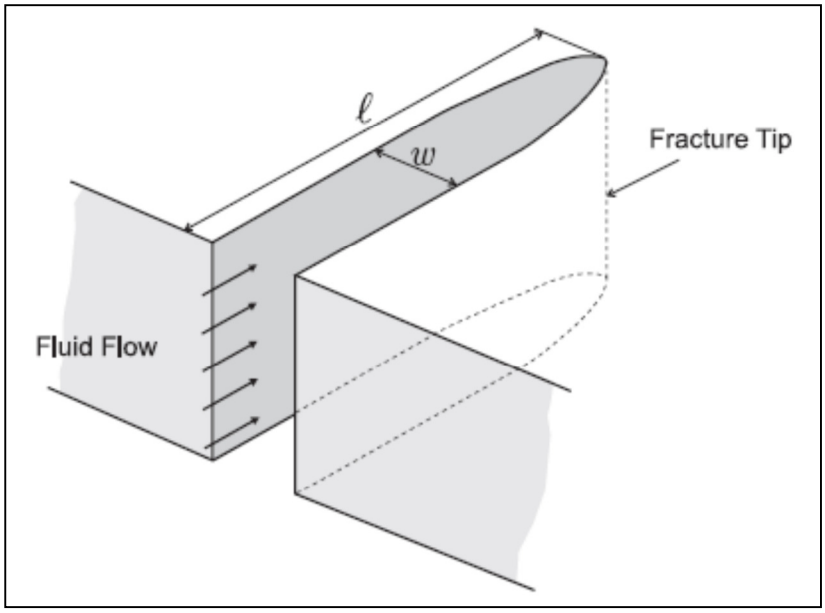

Figure 1-8 KGD Fracture Geometry (Adachi et al. 2007)

The PKN and KGD models are used primarily for determining fracture geometry and volume. They are also used to derive expressions for pressure within the fracture. The PKN is most commonly used for hydraulic fracture operations where long thin fractures are expected. KGD is suited for fractures where the length-to-height ratio approaches unity or less. The models are constrained by several assumptions. A plane strain condition exists for the PKN fracture in the vertical plane and for the KGD fracture in the horizontal plane. Both models assume a constant height that is independent of fracture length. The models do not consider geomechanical effects such as stress increases or poroelastic volume changes, nor can they accommodate the presence of discontinuities (joints, bedding planes) that could affect the behaviour of the hydraulic fracture.

Despite these limiting assumptions, the PKN and KGD models can provide insight into several different mechanisms associated with hydraulic fracture. They are widely accepted as first order approximations of fracture geometry and volume, and they have been used extensively to estimate the pad volume required to obtain the hydraulic fracture which would allow proppant entry (Adachi et al, 2007). The PKN and KGD models, with some modifications, have also contributed to the modelling of proppant

transport which has led to a reduction of unexpected proppant bridging and screen-outs (Adachi et al. 2007). These models have also been used to show the sensitivity to input parameters such as treatment volumes, fluid viscosity effects, leak-off, and injection rate. These parameters will be expanded on in Chapter 2.

Several studies have shown that both the PKN and KGD bi-wing models are often too much of a simplification of the hydraulic fracturing process in the rock mass. The presence of joints and bedding planes will affect the shape of the overall hydraulic fracture, generating a multi branched and complex form as the propagating hydraulic fracture interacts with the natural discontinuities. The selection of a fixed height for the models and a constant value for the fracture toughness can also affect the applicabilityof the model. The PKN and KGD fracture models should be applied only with an understanding of their limitations.

1.4.2 Numerical Models

Numerical methods are more common and more appropriate when dealing with the complexity and non-linearity involved in modelling fracture mechanisms in porous naturally fractured media. The most common methods include (Jing and Hudson 2002):

- Continuum methods – finite difference, finite element, boundary element
- Discrete methods – discrete element, discrete fracture network
- Hybrid continuum/discrete methods
- Coupled thermo-hydro-mechanical (THM) models implemented through finite element or finite difference numerical approaches
- Inversion of actual data using inverse solutions methods that may be direct inversions, or error minimization methods based on one or more of the forward models listed above

The choice of method should rely on several aspects of the physical problem, including the scale of the process being simulated and the natural fracture system geometry within the reservoir. Discrete

mathematical models (such as discrete element methods, etc.) are generally applied when there is good reason to believe that the rock masses are naturally fractured and that large-scale displacements (opening and shearing) of these discontinuities will have a major effect on the HF modeling. Continuum approaches are best suited for homogenous rock masses or for cases where there is reason to believe that the effect of natural fracture on the HF response will be inconsequential (Jing and Hudson 2002).

Each method has advantages and disadvantages and should be chosen based on the data available and the goals of the model (Jing 2003). For instance, a continuum finite element model may not be suitable for modelling fracture propagation through a heavily fractured medium, and a THM model would be needed for a situation where there will be important temperature effects arising because of injection of a hot or cold fluid over a long time period (e.g. steam fracturing in heavy oil stimulation, or long-term disposal of cold water).

1.4.3 Uncertainty in Modelling

Any model of the subsurface will possess some degree of uncertainty that will generate interest in approaching problems in a probabilistic manner (e.g. sensitivity analysis or stochastic variation of properties). This interest may, if the models are simple enough, translate into a risk assessment analysis. Some factors that contribute to uncertainty are (Hack et al. 2006):

- Estimation errors (e.g. estimation of earth stresses)
- Modelling constraints (e.g. inability to discretize adequate detail)
- Measurement errors and scale issues (e.g. failing to understand the difference between rock specimen stiffness modulus and rock mass stiffness modulus)
- Ignorance, unforeseen features, events, and processes (e.g. encountering an unidentified zone of high fluid leak-off capacity or an unexpected basal aquifer)
- Simplifications and generalisations due to information overload (e.g. assuming a single stiffness modulus in a case where stiffness differences will restrict fracture height growth)
- Human error

It is not possible to know every aspect of the underground conditions in which a fracture job will take place. Even if the uncertainties listed above are largely eliminated, there will remain some unknowns that could cause the actual hydraulic fracture process to severely deviate from the predictions of the model.

1.4.4 Simplification of Models

Despite the availability of numerous mathematical and advanced coupling solutions, many hydraulic fracturing jobs are planned with simple and quick commercial software programs that were originally developed for conventional or carbonate reservoirs exploited through vertical wells, with vertical HF propagation entirely and with no possibility of one fracturing stage affecting another. There are several excellent reasons for simple models to be used over complex modelling methods.

For example, if modeling results are incoherent or are demonstrated to be systematically incorrect, the time and financial commitment that is needed to produce a fully representative complex model will not be seen as a valuable investment. If the difference in overall gas production that may be achieved is viewed as not significant enough to invest time and money into a complex mathematical model when a simpler approach can be used, the complex modeling will be avoided. The same may be said for an overly simplistic model that leads to poor engineering decisions. Model usefulness, whether it is a complex or simple model, must be demonstrated in practice, and this is a challenging task.

The simple models that are commonly used are focused on prediction of overall production success of a fracture job rather than evaluating or understanding the geomechanical factors governing fracture propagation and stress redistribution. The models often rely on bi-wing planar fracture assumptions to reduce geometric complexities and to be able to apply the PKN and KGD method. Then, they may be repeatedly "calibrated" to field data to improve their use as predictive tools, even if the underlying physical basis of the model is questionable or incomplete.

In order to be effective, to some extent, the following features should be included in a model (Jing 2003).

- Relevant physical processes and their mathematical representations, such as the incorporation of thermoelastic effects when appropriate (usually associated with long-term injection)
- Relevant mechanisms and constitutive laws for the important rock units and rock mass fabrics (e.g. introducing Mohr-Coulomb slip potential for representation of the response of a large fault)
- Existing state of rock stress (e.g. including horizontal stress differences for different strata)
- Temperature and pressure, as essential initial conditions
- Presence of natural joints in cases where strong fabric such as one dominant joint set is known to exist
- Reasonable degree of in-homogeneity at different locations throughout the rock mass, based upon the geomechanical earth model, geophysical data, and core testing
- Anisotropic properties if appropriate, particularly in laminated or thinly bedded rock masses
- Time and rate dependent behaviour such as the non-Newtonian behaviour of certain viscous fracturing fluid formulations
- Variations in properties in the rock mass at different scales such as the matrix permeability versus the rock mass permeability dominated by natural fractures
- Scale effects such as a HF interacting with one discontinuity such as a fault versus interaction with many discontinuities such as a jointed rock mass
- Effects of engineering processes on the constitutive properties and geometry of the rock mass including changes in permeability over time as pressures change

Some methods will incorporate these elements in more effective ways than others and there will always remain unknowns and simplifications that must be made. The most important aspect of modelling is not how complex it can be or how many features it can incorporate, but how effective it is at incorporating the most important aspects of the physical system in order to produce results that are sufficiently representative of the physical processes that will occur. A model may focus more heavily on one feature

listed above than another in order to produce results that are in line with the goal of the program. No single approach can handle all the different cases and configurations considered.

1.5 Goal of Thesis

The main goal of this study is to present a simple analytical geomechanical model which utilizes existing field data to estimate stress changes during fracturing and the overall fracture geometry. The model will also show how those changes may affect subsequent stages. The intention is to create a simple and quick tool that can be used to assist with design decisions in formations that are similar geologic settings.

This thesis will began by examining field data from an existing hydraulic fracture job within the Montney Formation in Alberta, Canada. The breakdown and closure pressures from the field data will be compared to determine if a stress change is detected within the fracturing operation. The injection rate and injection volume from the data will be used to estimate an approximate size and shape of the fractured area. The stress change from the fracture will be compared to the breakdown pressures from the subsequent stages to determine if the model is accurate. The model could then potentially be used to estimate how fracture operations within a similar formation may be affected by stress changes.

Hydraulic fracture technologies, property testing, operations design and monitoring, and post process analysis are discussed in Chapter 2. Chapter 3 introduces geomechanical effects and the concept of stress shadow in more detail. Governing equations for fracture initiation and stresses within the formation will also be reviewed. The analytical equations for stress change around an ellipsoidal equation are presented in Chapter 4. Chapter 4 will also discuss the full work flow and equations of the stress shadow model. Chapter 5 reviews the case study field data. Chapter 6 details the results of the model when used in conjunction with the field data. Conclusions and recommendations are made in Chapter 7.

Chapter 2 Multi-stage Hydraulic Fracturing in Unconventional Reservoirs

2.1 Design and Planning of Fracture Operations in Unconventional Reservoirs

Massive multi-stage hydraulic fracturing (MSHF) operations are planned and designed based on various geologic properties and operational considerations. The primary reservoir parameters needed to estimate if the well will be economically feasible include reservoir pressure, porosity, permeability, mineralogy, and oil and water saturation (Jones and Britt 2009). Once the well has been determined to be economically viable, the geomechanical properties of the formation must be established. These include the minimum horizontal stress magnitude and direction, Young's modulus, Poisson's ratio, reservoir temperature, and leak-off coefficient (Jones and Britt 2009).

Pre-fracture treatment design is completed with the intention of optimizing production and minimizing unknowns that could potentially cause operational issues. The analyses usually are based on information obtained through dipole sonic logs, borehole breakout analysis, core analysis, and *in situ* stress tests (Jones and Britt 2009). The pre-fracture treatment analyses will be expanded upon in Section 2.3.

Several parameters are monitored during the hydraulic fracture process. The primary property measured during the fracture process is the bottom-hole treatment pressure (BHTP) which is generally monitored directly or calculated from surface pressure values (Jones and Britt 2009). Microseismic monitoring is also used to monitor the fracture process, though usually the results from the microseismic array are not available until after the MSHF operation has been completed. Proppant and fracture fluid tracing data, gamma ray and other log data, tiltmeter data, and transient pressure information may also be collected and used during MSHF operations, or to do post-analysis of the stimulation. The information gathered during the MSHF job will be discussed in detail in Section 2.4.

Post-fracture analysis can provide valuable insights into how closely the actual MSHF results matched the predictions from the design procedure. Adjustments can be made to future designs in similar formations based on the results of the post-fracture analysis. Pressure transient analysis (PTA) and flow regime

calculations are generally completed to validate reservoir properties (Jones and Britt 2009). Post-fracture analysis will be reviewed in more detail in Section 2.5.

2.2 Hydraulic Fracture Technology

The technology used to implement MSHF is variable and extensive as there must be options to meet a wide range of formation conditions. No two MSHF operations are likely to exist under identical conditions and therefore the technology must be able to adapt to the specific parameters of the target formation. For instance, the depth of the formation may dictate what kind of perforation method can be used, or clay minerals present in the rock mass may eliminate certain fracturing fluids as viable options. The sections below will outline the major equipment deployment pertinent to the stress shadow model and analyses presented in this thesis.

2.2.1 Cemented Casing Plug and Perforation Method

The cemented casing, plug and perforation (CCPP) completion method places several closely spaced (20-100m) perforations points within a hydraulic fracture interval (Blanton and Mackenzie 2006). A perforation gun is set down hole and fires in a planned perforation sequence to create the hydraulic fracture initiation points. A wireline is used to pull out the perforation apparatus and the interval is sealed with packers or bridge plugs, then fractured. Intervals are fractured sequentially from the toe of the well (the interval farthest from the wellhead) to the heel (the interval closest to the wellhead). The perforation clusters can have anywhere from three to seven fracture points spaced out at equal distances along the section. The spacing between the individual fracture initiation points is generally small and almost always uniform. Figure 2-1 shows a basic schematic of a CCPP well.

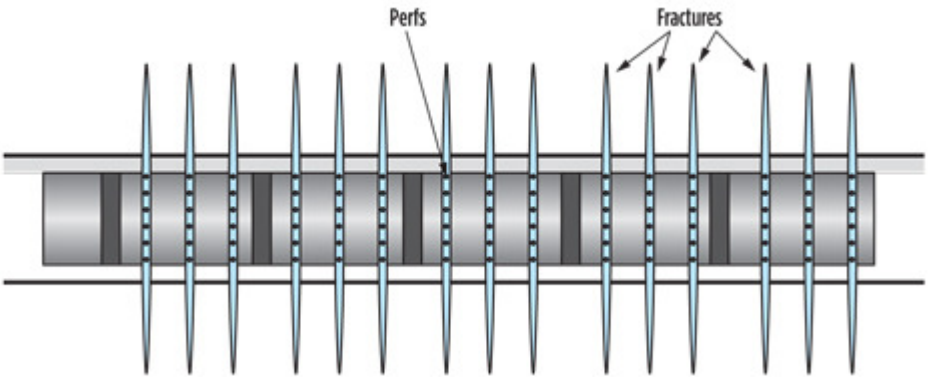

Figure 2-1 Basic Schematic of a Plug and Perforation Well Set Up (Daneshy 2013)

The CCPP method is preferred in deeper wells where the mechanical stability of the wellbore may be low. The numerous perforations provide several points for hydraulic fractures to grow from. If one fracture does not initiate or a screen-out (a condition where the proppant creates a bridge across the perforation or fracture and prevents flow) takes place in one or more perforation, other perforation points will still be able to take fluid and proppant to create a hydraulic fracture.

It is usually assumed that increasing the number of perforations and clusters will increase fracture complexity and therefore cause an increase in gas production. However, if geomechanical effects are incorporated, evidence shows that more perforations in a small interval may not be the optimal method of resource extraction (Olson 2008). Several studies have proposed that the cost of extra perforation clusters and single perforation points is not always compensated for by increased production (Dohmen et al. 2014). There is evidence which shows that not all perforation clusters contribute to production (Miller et al. 2011). In the cases examined, one perforation cluster will contribute a significantly higher amount to the production than the clusters on either side of it (Miller et al. 2011). It has also been shown that insufficient space between perforation clusters will cause the width and length of the middle fracture initiated by the middle cluster to decrease and will also reduce the complexity of the fractures (Olson 2008). The geomechanical interactions caused by several closely spaced hydraulic fractures can have a significant effect on overall production. This topic will be expanded upon further in Chapter 3.

2.2.2 Open Hole Methods

Open hole methods requires the formation to be mechanically stable as no casing or cement is used to maintain wellbore stability for some time before equipment is placed downhole. The fracturing fluid is in direct contact with the formation during open-hole methods. The most popular open hole system is the ball drop method, also referred to as sliding sleeve completions. Casing with swelling packers and sliding sleeves is placed in the horizontal open-hole section. Frac-ports which are sealed with closed sleeves are placed within each interval. The fracturing takes place from the toe of the well to the heel as the sleeves are opened sequentially to allow each individual interval to be pressurized and fractured. The most common method of opening the sleeves is to drop a ball of a specific size down the well until it seats in the correct sleeve. A pressure differential is implemented to force the sleeve to slide open and allow the fracturing fluid to enter the correct interval. Once the prescribed amount of fracture fluid is pumped down, another slightly larger ball is pumped down to seal the interval and begin fracturing of the next one. Figure 2-2 shows a basic schematic of an open hole ball drop well.

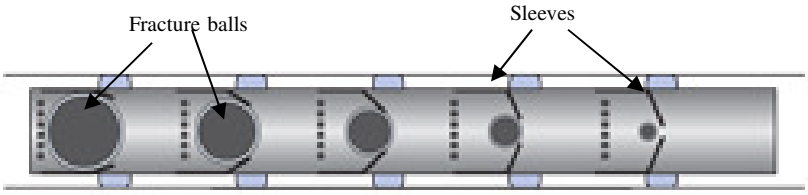

Figure 2-2 A Basic Schematic of an Open Hole Ball Drop Well (Daneshy, 2013)

The ball drop completion method is done with continuous injection which greatly decreases the time needed to fracture the entire well, as compared with CCPP methods (Daneshy 2013). There is no need to use wirelines or perforation guns which makes the equipment and operational procedures simpler. However, accurate pumping rates and volumes are needed to insure each interval is sufficiently fractured before moving onto the next interval. Screen-outs are more common than in CCPP methods, especially near the toe of the well. Deep wells cannot generally use ball drop methods as the frictional forces down the well often prevent the ball from seating near the toe of the well.

.

The ball drop method allows fractures to initiate at any point along the interval between the packers, which means the fluid can take advantage of any natural planes of weakness and joints present in the interval. Many MSHF designs are based on the assumption that the fracture will initiate from the middle of the interval though this is not likely to be the case. If there is a plane of weakness closer to the edge of the interval the initiation point may not be from the center point. Also, the swelling packers that are used to separate intervals may modify the stresses somewhat, making it easier to initiate hydraulic fractures near the packers. If the fracture initiates too closely to the edge of the interval, it may cause stress changes to occur in the rock within the next stage at a greater intensity than if it initiates at the center of the interval, further modifying the rock response and making it less likely that the fracture initiates in the centre of the interval. Stress interactions will be discussed further in Chapter 3.

2.2.3 Hydraulic Fracture Fluids and Proppant

MSHF operations must consider the type of fluid and the type and amount of proppant when designing a fracture plan. The fluid initiates the fracture, propagates within the formation (fracture extension), and effectively transports the proppant within the hydraulic fracture (Jones and Britt 2009). The grains of the proppant must be large enough and strong enough to keep the fracture open once the pumping is completed.

The fluids are selected based on several criteria. Generally they should be selected so they do not react negatively with the formation (e.g. fresh water may cause smectite-bearing formations to swell which will impair fracture conductivity), have enough viscosity to transport the proppant but not so much that the pumping pressure increases significantly, and prevent fluid loss into the rock matrix (Jones & Britt, 2009). The polymers used in the hydraulic fracture fluid to generate viscosity should also be able to break down easily (i.e. de-polymerize and lose viscosity) in order that they can be removed more easily from the formation during the fracturing back-flow period. The most commonly used fluids include slickwater (a water based non-viscous fluid using agents that reduce frictional pressure losses during flow

in thin fractures) and aqueous-based cross-linked gels or foams (more viscous chemical based fluids designed to transport proppant more effectively). Less commonly, agents such as liquid CO_2, N_2, or gelled propane can be used. Although far more expensive, these fluids have the advantage that they do not cause any formation damage.

The viscosity of the fluid can influence the shape of the fracture. In general, less viscous fluids will create long thin fractures where-as highly viscous fluids will cause induced fractures to be shorter in length, more circular in aspect, and of greater aperture (fatter) (Beugelsdijk et al. 2000). Lower viscosity fluids tend to increase the complexity of the fracture geometry (Cipolla et al. 2009), likely because the pore pressures can more easily penetrate the natural joints and bedding planes, adding shear slip and joint dilation. The shape and size of the fracture will also affect the geomechanical properties of the rock mass; larger and more complex, wider fractures will lead to larger changes to the *in situ* stress state than a shorter and simpler fracture would. In particular, larger fracture aperture should lead to larger stress changes in the direction normal to the induced fracture, thus the volumetric component of deformation during fracturing is important to the issue of stress change.

2.3 Pre-Fracture Formation and Well Testing

Testing the target formation to determine geological and mechanical properties is part of the design of a MSHF operation. Pre-fracture testing is usually done to determine important geomechanical aspects of the formation (*in situ* stress, Young's modulus, etc.) as well as a wide range of geologic properties which will affect production (porosity, permeability, etc.). A good estimation of the formation's properties is valuable when it comes to planning a MSHF operation, as well as to the post-fracturing analysis.

2.3.1 Determination of Geomechanical Properties

The *in situ* stress state of the target formation is the major geomechanical control on the initiation and propagation of a hydraulic fracture. The hydraulic fracture will propagate approximately perpendicular to the minimum principal compressive stress direction. The fracture will initiate and propagate if it can both

overcome the intrinsic fracture toughness of the rock and the closure pressure of the formation, taken to be equal to σ_h. The mechanisms of stress, strain, and fracture will be discussed in detail in Chapter 3.

There are several tests and procedures that can be done to determine the stress in the target formation. They can be grouped into three main types of tests: logging while drilling (LWD), wireline logging methods and direct well testing (Fjaer et al. 2008).

Dipole or quadrupole multiple-receiver sonic logs are used to make a first-order estimate of the minimum compressive horizontal stress magnitude and orientation as these will affect the propagation and final geometry of the hydraulic fracture (Dutton et al. 1982) and are needed in design calculations. The shear and compressional sonic velocities from these logs are used to calculate the dynamic Young's modulus and Poisson's ratio (Jones and Britt 2009). Some acoustic logs can be done through LWD methods in order to determine the mechanical properties in real time while drilling. There are no direct logging methods available to determine the *in situ* strength parameters and actual stress state (Fjaer et al. 2008). Most logging methods use an empirical correlation to relate acoustic velocities to strength parameters, and careful calibration of the geophysical logs in a region is required to extract reliable information about stress state and orientations, as well as mechanical properties (dynamic moduli at the borehole scale are not the same as static moduli at the scale of hydraulic fracturing).

Temperature logging is commonly done to determine the geothermal gradient and bottom-hole temperature. Temperature can have a significant effect on the elastic properties of rock and should be considered when using equations which apply to geomechanics.

Core analysis can be used to obtain Young's modulus and Poisson's ratio for use in design (Jones and Britt 2009) and for calibrating geophysical logs so that they can be used to interpolate and correlate values. Triaxial testing can be done on solid undisturbed cylindrical specimen to determine Young's modulus under static conditions. It should be noted that usually every effort is made to ensure the sample is undisturbed and that prepared specimens are tested under conditions similar to those of the reservoir; however, sample degradation and disturbance can skew the outcome of the tests. Core analysis should be

cross-referenced with the dipole sonic logs and other geophysical logs of the formation to ensure accuracy in depth and to identify and eliminate poor quality data.

Borehole geometry logs are used to measure the overall shape of the hole to identify wellbore breakouts or elliptical geometry. Consistently oriented elliptical cross sections in multiple boreholes in the same area suggest that there is a preferential stress orientation in the area and this will therefore almost certainly indicate the minimum compressive horizontal stress direction (Jones and Britt 2009) determining the optimum azimuth along which the well should be drilled. Generally wells are drilled along the same azimuth as the minimum compressive horizontal stress direction (Jones and Britt 2009) to foster the development of transverse fractures during stimulation.

It can be difficult and complicated to determine the in-situ stress state of the formation, especially in areas without a strong tectonic imprint and in cases where borehole breakouts are inconsistently oriented or poorly developed. However, accurately determining stress gradients and relevant treatment pressures must be carried out for pre-fracture planning. The pressure at which the fracture closes (p_c) is usually assumed to be equal to the minimum compressive horizontal stress of the formation (σ_h) but it has been shown that closure of the fracture is not instantaneous (Warpinski et al. 1998). The fracture closure process is gradual and can make the selection of the closure pressure from field data difficult. Even if the two faces of the fracture are touching, the fluid within it may still be free to flow (Fjaer et al. 2008). For the purposes of this thesis, the closure pressure will be assumed to be the best estimate of the minimum compressive horizontal stress.

Different tests can be used to determine closure pressure. These include pump in/decline (PID) tests and pump in/flowback (PIFB) tests (Jones and Britt 2009).

The PID test is a fairly simple type of test to run. One type of PID is called the Microfrac™ test and has been examined in detail in Warpinski and Teufel (1989) and McLennan and Roegiers (1982). A small amount of fracturing fluid is injected into the formation at a low rate and the decline of pressure is monitored after the test has been shut in. An instantaneous shut in pressure (ISIP) is selected as a close

approximation of closure pressure after several tests have been run. The ISIP will act as an upper bound for closure pressure (Jones and Britt 2009). An example of a Microfrac™ test is shown in Figure 2-3.

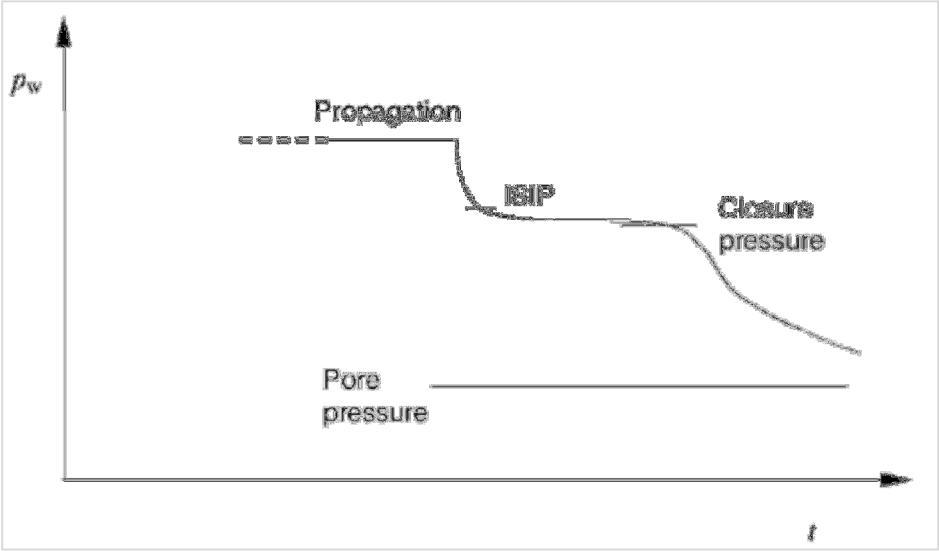

Figure 2-3 An example of a Microfrac test (Fjaer et al. 2008)

It is considered good practice to plot the pressure vs. the square root of shut-in time to select the closure pressure. Closure pressure is indicated when the slope of the line changes, indicating a change in linear flow. An example of a square root time plot with a closure pressure selected is shown in Figure 2-4.

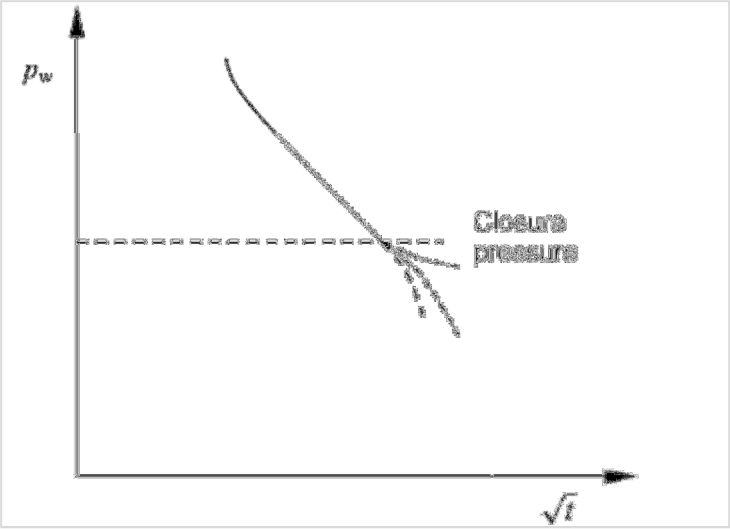

Figure 2-4 An Example of a Square Root Time Plot (Fjaer et al. 2008)

PIFB tests are slightly more complicated when it comes to determining closure pressure, but can be more effective in extremely low permeability formations (Jones and Britt 2009). PID tests take a long time to complete in low permeability, low porosity reservoirs whereas PIFB tests are completed fairly quickly. In PIFB tests, the injection is immediately followed by a constant rate flowback period. The rate of flowback is meant to match the rate of leak-off into the formation. During flowback, a characteristic reverse curvature occurs in the pressure decline when closure pressure is reached (Jones and Britt 2009). PIFB tests can be difficult to interpret and can be operationally intensive, so they are generally done only if PID tests fail. An example of a PIFB test is show in Figure 2-5.

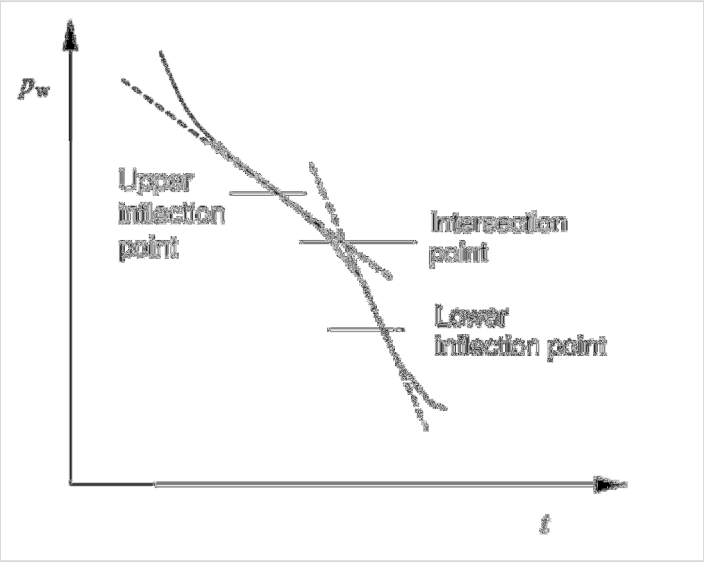

Figure 2-5 An Example of a PIFB Test with Typical S Shaped Curve (Fjaer et al. 2008)

The vertical stress is usually determined through use of density logs. The density recorded from the log integrated over the vertical depth of the well is considered to give a reasonably accurate measurement of vertical stress in areas of low tectonic activity (Fjaer et al. 2008). From such tests, from modeling, and from previous experience, the minimum pressure needed to create the fracture, the proppant size and strength requirements, and the pressure at which the fracture will propagate (Jones and Britt 2009) can be assessed to aid in hydraulic fracture design.

2.3.2 Determination of Geological Formation Properties

Porosity and permeability are important properties to determine before a well can be deemed economically viable; they are the primary governing parameters of gas flow to the hydraulic fracture and wellbore.

Porosity is the ratio of the volume of the void space between the grains of the rock to the total volume of rock mass. It can be determined through core testing, though undamaged whole core is needed. If the core is undisturbed it can be tested for porosity under similar stress conditions to those found in the targeted rock mass. Any values obtained in the lab through core testing should be compared to the

porosity values gathered through wireline logs. The two main types of logs used to determine porosity are density logs and nuclear magnetic resonance (NMR) logs.

Permeability is a measure of the ability of the rock to transmit fluids under a pressure gradient. It can be affected by many factors including testing scale, pore types and size, effective stresses, pore pressure, and grain shape (Cui and Brezovski 2013). Core samples are tested using a variety of different approaches including pressure pulse decay and pressure fall-off methods (steady-state methods are too time consuming in low permeability materials). Care should be taken to ensure that the samples are representative of the formation and tested under the correct confining stresses because permeability in small pores and microcracks is sensitive to the effective stress level. A detailed examination of measuring permeability in core samples can be found in the study by Cui and Brezovski (2013). Permeabilty can also be measured through the use of well-test analysis, including injection tests, as mentioned in the previous section.

Mineralogy is generally established through thin section examination , X-ray diffraction, oxides analysis, and scanning electron microscope (SEM) analysis. The mineralogical composition of the rock affects the strength and mechanical behavriour of the overall rock mass (Fjaer et al. 2008). The rock is more likely to act in an elastic fashion if clay minerals are not present and as the amount of clay minerals increases, the formation tends to become more ductile. Estabilishing formation mineralogy will also help to select a fracturing fluid. Certain minerals (e.g. smectite) will react chemically with specific fracturing fluids and could negatively affect production.

2.4 Production Monitoring and Analysis

The amount and type of data collected during MSHF will depend on how much a company is willing to invest, and this can change as a project progresses. The more information gathered, the more can be said about the overall fracture geometry and effectiveness of the pre-fracture planning. Pressure recording and analysis is standard practice for all MSHF operations as it is often the only way that is used in real time to track how the formation is reacting to the injection process. Data purely for use in determining fracture

geometry is not always gathered but are considered valuable for planning future jobs within similar formations.

2.4.1 Fracture Geometry Data

Tiltmeters are highly sensitive sensors which are used to measure the change in inclination of a surface. It is assumed that the Earth will respond in an elastic manner to the deformations caused by the opening of hydraulic fractures (Jones and Britt 2009). To make sense of the recorded data, the measured tilts recorded on the surface are compared with theoretical values for possible combinations of fracture azimuth and dip so that fracture orientation can be inferred from the information gathered from surface tiltmeters. Downhole tiltmeters are also used to record deformations, and these are used to more accurately estimate fracture height rather than merely orientation (Jones and Britt 2009). Tiltmeters used in a downhole array must be placed in particular locations with respect to the well being stimulated in order to achieve maximum effectiveness for a MSHF process. Too close to one portion of the MSHF well means that the formation response for more distant stages will be difficult to collect and analyze; too far from the well means the signals would be too weak to achieve the precision desired.

Microseismic monitoring has become the most commonly used method to estimate stimulated volume of the hydraulic fracture. Microseismic events are caused by small shifts in the earth which emit elastic compressional and shear waves (Jones and Britt 2009). They are caused when shear slip of natural joints or bedding planes occurs around a hydraulic fracture during injection. Tensile stresses formed at the tip of the hydraulic fracture, along with an overall increase in formation stress and pore pressure, plus the geometrical distortion imposed by the thin ellipsoidal shape of the induced fracture, cause significant shear stress changes within the formation, in combination with a reduction in effective stresses. These processes contribute to the shear slippage of planar weakness features in the formation. Geophones are placed around the fracture operation to measure wave arrival times. Location, magnitude, and direction can be calculated from this information. It should be noted that the size and magnitude of the

microseismic events does not delineate the size of the hydraulic fracture and should be interpreted more as a stimulated volume. This concept will be expanded on in Chapter 3.

2.4.2 Pressure Monitoring

The pressure needed to maintain fracture growth during MSHF is one of the most important parameters to monitor during the fracture process. It provides insight to many different aspects of the fracture treatment process. Surface pressure data is most commonly recorded, though it is recommended that bottom-hole treatment pressure (BHTP) should act as the primary source of information for the fracture treatment process (Jones and Britt 2009). BHTP is needed to determine the net fracture pressure defined by equation 2.1.

$$p_n = p_f - p_c \quad (2.1)$$

Where p_n is the net fracture pressure, p_f is the BHTP within the fracture required for propagation, and p_c is the closure pressure (equal to the minimum principal stress). It is the pressure available to create width within the fracture and to force propagation of the induced fracture through the rock mass (Smith & Montgomery, 2015). Net fracture pressure is used in design to determine the main fracture treatment pressure and to analyze on-site fracture pressures. The concept of net pressure will be expanded on in Chapter 3.

BHTP is also needed to monitor the completion of Minifrac™ tests which are used to determine the mechanics of fracture growth (Jones and Britt 2009). Minifrac™ tests are done before individual stages to confirm stress states predicted by pre-fracture analysis and to determine leak-off properties. They are used to estimate breakdown pressure (p_b), instantaneous shut in pressure (ISIP), and p_c of an interval. They also provide insight into the mechanics of fracture propagation, fracture geometry, *in situ* stress contrast, and fracture fluid efficiency (Jones and Britt 2009). Figure 2-6 presents an idealized pressure curve for a Minifrac™ test.

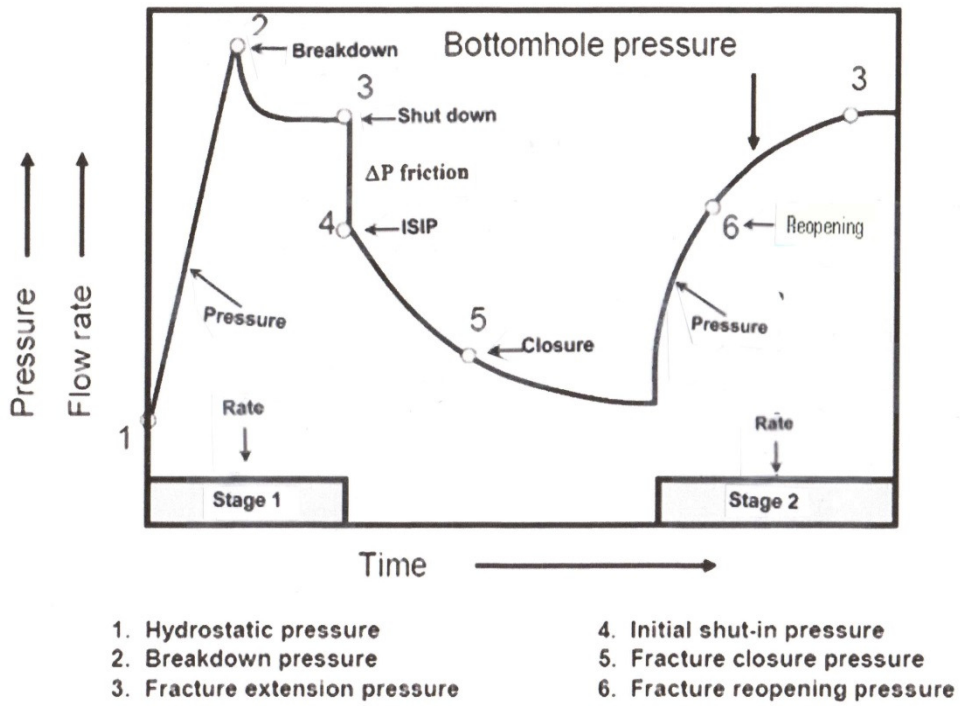

Figure 2-6 Idealized Pressure Curve for a Minifrac™ Test (National Energy Board 2013)

Pressure response during MSHF is the main diagnostic tool used for making real-time decisions regarding the fracture treatment (Smith and Montgomery 2015). Pressure fluctuations during treatment can be classified into four different categories (Smith and Montgomery 2015):

- Mechanical malfunctions such as pump and blender failures, closed valves, plugged lines, or casing failures.
- Changes in fracture fluid properties such as fluctuations in viscosity or proppant concentrations.
- Changes in the type of fracture propagation
    - A rapid increase in pressure may indicate a fracture which has stopped propagating – screen-outs may occur.
    - A rapid decrease in pressure may indicate that the hydraulic fracture has encountered a plane of weakness or is rapidly expanding or has changed direction

- Instantaneous increase in pressure indicates either an imminent blowout from a change in reservoir pressure or that the fracture has screened-out near the wellbore (entrance to the fracture is blocked).

- Changes in the formation – mechanical or geological
  - The value of σ_h is changing which results in a gradual change of treatment pressure needed to propagate the fracture.
  - Faults, joints or bedding planes may cause the fracture to branch.

2.5 Post-Fracture Production Analysis

Post-fracture production analysis is mainly concerned with evaluating reservoir and fracture behaviour. Pressure transient analysis (PTA) is used to evaluate flow regime (i.e. radial, linear, etc.) and fracture growth. Specialized plots, including G Function analysis, Square Root Time plots, and Nolte-Smith Log-Log interpretation are used to evaluate fracture behaviour. These plots are primarily based on PKN and KGD geometry assumptions. For more information on post-fracture pressure analysis, please see Smith and Montgomery, 2015.

Direct measurements of reservoir properties may include temperature surveys, tracer logs, and tiltmeter data. Temperature surveys are used to monitor changes in the rock after pumping is completed. They are limited to monitoring temperature anomalies within two meters of the wellbore and must be completed within 36 hours of fracturing (Smith and Montgomery 2015). Radioactive and chemical tracer logs are used to determine the propagation path of the fracture fluid. The radioactive tracer tests are limited to the area near the wellbore (< 1 meter) due to limitations of the gamma ray tool. However the information can be useful to determine fracture width (Smith and Montgomery 2015).

There are relatively few post-fracture production analyses which focus on validating the geomechanical properties that were established at the beginning of MSHF operations. It is difficult to determine the final size and shape of the hydraulic fracture, as well as the final propagation path the fracture took. Microseismic analysis may offer some insight into the general overall size of the final stimulated volume,

but often cannot show the exact dimensions of the final hydraulic fracture. An in-depth understanding of the geomechanics and the effects of the changes of the *in situ* stress regime are needed in order to estimate how large a fracture became and why it took the path it did.

Chapter 3 Geomechanics of Unconventional Resources – Governing Equations

3.1 Geomechanics of Shale Gas Plays

The propagation behaviour of a hydraulic fracture is largely controlled by the *in situ* stresses. In general, the fracture will propagate perpendicular to the direction of minimum compressive stress. Local planes of weakness, such as natural joints or faults, will also have an influence on the direction of the hydraulic fracture, but at a smaller and more localized scale. It has been shown that the induced fracture is likely to locally follow the path of least resistance while still maintaining an average perpendicular relationship with the minimum horizontal stress). Horizontal wells to be stimulated by MSHF are aligned parallel to the direction of σ_h (which is usually the minimum principle compressive stress) to give fracture orientations transverse to the wellbore. It is assumed that the induced hydraulic fractures for the various stages will propagate parallel to each other barring small localized directional changes due to weak planes in the rock. Fracture stages are planned for maximum coverage of the volume around the wellbore with as little overlap as possible.

3.2 Stress and Strain in Geomechanics

Stress is a measurement of force per unit area. For the purposes of this thesis, stresses will be negative in compression and positive in tension. It should be noted that this is the opposite of the usual rock mechanics convention, but in line with standard continuum mechanics sign conventions. Stress can be written in the following tensor when considering a three-dimensional material model:

$$\boldsymbol{\sigma} = \begin{bmatrix} \sigma_{11} & \sigma_{12} & \sigma_{13} \\ \sigma_{21} & \sigma_{22} & \sigma_{23} \\ \sigma_{31} & \sigma_{32} & \sigma_{33} \end{bmatrix} \tag{3.1}$$

where σ_{11}, σ_{22}, and σ_{33} are the diagonal components of the stress tensor. At the material point, there will be three orthogonal planes on which there are no shear stresses. These planes are called principal planes

and the stresses normal to them are called principal stresses. The principal stresses are denoted as σ_1, σ_2, and σ_3 and are the eigenvalues of $\boldsymbol{\sigma}$. The eigenvectors of $\boldsymbol{\sigma}$ correspond to the directions of the principal stresses. The three principal stresses in the ground are usually parallel and normal to the ground surface i.e. the vertical stress (σ_v), the minimum horizontal stress ($\sigma_h = \sigma_1$), and the maximum horizontal stress ($\sigma_H = \sigma_3$). Usually in MSHF, which takes place at least 1 km beneath the surface, $\sigma_h = \sigma_1$. The overburden stress or vertical stress is often the overall maximum compressive stress, but not in regions which have experienced tectonic compression.

Strain is a measurement of deformation of a material. Under small deformations, the symmetric strain tensor is:

$$\boldsymbol{\epsilon} = \begin{bmatrix} \epsilon_{11} & \epsilon_{12} & \epsilon_{13} \\ \epsilon_{12} & \epsilon_{22} & \epsilon_{23} \\ \epsilon_{13} & \epsilon_{32} & \epsilon_{33} \end{bmatrix} \tag{3.2}$$

For the purposes of this study, the rock deformations will be assumed to be linear and so the components of the strain tensor are given by:

$$\epsilon_{ij} = \frac{1}{2}\left(u_{i,j} + u_{j,i}\right), \qquad \text{i, j, = 1..3} \tag{3.3}$$

where $\boldsymbol{u}$ is the displacement field, u_i is ith-component of the displacement field and $u_{i,j}$ is the partial derivative of u_i with respect to x_j.

The following conditions apply for linear elastic behaviour:

- The deformations are reversible.
- The deformations and strains are small.
- There is a linear relationship between stress and strain.

Assuming isotropic behaviour, the constitutive equation for linking stress and strain is:

$$\sigma_{ij} = \lambda\epsilon_{mm}\delta_{ij} + 2G\epsilon_{ij} \tag{3.4}$$

where λ and G (shear modulus) are Lamé constants, ϵ_{mm} is the volumetric strain, and δ_{ij} is the Kronecker delta:

$$\delta_{ij} = \begin{cases} 1, & i = j \\ 0, & i \neq j \end{cases} \tag{3.5}$$

In one-dimension, equation 3.6 is commonly called Hooke's Law:

$$\sigma = E\epsilon \tag{3.6}$$

where E is the elastic modulus of the material. In more general terms, Hooke's Law is defined by:

$$\sigma_{ij} = C_{ijkl}\epsilon_{kl}\,, \qquad \text{i, j, k, l = 1..4} \tag{3.7}$$

where $\boldsymbol{C}$ is the stiffness tensor. For an isotropic material, $C_{ijkl} = C_{jikl} = C_{jkil} = C_{jilk}$. The equation for C_{ijkl} then becomes:

$$C_{ijkl} = \lambda\delta_{ij}\delta_{kl} + 2G(\delta_{ij}\delta_{jl} + \delta_{il}\delta_{jk}) \tag{3.8}$$

Poisson's ratio (ν) can be defined for a uniaxial stress state; a strain in the axial direction (ϵ_{11}) leads to strain (ϵ_{zz}) perpendicular to the loading direction. Poisson's ratio is:

$$\nu = -\frac{\epsilon_{11}}{\epsilon_{22}} \tag{3.9}$$

The shear modulus, G, is a measure of resistance to shear stress and may also be written as:

$$G = \frac{1}{2}\frac{\sigma_{ij}}{\epsilon_{ij}}, \quad where\ i \neq j \tag{3.10}$$

The bulk modulus, K, is defined as the ratio of applied isotropic stress to the volume change. It is a measure of compressibility and can be written as:

$$K = \frac{1}{3}\frac{\sigma_{ii}}{\epsilon_{jj}} \tag{3.11}$$

The following equations summarize some commonly used relationships between $G,\ \lambda, E, \nu$ and K:

$$K(\lambda, G) = \lambda + \frac{2}{3}G \tag{3.12}$$

$$K(E,v) = \frac{E}{3(1-v)} \tag{3.13}$$

$$\lambda(E,v) = \frac{vE}{(1+v)(1-2v)} \tag{3.14}$$

$$G(E,v) = \frac{E}{2(1+v)} \tag{3.15}$$

The fluid within the pore spaces of a rock is an important aspect of geomechanics. The fluid will carry part of the total stresses applied to the system (Fjaer et al. 2008). The presence of fluid adds additional complications to the system as it will act as a poroelastic system, with the fluid reacting differently to applied stresses than the solid would due to different compressibility values.

However, it has been shown that the deformation of the rock is primarily dependant on the stresses transmitted through the solid phase of the rock (Terzaghi 1943). Terzaghi stated that the shear strength of the rock depends only on the difference between the normal stress and the pore pressure. He introduced the concept of effective stress which was more expanded on by Biot to include a stress-change partitioning co-efficient -α (Biot 1941):

$$\sigma'_{ij} = \sigma_{ij} - \delta_{ij}\alpha p_f \tag{3.16}$$

Where $\boldsymbol{\sigma}$ is the total stress, α is the Biot co-efficient, and p_f is the fluid pressure. Poroelastic effects related to fluid pressure and effective stress will not be considered in this thesis.

Unconventional reservoirs often exhibit anisotropic and non-elastic behaviour. This can be due to high clay content within the formation (increase in clay results in an increase in plastic behaviour), bedding planes and overall structure of the formation (E and ν will be different in different directions if the formation is bedded), and variations in material properties at varying scales across the formation. In this thesis, the rock mass will be assumed to be a linear, elastic, and isotropic material. The majority of the modelling will be done considering total stress changes only.

3.3 Hydraulic Fracture Mechanics

Hydraulic fracturing, in its simplest form, can be described as the process in which fluid is pumped into a well faster than it can leak off into the formation, which causes the pressure to rise to the point where an extensional plane opens within the rock mass (Smith and Montgomery 2015). For further extension of the fracture, the fluid must then be continually pumped in at a rate and pressure which will cause the fracture to propagate. In order for a fracture to propagate, the pressure within the fracture must overcome the compressional forces and the fracture toughness of the rock mass. Several different factors govern the initiation and propagation of a hydraulic fracture; however, *in situ* stresses and reservoir pressures play primary roles (Smith and Montgomery 2015).

3.3.1 Linear Elastic Fractures

The study of linear elastic fracture mechanics attempts to characterize a material's resistance to fracture by defining a property called fracture toughness (Fischer-Cripps 2007). The quantification of fracture toughness began in 1913 with Inglis (Inglis 1913) who showed that stress magnification at the edge of an elliptical hole in a stressed medium depended on the radius of curvature of the hole. The smaller the radius of curvature, the larger the stress concentration became. The stress concentration factor, k, can be defined as:

$$k = 1 + 2\sqrt{\frac{c_r}{\varphi}} \tag{3.17}$$

where c_r is the half length of the major axis and φ is the radius of curvature at the tip of the hole. This work was expanded on by Griffith in 1921 (Griffith 1921) when the concept of minimum potential energy was applied to fracture mechanics using the energy balance criterion. He proposed two conditions for fracture growth (Fischer-Cripps 2007):

1. The stress at the crack tip is a function of the stress concentration factor, k, which depends on the ratio of the fracture radius of curvature to its length. The stress at the crack tip must be enough to cause the bonds at the crack tip to fail.

2. In order for a fracture to extend, the amount of strain energy released per unit of fracture extension must be greater than or equal to the rate of surface energy required for the two new fracture faces to form.

The first condition relies on a stress concentration factor which means the value of stress at the tip of the fracture can be calculated as a finite value.

If the fracture tip is assumed to be sharp (r approaches 0), the normal stress at the crack tip tends to infinity in a perfectly elastic body. The asymptotic normal stress at a crack tip is:

$$\sigma_{yy} = \frac{K_{IC}}{\sqrt{2\pi r}} \cos\frac{\theta}{2} \left(1 - \sin\frac{\theta}{2} \sin\frac{3\theta}{2}\right) \tag{3.18}$$

where K_{IC} is the mode I critical stress intensity factor for a mode I tensile fracture, and r and θ are expressions of polar co-ordinates. It is noted that σ_{yy} is singular at the crack tip, where r is equal to zero. K_{IC} is a material property and defines the onset of fracture extension and is related to fracture toughness (Fischer-Cripps 2007). K_I characterizes how quickly the crack tip stress approaches infinity under pure extensional loading. Let K_I be the stress intensity factor which will not cause fracture extension. For a fracture of length 2c loaded by a remote stress, σ^a, acting perpendicular to the crack, with Y acting as a geometric factor, the equation for K_I is:

$$K_I = \sigma^a Y \sqrt{\pi c} \tag{3.19}$$

Equation 3.18 suggests that the stress at the crack tip is infinite; however, Griffith's second condition of energy balance must be satisfied in order for a fracture to propagate when a stress increment is applied (Fischer-Cripps 2007).

The second condition can be mathematically written as:

$$\frac{dU_s}{dc} \geq \frac{dU_\gamma}{dc} \tag{3.20}$$

where U_s is the strain energy, U_γ is the surface energy, and c is the fracture half length. Further work by Griffith (Griffith 1921) showed that the strain energy released by a double-ended narrow elliptical crack of length $2c$ in an infinite plate is:

$$U_s = \frac{\pi\sigma_a^2 c^2}{E\prime} \tag{3.21}$$

where σ_a is the total applied stress and c is the fracture half length, and E' is plane strain Young's modulus (i.e, E' = E/(1-v^2)).

The total surface energy for two surfaces of length $2c$ can be written as:

$$U_\gamma = 4\gamma c \tag{3.22}$$

where γ is the fracture surface energy of the solid. The fracture surface energy may include energy dissipative mechanisms such as phase transformations, microcracking, and plastic deformation (Fischer-Cripps 2007).

By combining equations 3.21 and 3.22, the critical condition for crack growth becomes:

$$\frac{\pi\sigma^2 c}{E'} \geq 2\gamma \tag{3.23}$$

Equation 3.23 shows that a fracture will not extend unless the strain energy released becomes equal to or greater than the surface energy for the newly formed crack segments (Fischer-Cripps 2007). Figure 3-1 illustrates the strain energy released and the surface energy as a function of fracture length. It shows a configuration where fracture propagation changes from stable (quasi-static) to unstable (dynamic) at a crack length of c_c.

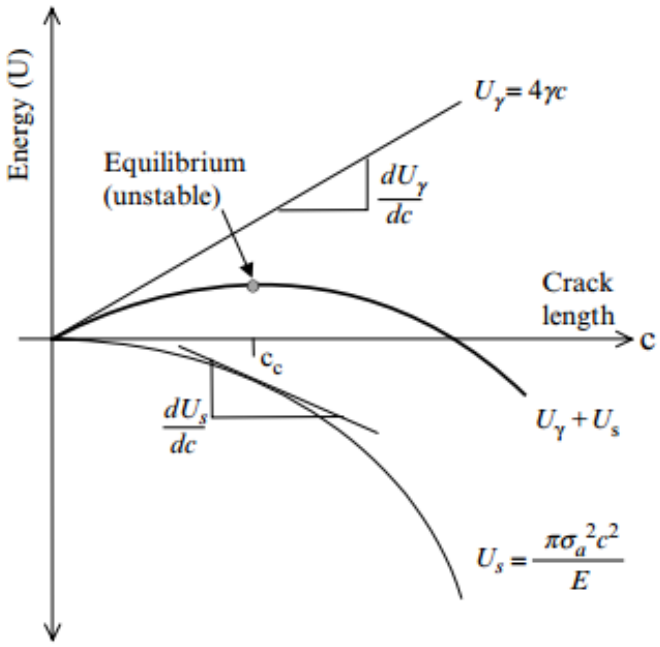

Figure 3-1 Energy vs. crack length for a fracture increasing in length (Fisher-Cripps 2007 – pg 35)

In Figure 3-1, U_s decreases exponentially as the crack length increases, and U_γ increases linearly as the crack length grows. At the point c_c, the reduction in strain energy due to the formation of a crack becomes equal to the surface energy required to created new crack surfaces. The fracture will propagate at this point. Beyond c_c, the released strain energy that is available is greater than the energy required to create fracture surfaces. This leads to unstable crack growth and constant spontaneous extension of the fracture.

The energy balance criterion is an indication of whether or not fracture growth is possible; however, the stress state at the tip of the fracture will determine if the fracture will actually propagate or not. A fracture will not extend if the stress is insufficient to break the bonds at the crack tip. The fracture toughness and stress intensity factor are incorporated into fracture propagation conditions.

3.3.2 Fracture Toughness in Hydraulic Fracturing of Unconventional Reservoirs

Fracture toughness is the ability of a material to resist fracture propagation. Most consolidated rock formations will act as elastic, brittle, materials under tensile loadings at the tip of a crack (Smith and Montgomery 2015). Fracture toughness for a rock mass can be defined by one of two material properties:

- Critical stress intensity factor (K_{IC})
- Strain energy release rate (G_F)

G_F is the strain energy release rate per area of fracture. It is equivalent to

$$G_F = \frac{\pi\sigma^2 c}{E'} \tag{3.24}$$

K_{IC} and G_F can be related to each other through the following equation under plane strain conditions:

$$G_F = \frac{1-\nu^2}{E} {K_{IC}}^2 \tag{3.25}$$

The value of K_{IC} has a large range of values that do not seem to depend on rock type (Smith and Montgomery 2015). There is a general trend that shows that K_{IC} will increase gradually with an increase in net confining pressure. It is generally agreed that fracture toughness will have a significant influence on hydraulic fracture propagation in cases where a low viscosity fluid is used, radial unconfined fractures are formed, and the formation has a lower elastic modulus (Smith and Montgomery 2015).

3.3.3 Pressure Definitions for MSHF

There are several different pressures that can be defined when discussing the propagation of a hydraulic fracture. These include net pressure (p_n), the bottom hole test pressure (BHTP) within the fracture (p_f), pressure in the fracture tip (p_{tip}), viscous pressure (p_v), closure pressure (p_c), breakdown pressure (p_b), instantaneous shut in pressure (ISIP), and the pressure measured at the surface ($p_{surface}$). An overall look at the pressures is presented in Figure 3-2.

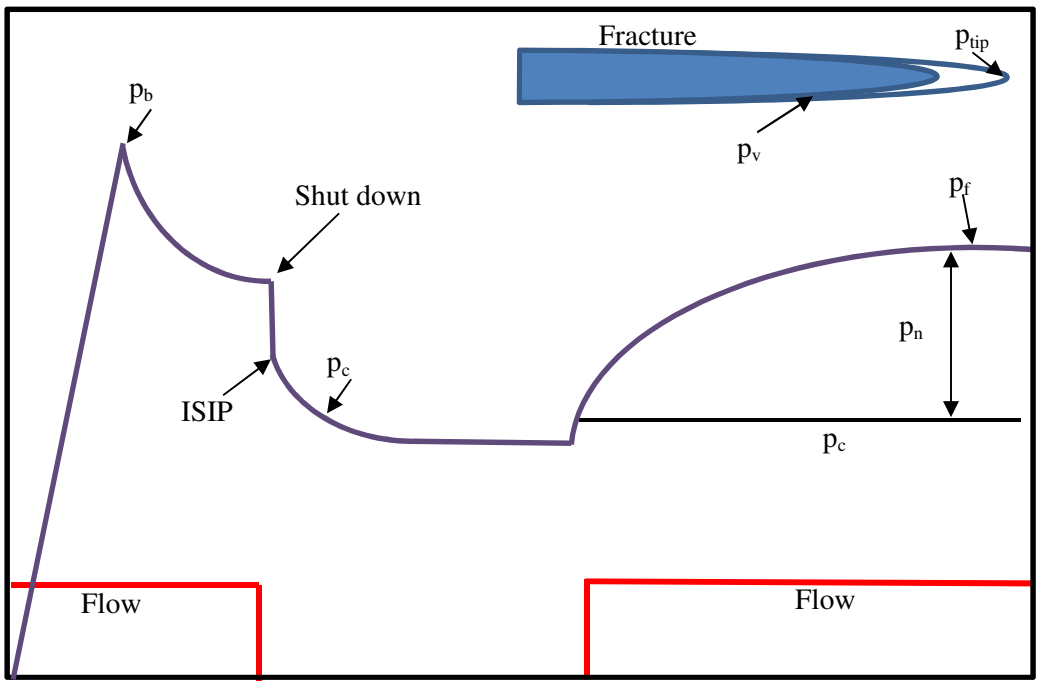

Figure 3-2 Pressure diagram for a stage of MSHF

Net pressure (p_n) counteracts the stress in the rock perpendicular to the fracture. In its simplest form, it is defined by (2.1). It is the pressure needed to open a fracture (Smith and Montgomery 2015). Net pressure will vary along the length of the fracture and will also vary with pumping time. The net pressure within a propagating fracture can be broken down into several components. If the fracture is propagating, there must be a critical net pressure within the tip region, p_{tip}. There must also be a viscous pressure (p_v) to account for fluid friction pressure losses along the fracture between the wellbore and the tip as the fracture extends. There will also be a near-wellbore pressure drop, generally taken to be the result of frictional pressure losses as the fluid passes through the perforations and other near-wellbore constrictions. The two components needed to push viscous fluid to the fracture tip and therefore cause propagation are p_v and p_{tip}. Assuming a viscous fluid in laminar flow conditions, these pressures can be expressed as:

$$p_v = \frac{E'}{H}\left[\frac{8(Q/2)\mu L}{\pi E'}\right]^{1/4} \tag{3.26}$$

$$p_{tip} = K_{IC}\sqrt{\frac{\pi}{4R}} \tag{3.27}$$

Derivations of the previous equations can be found in Smith & Montgomery, 2015. H is the assumed fracture height, L is the length, and μ is the viscosity of the fluid. The pressure driving the fracture will depend on different factors. For example, if the fracture is wide all along its length, p_{tip} is also very large and the viscous pressure loss becomes negligible (Smith and Montgomery 2015). Alternatively if the fluid viscosity is high then the pressure drop along the length of the fracture will become so high that the pressure at the tip will be inadequate to cause propagation. The relationship between the viscous and tip pressures and the net pressure becomes:

$$p_n = \left[p_{tip}^e + p_v^e\right]^{1/e} - \sigma_h \tag{3.28}$$

where e is equal to 3 for a Newtonian fluid.

Tip behaviour of a pressurized crack is often seen to differ from the assumed linear elastic fracture mechanics. This is often attributed to a dry region within a fracture (Smith and Montgomery 2015); due to viscous and capillary effects, fluid is unable to reach the very narrow widths just behind the fracture tip. The fluid lag can be shown to be equivalent to an additional fracture toughness:

$$K_{IC}^{Eff} = K_{IC} + K_{IC}^{Lag} \tag{3.29}$$

where K_{IC}^{Lag} can be found for a radial fracture geometry (Smith and Montgomery 2015):

$$K_{IC}^{Lag} = 2p_{net-tip}\sqrt{\frac{R}{\pi}}\,\frac{p_{net-frac}}{p_{net-frac}+p_{net-tip}} \tag{3.30}$$

where $p_{net-tip}$ is the pressure difference needed to close the unwetted fracture tip, R is the radius of the fracture, and $p_{net-frac}$ is the net pressure at the entrance to the tip region .

Closure pressure, p_c, is the pressure at which an open fracture will revert back to its original closed state. As discussed in previous sections, this is considered to be the minimum compressive principal stress. It

will be equal to or less than p_b, the pressure required to initiate a fracture and less than p_n, the pressure required to propagate the fracture (Jones and Britt 2009).

Breakdown pressure, p_b, is the fluid pressure at which the rock initially cracks during MSHF treatments. It is primarily influenced by the near-wellbore stress state (Smith and Montgomery 2015). The rock fails in tension when the following condition is fulfilled (assuming the minimum compressive horizontal stress is also the minimum principal stress) (Smith and Montgomery 2015):

$$\sigma_h = -T_0 + p_b \tag{3.31}$$

where T_0 is the tensile strength of the rock. Breakdown pressure can be derived for linear elastic rock by using the radial and tangential stress equations for stress around a borehole. It should be noted that in this thesis that the breakdown pressure is considered to be influenced by more than just the immediate area outside of the wellbore. A small initial break may occur when the area right outside the borehole is fractured, but in order for the fracture to propagate it must overcome more than just the near wellbore conditions. The high injection rates and volumes used in fracturing are generally very high and so the instantaneous break in the rock which is recorded on pressure monitors will likely be through more than just the first few centimeters of available rock face.

Instantaneous shut in pressure (ISIP) is equal to the injection pressure in the fracture right outside the wellbore just after pumping has ceased (no inertial effects and friction losses, but with the injection valve closed (no leak-off to surface allowed). The ISIP is not considered to be a measure of fracture closure pressure, though it can be used as an upper bound for p_c. It is more of a measure of minimum fracture propagation pressure at the tip (Smith and Montgomery 2015). It is analogous to the BHTP right when the pumps have turned off and therefore can give an idea of p_n right at shut-in.

The surface pressure ($p_{surface}$) is a quantity that is generally calculated during design and monitored during MSHF. It is given by (Smith and Montgomery 2015):

$$p_s = p_c + p_n + \Delta p_{perf+pipe} - p_{Head} \tag{3.32}$$

where $\Delta p_{perf+pipe}$ is approximately proportional to the square of the flow rate, and p_{head} is the head loss.

3.3.4 Fluid Flow within a Hydraulic Fracture

Fracture mechanics must consider a material balance to account for the total amount of fluid that is injected into a fracture (Jones and Britt 2009). This relationship can be described as:

$$V_p = V_F + V_L \tag{3.263}$$

Where V_p is the total volume pumped into the formation, V_F is the volume of fluid within the fracture, and V_L is the volume of fluid lost into the formation. The principle of material balance must be taken into account when creating fracture models that are focused on fluid flow within the fracture.

The governing equations and assumptions regarding fluid flow within a hydraulic fracture are often only done in one dimension to limit the complexity of the problem (Smith and Montgomery 2015). More detail on fluid flow within a fracture can be found in Smith and Montgomery (2015).

3.4 Stress Shadow

The stress shadow effect in MSHF occurs when a previous hydraulic fracture stage (or previous stages) significantly alters the stress condition in the surrounding rock around the propagating fracture so that it may adopt a different orientation and propagation direction than a "virgin" fracture. Depending on the spacing of the stages, there is a potential for the permanent volumetric strain associated with fracturing to generate the stress shadow that alters stresses in the rock in which subsequent fracture stages will occur.

Stress shadowing during hydraulic fracture operations has been modeled several times and it is generally agreed that the following are events seen due to stress shadows in fracture operations:

- An increase in the minimum horizontal stress magnitude (Cheng 2009), (Olson 2008), (Nagel and Sanchez-Nagel 2011), (Roussel and Sharma 2011).
- Maximum horizontal stress will increase, but at a slower rate and overall magnitude than the minimum horizontal stress (Cheng 2009).

- Subsequent fractures may not propagate in the same orientation or direction as previous fractures due to the change in σ_1 (Olson 2008), (Roussel and Sharma 2011), (Roussel et al. 2012).
- Fractures may propagate in a direction that will cause them to terminate in previously fractured intervals (Olson 2008), (Roussel and Sharma 2011).
- Full 90° rotation of fracture propagation direction is possible if the minimum horizontal stress is increased past the point of the maximum horizontal stress (Roussel et al. 2012).
- Widths of fractures propagating from the middle of a perforation cluster may be smaller than those at the edges of the perforation cluster (Olson 2008).
- Stress shadow extents increase with fracture heights (Nagel et al. 2012).

3.5 Stress Shadow Models and Field Results

Few studies compare the results of the mathematical models to field results. In two studies (Nagel et al. 2013), (Rios et al. 2013), it was shown that a continuum model was able to closely match the field data from a multistage hydraulic fracture operation. Instantaneous shut in pressure (ISIP) was used as a stand in for the minimum horizontal stress. Good matches were achieved between the modeled data and the observed data for stages near the toe of the well. However, closer to the heel, the predicted ISIP values were much higher than those recorded. This was attributed to either a change in stress regime or a full rotation of the hydraulic fractures. The field study concluded that when the spacing between stages is greater than the fracture height, the stress shadow effect is negligible. However, if the fracture height is similar or much larger than stage spacing, the increase in the minimum horizontal stress will have an effect on adjacent stages.

Another study (Yu et al. 2013) verified a commercial model of hydraulic fracturing against data from hydraulic fracturing operations in the Barnett shale. The study pointed out that many models used to evaluate MSHF operations assume parallel transverse fractures and do not account for mechanical interference from stress changes. The paper focused more on gas production rates than directly

comparing stress values. They note that gas production is initially high when many closely spaced fractures are used, but then will steeply drop off. It is concluded that fracture interference is the main cause of the decrease in production and that inner fractures in a cluster will contribute less than outer fractures, which matches with conclusion from other studies.

Recently there has been a movement towards models that do not rely on complex mathematical formulas. The reasoning behind this is twofold: first, more complex models rely heavily on the expertise of the person using them (Bunger et al. 2013) as they are not simple enough to use without training and knowledge of advanced mathematics; second, complex models are not seen as a worthwhile investment unless the reservoir properties are well characterized (Bunger et al. 2013). Without accurate characterization of properties, the models may be correct in terms of physical processes, but incorrect in terms of geomechanical properties. They therefore rely on a wide range of parametric analysis and require many more parameters than are confidently available from the data. Without reliable properties, the model is often not seen as a worthwhile endeavor, and rarely are attempts made to calibrate the models because of an inadequate or incomplete database.

Simpler models which rely on the well-known radial and PKN geometries have recently been reexamined as a way to produce rough but useful predictions (Bunger et al. 2013). Several assumptions are made to simplify the process. In the study (Bunger et al. 2013), it was found that by neglecting source geometry, restricting height growth, fluid leak-off, and proppant transport effects, a model of perforation cluster initiation could be matched to field results in the Barnett shale. However, clusters had to be more than 1.5 to 2.5 fracture heights apart in order to negate mechanical interactions of fractures (Bunger et al. 2013).

Comparison of models to field data is both an uncertain and complicated process due to many unknowns and assumptions. It may not be possible to accurately recreate field results in a mathematical model, but it is possible to create a model which produces useful predictions and information for future operations in similar circumstances.

3.6 Optimization of Massive Multistage Hydraulic Fracturing Using Geomechanics

The optimization of fracture stage spacing is an important aspect of MSHF. The stages should cover as much of the formation as possible while avoiding fracture overlap between intervals. Much of the optimization is done by using both PKN and KGD models to predict fracture height and width and to plan the stages accordingly. Geomechanical effects such as stress changes and permanent volumetric strain from shearing and dilation are not considered in these production forecasting models.

It has been shown that most induced hydraulic fractures do not have a geometric configuration which matches the biwing planar fracture geometries inherent in the PKN and KGD models (Nagel et al. 2012). Instead, microseismic data and laboratory experiments suggest that fractures are multi-branching and complex rather than singular and planar. Fractures will also tend to grow in an upwards direction, as the fracture fluid gradient is generally less than the gradient of the minimum compressive stress. This fact, paired with the stress changes caused by the induced fractures that can affect subsequent stages, can impair the utility of the PKN and KGD predictive models.

Many MSHF operations try to put as many stages into a well as possible to try to access the maximum amount of resource. However, evidence has shown that adding stages does not always translate to an increase in production (Dohmen et al. 2014). Studies have shown that more stages may actually lead to less production in the long term. One of these studies completed in the Bakken Formation is illustrated below in Figure 3-3.

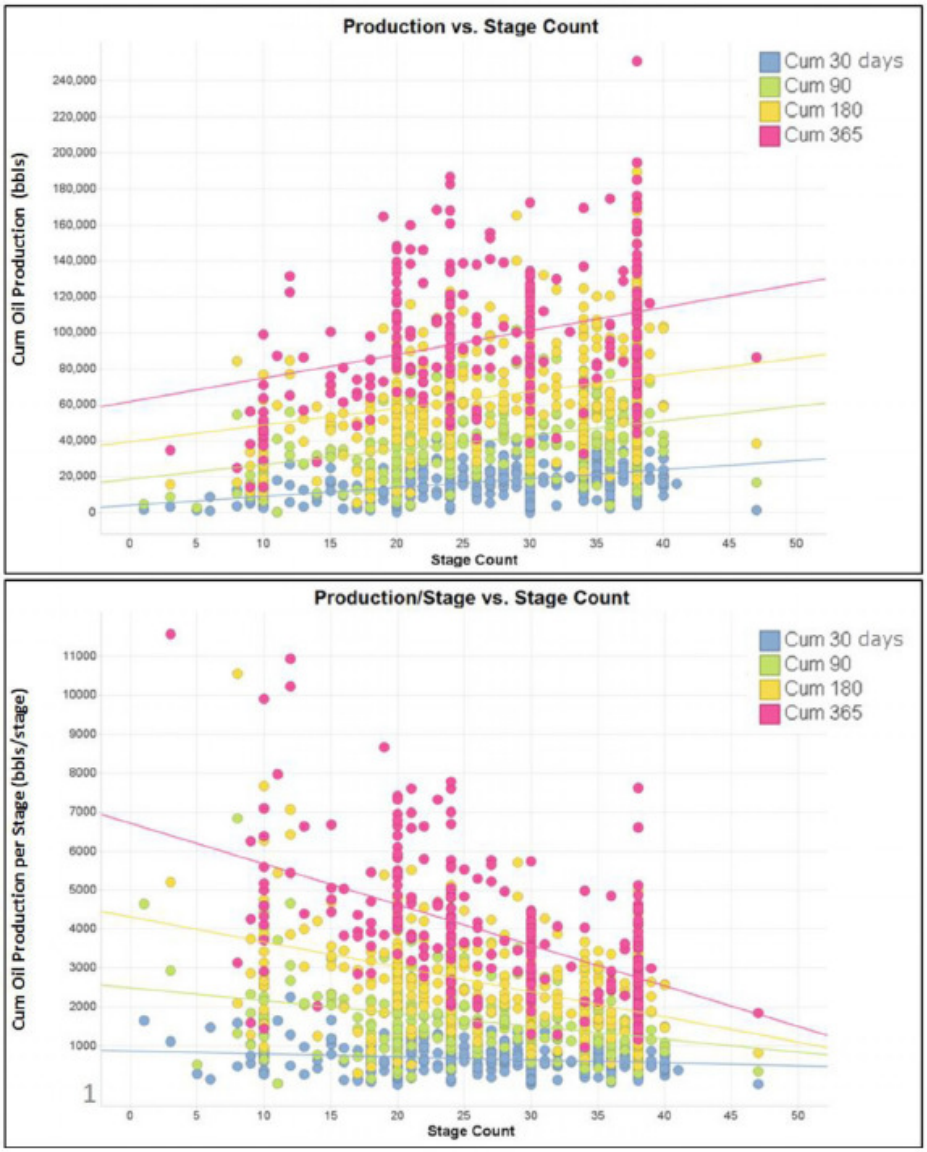

Figure 3-3 Production per well in the Bakken Formation (Dohmen et al. 2014)

There are many possible explanations for a drop in production with more stages, but from a geomechanical point of view, the reasons could be directly related to stress shadowing. As discussed previously, stress shadowing has been shown to limit both the height and the width of hydraulic fractures, as well as causing orientation changes that would reduce the total volume of the reservoir contacted by a fracture network. Reduced height and width of induced fractures leads to an overall reduction in fracture volume and therefore a decrease in overall fracture conductivity in the stimulated zone. In general, larger

fractures (larger area and aperture) increase the effective porosity of the rock on a greater scale than fractures limited in growth by stress shadow effects. Propagation and orientation of induced hydraulic fractures may also be affected by stress shadowing. Microseismic monitoring has shown both fracture rotation and propagation of fractures into other zones due to stress interference (Nagel et al. 2013), Dohmen et al. 2014). Depending on the zone the fractures are forced into, this could have negative effects on production, or at least not contribute to production. Neglecting the geomechanical effects of hydraulic fracturing when trying to optimize spacing of fracture stages may lead to inaccurate predictions and sub-optimal MSHF designs.

Current models which use advanced mathematical numerical models to model and predict stress shadowing are time intensive and computationally expensive to implement. They require specialized knowledge in order to be accurately and effectively implemented, which may at times prohibit or inhibit their use for real world applications. At the same time, the PKN and KGD models which are still widely used for predictive modelling of fracture geometry were never meant to incorporate the geomechanical effects of permanent volumetric strains and stress alterations. A simple model which can incorporate stress changes could be useful to the optimization of stage spacing.

Chapter 4 Modelling of Multistage Hydraulic Fracturing with Consideration of Geomechanics

The model presented in this thesis is a simple linear elastic model which assumes a homogeneous isotropic medium and is intended to act as an analytical geomechanical model of hydraulic fracture induced stress changes. The model will be used in conjunction with field data collected from wells within the Montney Formation, which demonstrate possible stress interference within the production data. The final model will show stress changes which occur during fracturing and demonstrate how the change in stress may affect the adjacent and subsequent stages. This simple and easy to use model may be used to assist with design and planning of MSHF operations within formations similar to the original case study that was used for calibration.

The field data, including the total volume of injected fluids, geomechanical properties, porosity, and initial *in situ* stresses, are used to determine the resulting volume of a stimulated area (fracture) in the subsurface. The total final volume is then used to estimate an approximate shape and size of the fracture while considering energy minimization and fracture toughness. The changes in stress in the surrounding rock mass are calculated using the solution given by Eshelby (1957), which is a mathematical solution used to determine the elastic stress field around an ellipsoidal inclusion. The stress changes calculated by the program are compared to breakdown pressures in the next interval to see if the overall change in stress can be approximated using this solution. The program is outlined visually in the figure below where the stress shadow at the next injection point (which is caused by the stimulated volume of the modelled fracture) is represented by the equation $\sigma_{1\,initial} + \Delta\sigma_1$.

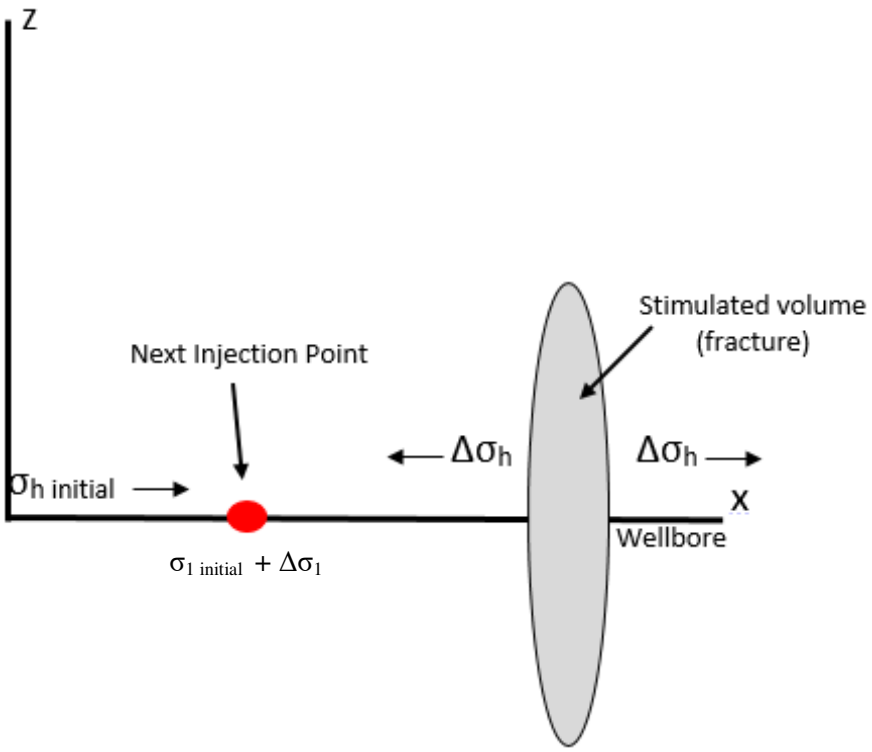

Figure 4-1 Representation of stress change model

4.1 The Eshelby Solution

The Eshelby solution was first proposed in 1957 by J.D. Eshelby for the elastic stress and displacement field in and around an ellipsoidal inclusion within a material matrix. The inclusion is located within an infinite, homogeneous, and isotropic elastic domain (Eshelby 1957). The inclusion undergoes a change in shape and size which translates to a change in the stress and strain within the medium surrounding the inclusion and within the inhomogeneity itself. It was found that the elastic stress and strain within the inclusion are constant throughout the ellipsoid (Eshelby 1957). Eshelby presented solutions for the elastic field far from the inclusion, the stress and strain components at a point immediately outside the inclusion, the total strain energy in the medium and in the inclusion, the interaction energy of the inhomogeneity with an elastic field, and the change in the gross elastic constants of a material (Eshelby 1957).

The Eshelby solution first computes the stresses within an ellipsoidal inclusion by mathematically removing the inhomogeneity from the matrix and applying a change in shape, which causes the inclusion to undergo a transformation strain. Eigenstrains, ϵ^*, are defined as the strain state that the inclusion will enter if the constraint of the material around it is removed (Mura 1987), (Meng et al. 2011). This is also known as the stress-free strain state. Tractions are then applied to the boundary of the inhomogeneity such that the elastic strain is equal and opposite to the transformation strain. The inclusion is then placed mathematically back into the infinite medium and the boundary tractions are removed. The resulting strain within the inclusion was found to be uniform (Eshelby 1957).

4.1.1 Equations for Inclusions and Eigenstrains

Mura, (1987) defined the inclusion as a subdomain, Ω, in the domain of the medium, D. His formulation assumes that the elastic moduli of the inclusion and the medium differ from each other, i.e. C^*_{ijkl} in $\Omega \neq C_{ijkl}$ in D-Ω. It also assumes that there is a remote homogeneous stress, σ_{ij}^{∞}, that is constant, acting at infinity (i.e. a far-field constant boundary stress condition).

It is important to note the inclusion of the fictitious eigenstrain in this program provided by Meng, 2011. The Eshelby solution was originally formulated for an inclusion with the same properties as the surrounding matrix. Eshelby proved that a solution could be found for an inclusion with a different Poisson's ratio and Young's modulus by choosing the eigenstrain properly. This is known as the inhomogeneity problem instead of the inclusion problem, in which all properties are constant from the inclusion to the matrix. The fictitious eigenstrain represents an arbitrary eigenstrain that the inhomogeneity was initially subjected to and will need to be considered if the inclusion has different properties from the matrix.

Mura (1987) presented equations to solve for the fictitious eigenstrain, ϵ_{ij}^*, as well as stress and strain fields for the inclusion and the medium. Equations 4.1 through 4.5 present the equations developed by Mura (1987) for fictitious eigenstrain, strain within the inhomogeneity, stress within the inhomogeneity,

strain within the medium at a specified distance from the inclusion, and stress within the medium at some distance, x, from the inclusion respectively.

$$\left(\Delta C_{ijkl} S_{klmn} - C_{ijkl}\right)\epsilon^{*}_{mn} = -\Delta C_{ijkl}\epsilon^{\infty}_{kl} - C^{*}_{ijkl}\epsilon^{p}_{kl} \tag{4.1}$$

$$\epsilon_{ij} = \epsilon^{\infty}_{ij} + S_{ijmn}\epsilon^{*}_{mn} \quad in\ \Omega \tag{4.2}$$

$$\sigma_{ij} = \sigma^{\infty}_{ij} + C_{ijkl}(S_{klmn}\epsilon^{*}_{mn} - \epsilon^{*}_{mn}) \quad in\ \Omega \tag{4.3}$$

$$\epsilon_{ij}(x) = \epsilon^{\infty}_{ij} + D_{klmn}(x)\epsilon^{*}_{mn} \quad for\ x \in D - \Omega \tag{4.4}$$

$$\sigma_{ij}(x) = \sigma^{\infty}_{ij} + C_{ijkl}D_{klmn}(x)\epsilon^{*}_{mn} \quad for\ x \in D - \Omega \tag{4.5}$$

In these equations, $\Delta C_{ijkl} = C_{ijkl} - C^{*}_{ijkl}$, ϵ_{ij}^{∞} is the remote strain, ϵ^{p}_{kl} is the eigenstrain that the inhomogeneity was initially subjected to, σ_{ij}^{∞} is the remote stress, S_{ijkl} is the Eshelby tensor ($S_{ijkl} = S_{jikl} = S_{ijlk}$), and D_{ijkl} is the exterior elastic field tensor. Both S_{ijkl} and D_{ijkl} are defined in detail in Meng (2011). Displacement is calculated through equation 4.6 from Mura (1987).

$$u_i(x) = \frac{1}{8\pi(1-v)}(\psi_{,jli}\,\epsilon^{*}_{ij} - 2v\epsilon^{*}_{mm}\Phi_{,i} - 4(1-v)\epsilon^{*}_{il}\Phi_{,l}) \tag{4.6}$$

Where Φ and ψ are complex functions specified by Ferrers (1877) and Dyson (1981), referred to in Meng (2011).

4.1.2 MATLAB Code for Eshelby Solution

MATLAB codes for the Eshelby solution have been developed by several different sources. The solution chosen by Meng (Meng et al. 2011) is a quasi-analytical expression based on the Eshelby solution for the interior and exterior elastic fields. It is considered to be quasi-analytical as it employs a numerical routine developed by Igor (Igor 2005) to approximate an elliptical integral with a tolerance on the order of 10^{-16}.

The process of calculations proceeds in the following manner. Young's modulus and Poisson's ratio of both the matrix and the inhomogeneity (inclusion) are specified by the user of the program. The

ellipsoidal dimensions, the remote stress, and the initial strain are also provided by the user. The stiffness tensors are then created and used to calculate the remote strain for the remote stress given. The Eshelby tensor for a given Poisson's ratio and ellipsoidal shape is built which then is used to calculate the fictitious eigenstrain. The 4^{th}-order Eshelby tensor that will be used to calculate the exterior strain and stress around the inclusion is then constructed along with the displacements in the matrix. The outputs are then plotted.

The program described above is simply used to implement the Eshelby solutions. Section 4.2 will present the use of the Eshelby solution in the context of hydraulic fracturing and stress shadow measurements.

4.2 Problem Description

Consider a horizontal well divided into several separate and laterally isolated stages. A single stage is stimulated when a volume of fracturing fluid and proppant is pumped down into the section. The injected material causes the rock formation to fracture and the fluid to propagate into the formation to form a hydraulic fracture.

The induced fracture increases the effective porosity of the formation (permanent volumetric strain). The final volume of the fracture is not necessarily equal to the injected volume due to the effective porosity of the rock, which may leak off some of the liquid. The stimulated volume will be larger than the injected volume because of the porous nature of the reservoir, combined with the fact that numerous natural fracture planes are stimulated, involving propping and shearing of pre-existing discontinuities in the case of stiff jointed rock masses (shale gas and shale oil reservoirs). Diagrams of the fracture are presented below:

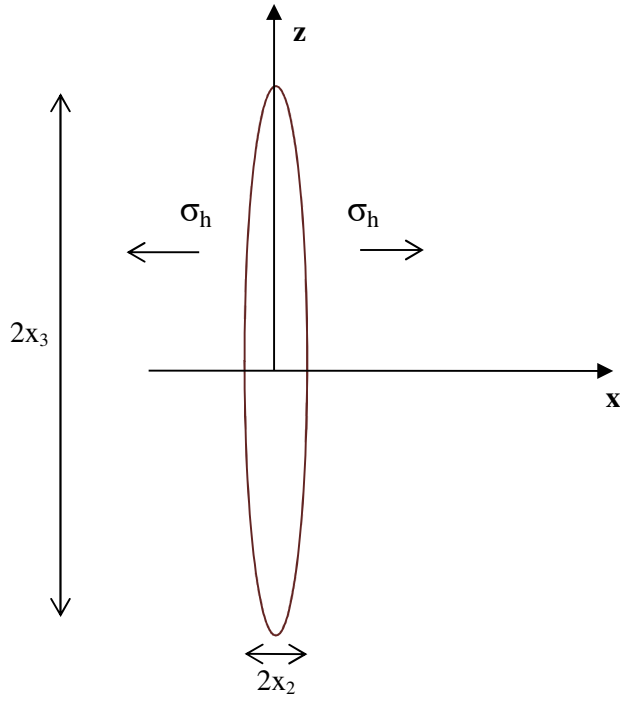

Figure 4-2 Initial Fracture Geometry – Side View

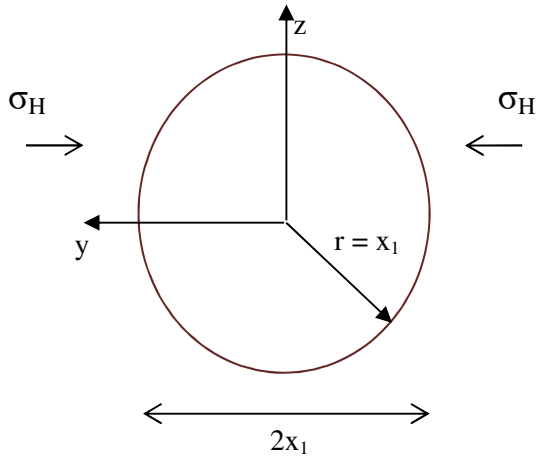

Figure 4-3 Initial Fracture Geometry - Top View

The x-direction corresponds to the direction of the horizontal well as well as the minimum compressive horizontal stress. The z-direction is vertical and perpendicular to the well direction and aligned with the vertical stress direction. The y-direction is horizontal and perpendicular to the x axis and is in the direction of the maximum horizontal stress. The semi-axis of the ellipsoids, x_1, x_2, and x_3, aligned with

the y, x, and z planes respectively, will be set considering the calculated stimulated volume and a ratio of x_3/x_2.

The stimulated volume is assumed to take the form of an ellipsoidal shape with the major axes in the plane perpendicular to the minimum horizontal stress. Therefore, we can assume $x_1 = x_3 \neq x_2$.

The rock will fail when the net pressure becomes high enough to overcome the minimum compressive principal stress, σ_1, and the toughness of the rock, represented in this case by K_{IC} and G_F. Both the breakdown pressure and the ISIP value of the stage will be considered when it comes to interpreting stress shadow effects. However, the recorded breakdown pressure from the production monitoring will be the primary value used in the comparison of calculated stress changes to the field data. Further justification of the use of breakdown pressure as an indication of stress shadowing is given in Chapter 3 and Chapter 5.

For the purposes of this model, the propagation of the fracture itself is not considered. Only the final geometry and stress change will be calculated for each stage. This is done to minimize computational complexity. Only the final volumetric deformation of the rock is needed to determine the effect of the stress change on the next stage.

The change in volume caused by the injection causes a change in the local *in situ* stresses in and around the fractured region in the reservoir. The stress change is calculated using the Eshelby solution discussed in Section 4.1. The model will begin with two unknowns: the final ratios of the semi-axes and the effective porosity of the rock, which in turn affect the overall size of the final stimulated volume. The stimulated volume is the final volume of the ellipsoid after the total volume has been injected. A range of ratios and effective porosities will cause stress changes which correspond to changes in the minimum horizontal stress (extensional stress or the closure stress) seen in the field data. Note that it is not possible to estimate the changes in the entire stress tensor; the only changed value that can be reliably assessed is the fracture closure pressure, and this value is not likely to be constant along the extent of the induced fracture surface, given the changes induced from the previous fracture stages.

In order to choose values for the semi-axes ratios and effective porosity, energy minimization will be considered. The fracture will take the form that minimizes the overall work needed to create the fracture surfaces. The program will search for the inclusion that minimizes the overall change in energy of the system. If a stress intensity factor and a strain energy release value are not considered in a fracture which is propagating, then the fracture will grow until it approaches a zero thickness value. Therefore energy minimization must be considered when determining the geometry of the fracture.

The total strain energy caused by the volume change is derived in the following sections. Once the geometry of the fracture which minimizes the change in energy is found, it is used to calculate the final stress change caused by the hydraulic fracture.

4.2.1 Strain Energy Minimization

Let V_I represent the total volume injected into the fracture stage. Let V_S be the volume of the stimulated area within the fracture stage. Due to effective porosity, $V_I < V_S$. V_S is assumed to undergo a uniform dilation. The volume change of V_s can be written as:

$$\Delta V_S = V_I \tag{4.7}$$

which then makes the volumetric strain:

$$\epsilon^T = \frac{\Delta V_s}{V_s} = \frac{V_I}{V_s} = \varepsilon_{kk} = \varepsilon_{11} + \varepsilon_{22} + \varepsilon_{33} \tag{4.8}$$

where ϵ^T is the total volumetric strain. Eshelby (1957), derived the total strain energy due to the introduction of an inhomogeniety of volume V_S into an infinite initially stress-free domain as:

$$E_{el} = 2G(\epsilon^T)^2 V_s \frac{(1+\nu)}{9(1-\nu)} \tag{4.9}$$

An additional energy term must be added to E_{el}, the total strain energy in the matrix and inclusion, due to the interaction of the inclusion with the initial *in situ* stress. This will give the total strain associated with the insertion of the injected volume into the initially stressed domain. From Eshelby (1957), the interaction energy of the elastic field with another field is:

$$E_{int} = -\int_{V_S} \sigma_{ij}^{A} \epsilon_{ij}^{T} \, dv \tag{4.10}$$

where σ_{ij}^{A} are the components of the *in situ* stress field and ϵ_{ij}^{T} are the components for the strain field of the inclusion. Assuming x, y, and z directions are aligned with σ_h, σ_H, and σ_v respectively, then the stress becomes:

$$\boldsymbol{\sigma^{A}} = -\begin{bmatrix} \sigma_h & 0 & 0 \\ 0 & \sigma_H & 0 \\ 0 & 0 & \sigma_v \end{bmatrix} \tag{4.11}$$

The volumetric strain is purely from dilation so we can write ϵ_{ij}^{T} as:

$$\epsilon_{ij}^{T} = \frac{1}{3}\varepsilon_{kk}\sigma_{ij} = \frac{1}{3}\frac{\Delta V_S}{V_S}\delta_{ij} = \frac{1}{3}\frac{V_I}{V_S}\delta_{ij} \tag{4.12}$$

The deviatoric part of the strain tensor, $'\epsilon_{ij}^{T}{}'$ is zero. Similarly, the deviatoric part of the stress tensor, $'\sigma_{ij}^{A}$ of the *in situ* stress is also zero. Eshelby (1957), showed that:

$$\sigma_{ij}^{A}\epsilon_{ij}^{T} = \frac{1}{3}\sigma^{A}\epsilon^{T} + {}'\sigma_{ij}^{A}\,'\epsilon_{ij}^{T} \tag{4.13}$$

where $\sigma^{A} = -(\sigma_h + \sigma_H + \sigma_v)$ and $\epsilon^{T} = V_I/V_S$. Combining the equations:

$$\sigma_{ij}^{A}\epsilon_{ij}^{T} = -\frac{1}{3}\left(\frac{V_I}{V_S}\right)(\sigma_h + \sigma_H + \sigma_v) \tag{4.14}$$

Inserting equation 4.14 into equation 4.10, the equation for internal energy then becomes:

$$E_{int} = \int_{V_S} \frac{1}{3}\left(\frac{V_I}{V_S}\right)(\sigma_h + \sigma_H + \sigma_v)\, dV \tag{4.15}$$

which becomes:

$$E_{int} = \frac{V_I}{3}(\sigma_h + \sigma_H + \sigma_v) \tag{4.16}$$

The total strain energy increase caused by injection of fluids into the formation is then:

$$E^{T} = E_{el} + E_{int} \tag{4.17}$$

$$E^{T} = 2G(\epsilon^{T})^2 V_S \frac{(1+v)}{9(1-v)} + \frac{V_I}{3}(\sigma_h + \sigma_H + \sigma_v) \tag{4.18}$$

substituting $\epsilon^T = V_I/V_S$, into equation 4.18 and simplifying, the total strain energy increase becomes:

$$E^T = \left[2G\frac{(1+\nu)}{9(1-\nu)}\epsilon^T + \frac{(\sigma_h+\sigma_H+\sigma_v)}{3}\right]V_I \tag{4.19}$$

The energy dissipated by fracture is proportional to fracture toughness and the overall area of the fracture surface. It can be written as:

$$E^F = G_F A \tag{4.20}$$

where G_F is the fracture toughness or fracture strain energy release rate of the formation and A is the cross sectional area (a circle) of the ellipsoidal inclusion normal to σ_h. The value of G_F will vary depending on rock type.

The change in effective porosity, $\Delta\phi$, is related to the injected volume and the final stimulated volume of the fracture. It is equivalent to the volumetric strain.

$$\Delta\phi = \frac{V_I}{V_S} = \epsilon^T \tag{4.21}$$

4.2.2 Methodology

The induced stimulated volume is represented by an inhomogeneity in the rock. Figures 4-2 and 4-3 in Section 4.2 show the initial inclusion geometry. The volume of the final stimulated ellipsoid, assuming $x_1 = x_3 \neq x_2$, can be calculated as:

$$V_s = \frac{4}{3}x_1^2 x_2 \tag{4.22}$$

Equation 4.22 applies only to circular ellipsoids. For a given stimulated volume, as the ratio of x_1 to x_2 increases, the fracture surface area will increase and the energy dissipated by fracture, E^F, will also increase. The algorithm seeks the values of x_1/x_3 and $\Delta\phi$ given an injected volume, V_I, which will minimize the total change in energy:

$$\Delta E = E_{el} + E_{int} + E^F \tag{4.23}$$

The total change in energy is a summation of the total strain energy in the matrix and the inclusion, the interaction energy, and the energy dissipated by the fracture.

Given V_I, for a range of potential $\Delta\phi$, a V_S is calculated for each $\Delta\phi$. $\Delta\phi$ is equal to the volumetric strain, ϵ^T. For each $\Delta\phi$, a range of values of x_1/x_3 are used to calculate the change in σ_h at the location of the next fracture stage. The combined values of $\Delta\phi$ and x_1/x_3 that result in a change in stress which falls within an acceptable range of the field breakdown pressure of the adjacent stage will be selected and plotted. The critical points for each x_1/x_3 occur where $\Delta\sigma_h$ from the model is equal to the $\Delta\sigma_h$ from the data.

Looking at E^T as a function of $\Delta\phi = \epsilon^T$ and considering:

$$E^T = 2G(\epsilon^T)^2 V_s \frac{(1+\nu)}{9(1-\nu)} - E_{int} \tag{4.24}$$

It is noted that E_{int} is a constant and only depends on V_I, which is a known value. Since $\epsilon^T = V_I/V_s$, it can be rewritten as:

$$E^T = 2G\frac{(1+\nu)}{9(1-\nu)}\epsilon^T V_I + E_{int} \tag{4.25}$$

The change in strain energy is a linear function with the slope dependent on the injected volume. This is represented by Figure 4-4

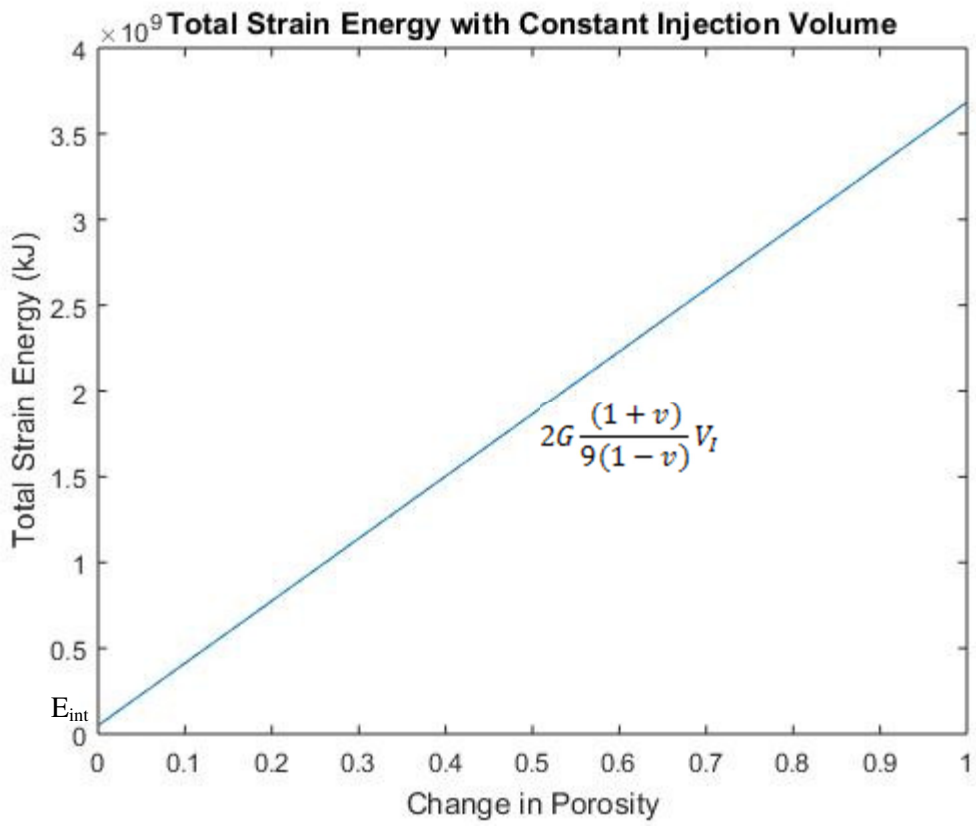

Figure 4-4 Change in Strain Energy with Constant Injection Volume - Sample chart

Figure 4-4 shows the work of expansion, which is the work required to accommodate the change in volume from the injected fluid and the resulting geometry of the ellipsoid. The total change in energy increases in a linear fashion as the change in porosity increases, showing that more energy is required to create a larger stimulated area. In the above graph, the injection volume is held constant while the final stimulated area of the ellipsoid is increased.

If the stimulated volume is held constant, and the injected volume is varied, the following relationship between the change in porosity and the total energy can be plotted:

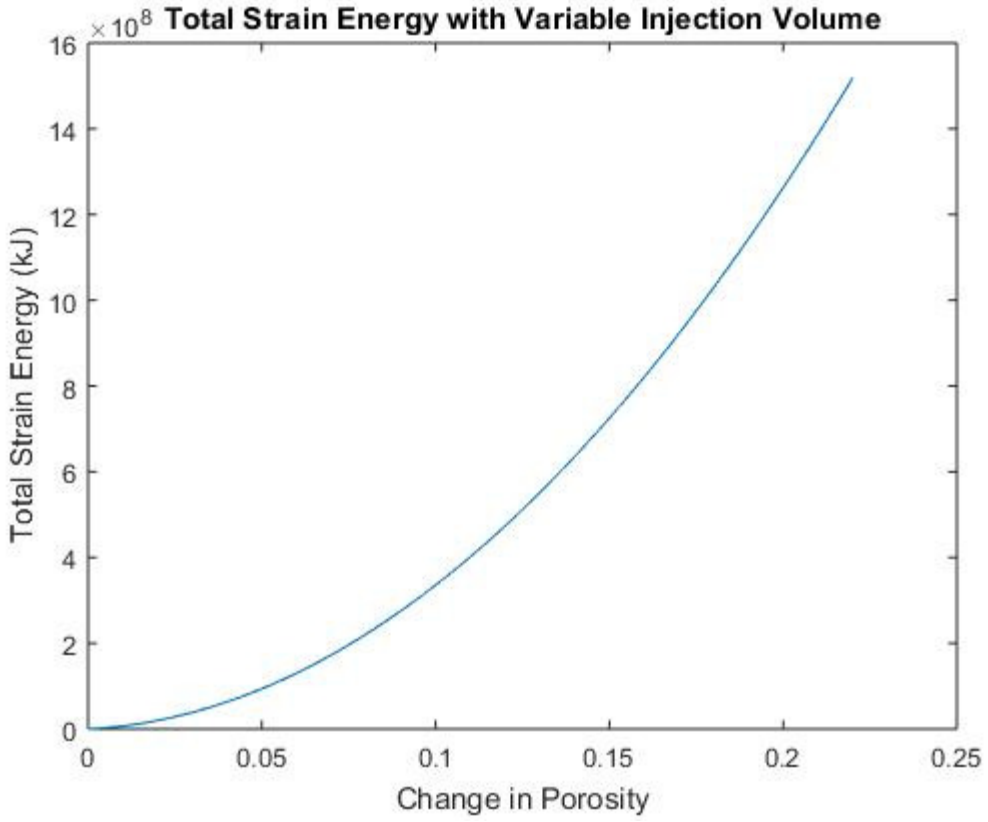

Figure 4-5 Change in Strain Energy with Variable Injection Volume – Sample Chart

Figure 4-5 shows that the total change in energy increases in a non-linear fashion as the injection volume increases. In this graph, the stimulated volume is held constant, while the injected volume is increased to the amount used in a typical fracture stage. The final volume of the ellipsoid does not change, so the porosity must rapidly increase in order to accommodate the increase in injected volume.

The fracture area can be written as:

$$A = \pi x_1^2 \tag{4.26}$$

Substituting equation 4.26 into equation 4.22 and rearranging,

$$\pi x_1^2 = \frac{3}{4x_2} V_S = A \tag{4.27}$$

Recalling that:

$$V_S = (\epsilon^T)^{-1} V_I \tag{4.28}$$

Equation 4.27 then becomes:

$$A = \pi x_1^2 = \frac{3}{4x_2} (\epsilon^T)^{-1} V_I = \frac{3}{4x_2} \frac{V_I}{\Delta\phi} \tag{4.29}$$

Looking at E^F as a function of $\Delta\phi = \epsilon^T$, the energy dissipated by the fracture can be expressed as:

$$E^F = G_F A = \frac{3G_F}{4x_2} V_I \frac{1}{\Delta\phi} \tag{4.30}$$

Plotting E^F as a function of $\Delta\phi = \epsilon^T$, we get the energy required to fracture the medium, or the work done by the fracture, assuming G_F is constant. We can plot this function considering the ratio of x_3/x_2.

It is noted that $E^T = E_{el} + E_{int}$ will vary with ϵ^T therefore E^F will vary with $1/\epsilon^T$. We can plot the change in total energy vs the volumetric strain to find which pairing of x_3/x_2 and $\Delta\phi$ values yields the minimum change in energy.

4.3 Scope and limitations

There are many underlying assumptions that are made with the model presented above. First, the rock mass is assumed to be homogeneous and isotropic for all material properties. While this is not true of unconventional reservoirs, the assumption can be made due to the relatively small variations in properties at the scale of a MSHF operation. This assumption may not hold for heavily laminated shales and siltstones, as anisotropy may affect material properties on a hydraulic fracture scale.

The medium is also considered to contain no natural fractures or planes of weakness. The Montney Formation is naturally fractured which would suggest the induced fracture would not be biwing or symmetrical in all directions, however this model is an estimation of the final stimulated volume of the fracture rather than an accurate representation of fracture geometry. Completely accurate fracture geometry is not required to determine a first order estimate of stress shadowing, but rather an idea of the overall fracture volume itself is more valuable in the determination of stress fields.

Plastic effects are neglected in this model and the rock mass is assumed to behave in a linear elastic fashion. The Montney Formation is very brittle with little clay content, so this assumption is applicable to

the wells from the case study; however, this model may not be applicable to a more clay based reservoir. Linear elastic behaviour is assumed for the sake of simplicity as well.

Fluid effects, viscous forces, and thermal effects are not considered to a great extent in this model. A fully coupled thermal and hydraulic model is too computationally intensive for the goals of this program. All fractures are assumed to be uniformly pressurized which means they exist only under a toughness dominated condition. Viscous dissipation of energy from the fluid flowing within the hydraulic fracture will result in a pressure gradient along the length of the fracture. This leads to a non-constant pressure distribution within the hydraulic fracture, causing different fracture apertures. For the purposes of this model, viscous dissipation and fluid compressibility are not considered.

While effective porosity is considered, fluid leak-off into the formation is not a part of this model. All fluids pumped into the formation are assumed to contribute to the final volume of the stimulated hydraulic fracture. The permeability of the Montney Formation is low (see Chapter 5), and therefore it can be assumed that loss of fluid into the formation is negligible.

Chapter 5 Hydraulic Fracture Field Data

Five horizontal wells were fractured within the Montney Formation using the ball drop method. Two additional wells were completed using the plug and perforation method. The production data from these wells is examined to determine if there are possible instances of stress interference in the pressure data recorded during the MSHF operation. There are several events that can be observed in pressure data which could indicate stress interference.

Stress shadow data can be gathered from net fracturing pressure data recorded in the field during hydraulic fracturing (Roussel et al. 2012). A steady increase in net pressure along fracturing stages would suggest little to no stress shadow interference, whereas an up and down trend in net pressure data could suggest that fractures are interacting due to stress shadow effects (Roussel et al. 2012)

5.1 The Montney Formation

All the wells in the dataset are drilled in the Montney Formation. The Montney straddles the northern Alberta-British Columbia border and covers approximately 90,650 km^2 and varies in geological properties from east to west (Keneti et al. 2012). Figure 5-1 shows the location of the Montney Formation in Canada.

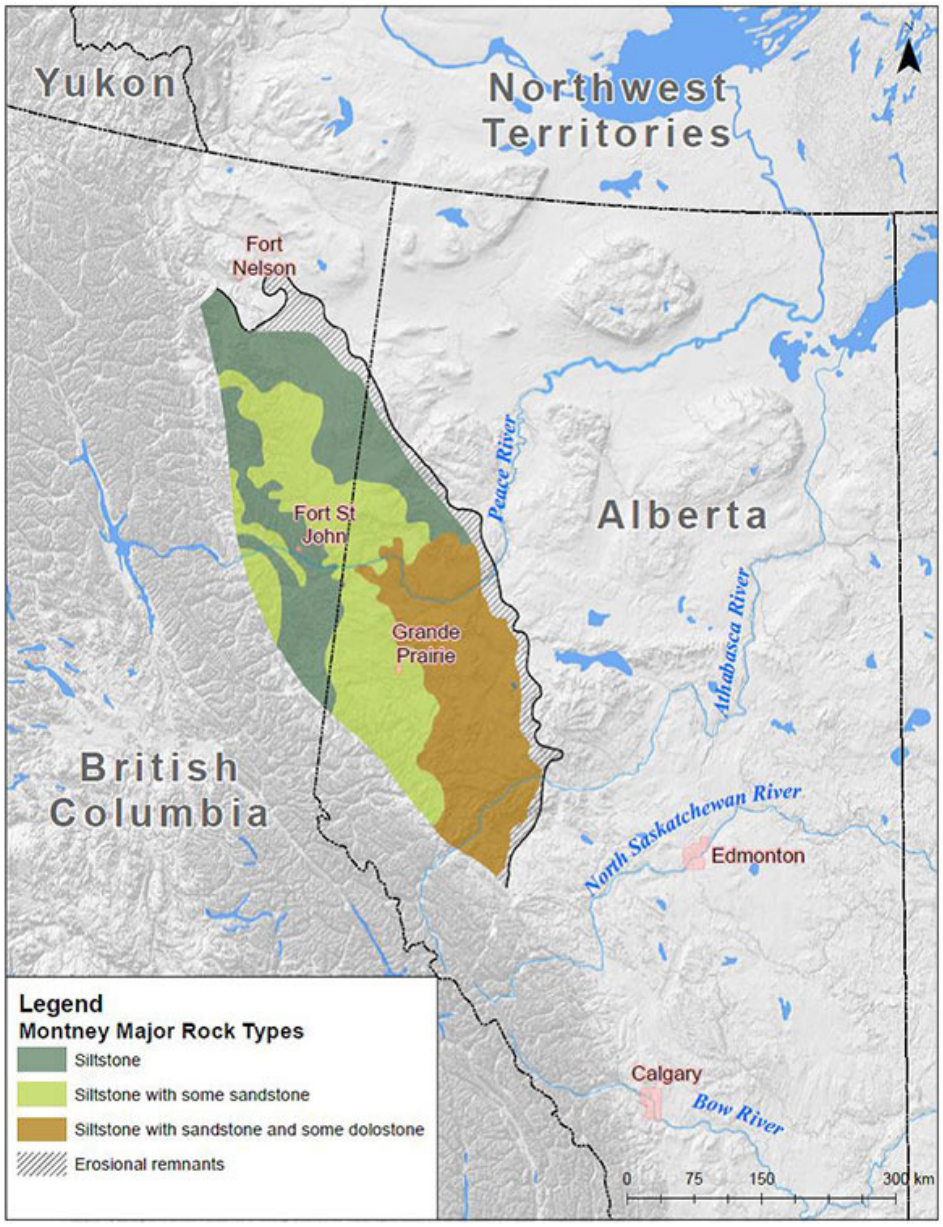

Figure 5-1 Location of Montney Formation (National Energy Board 2013)

The formation is primarily composed of brittle sandstones, siltstones and shales in the western area of the play and becomes more ductile and clay rich in the north (Keneti et al. 2012). The play is divided into several units, the most commonly known being the Upper, Middle and Lower Montney Formations. The lower Doig Formation is also sometimes considered to be a part of the Montney. These units can be further subdivided if desired. Figure 5-2 shows the division of the Montney Formation.

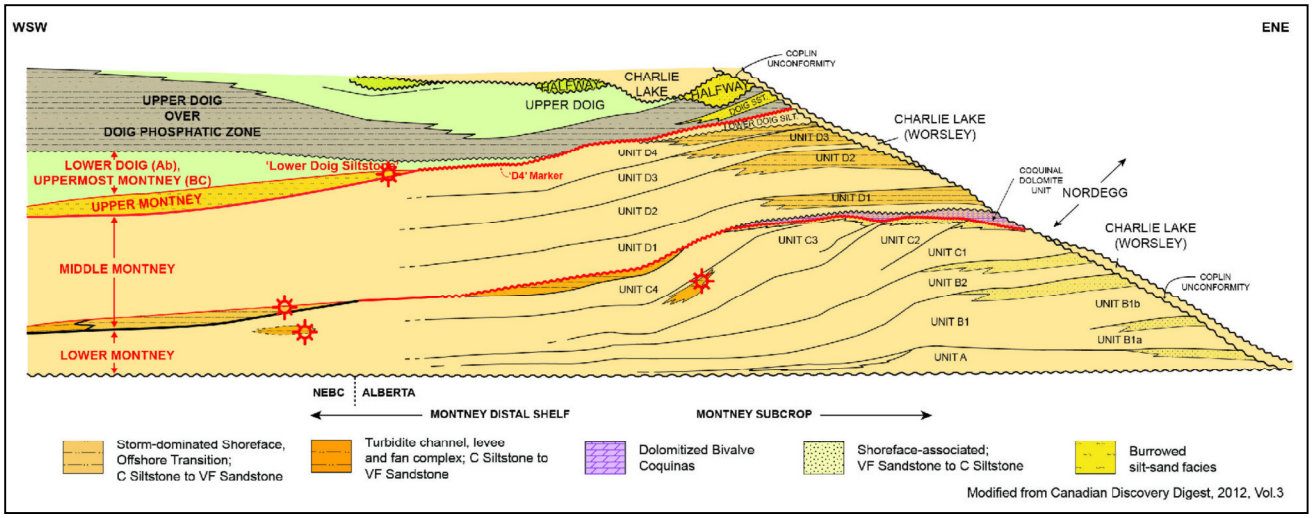

Figure 5-2 Cross section of the Montney Formation (National Energy Board 2013)

The formation produces both liquid-rich and dry gas. The geomechanical properties of the Upper, Lower, and Middle Montney Formation are not the same, but are comparable to a point where many hydraulic fracture operations and models will consider them to be the uniform. The Montney Formation is considered to be a brittle formation in comparison to other unconventional shale plays. They clay content is generally low, the Young's modulus value is high, and the Poisson's ratio is also low. Brittleness has been shown to increase the reach of a stress shadow when it causes the rock to become stiffer (Roussel et al. 2012). Due to the brittle nature of the Montney, it is more likely that stress shadow interactions will occur than in a more clay rich and ductile rock mass.

Natural fractures exist within the Montney Formation, as do local variations in geomechanical properties. The natural fractures can cause issues such as unexpected variations in fracture propagation direction even in wells which have high production values. Natural fractures and their effect on stress shadows will only be considered in this study as a property which may cause the field data to differ from the modeled data. Inclusion of an explicit natural fracture system and its effects on propagation and stress shadowing is outside the scope of this study.

5.2 Case Study Well Summary

The wells were drilled using horizontal completion methods in the various subsections of the Montney Formation. This study will not focus on the overall gas production or efficiency of the wells; instead, focus will be placed on the potential mechanical interactions. A summary of the basic well data is presented in Table 5-1.

Table 5-1 Well Summary

Well Name	Formation	Fracture Method	Intervals	Average Interval Spacing (m)	Total Vertical Depth (m)	Average Surface ISIP (MPa)
Well A	Upper Montney	Ball Drop	20	98.0	2152.8	27.5
Well B	Middle/Lower Montney	Ball Drop	20	90.0	2154.4	29.4
Well C	Upper/Middle Montney	Ball Drop	17	100	2130.0	38.2
Well D	Upper Montney	Ball Drop	18	105	2000.0	33.0
Well E	Upper Montney	Ball Drop	18	98.8	2087.0	27.0
Well F	Lower Montney	Plug/Perf	9 zones, 3-4 perfs per zone	50-60 (perf spacing)	2174.9	36.8
Well G	Upper Montney	Plug/Perf	8 zones, 4-5 perfs per zone	~50 (perf spacing)	2008.6	30.0

5.3 Pressure Data from Case Study Wells

The majority of pressure curves for ball drop wells contain a mini fracture test to determine ISIP and closure pressure, a period of pressurization while the ball is seated, treatment with acid and slickwater, and then constant treating pressure. In general, the treatment pressure remains fairly consistent throughout the fracture operation in one interval and is usually close in value to the treatment pressure in subsequent intervals. Figure 5-3 below shows the treatment pressure curves for intervals 4 and 5 in Well B.

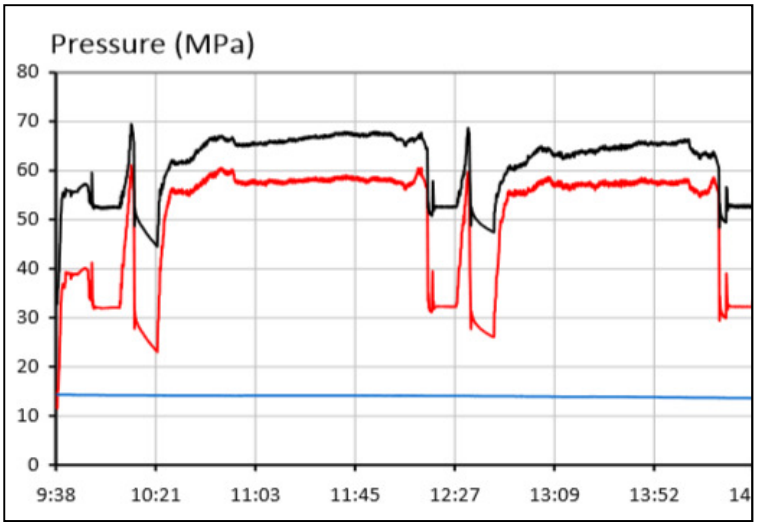

Figure 5-3 Pressure readings in a typical ball drop hydraulic fracture operation

In Figure 5-3 and all subsequent pressure figures in Chapter 5, the red line is the surface pressure read by mainline pressure monitors at the head of the well. The black line represents a calculated bottom hole pressure. A uniform calculation of pressure head is applied to all surface pressures to estimate the bottom hole pressure. The calculation does not account for horizontal well distance, which can affect friction losses, and should therefore be regarded as an estimation only. The thin blue line in the figure is a backup monitor pressure at the surface. In Figure 5-3, the backup monitor was not functioning correctly. Unless otherwise noted in the description of the figures, the flow rate associated with the pressure curves is as to be expected when pumping. Flow is increased during formation testing until breakdown is achieved. The flow is then cut off while pressure data is collected. Flow is then increased up to a steady rate which allows the fracturing liquid to enter the formation at a steady rate with no pressure build up or screen outs.

In Figure 5-3, it can be seen that two MicroFrac™ tests were completed between 9:38 and 10:21. At 10:21 the interval was pressurized and hydraulic fracturing began. A similar pattern can be seen for the next interval with a MicroFrac™ test at 12:27 and pumping to fracture starting at approximately 12:45.

The treatment pressure remains fairly constant but there are some points at which more pressure buildup occurs or a drop in pressure is seen. These are usually explained as a new fracture opening along the interval (ball drop is uncased), the fracture encountering an area of lower or higher stress, or interaction

with other existing fractures (closed or open planes of weakness). The general overall increase in treating pressure suggests an expanding hydraulic fracture as is expected during the stimulation stage.

Plug and perforation methods are similar to ball drop but do exhibit some differences. There are between 3 and 5 perforations per pressurized zone. The perforations are consistently spaced at approximately 50 m throughout the entire well. It is assumed that all perforations fire all perforations take an equal amount of fluid during pumping. An example of a typical cure for plug and perforation operations is shown below in Figure 5-4.

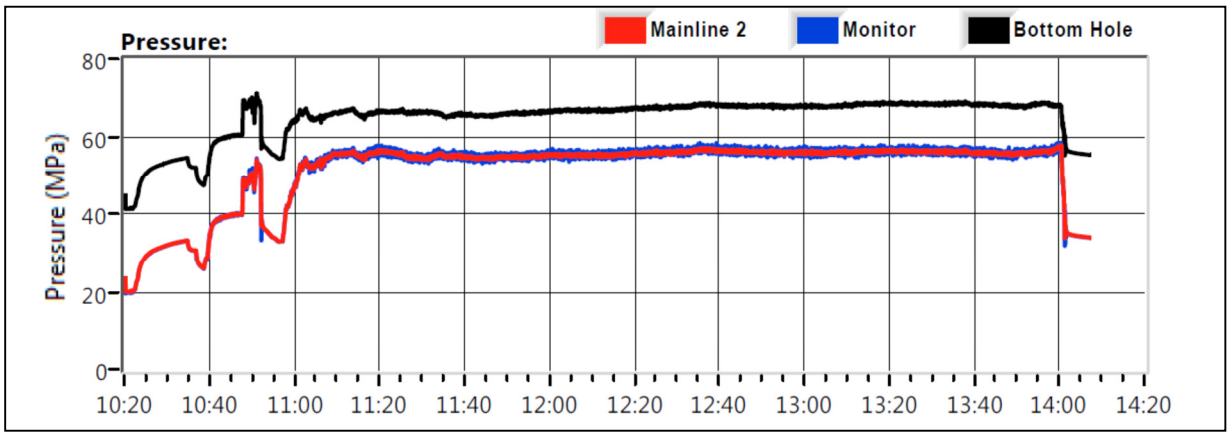

Figure 5-4 Pressure readings in a typical plug and perforation hydraulic fracture operationPressure readings in a typical plug and perforation hydraulic fracture operation

There were no anomalies in flow rate for the pumping curve above. The flow rate was held steady for the duration of the treatment from approximately 11:00 to 14:00.

The start of every pressure curve for both plug and perforation and ball drop operations begins with an acid soak. In the image above, the acid soak occurs from 10:20 until 10:40. The acid soak generally consists of a dilute acid solution being pumped down the hole to clean it out and dissolve carbonates near the wellbore. The following stage is the pad stage which involves pumping pure slickwater free of proppant down the well to assist with flow and placement of proppant in later stages. Proppant is added

to the slickwater at varying concentrations depending on the demands of the well. At the end of the pumping curve the well is usually flushed.

In Well A the treatment pressures for intervals 15-20 are significantly lower than the preceding intervals. While this could be due to smaller distance from the pump to these intervals, the rapid change from 55 MPa treatment pressure in interval 14 to approximately 40 MPa treatment pressure in interval 15 suggests there could be other issues contributing to the change. It has been suggested in other studies that fracture rotation due to stress shadow interference can lead to lower than expected treatment and breakdown pressures values (Rios et al. 2013). It may be possible that a re-orientation of the fracture direction resulted in lower treatment pressure.

Intervals 8-12 in Well B exhibit several rapid changes during treatment pressure that are not explained through pumping or flow rate data. Flow rate was held fairly constant despite many rapid drops in pressure. This could be a result of natural fractures. Figure 5-5 and Figure 5-6 below show a visual of the intervals.

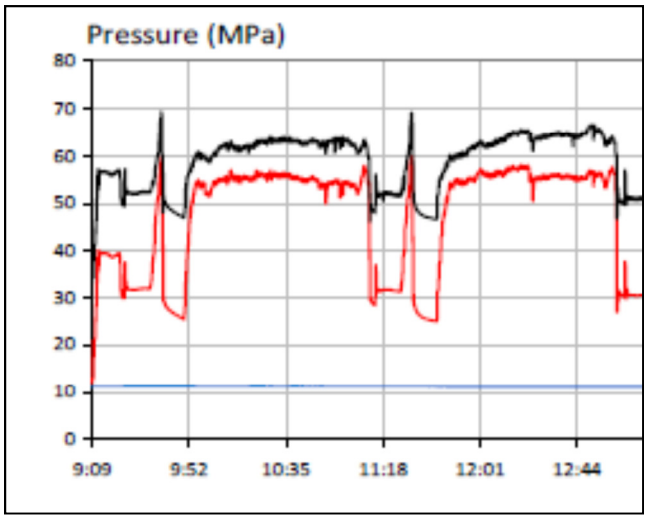

Figure 5-5 Intervals 8-9 pressure fluctuations

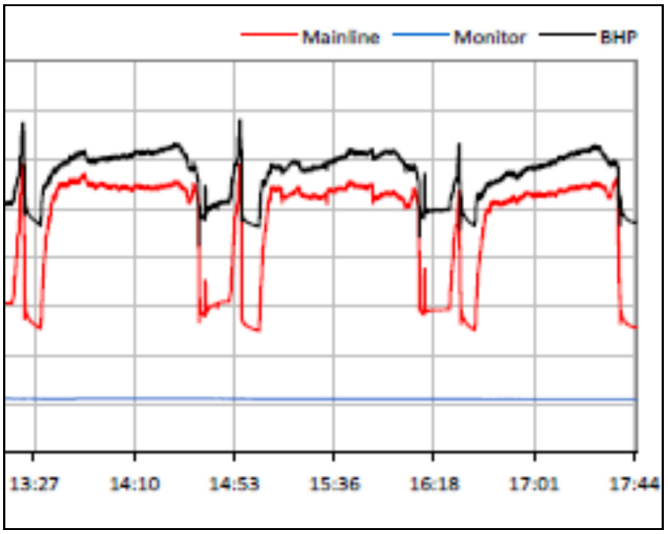

Figure 5-6 Intervals 10-12 pressure fluctuations

In interval 4 of Well C, there were some issues with the ball seating. The pressure increased well past the pressure needed to fracture the formation and the total volume pumped into the interval was much higher than usual. Figure 5-7 shows the interval.

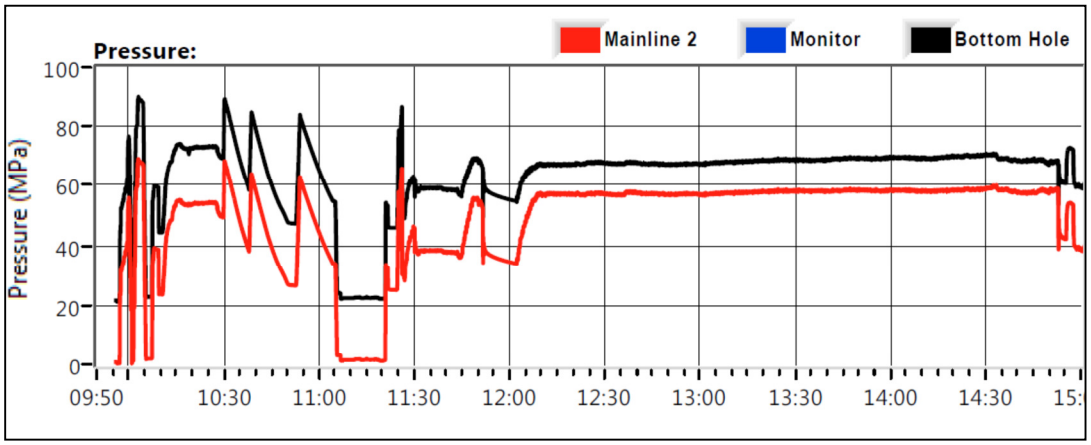

Figure 5-7 Interval with ball seat issues and pressure spikes

The pressure curve itself is fairly constant but there is the possibility that the high pressures from the time ahead of the constant curve could have affected the formation. Figure 5-8 shows interval 5 of the well.

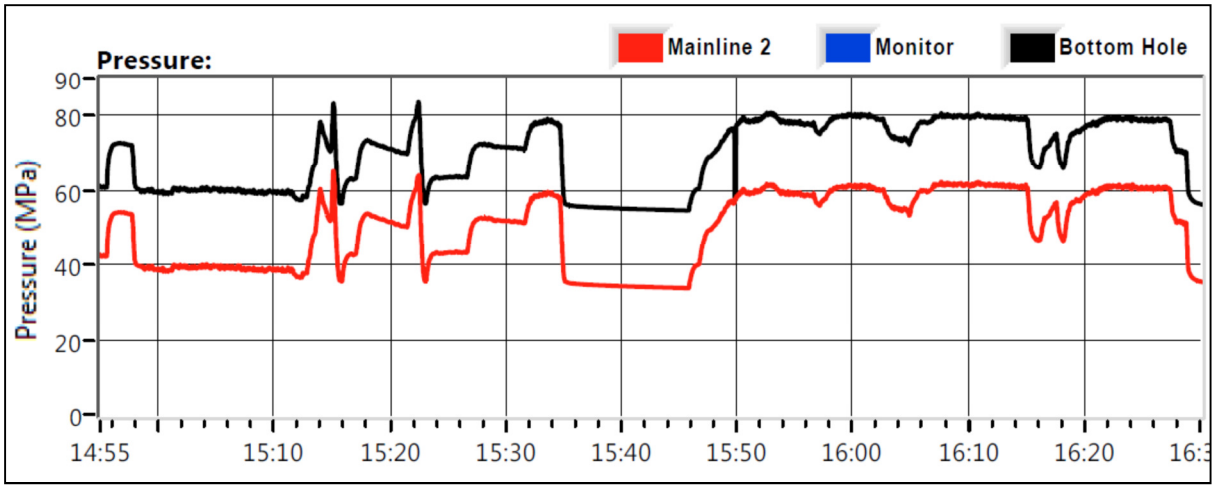

Figure 5-8 Interval with unexplained pressure issues

Zone 5 could not be fractured. They increased the pressure to approximately 63 MPa which did not cause the formation to breakdown. It is possible that the increased volume from zone 4 caused the stress to increase to a point where fracturing was no longer feasible. Zone 7 also was fractured using a very high volume of fluids, and zone 8 also could not be initiated even at a max treating pressure of 59 MPa. Zone 9 experienced issues as well. The ball would not seat and the pumping rate could not be increased beyond 2 m^3/min at 65 MPa. The same issue was encountered for intervals 11, with a high pumping volume, and 12, with no breakdown of the formation. It is possible that the stress change from the higher than average volumes of the previous stages had interfered with this section of the well. The remainder of the stages were stimulated at a lower volume that the first half of the well and experienced no further issues with breakdown achievement.

Zone 7 of Well F contains 4 perforations. It exhibits fairly constant treatment pressures until the last third of treatment time at which point two unexplained spikes and drop offs occur. Figure 5-9 shows zone 7.

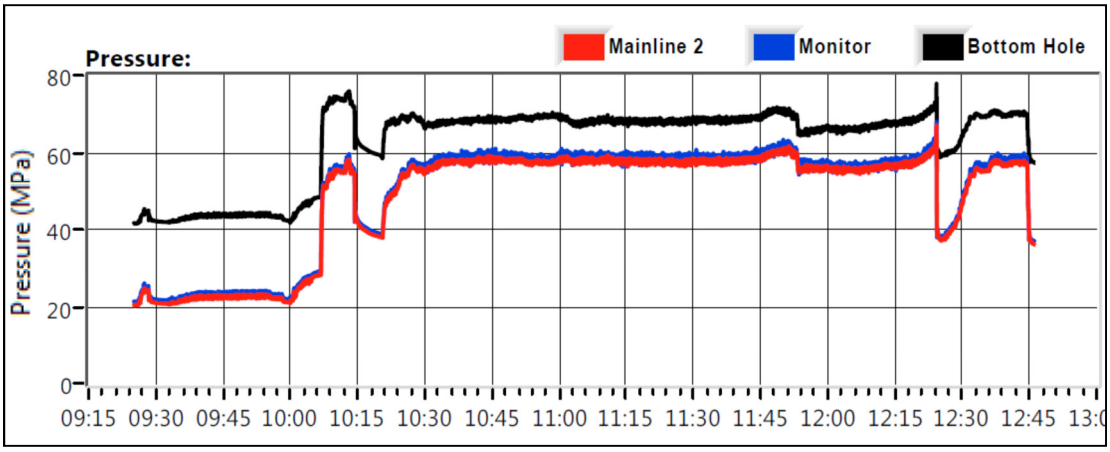

Figure 5-9 Pressure fluctuations in plug and perf operations

There is the possibility that the pressure drops and subsequent build ups are the result of a perforation initiating after the initial fracture began propagation. The drop which occurs around 11:50 in the data is not matched by a drop in flow rate. The flow of fluid into the interval remained constant despite the pressure build and drop. The large build at 12:20 was also not reflected in flow data, however the pump was shut off around 12:25 when the rapid pressure rise suggested that a blowout could be imminent. An investigation into local stress shadowing between the closely spaced perforations will be completed to see if the minimum horizontal pressure was increased to a point that would prevent all perforations from initiating.

5.3.1 Increased and Fluctuating Breakdown Pressures

Many of the wells do not demonstrate significantly different ISIP or breakdown pressure values from stage to stage. The stage spacing is between 90 and 100 m for the majority of the wells, which is considered to be quite large.

Well B does however show a pattern of fluctuations between breakdown pressures in its later stages. The breakdown pressure for interval 15 is 36 MPa, followed by 30 MPa in interval 16, then an increase back to 35 MPa in interval 17, falling to 29 MPa in interval 18, and increasing back to 34 MPa in interval 19. This may be indicative of stress shadow interference. Well E shows a fluctuation from 30 MPa to 38

MPa and back down to 31 MPa in the next interval. The final three intervals on the well also exhibit a similar pressure pattern.

5.3.2 Breakdown Pressure and ISIP Values as an Indication of Stress Changes

The data contains some information on both breakdown pressure and ISIP values. The ISIP values for most of the intervals were estimated by selecting a value from the curve of the field MicroFrac™ test. Square root time plots were not completed. It should be noted that selecting the ISIP value from a MicroFrac™ test can be arbitrary and have a large range of values. ISIP will act as an upper bound for the closure pressure of the formation when it is available. In several of the test cases, the ISIP was not estimated for each stage, but rather only once at the start of daily operations. Not all stages have an accurate ISIP value. In these cases, the ISIP value will not be considered.

Breakdown pressure is generally a measure of near-wellbore stress conditions. There are many factors that can influence the breakdown pressure, including formation damage, skin effects, and rock structure changes near the annulus. Many of the factors affecting breakdown pressure will cause a decrease in magnitude of the value at which the rock fails. Natural weaknesses in the rock and formation damage often make it easier for the rock to crack. If there is a significant increase in breakdown pressure, it suggests that either the fracture initiation point is in an area with rock structure that has made it more difficult for the formation to break or the minimum horizontal stress has been increased.

Several intervals exhibit breakdown pressures that fluctuate significantly from one interval to the next. For these wells, breakdown pressure will be the main indication of stress change. In other wells, certain intervals were unable to be fractured. These intervals will be examined to see if the previous stages had increased the stress to the point where the formation would not break, even under the maximum pressure applied during the attempted fracturing.

The use of breakdown pressure as a measure of stress change is not ideal, however the goal of this program is to use the data available from a typical hydraulic fracture operation. If the breakdown

pressure is considered to be representative of the rock conditions not just immediately outside the wellbore, but also several meters into the formation, it can give a better indication of a stress increase.

5.4 Geomechanical Properties of the Montney Formation

The Montney Formation varies from over-pressured (the pore pressure gradient is larger than hydrostatic) to normally pressurized depending on the location of the wells. However, only total stresses will be considered for this project. The *in situ* stress magnitudes have been determined through density logs, stress correlations, and pressure testing methods discussed in Chapter 2.

The values of the geomechanical properties are fairly consistent throughout the formation, though there is some variation. The values for Young's modulus, Poisson's ratio, shear modulus, and critical stress intensity factor have been chosen based on numerous field and lab tests. Effective porosity estimates are also included, however these values act only as a starting point for the program. They are presented in Table 5-2.

Table 5-2 Geomechanical Properties of the Montney Formation

Geomechanical Property	**Minimum**	**Average**	**Maximum**	**Source**
Young's Modulus (E)	19.4 x10^6 KPa	21.0 x10^6 KPa	32.5 x10^6 KPa	Triaxial lab tests (provided by client)
Poisson's Ratio (ν)	0.19	0.21	0.26	Triaxial lab tests (provided by client)
Fracture Energy (G_F)	1.27 MPa $m^{0.5}$	1.34 MPa $m^{0.5}$	1.46 MPa $m^{0.5}$	(Ouchterlony, 1990)
Effective Porosity (ϕ)	1.5%	2.0%	3.0%	Wellbore Logs (provided by client)
Bulk Density (ρ)	2.5 gm/cc	2.61 gm/cc	2.63 gm/cc	Density Logs (provided by client)

5.5 Estimation of Fracture Energy

The fracture energy and therefore the energy dissipated by fracture, E^F, (Equation 4.30) will likely be higher in the field than the fracture energy estimated through laboratory experiments. The equation for energy dissipated by fracture is presented below:

$$E^F = G_F A = \frac{3G_F}{4x_2} V_I \frac{1}{\Delta\phi} \tag{5.1}$$

The fracture energy, G_F, is multiplied by the area of the fracture to estimate the total amount of energy dispelled through the fracturing process. The surface area of the fracture is likely to be much higher than the area estimated by the program presented in this thesis. This is due to the assumption in the program that the fracture will be a simple ellipsoid. In reality, the fracture is likely to be a multi-branching, non-uniform shape which creates a significantly higher amount of surface area. E^F and therefore the total change in energy of the system will likely be much higher in the physical system than in the model. This will be discussed further in Chapter 6 and Chapter 7.

Chapter 6 Case Study Outputs and Analysis

Three cases are examined in this study. The three cases each deal with a different indication of stress shadow interference (i.e., breakdown pressure increases, non-initiating intervals). The first case study is focused on fluctuating breakdown pressures, where 5 intervals show a pattern of uniformly increasing and decreasing values of p_b. The study attempts to estimate the geometry of the hydraulic fractures which would cause the recorded breakdown pressure. The second study examines the intervals in which fractures could not be initiated even at high treatment pressures. The highest recorded pressure will be compared to the value of stress change that the previous hydraulic fracture stage could have caused. The third study examines the stress shadowing effects in a plug and perforation interval. Specific focus will be placed on how the stress changes based on which perforation has taken the most volume.

6.1 Case 1 – Fluctuating Breakdown Pressure

Well B contains 20 intervals in an open-hole ball drop system at a vertical depth of 2154.4 m. Slickwater was used to fracture all intervals. For the purposes of this study, all fractures were assumed to initiate at the centre of the interval. The formation is considered to be homogenous, elastic, and laterally infinite. The height of the formation is large enough that the height growth of the stimulated area will not be confined by barriers caused by a change in rock type. The ellipse of the stimulated area is assumed to be symmetric about the wellbore. Growth is equal in all directions as governed by the predetermined ratio of the ellipse. The majority of these assumptions allow for the stress change caused by the injection of fluid to be uniform and symmetric around the injection point. Variations in the geomechanical properties of the rock, porosity, natural fractures, and *in situ* stress may cause the actual physical stimulated area to not be symmetrical about the wellbore, but for the purposes of this study, this effect is not considered. Principal stress directions are assumed to line up with $\sigma_v, \sigma_H,$ and σ_h. The breakdown pressure is assumed to be an upper limit estimation of the minimum principle stress. Figure 6-1 shows the breakdown pressures in comparison to the ISIP values recorded at the well site.

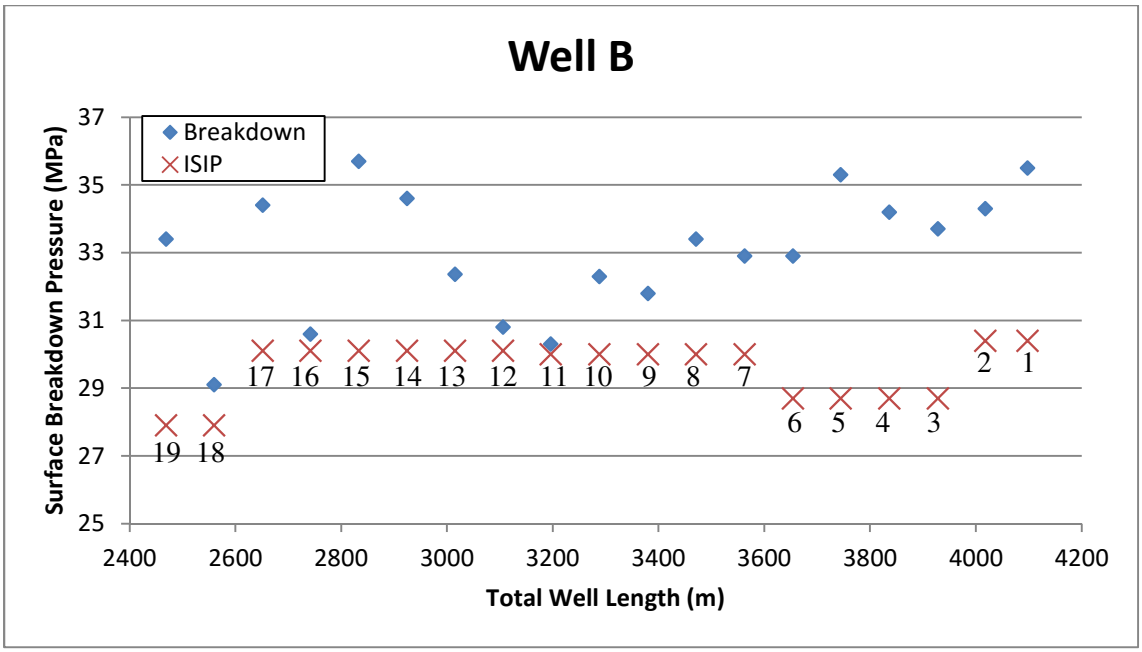

Figure 6-1 Breakdown Pressures and ISIP Values along the Well

No breakdown pressure was recorded for the last interval. It should be noted that the ISIP values were recorded to be the exact same for the majority of the intervals. Examination of the treatment curves shows that the ISIP values were estimated for each day rather than each stage. It can be seen in the data that stages 12 through 17 all have the same ISIP value and were all completed on the same day. The MicroFrac™ test was done at the start of interval 12 and that value was applied to the remainder of the stages. Because of this, the ISIP values for this well will not be considered when looking at stress changes between intervals. The recorded values cannot act as a measure of stress change within each interval. However, they can give us an idea of the initial minimum horizontal stress. The first ISIP test recorded a value of 30.4 MPa as a top end estimate of minimum horizontal stress in undisturbed rock.

It is interesting to note that the breakdown pressures tend to fluctuate up and down across most of the well. There is usually a period of building followed by a rapid decrease in value, especially evident in the build in breakdown pressure of the stages 11-15, followed by a rapid drop in stage 16. This could be indicative of a steady increase in the minimum horizontal stress followed by a fracture rotation. For the purposes of the model, only the last four stages will be considered for analysis.

The last four stages show a rapid up and down pattern. The breakdown pressure fluctuates between what could be considered an altered stress state (~34 MPa) and the undisturbed *in situ* state (~30 MPa). If the intervals which broke at higher pressures produced a rotated fracture, it is possible the fracture would not cause as much of a stress change in the adjacent interval which causes the formation to break at the original minimum horizontal stress state.

6.1.1 Model Inputs

The details of the intervals are presented in Table 6-1 below.

Table 6-1 Interval Data Well B

Interval	p_b (MPa)	Δp_b (MPa) (% change)	Distance from Previous Zone (m)	Total Injected Volume (m^3)
15	35.7	1.1 (3.2%)	91.1	1143.9
16	30.6	-5.1 (-14.3%)	91.8	1230.4
17	34.4	4.2 (+12.4%)	90.1	1200.0
18	29.1	-4.7 (-15.4%)	91.7	1262.3
19	33.4	4.3 (+14.8%)	91.0	1230.0

Overall, the average percent change in breakdown pressure between intervals is 5.8%, with the median value being 4.1%. The four final intervals experienced a significantly higher change in p_b than the other intervals. This section will focus specifically on the stress change between intervals 16 and 17.

The inputs for the model can be found in Section 5.4. The average values of the geomechanical properties were used for the initial model. The fracture is assumed to be a stimulated area with pore space uniformly filled with incompressible slickwater. The model requires the inputs of Young's modulus and Poisson's ratio for the inclusion. Since the inclusion is considered to be a stimulated area of the formation rather than a true fluid-filled fracture, the geomechanical properties of the stimulated area will be the same as the undisturbed formation. The amount of fluid is small compared to the overall volume of the rock that is being stimulated, therefore it can be assumed that Young's modulus and Poisson's ratio of the affected area will not change significantly once the fluid is injected The inclusion is subjected to an initial eigenstrain equal to $\Delta\phi$. The initial *in situ* stress conditions are considered to be 51 MPa, 40

MPa, and 30 MPa for σ_v, σ_H, and σ_h respectively. Density logs were used to determine σ_v. The minimum horizontal stress was estimated from ISIP values in undisturbed rock.

6.1.2 Calculated Stress Changes

Figure 6-2 shows an example of stress changes along the wellbore trace.

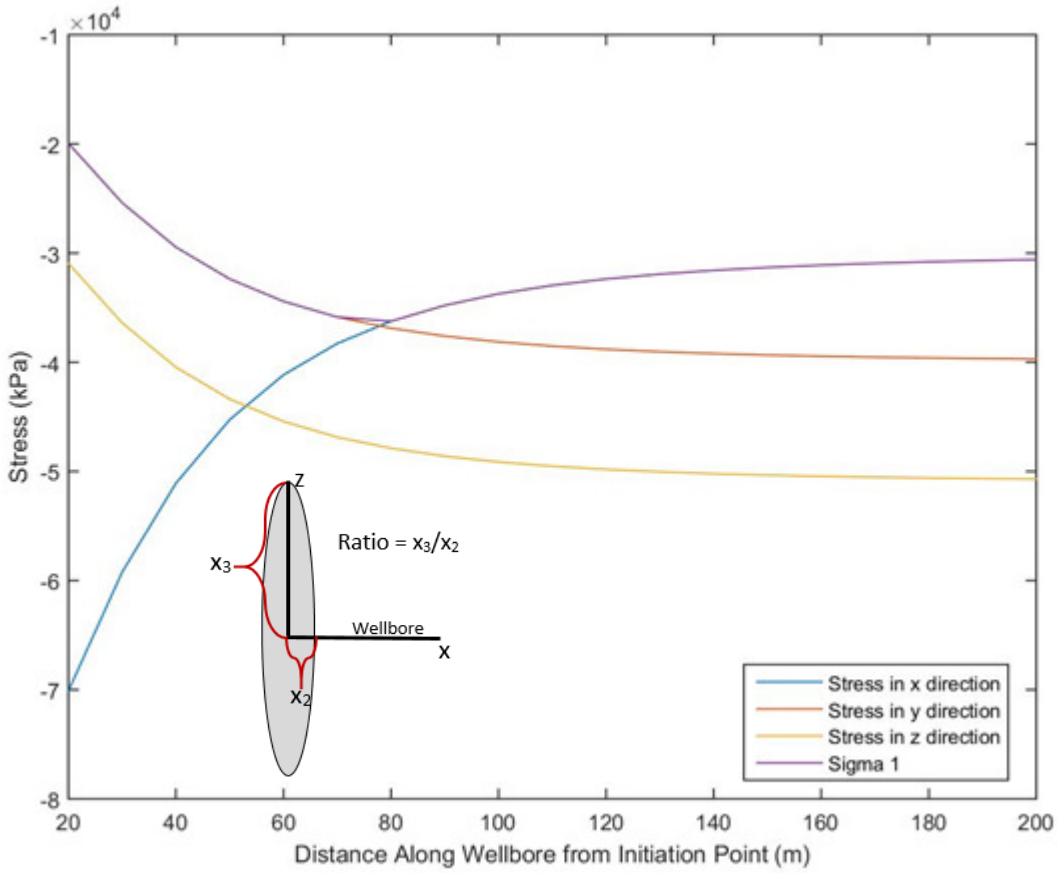

Figure 6-2 Example of Stress along the Wellbore (Ratio = 4, $\Delta\phi$ = .006)

In Figure 6-2, a ratio of $x_3/x_2 = 4$ is used. This means the height of the stimulated volume in the vertical direction (z-direction) is four times as large as the length of the stimulated volume along the wellbore (x-direction). The stress contours begin at the edges of the stimulated area.

In this case, the half-length of the width of the stimulated area along the wellbore is approximately 14.5 m, which is large for a fracture, but reasonable if a stimulated volume is being considered. The height in

the z-direction is 58.1 m. The stress state of the Montney formation suggests that the fractures will be long and thin rather than short and rounded, but a ratio of 4 (x_3/x_2) for a stimulated volume is not unreasonable. The horizontal compressive stress in the x-direction is significantly increased in compression near the edges of the stimulated area, and decreases as the distances from the initiation point increases until the stress state returns to the original assumed *in situ* condition. The compressive stresses in the y-direction and z-direction are reduced near the stimulated area and return to the *in situ* undisturbed state farther away from the fracture. Though the stresses in the y and z-direction are different in magnitude, the trends in the data of the two curves are the same. This is due to x_3 being equal to x_1 (semi axis along z is equal to the semi axis along y). The fracture geometry plays a large part in how the stress around the stimulated area is distributed. This will be expanded on further in this section.

For graphs showing the stress change for different cases of change in porosity and change in ratio for stage 16 to 17, please reference Appendix A. Tables 6.2 through 6.5 summarize the stress changes and geometries which produce a stress similar to the breakdown pressure recorded in the field, which in this case is 34.4 MPa. The cells highlighted in green show the porosity and ratio combinations which produce the desired stress change.

Table 6-2 Minimum Compressive Stress (kPa) at Initiation Point of Stage 17 due to an elliptical stimulated volume at Stage 16

Porosity	Ratio = x_3/x_2					
	2	4	6	8	10	12
0.001	-33883	-32582	-32046	-31723	-31500	-31335
0.006	-35750	-34790	-34259	-33880	-33586	-33346
0.011	-36155	-35398	-34947	-34611	-34340	-34113
0.016	-36351	-35714	-35320	-35019	-34772	-34561
0.021	-36471	-35914	-35561	-35288	-35060	-34864
0.026	-36553	-36054	-35733	-35482	-35270	-35087
0.031	-36614	-36159	-35864	-35630	-35432	-35260
0.036	-36661	-36242	-35967	-35748	-35562	-35399
0.041	-36651	-36309	-36051	-35845	-35669	-35514

Table 6-3 Height (m) of Stimulated Area for Stage 16

Porosity	Ratio= x_3/x_2					
	2	4	6	8	10	12
0.001	83.75	105.52	120.79	132.95	143.21	152.19
0.006	46.09	58.07	66.47	73.16	78.81	83.75
0.011	37.66	47.45	54.31	59.78	64.40	68.43
0.016	33.24	41.88	47.94	52.76	56.83	60.40
0.021	30.36	38.25	43.78	48.19	51.91	55.16
0.026	28.27	35.62	40.77	44.88	48.34	51.37
0.031	26.66	33.59	38.45	42.32	45.59	48.45
0.036	25.36	31.96	36.58	40.26	43.37	46.09
0.041	24.29	30.60	35.03	38.56	41.53	44.14

Table 6-4 Width (m) of Stimulated Area for Stage 16

Porosity	Ratio= x_3/x_2					
	2	4	6	8	10	12
0.001	41.88	26.38	20.13	16.62	14.32	12.68
0.006	23.05	14.52	11.08	9.15	7.88	6.98
0.011	18.83	11.86	9.05	7.47	6.44	5.70
0.016	16.62	10.47	7.99	6.60	5.68	5.03
0.021	15.18	9.56	7.30	6.02	5.19	4.60
0.026	14.14	8.90	6.80	5.61	4.83	4.28
0.031	13.33	8.40	6.41	5.29	4.56	4.04
0.036	12.68	7.99	6.10	5.03	4.34	3.84
0.041	12.14	7.65	5.84	4.82	4.15	3.68

Table 6-5 Stimulated Volume (m^3) for Stage 16

Porosity	Ratio= x_3/x_2					
	2	4	6	8	10	12
0.001	1230400.00	1230400.00	1230400.00	1230400.00	1230400.00	1230400.00
0.006	205066.67	205066.67	205066.67	205066.67	205066.67	205066.67
0.011	111854.55	111854.55	111854.55	111854.55	111854.55	111854.55
0.016	76900.00	76900.00	76900.00	76900.00	76900.00	76900.00
0.021	58590.48	58590.48	58590.48	58590.48	58590.48	58590.48
0.026	47323.08	47323.08	47323.08	47323.08	47323.08	47323.08
0.031	39690.32	39690.32	39690.32	39690.32	39690.32	39690.32
0.036	34177.78	34177.78	34177.78	34177.78	34177.78	34177.78
0.041	30009.76	30009.76	30009.76	30009.76	30009.76	30009.76

From the tables above, it can be seen that the stress change is largely controlled by fracture height. The change in minimum compressive stress will be similar in value for all fracture geometries that are close in height, despite the overall final stimulated volume or porosity. The width of the fracture will also influence the stress change. The larger the width is compared to the height (i.e. a smaller ratio), the higher the minimum compressive stress change will be. An increase in ratio (the width is smaller compared to the height) for a constant porosity leads to an overall decrease in the magnitude of stress change at the next injection point. This can be seen in Figure 6-3 below.

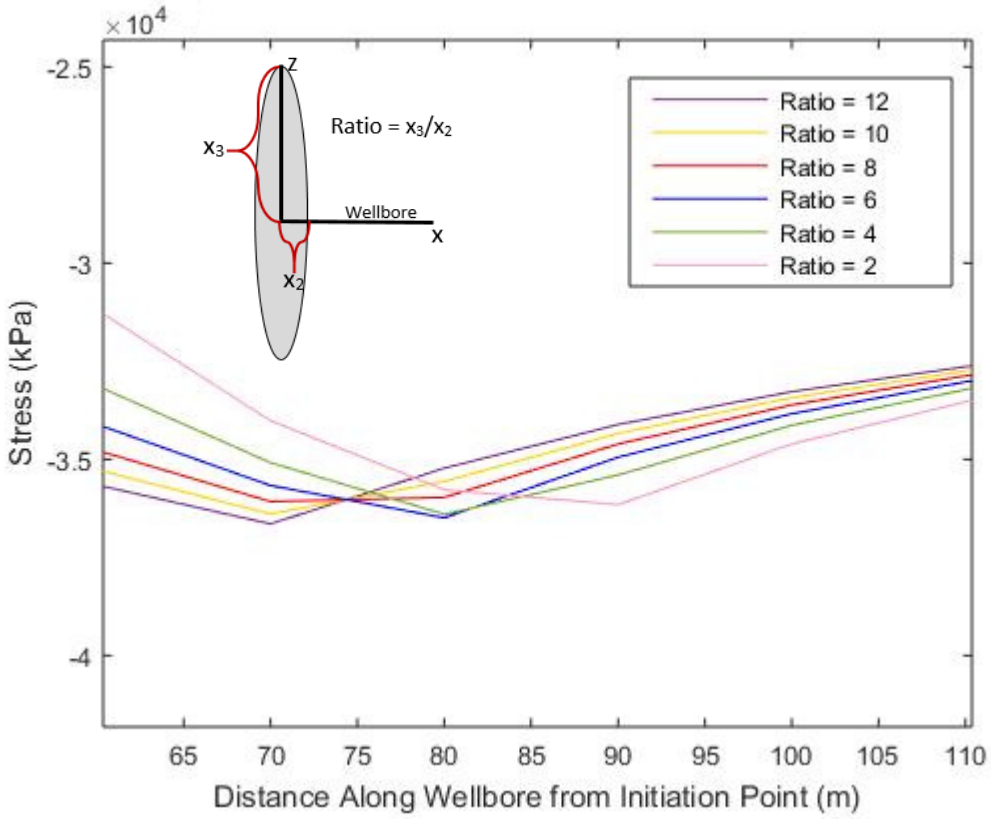

Figure 6-3 Change in σ_1 for a constant $\Delta\phi = 0.011$

The relationships presented in Figure 6-3 for a constant porosity and a decreasing ratio are as follows:

- Height decreases as ratio decreases
- Width increases as ratio decreases
- Stress increases as ratio decreases

- Stimulated volume remains the same

The proportional decrease in fracture width leads to a decrease in the overall stress change. The fracture is greater in height as the ratio increases, but it is getting thinner overall which causes the stress change to be smaller. It should be noted that the stress change is not dependent solely on width. The overall ratio of height to width must be considered. A fracture with a large width compared to the height will cause larger stress changes than a fracture with an equivalent width but with a much longer height. An example taken from the outputs of case 1 is presented in the table below.

Table 6-6 Comparison of Stress Change for a Constant Width

Fracture Width (m)	Fracture Height (m)	Fracture Volume (m^3)	Ratio	$\Delta\phi$	σ_1 at Next Injection Point (kPa)
12.68	25.36	34177.78	2	0.036	-36661
12.68	152.19	1230400.00	12	0.001	-31335

It can be seen from the table above that the ratio of 2 produces a larger overall stress (36.7 MPa) than a ratio of 12 (31.3 MPa) despite the fractures having the exact same width.

Similar fracture heights produce similar changes in overall stress despite the ratio and porosity of the stimulated area. This can be seen in the table of case 1 data below.

Table 6-7 Comparison of Stress Change for a Constant Height

Fracture Height (m)	Fracture Width (m)	Fracture Volume (m^3)	Ratio	$\Delta\phi$	σ_1 at Injection Next Point (kPa)
47.45	11.86	111854.55	4	0.011	-35398
47.94	7.99	76900.00	6	0.016	-35320
48.19	6.02	58590.48	8	0.021	-35288
48.34	4.83	47323.08	10	0.026	-35270

The heights are within 1 m of each other and the resulting change in stresses are all approximately 35.3 MPa despite the volumes, ratios, porosities and widths of the fractures varying by significant amounts.

Figure 6-44 illustrates the minimum horizontal stress change along the wellbore for a constant ratio and a range of porosities. The relationships presented in Figure 6-4 for a constant ratio and an increased change in porosity are as follows:

- Height decreases as change in porosity increases
- Width decreases as change in porosity increases
- Stress increases as change in porosity increases
- Stimulated volume decreases as change in porosity increases

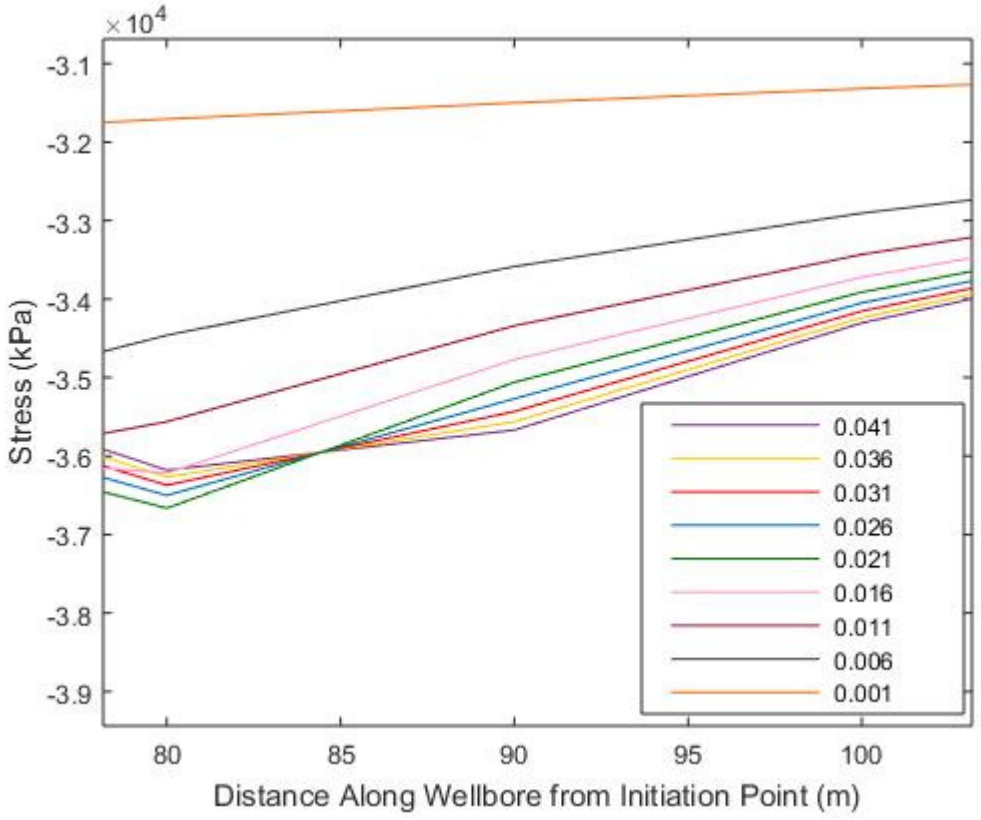

Figure 6-4 σ_1 along the Wellbore for a constant ratio of 10 and a range of porosities

The minimum compressive stress at the initiation point will increase with increasing porosity if the ratio is held constant. The height, width, and stimulated volume of the fracture will decrease as the porosity increases if the ratio is held constant. This means that the minimum compressive horizontal stress at the next initiation point will increase as the stimulated volumes decreases in width, height, and stimulated

volume. This may seem fairly counter-intuitive; however, as shown above, the change in stress is heavily dependent on fracture geometry (ratios of width to height) rather than how large the stimulated area is. For a constant ratio and a changing porosity, the height still has an inverse relationship to the stress change. This suggests that height can give a good approximation of how much stress around a stimulated volume will change despite other changing variables. The final stress at the next initiation point vs the height of the stimulated volume is plotted below in Figure 6-5.

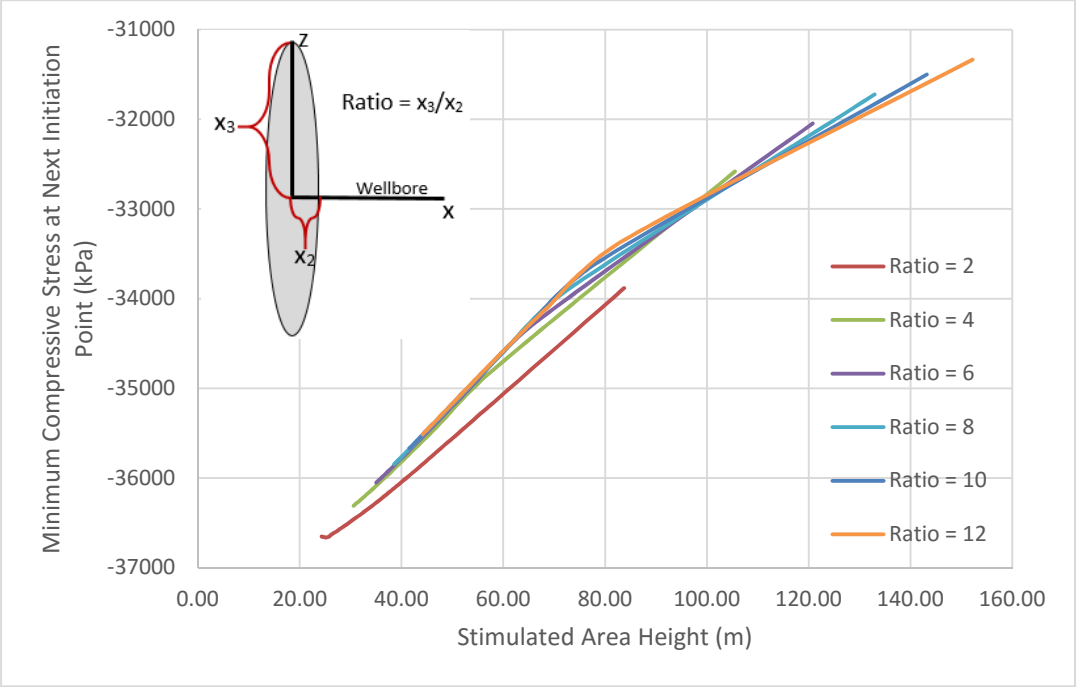

Figure 6-5 Minimum Compressive Stress at next Initiation Point based on Final Fracture Height

In Figure 6-5, the change in porosity decreases with increasing height. The data from the stimulated area with a ratio of 2 does not fit with the rest of the data. This could be due to the elliptical integration (Igor 2005) used in Matlab. The function becomes less accurate the more the ellipsoid tends towards a sphere.

In Figure 6-3 and 6-4 above, there is an inflection point in each set of data where σ_1 goes from increasing in compression to decreasing back towards the undisturbed stress state. In Figure 6-3, for all ratios at a $\Delta\phi$ of 0.011, σ_1 is aligned with σ_{22} (y-direction) initially before it becomes realigned with σ_{11} (x-direction) along the wellbore. The inflection points represent the point at which this change occurs which

will be referred to as the crossover point. The stress change in the x-direction initially is so large that it is no longer the minimum compressive stress (σ_1). The crossover points range from approximately 70-90 m away from the initiation point in Figure 6-3. In Figure 6-4, for a constant ratio of 10, the crossover points fall between 80 and 90 m away (approximately at 85 m) from the initiation point for a $\Delta\phi$ between 0.041 – 0.016. The fractures created by a $\Delta\phi$ between 0.011 and 0.001 do not have inflection points. The stress change these $\Delta\phi$ values produced did not cause σ_1 to become aligned with the y-direction at any point. It is important to note that stage 17 will begin propagating after the inflection points in all cases so σ_1 will be aligned with the x-direction and no fracture rotation will occur.

Figure 6-6 shows the minimum horizontal stress value at the initiation point of stage 17 for a variety of ratio and porosity values. The red dots show where the closest values to the desired breakdown pressure of 34.4 MPa were achieved. The red line represents 34.4 MPa.

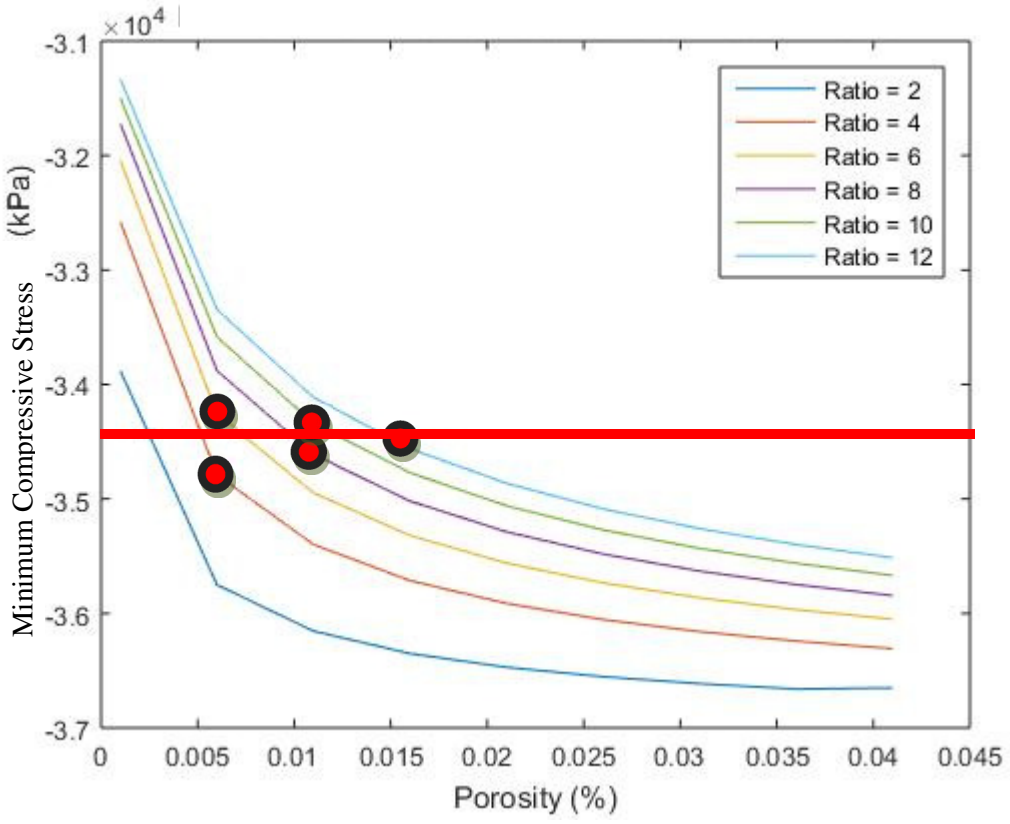

Figure 6-6 σ_1 at Initiation point of Stage 17 for various ratio and porosity values

The table below shows the selected values presented in Figure 6-6 above and compares them to the desired stress change of 34.4 MPa.

Table 6-8 Selected Fracture Geometries and Stresses

Ratio	$\Delta\phi$	Stress at Initiation Point (kPa)	$p_b - \sigma_1$ (kPa) (% change)	Fracture Height (m)	Fracture Width (m)
4	.006	-34790	390 (1.13%)	58.07	14.52
6	.006	-34259	-141 (-0.41%)	66.47	11.08
8	.011	-34611	211 (0.61%)	59.78	7.47
10	.011	-34340	-60 (-0.17%)	64.40	6.44
12	0.016	-34561	161 (0.47%)	60.40	5.03

6.1.3 Energy Dissipated by Fracture

The energy dissipated by fracture at stage 16 for a range of ratios and porosity values is plotted in Figure 6-7.

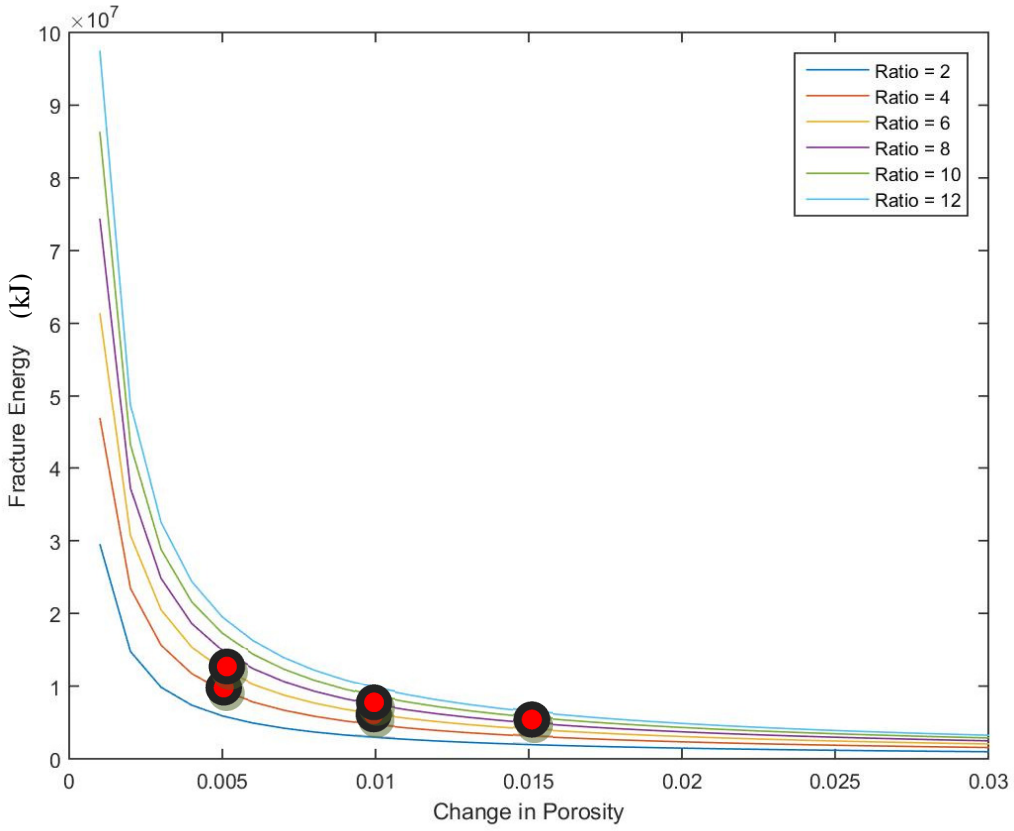

Figure 6-7 Energy Dissipated by the Fracture for Case 1 – Stages 16 to 17

It can be seen that less energy is dissipated by fracture when the ratios of the ellipsoid are small. The overall energy dissipated decreases in general as the change in porosity increases. It can be seen that all ratios begin to approach the same value of energy dissipation as the change in porosity increases past 3%.

6.1.4 Energy Minimization

The total change in energy caused by the inclusion at stage 16 in case 1 is presented in Figure 6-8. The overall change in energy for all ratios starts fairly high and then drops to a minimum as the porosity increases. The change in energy then begins to increase again with increasing porosity.

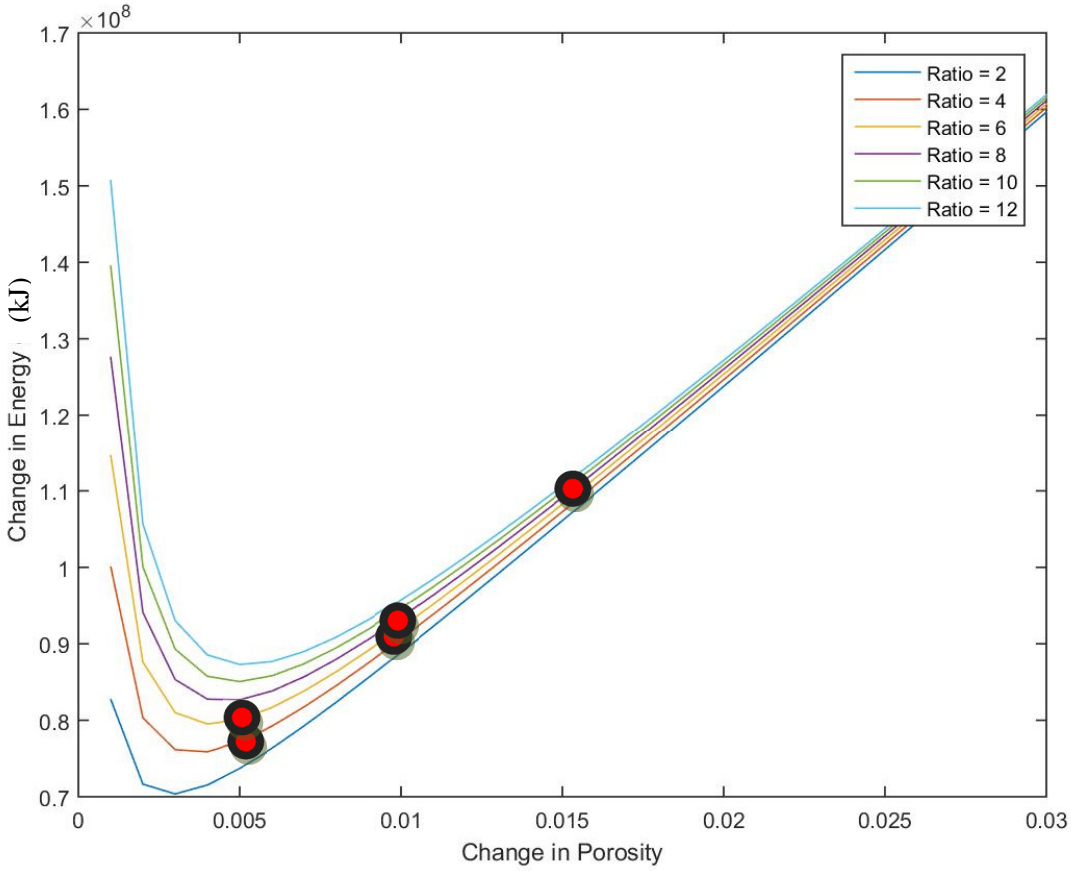

Figure 6-8 Total Change in Energy due to Inclusion at Stage 16

The graph suggests that the stimulated area most likely to form if we are considering energy minimization is the ellipsoid produced by a ratio of 4 and a change in porosity of 0.6 %. The final dimension of the

ellipsoid would be 58.07 m in the z-direction and y-direction (vertical and perpendicular to the well respectively) and 14.52 m in the x-direction (along the well).

6.1.5 Observations and Comments

Appendix A contains several graphs showing stress changes along the well for varying fracture geometries and formation porosities. It can be seen in the graphs in Appendix A that the extent of the stress alteration is dependent on fracture width and height. The final geometry that is selected through the method of energy minimization has a large width for a stimulated area, however it is not unreasonable. The program looks at the overall stimulated area rather than a single planar fracture. A single planar fracture may not have a width with semi-axis of 14.52 m, but a multi-branching fracture could potentially have branches which extend far enough out to create a large overall stimulated volume semi-axis width.

It can be seen that stimulated areas with a smaller width (large ratio value) and overall smaller stimulated volume produce a greater change in energy, despite all having similar fracture heights (see Figure 6-8). The energy dissipated by the fractures which produce the appropriate stress shadow is fairly constant in value (see Figure 6-7). This suggests that the major change in total energy is caused by the total energy which is a sum of the total strain energy and the interaction energy. The interaction energy is dependent on the constant value of the three initial principal stresses and the injection volume. This suggests the change in strain energy is the driving force behind the energy minimization. It relies on the stimulated volume which varies between the fractures which cause the desired stress change.

The height of the fracture appears to be the determining factor on the magnitude of the stress change despite changes in ratio and porosity. Fracture width will also influence stress change, but it must be considered in conjunction with the overall fracture height. Interestingly, the final volume of the fracture does not seem to have a significant impact on the overall stress change when compared with the effects of geometry on the final stress state.

The rotation of fractures is likely to occur if the next fracture initiates close to the stimulated area. Figures 6-3 and 6-4 can be used to determine a rough estimate of the minimum distance between fractures

needed to prevent rotation. It should be noted that if the initiation point of the next stage falls before the inflection point (where $\sigma_{yy} < \sigma_{xx}$), then the trends identified in the above section will not hold. The reason for this has to do with the trend of $\sigma_1$before the cross over point. Figure 6-9 shows the stresses in the x, y, and z direction as well as the overall least principal compressive stress.

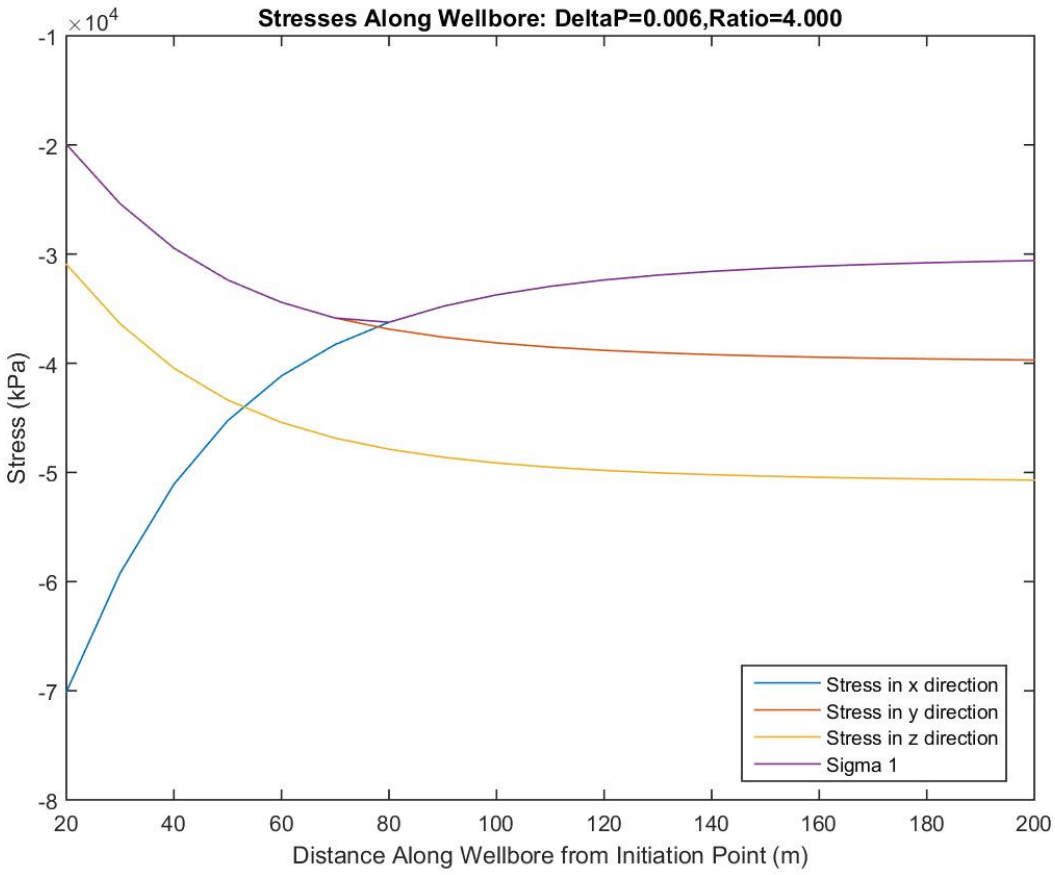

Figure 6-9 Stress along Wellbore

It can be seen from the figure above that $\sigma_1$is initially aligned with the stress in the y-direction and then changes to be aligned with stress in the x-direction. The trend of $\sigma_1$initially increases in compression as the stress in the y-direction increases to its original *in situ* state before hitting the inflection point where the stress in the x-direction becomes σ_1 and begins to decrease to its original *in situ* state. If σ_1 is along the y-direction, the trends relating height, width, porosity, and ratios will need to be re-examined.

6.1.6 Stages 18 – 19

Similar trends were seen when the stress change between stages 18 and 19 were modelled. The stress went from 29.1 to 33.4 in between stages 18 and 19. Tables 6-9 through 6-11 summarize the results of the modelling below:

Table 6-9 Minimum Compressive Stress at Stage 19 due to Injection at Stage 18 (kPa)

Porosity	Ratio = x_3/x_2						
	2	4	6	8	10	12	14
0.001	-33950	-32617	-32070	-31742	-31515	-31347	-31217
0.006	-35879	-34886	-34337	-33947	-33645	-33399	-33193
0.011	-36299	-35514	-35048	-34701	-34422	-34188	-33987
0.016	-36503	-35841	-35433	-35122	-34866	-34649	-34459
0.021	-36628	-36049	-35683	-35400	-35164	-34962	-34783
0.026	-36643	-36195	-35862	-35601	-35382	-35192	-35024
0.031	-36612	-36304	-35997	-35755	-35550	-35371	-35212
0.036	-36587	-36390	-36104	-35877	-35684	-35515	-35363
0.041	-36568	-36459	-36192	-35977	-35795	-35634	-35489

Table 6-10 Height of Stimulated Area (m) for Stage 18

Porosity	Ratio = x_3/x_2						
	2	4	6	8	10	12	14
0.001	84.47	106.43	121.83	134.09	144.44	153.49	161.58
0.006	46.49	58.57	67.04	73.79	79.49	84.47	88.92
0.011	37.98	47.85	54.78	60.29	64.95	69.02	72.66
0.016	33.52	42.23	48.35	53.21	57.32	60.91	64.12
0.021	30.62	38.57	44.16	48.60	52.35	55.63	58.57
0.026	28.51	35.92	41.12	45.26	48.76	51.81	54.54
0.031	26.89	33.88	38.78	42.68	45.98	48.86	51.44
0.036	25.58	32.23	36.90	40.61	43.74	46.49	48.94
0.041	24.50	30.86	35.33	38.89	41.89	44.51	46.86

Table 6-11 Width (m) of Stimulated Area for Stage 18

Porosity	Ratio = x_3/x_2						
	2	4	6	8	10	12	14
0.001	42.23	26.61	20.30	16.76	14.44	12.79	11.54
0.006	23.24	14.64	11.17	9.22	7.95	7.04	6.35
0.011	18.99	11.96	9.13	7.54	6.49	5.75	5.19
0.016	16.76	10.56	8.06	6.65	5.73	5.08	4.58
0.021	15.31	9.64	7.36	6.08	5.24	4.64	4.18
0.026	14.26	8.98	6.85	5.66	4.88	4.32	3.90
0.031	13.44	8.47	6.46	5.34	4.60	4.07	3.67
0.036	12.79	8.06	6.15	5.08	4.37	3.87	3.50
0.041	12.25	7.72	5.89	4.86	4.19	3.71	3.35

The cells highlighted in green show the geometry and porosity values which yield the desired stress change. It is interesting to note in this case that only a .06% change in porosity produced a small enough stress change to be considered valid. The heights of the stimulated area are fairly similar, but do vary by about 10 m. The data follows the same trends as mentioned in the previous section where the height is the main controlling factor on the overall stress change at the next fracture point.

The final stress at in initiation point of stage 19 is presented below in Table 6-12 and Figure 6-10.

Table 6-12 Selected Fracture Geometries and Stresses

Ratio	$\Delta\phi$	Stress at Initiation Point (kPa)	$p_b - \sigma_1$ (kPa) (% change)	Fracture Height (m)	Fracture Width (m)
10	.006	-33645	245 (-0.73%)	79.49	7.95
12	.006	-33399	1 (0.00%)	84.47	7.04
14	.006	-33193	207 (0.62%)	88.92	6.35

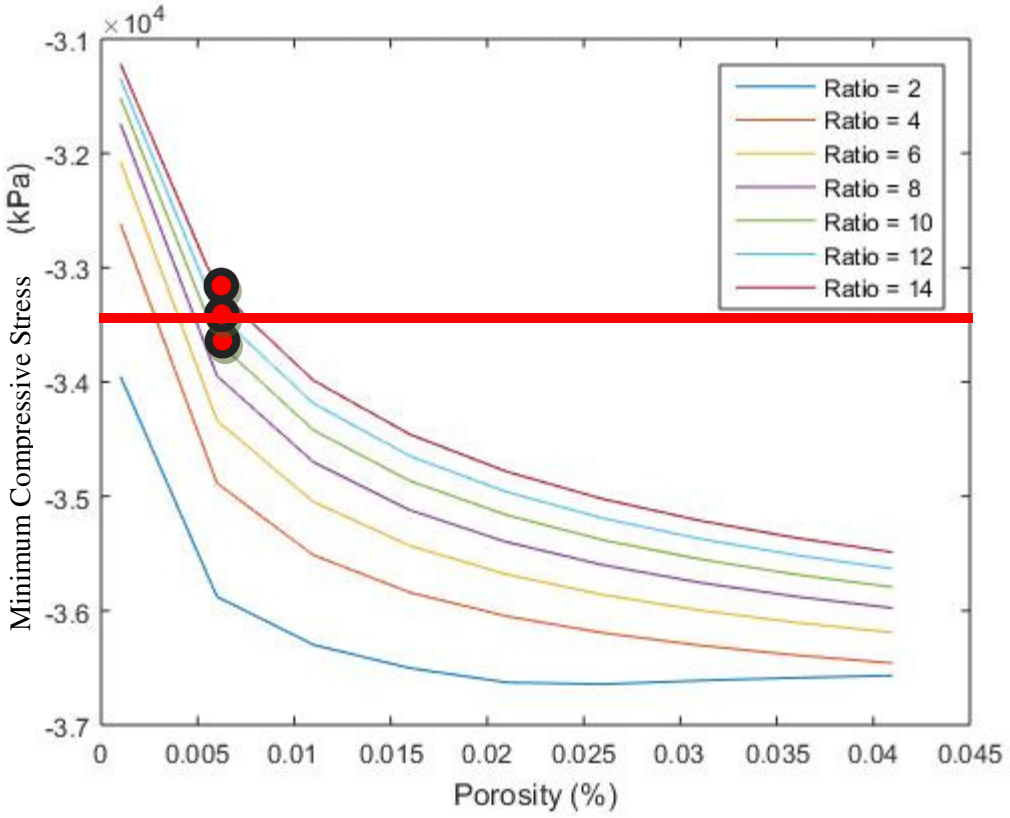

Figure 6-10 Minimum Compressive Horizontal Stress at Stage 19

The red line in Figure 6-9 represents the desired breakdown pressure of 33.4 MPa. It can be seen that the higher ratios, and therefore thinner fractures, produce a small enough stress change at the stage 19 to be considered valid. It appears as if smaller change in porosity values and larger ratios would produce a better representation of the stress change in this case. Energy dissipated by fracture and total change in energy are shown below.

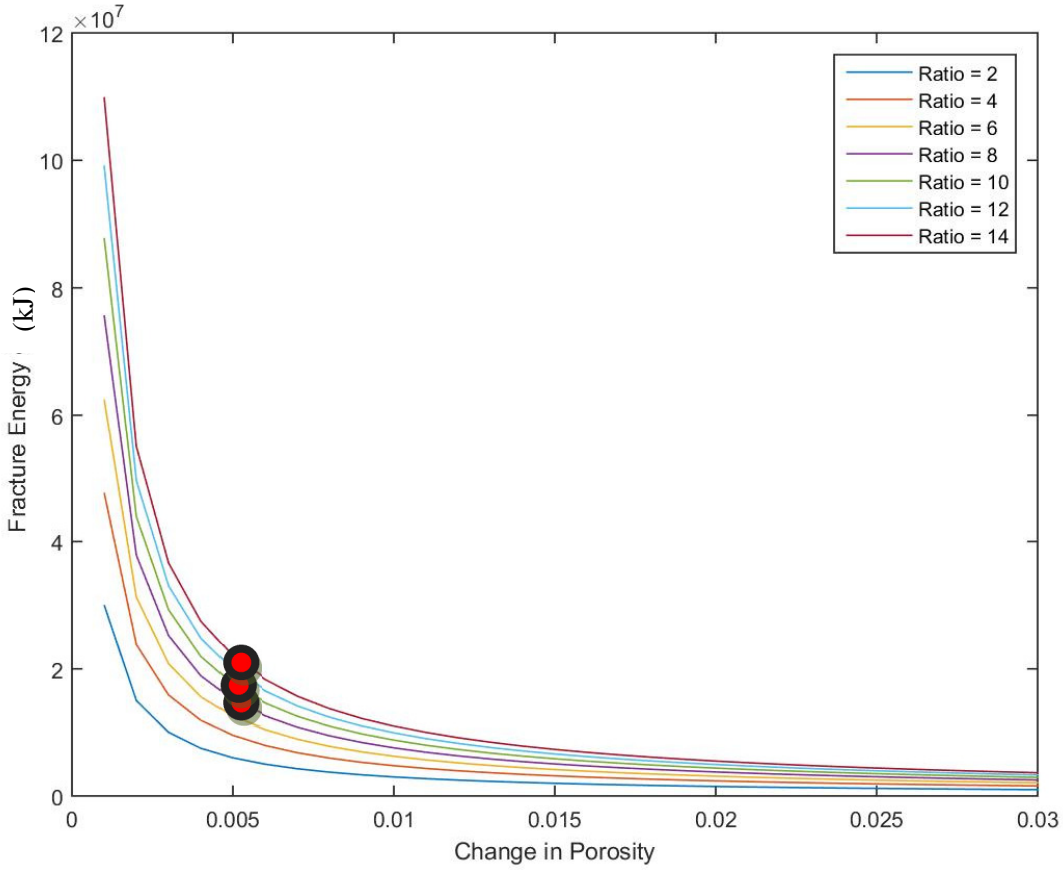

Figure 6-11 Energy Dissipated by the Fracture for Stage 18

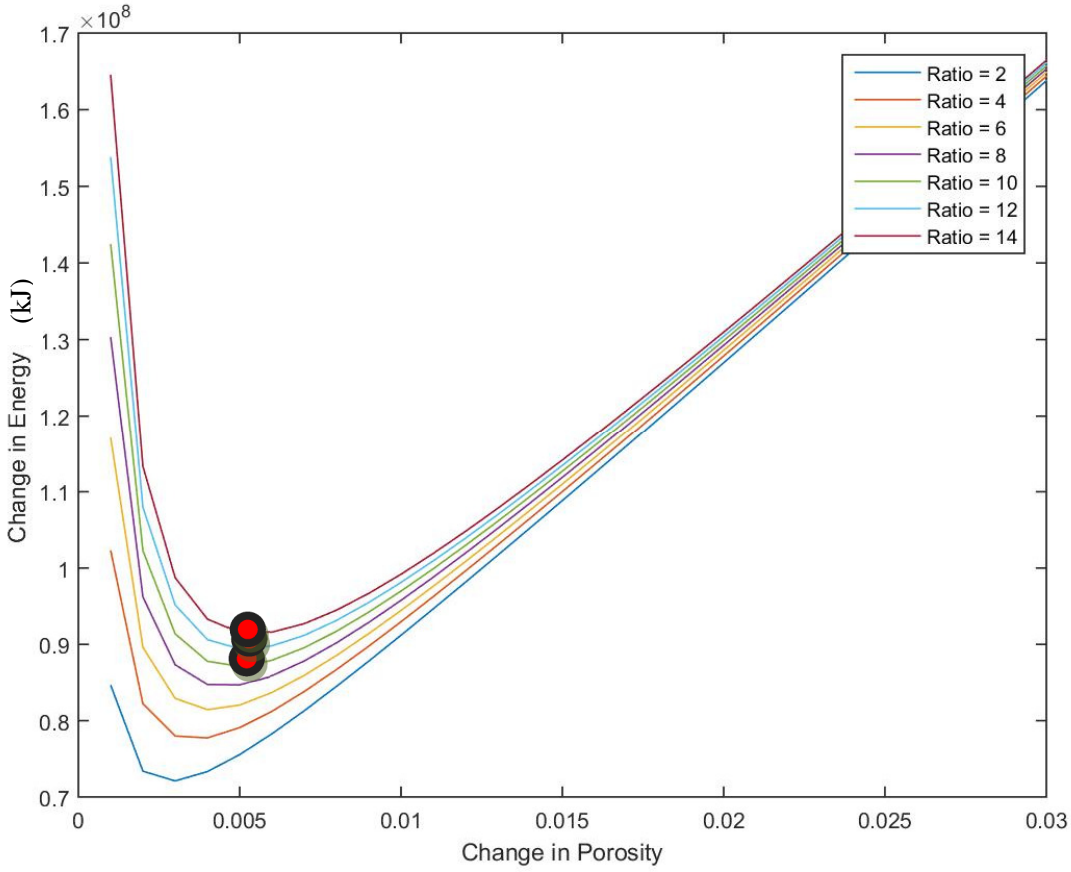

Figure 6-12 Total Change in Energy caused by Stage 18

The geometry which minimizes the change in energy is produced by a ratio of 10 and a change in porosity of .06%. The height of the fracture is 79.4 m and the width is 7.95 m.

The overall stress change between the stages in Case 1a (4.2 MPa) and in Case 1b (4.3 MPa) are very similar, as are the injected volumes (1230.4 and 1262.3 respectively); However, the heights produced by the program to achieve the desired breakdown pressures are fairly different between the cases. Case 1a fracture heights range from approximately 58 m to 66 m whereas case 1b heights are between 79 m to 88 m. By the analysis presented above, similar fracture heights should produce similar stress changes. This could be explained by the breakdown pressures recorded at the stages 16 and 18. At stage 16 the breakdown pressure is 30.6 MPa, which is fairly close to the input for σ_h for the program (30 MPa). The breakdown pressure at stage 18 is 29.1 MPa, suggesting that the minimum compressive horizontal stress

at that location might actually be lower than the assumed 30 MPa. If the program is run with a minimum compressive horizontal stress of 29.1, the heights which produce an approximate stress of 33.4 MPa at the next initiation point have heights that are very similar to case 1, suggesting that the input for minimum compressive stress should change based on the breakdown pressure. The results of using 29.1 as the initial *in situ* minimum compressive stress are presented in the table below:

Table 6-13 Fracture Geometries to produce 33.4 MPa at Stage 19 using 29.1 MPa as *In Situ* Minimum Compressive Stress

Ratio	$\Delta\phi$	Stress at Initiation Point (kPa)	$p_b - \sigma_1$ (kPa) (% change)	Fracture Height (m)	Fracture Width (m)
6	0.006	-33437.08	-37 (0.11%)	67.04	11.17
10	0.011	-33521.51	-122 (0.36%)	64.95	6.49
12	0.011	-33287.69	112 (-0.33%)	69.02	5.75
14	0.016	-33559.38	-159 (0.47%)	64.12	5.48

The fracture heights are much similar to case 1 if an original *in situ* value of 29.1 MPa is used. They range from 64.12 m to 69.02 m which match fairly well with the heights of 58 m to 66 m from case 1a. The overall change in stress is then 4.3 MPa from 29.1 to 33.4 MPa rather than 3.4 MPa change from 30 MPa to 33.4 MPa. The fracture which minimizes energy in this case has a ratio of 6, change in porosity of 0.06%, a fracture height of 67.04, and a width of 11.17.

6.2 Case 2 – Breakdown not achieved

Well C consists of 17 stages in an open hole system fractured with slickwater. The total vertical depth of the well is 2130 m. Several stages were stimulated with a volume that was higher than the average injected volume for the stages. The intervals following them were unable to be fractured by the pressures and rates achievable by the pumps. Figure 6-13 and Figure 6-14 show the breakdown pressures and injected volumes respectively.

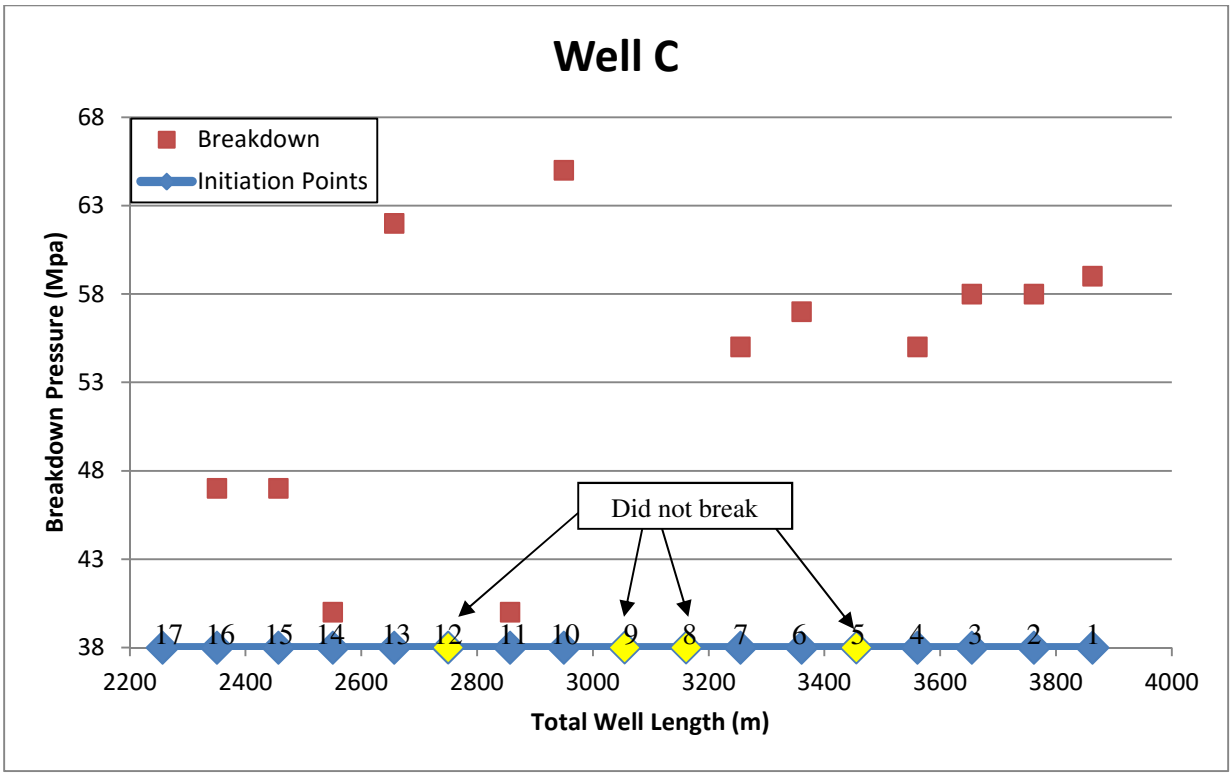

Figure 6-13 Breakdown Pressures along well

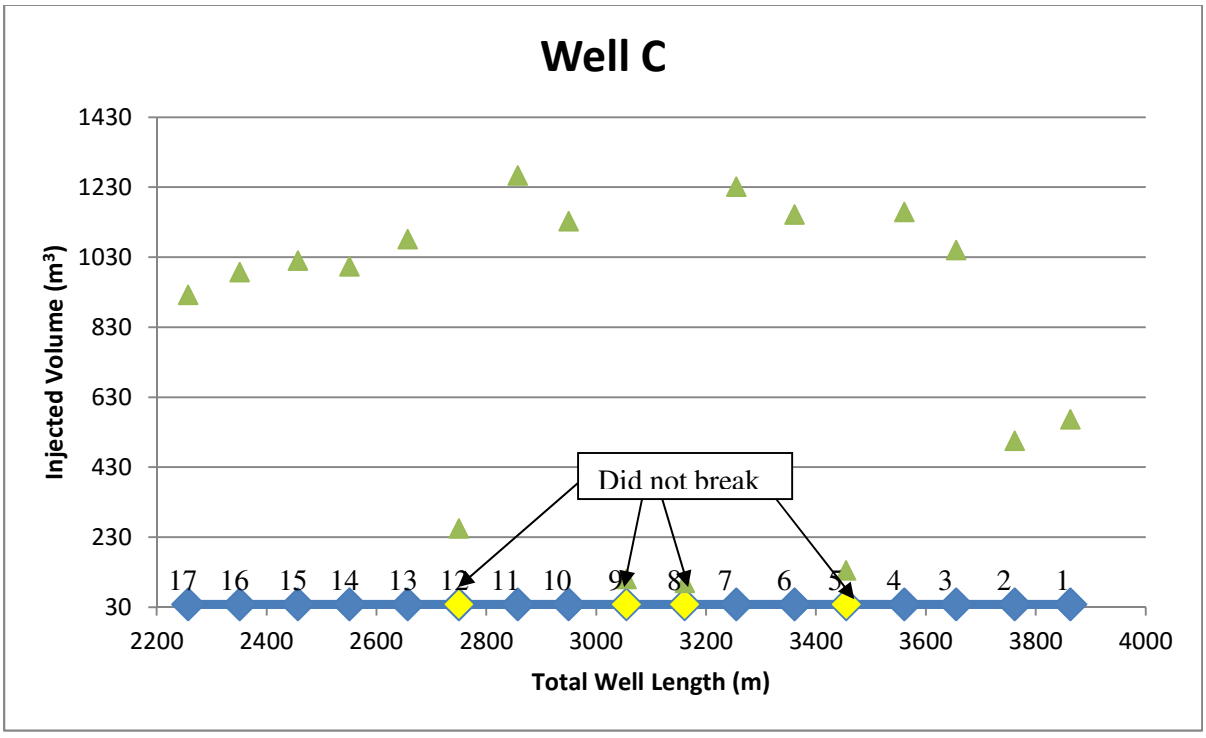

Figure 6-14 Injection Volumes along well

All intervals that could not be broken were subjected to pressures between 60 and 65 MPa. Interval 10 was able to be fractured at 65 MPa, which is significantly higher than the average p_b of 53.5 MPa. It occurred after two intervals which could not be fractured, suggesting that the stress change from previous stages could be laterally extensive. There is also a significant difference between the p_b values for intervals 10 (65 MPa) and 11 (40 MPa). Again, if the formation was stressed enough that the minimum compressive horizontal stress was increased to be close in magnitude to the maximum horizontal stress, there is the possibility of fracture rotation.

6.2.1 Model Inputs

The inputs for the geomechanical properties of the model can be found in Section 5.4. The average values of the geomechanical properties were used for the initial model. The initial *in situ* stress conditions are considered to be 51 MPa, 45 MPa, and 40 MPa for $\sigma_v, \sigma_H,$ and σ_h respectively as determined by density logs and field testing outlined in Chapter 2. These numbers were taken from field data. Table 6-14 summarizes the intervals in this well.

Table 6-14 Interval Data for Well C

Interval	Total Injected Volume (m^3)	p_b (MPa)	Distance from Previous Zone (m)
1	565.8	59	First Stage
2	505.4	58	101
3	1050.0	58	107
4	1158.6	55	94
5	134.4	Did Not Break	110
6	1151.1	57	94
7	1230.4	55	106
8	99.5	Did Not Break	94
9	110.4	Did Not Break	106
10	1132.0	65	105
11	1263.2	40	93
12	254.6	Did Not Break	107
13	1080.7	62	93
14	1002.9	40	106
15	1019.0	47	94
16	986.3	47	106

After the 12th interval the injection volume was lowered to between 900 m^3 and 1000 m^3 which resulted in no more missed intervals. The stress change between stages 4 and 5 is examined to determine what maximum injection volume and geometry will produce a stress of less than 65 MPa. It is assumed that if the stress is at 65 MPa or below, the fracture can be initiated. It should be noted that it is very likely that due to injection, the minimum compressive horizontal stress will actually increase beyond the vertical and maximum horizontal stress. If this is the case, the fracture is likely to propagate horizontally along the well. This could be a major factor in why the stages are not initiating properly. However, in this model the semi-axes of the z and y-directions are set to be equal, meaning the stress change in the z-direction will be equivalent in value to the stress change in the y-direction, so it is unlikely that the maximum compressive horizontal stress will increase beyond the vertical stress.

6.2.2 Calculated Stress Changes for Stage 4 to Stage 5

Appendix B shows the stresses in the x, y, and z-directions, as well as σ_1 along the wellbore. It can be seen that the σ_1 mostly aligns with the y-direction rather than the x-direction.

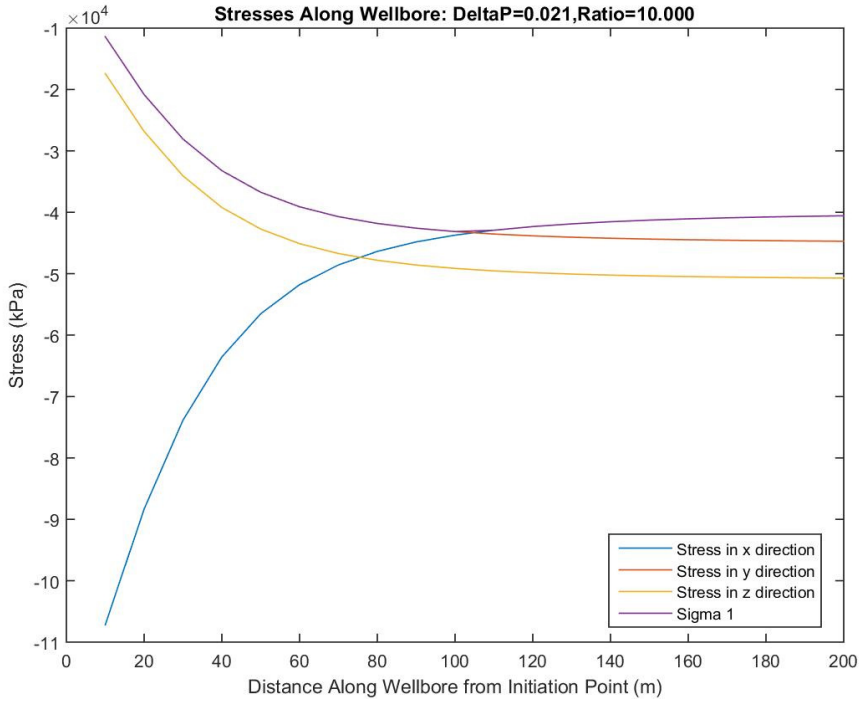

Figure 6-15 Stress along Wellbore for Case 2

In Figure 6-15, the minimum compressive stress is aligned with the y-direction (perpendicular to the well) for a large section of the well. The cross over point occurs around 105 m from the initiation point, where σ_1 realigns with σ_{11} in the x-direction. In this case the fracture in stage 5 (110 m from stage 4) would have initiated perpendicular to the wellbore, however that is not the case for all ratio and porosity combinations in the data set. Many of the inflection points occur just before or just after 110 m from the initiation point of stage 4 (which is the initiation point of stage 5). Fractures that start in areas where σ_1 is aligned with the y-direction do not follow the trends of stress decrease and increase identified in case 1. The fractures in case 1 all initiated in areas where σ_1 is along the wellbore.

Tables 6.15 through 6.17 summarize the stress changes and geometries which are produced when the injected volume is 1158.6 m^3.

Table 6-15 Minimum Compressive Stress at Stage 5 due to Injection at Stage 4 (kPa)

Porosity	Ratio = x_3/x_2					
	2	4	6	8	10	12
0.001	-42412.4	-41762.3	-41460.4	-41266.6	-41126.9	-41019.8
0.006	-43190.6	-42810	-42581.8	-42411	-42272.9	-42156.9
0.011	-43329.7	-43055.4	-42874.9	-42734.6	-42617.8	-42517.2
0.016	-43294.4	-43176.9	-43024.6	-42904	-42802.1	-42713.1
0.021	-43273.2	-43251.9	-43118.7	-43011.9	-42920.8	-42840.6
0.026	-43258.7	-43303.8	-43184.4	-43087.9	-43005.1	-42931.7
0.031	-43248.1	-43328.9	-43233.5	-43145.1	-43068.8	-43000.9
0.036	-43240	-43313.9	-43271.8	-43189.9	-43119	-43055.6
0.041	-43233.4	-43301.9	-43302.8	-43226.3	-43159.8	-43100.3

The trend of decreasing stress as the ratio increases for a constant change in porosity is not consistent for several constant change in porosity values, in particular for 0.041. The stress increases as the ratio increases before decreasing again. This is due to σ_1 rotation. Figure 6-16 shows the stress at the midpoint of stage 5 caused by the stimulated area at stage 4.

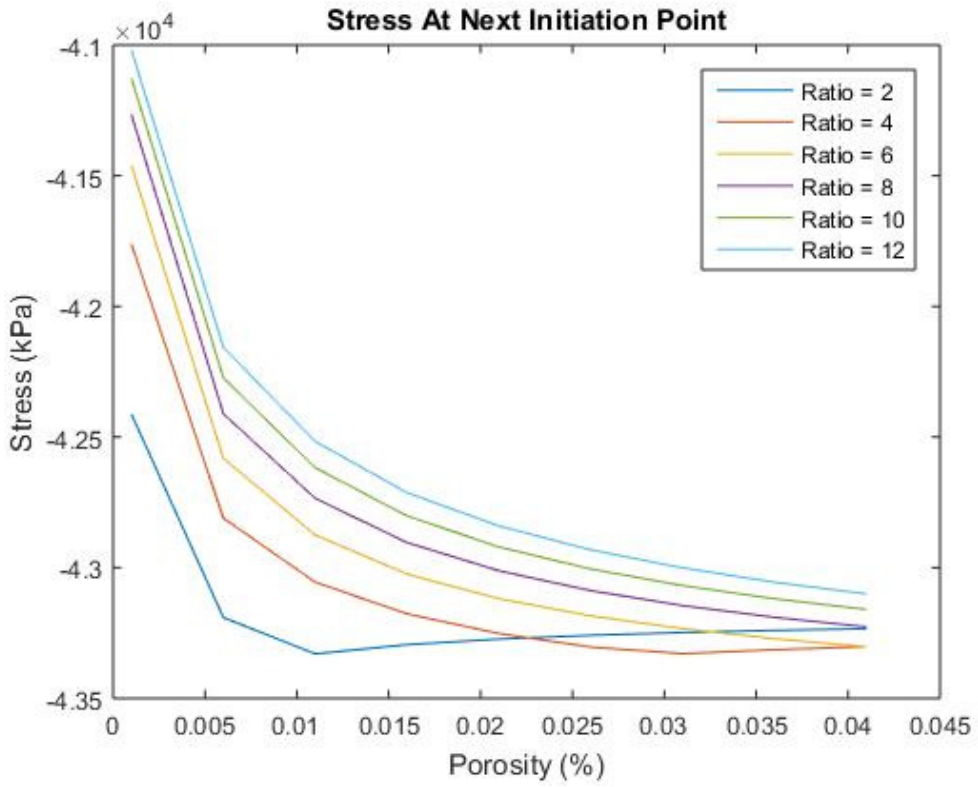

Figure 6-16 Minimum Compressive Stress at Stage 4

Figure 6-16 shows that the stress at stage 4 decreases with porosity for most ratios, however for ratios of 2 and 4 the stress increases after a porosity change of 0.006 and 0.031 respectively. The cross over point occurs after the 110 m distance between the two intervals, so the fractures with ratios and change in porosity values mentioned above begin to grow in a stress state where the minimum compressive stress is not aligned with the wellbore.

It can be seen from the table and figure above that no ratio and porosity combination produced a stress change near 65 MPa, suggesting that it was possible to fracture the interval if only stress shadowing is considered. However, if the breakdown pressures for the interval are examined, it can be seen that the first breakdown pressure (59 MPa), in what is theoretically undisturbed rock, is much higher than the *in situ* minimum compressive stress estimate (along the wellbore) of 40 MPa. Even if we consider the breakdown pressure as an upper bound for the minimum compressive stress, it is unlikely that the breakdown pressure would be 19 MPa higher than the closure pressure of the formation. The assumed

initial *in situ* stresses may be incorrect. A breakdown pressure of 59 MPa is significantly higher than the assumed maximum compressive stress of 51 MPa. If the well is to be analyzed, a better understanding of the undisturbed stresses are required.

From the analysis above, it can be concluded that a stress increase to 65 MPa is not achieved at stage 5. The principal stresses would all have to increase significantly along the wellbore past their initial values in order for 65 MPa to be the least principal compressive stress. This suggests that there may be more than stress shadowing causing the issues with breakdown pressure.

6.2.3 Stress Changes for Various Stages along the Well

More data is needed to explain the jumps in breakdown pressure along the well. It is very likely that the assumed undisturbed *in situ* stresses in each of the three principal directions are incorrect. There is also the possibility that the stress regime changes partly down the well. The following is an analysis of the stages along the well.

The first three stages with breakdown pressures of 59, 58, and 58 MPa likely did not experience stress interference. The first stage is in undisturbed rock and has a low injection volume (565.8 m^3). The second stage also has a low injection volume (505.4 m^3). The injection volume of stage 1 does not cause enough of a stress change to affect stage 2 which is 101 m away, nor does the low volume of stage 2 effect the stresses at stage 3. For modelling purposes, if all stresses in the principal directions are assumed to be equal to 58 MPa (as it is unknown which direction is actually the minimum compressive stress, and the magnitudes of stress are also unknown), it can be seen that low injection volumes in stages 1 and 2 have little effect on the stress 101 m away. This assumption of equal stresses for modelling purposes will be explained in more detail in Section 6.2.4.

The majority of the final stress values predicted by the program at stages 2 and 3 are very close in value to 58 MPa, with the closest being highlighted in green in the tables below. The final stress values range from 57.8 to 58.5 MPa with an average value of 58.0 at stage 2, and 57.2 to 57.6 MPa, with an average value of 57.3 MPa at stage 3.

Table 6-16 Minimum Compressive Stress at Stage 2 due to Injection at Stage 1 (kPa)

Porosity	Ratio					
	2	4	6	8	10	12
0.001	-58139	-58335	-58434	-58499	-58548	-58586
0.005	-57927	-58028	-58091	-58140	-58180	-58214
0.011	-57888	-57962	-58010	-58049	-58081	-58109
0.016	-57870	-57930	-57970	-58003	-58030	-58055
0.021	-57860	-57911	-57946	-57974	-57998	-58020
0.026	-57853	-57898	-57928	-57954	-57976	-57995
0.031	-57847	-57888	-57916	-57939	-57959	-57977
0.036	-57843	-57880	-57906	-57927	-57946	-57962
0.041	-57840	-57874	-57898	-57918	-57935	-57950

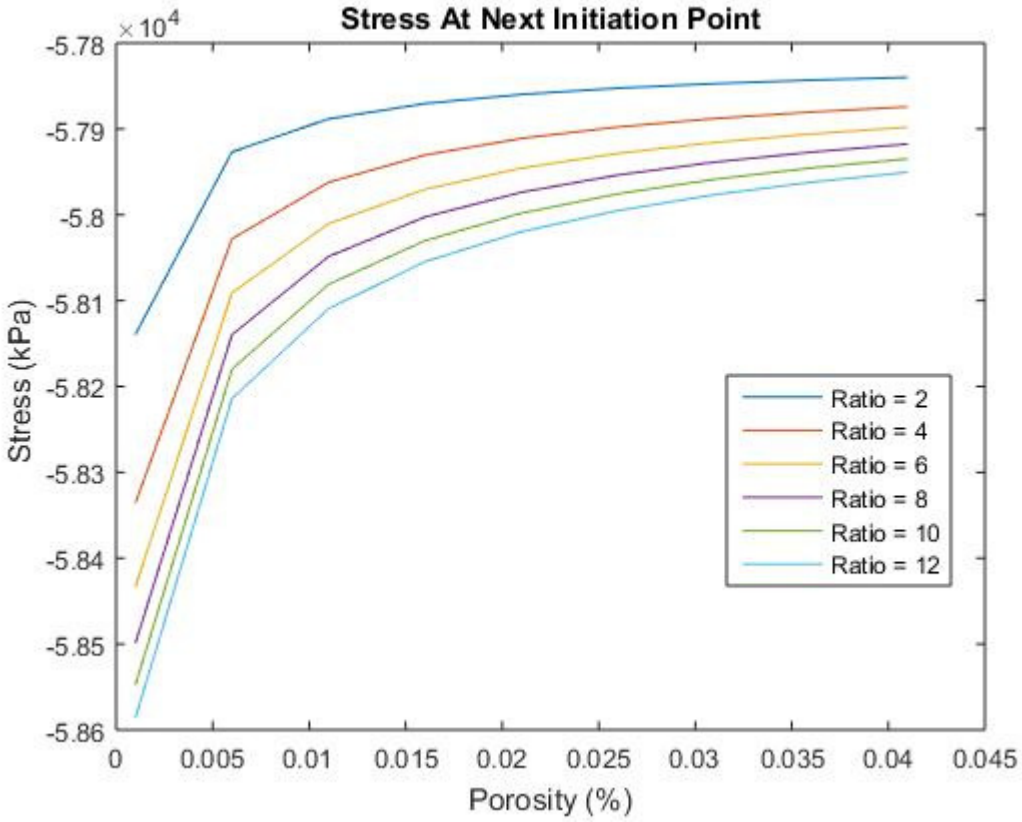

Figure 6-17 Minimum Compressive Stress at Stage 2 due to Injection at Stage 1

Table 6-17 Minimum Compressive Stress at Stage 3 due to Injection at Stage 2 (kPa)

Porosity	Ratio = x_3/x_2					
	2	4	6	8	10	12
0.001	-57381	-57499	-57563	-57606	-57640	-57667
0.006	-57262	-57317	-57353	-57381	-57404	-57425
0.011	-57241	-57281	-57307	-57329	-57347	-57363
0.016	-57232	-57264	-57285	-57303	-57318	-57332
0.021	-57226	-57253	-57272	-57287	-57301	-57313
0.026	-57222	-57246	-57263	-57276	-57288	-57299
0.031	-57220	-57241	-57256	-57268	-57279	-57289
0.036	-57218	-57237	-57251	-57262	-57272	-57281
0.041	-57216	-57234	-57246	-57257	-57266	-57275

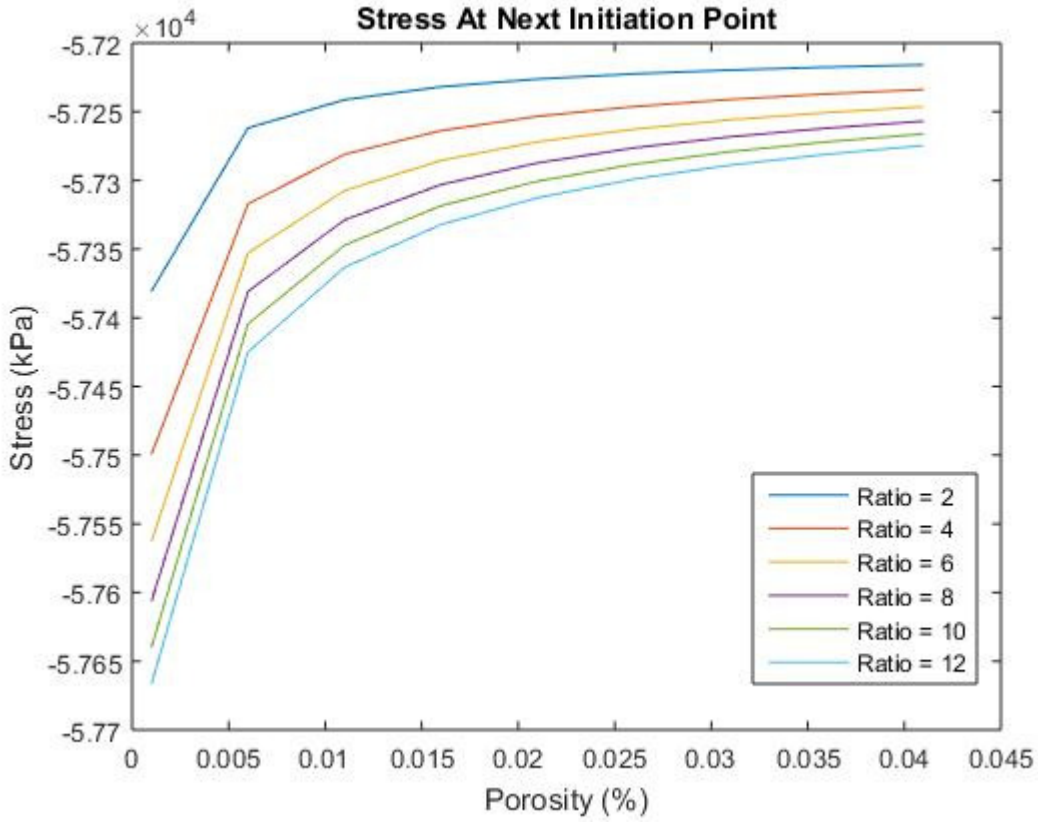

Figure 6-18 Minimum Compressive Stress at Stage 3 due to Injection at Stage 2

The trends in the data in Figure 6-17 and Figure 6-18 are opposite of those seen in case 1 as the initiation point is in an area where the least principal compressive stress is not aligned with the x-direction. Despite this, it is unlikely fracture rotation would be significant in Stage 3. The stresses in all directions are all

almost the same as they have all almost returned to their original *in situ* state. If the fracture was to grow laterally along the well, it would soon hit the point where all the stresses equalize and it would propagate equally in all directions. This is due to the assumption that $\sigma_h = \sigma_H = \sigma_v$. This assumption will be explained in more detail in Section 6.2.4. Figure 6-19 shows how the stresses approach each other at the injection point of stage 3.

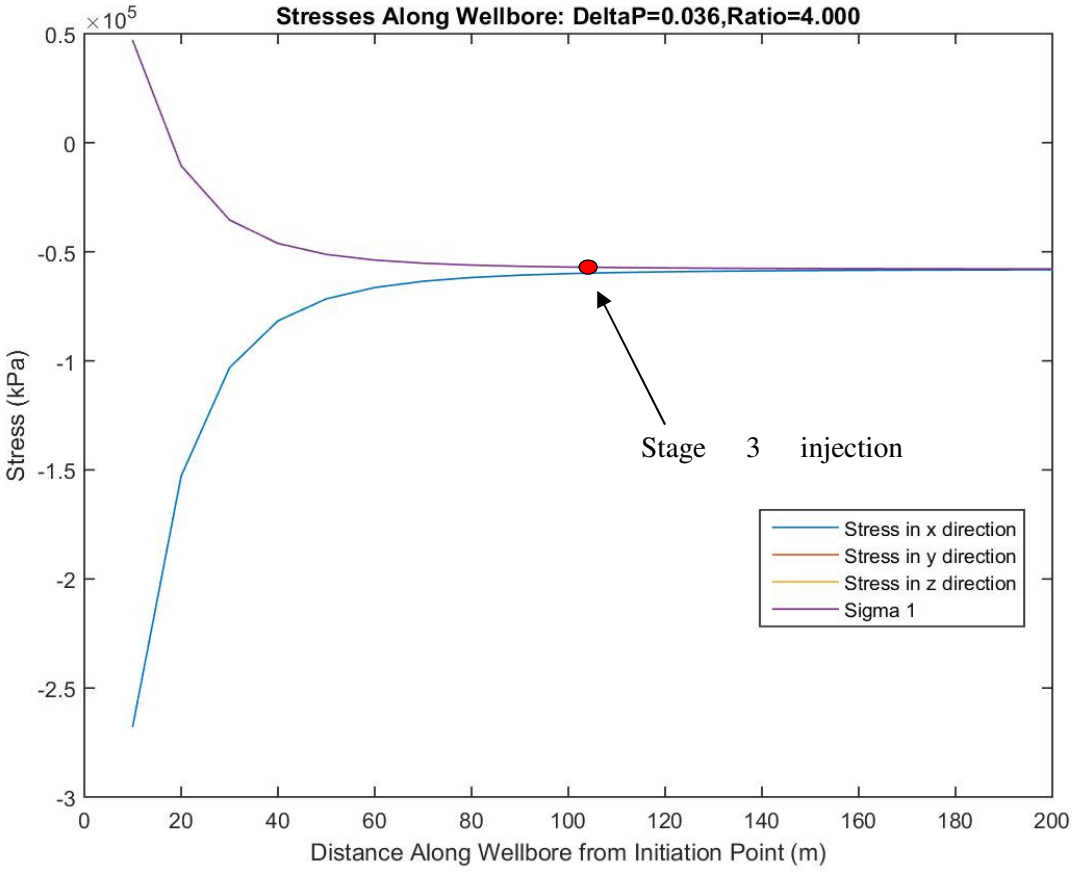

Figure 6-19 Stresses Caused by Injection at Stage 2

From the analysis above, and considering energy minimization, the most likely semi-axes lengths of the fracture at stage 1 are 44.82 vertically and 11.21 in the x-direction for a ratio of 4 and a change in porosity of 0.06%. Stage 2 will have a stimulated area half-length of 62.26 m the z-direction, and 5.19 m along the x-direction for a ratio of 12 and a change in porosity of 0.06%.

Stage 3 has a significantly higher injection volume (1050.0 m^3) than the previous stages. If we again assume 58 MPa as the stress in all directions from the breakdown pressure of stage 3, we can see that a change in stress from 58 MPa at stage 3 to 55 MPa at stage 4 is indeed possible given the data presented in the table and figure below. In this case, the minimum principal compressive stress is either in the y or z-direction.

Table 6-18 Minimum Compressive Stress at Stage 4 due to Injection at Stage 3 (kPa)

Porosity	Ratio = x_3/x_2					
	2	4	6	8	10	12
0.001	-56259	-56815	-57051	-57195	-57296	-57371
0.006	-55497	-55883	-56102	-56260	-56384	-56486
0.011	-55336	-55637	-55819	-55957	-56068	-56162
0.016	-55259	-55511	-55669	-55790	-55891	-55977
0.021	-55212	-55432	-55572	-55682	-55774	-55853
0.026	-55180	-55376	-55503	-55604	-55689	-55763
0.031	-55157	-55335	-55451	-55544	-55623	-55693
0.036	-55138	-55302	-55410	-55497	-55572	-55637
0.041	-55124	-55276	-55377	-55459	-55529	-55591

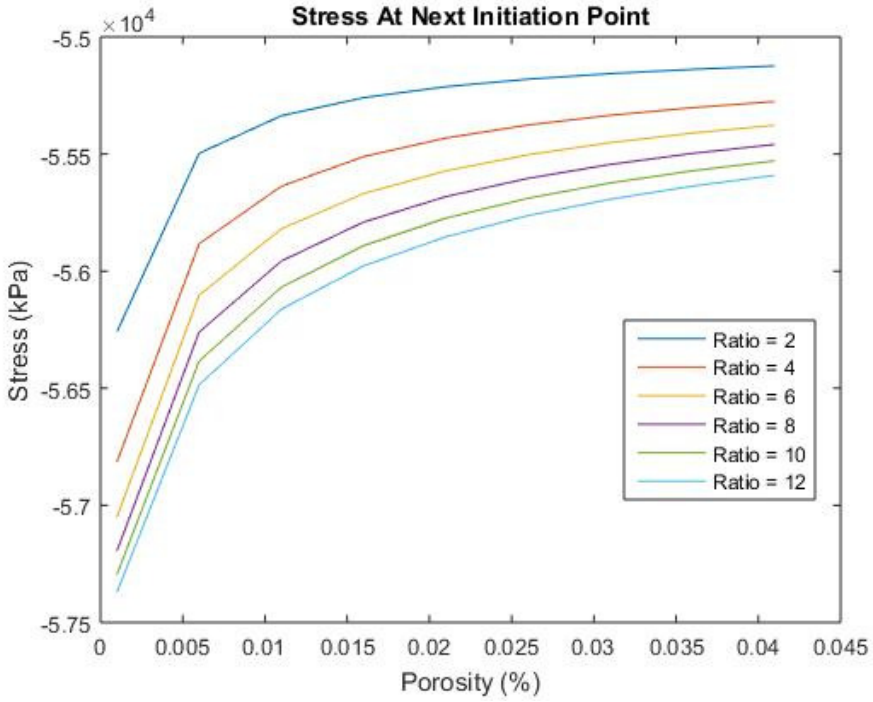

Figure 6-20 Minimum Compressive Stress at Stage 4 due to Injection at Stage 3

The stress at stage 4 predicted by the program ranges from 55.1 to 57.4 MPa, with an average value of 55.8 MPa. The fracture at stage 4 is likely to begin in a stress regime where the minimum compressive stress is no longer parallel to the wellbore. σ_1 is no longer aligned with the x-direction if the assumption is made that all directions begin with an equal stress. The fracture at stage 4 will likely be rotated and will no longer be perpendicular to the wellbore as the stresses 94 m from stage 3 are not yet converging to a single value, as seen in Figure 6-20 below.

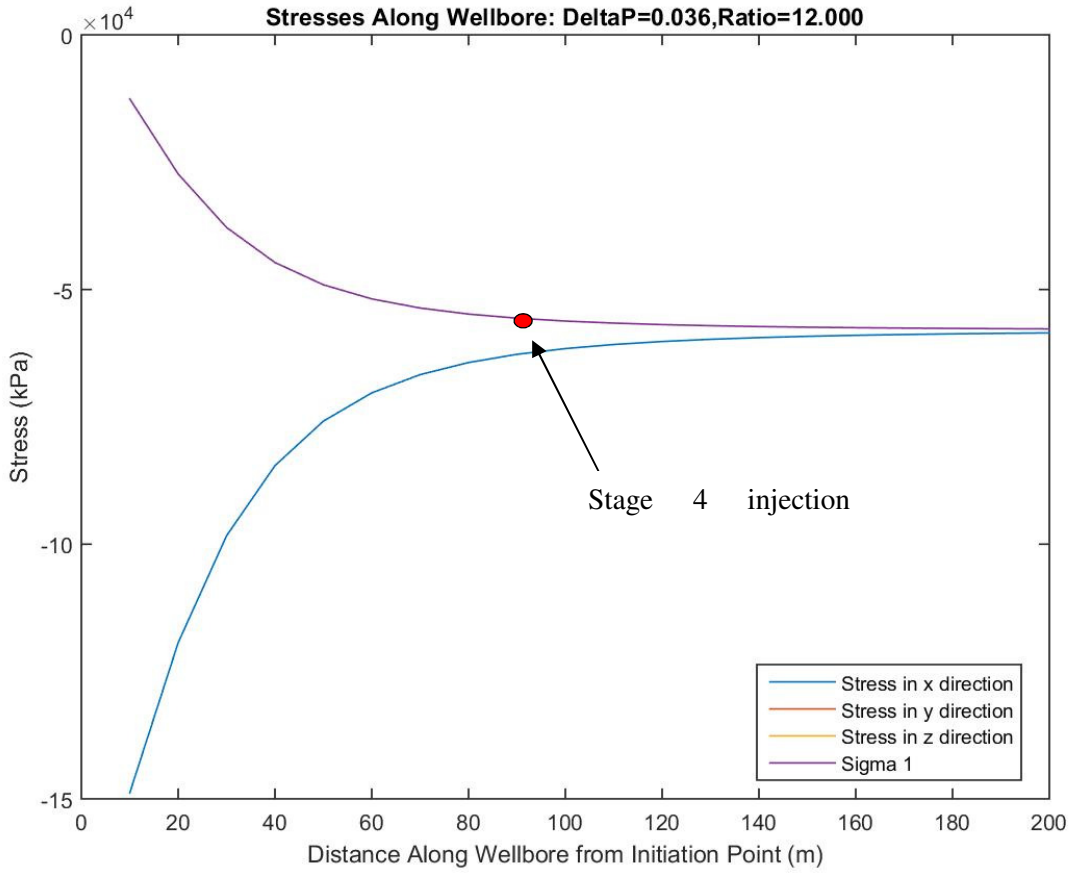

Figure 6-21 Stress caused by Injection at Stage 3

The most likely geometry of the fracture at stage 3 occurs at a ratio of 4 and a change in porosity of 0.31%. The length of the semi axes are 30.31 m and 7.58 m in the z and x-directions.

Without knowing the real value of the *in situ* stresses in the vertical and horizontal direction, it is not possible to know if the fracture is propagating along the wellbore or vertically. If the fracture is propagating along the wellbore, it could explain why stage 5 does not initiate. It is not possible to know anything about the fracture geometry at stage 4 as there is no stress information at stage 5.

Stage 6 likely begins in undisturbed rock as stage 5 did not initiate and no stress change would have occurred. The breakdown pressure at stage 6 is 57 MPa which is fairly close to the undisturbed breakdown pressure seen in stage 1. Stage 7 had a recorded breakdown pressure of 55 MPa. Using the program with $\sigma_v, \sigma_H,$ and σ_h set to 57 MPa, and an injection volume of 1151 m^3 at stage 6, we can see from the figure and table below that a stress change to 55 MPa at stage 7 could occur.

Table 6-19 Minimum Compressive Stress at Stage 7 due to Injection at Stage 6 (kPa)

Porosity	Ratio = x_3/x_2					
	2	4	6	8	10	12
0.001	-55799.8	-56122.4	-56272.5	-56368.8	-56438.3	-56491.6
0.006	-55414.2	-55602.7	-55715.8	-55800.5	-55869	-55926.6
0.011	-55340	-55481.2	-55570.6	-55640.1	-55698	-55747.8
0.016	-55305	-55421	-55496.4	-55556.1	-55606.6	-55650.7
0.021	-55284	-55383.9	-55449.8	-55502.7	-55547.8	-55587.6
0.026	-55269.7	-55358.2	-55417.3	-55465.1	-55506.1	-55542.4
0.031	-55259.2	-55339.1	-55393	-55436.8	-55474.5	-55508.2
0.036	-55251.2	-55324.4	-55374	-55414.5	-55449.7	-55481
0.041	-55244.7	-55312.5	-55358.7	-55396.5	-55429.5	-55458.9

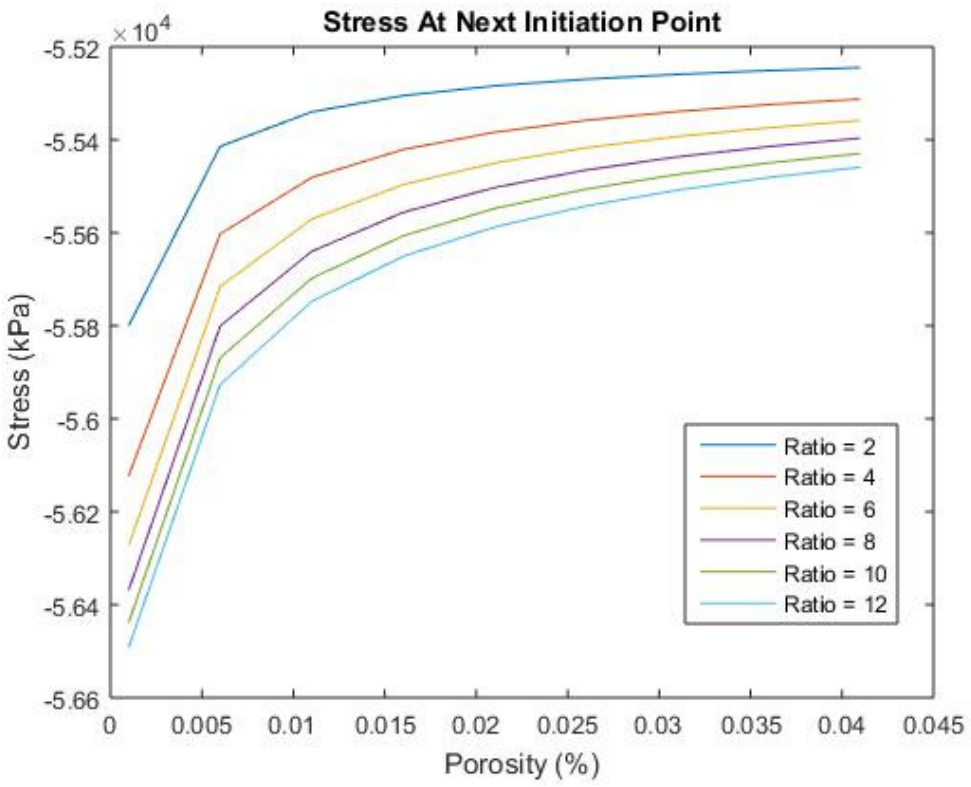

Figure 6-22 Minimum Compressive Stress at Stage 7 due to Injection at Stage 6

The stress at stage 7 predicted by the program ranges from 55.2 to 56. 5 MPa with an average value of 55.6 MPa. The stimulated area produced at stage 6 is likely 32.51 m in the z-direction (half -ength) and 16.25 m in the x-direction (half-width). A ratio of 2 and a change in porosity of 0.16% produces this geometry. Stage 7 has an injection volume of 1230 m^3 which is much higher than previous intervals. From the data above, it is likely that stage 7 began in a stress condition where the minimum compressive stress was no longer aligned with the well, suggesting that it is a rotated fracture. The high injection volume at stage 7, combined with the possibility of rotation, could have led to stages 8 and 9 not initiating.

The breakdown stress at stage 10 is 65 MPa which is very high. It is then followed by a breakdown stress of 40 MPa at stage 11. If a breakdown stress of 65 MPa is used as the *in situ* stress in all directions and an

injection volume of 1132 m^3 is input into the program, the minimum compressive stress at stage 11 does not reach 40 MPa as seen in Table 6-20 below.

Table 6-20 Minimum Compressive Stress at Stage 11 due to Injection at Stage 10 (kPa)

Porosity	Ratio = x_3/x_2					
	2	4	6	8	10	12
0.001	-63165.8	-63765.4	-64016.1	-64168.3	-64274	-64352.7
0.006	-62326.2	-62754.8	-62995	-63167.2	-63301.7	-63411.6
0.011	-62147.2	-62482.6	-62684.2	-62835.5	-62957.9	-63060.8
0.016	-62060.7	-62342.3	-62517.5	-62652.2	-62763.3	-62858.2
0.021	-62008	-62253.7	-62410	-62532	-62633.7	-62721.7
0.026	-61971.9	-62191.6	-62333.5	-62445.4	-62539.6	-62621.6
0.031	-61945.3	-62145.1	-62275.6	-62379.4	-62467.3	-62544.3
0.036	-61924.7	-62108.7	-62230	-62327	-62409.6	-62482.3
0.041	-61908.2	-62079.3	-62192.8	-62284.1	-62362.2	-62431.2

It is interesting to note that the minimum compressive stress will at one point be 40 MPa, but it will be achieved very close to the edge of the stimulated area and still within the interval for stage 10. This is show in Figure 6-23 below.

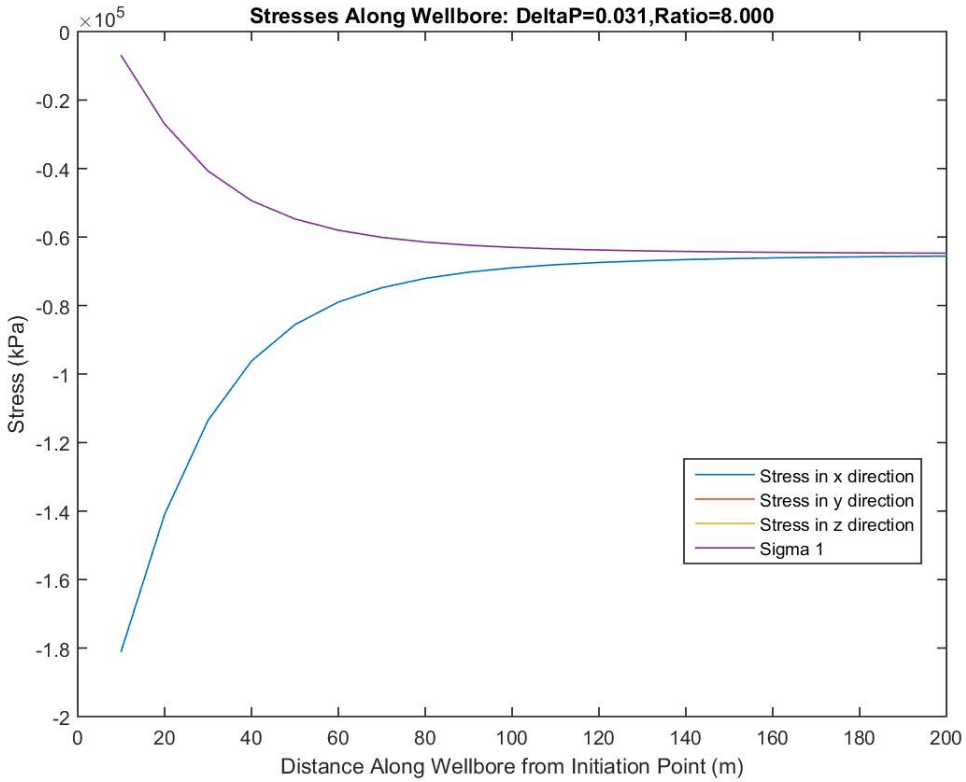

Figure 6-23 Stress along Wellbore due to Injection at Stage 10

A minimum compressive stress of 40 MPa is achieved around 25 m from the injection point of stage 10. It is unlikely stage 11 initiated in this location though, as it is still within the bounds of interval 10. If it is assumed that the fracture at stage 10 was rotated and propagating along the wellbore, with the width greater than the height, a minimum compressive stress near 40 can be achieved as seen in the table below. W > 93 indicates that the width of the fracture produced by the program was greater than the distance to the initiation point of stage 11.

Table 6-21 Minimum Compressive Stress at Stage 11 if Stage 10 has a Rotated Fracture

Porosity	Ratio = x_3/x_2					
	0.05	0.1	0.15	0.2	0.25	0.3
0.001	W > 93 m	W > 93 m	W > 93 m	W > 93 m	W > 93 m	W > 93 m
0.006	W > 93 m	W > 93 m	W > 93 m	W > 93 m	-4.06265	-51298.8
0.011	W > 93 m	W > 93 m	W > 93 m	-35050.1	-54798.4	-58016
0.016	W > 93 m	W > 93 m	W > 93 m	-53187	-57843	-59340.8
0.021	W > 93 m	W > 93 m	-39828.8	-56476.8	-58947.8	-59920.9
0.026	W > 93 m	W > 93 m	-50581	-57861.8	-59526.2	-60251.5
0.031	W > 93 m	W > 93 m	-54140.4	-58630.1	-59885.5	-60467.3
0.036	W > 93 m	W > 93 m	-55915.1	-59121.5	-60131.9	-60620.3
0.041	W > 93 m	-4290.73	-56980.5	-59464.3	-60312.5	-60735.1

From the data above, the likely geometry of the fracture at stage 11 is rotated so the semi axis along the z-direction is 22.41 m long, and the semi axis along the x-direction is 89.66 m. The width is larger than the height. The stress along the wellbore for this geometry is presented below.

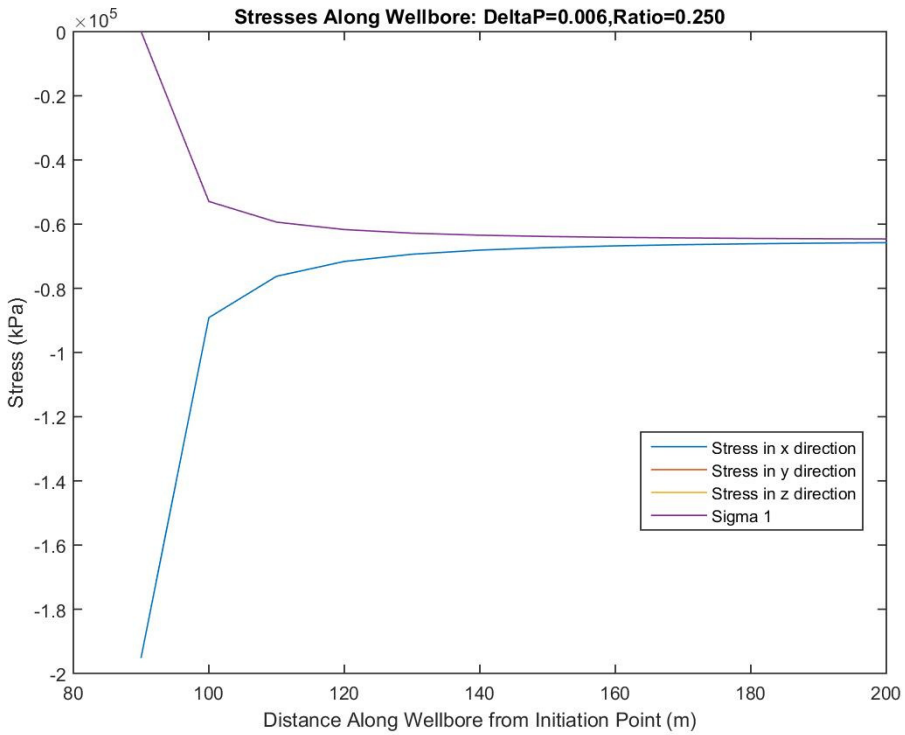

Table 6-22 Stress along the Wellbore caused by Stage 10

This stress regime suggests that the fracture in stage 11 initiates approximately 4 m away from the edge of the previously stimulated interval (93 m from stage 10 injection point). This may not be realistic in the real physical situation. Another explanation for this is that the stress regime is changing along the well. It is difficult to tell without more accurate stress measurements.

Stage 12 did not initiate. If stage 11 did initiate close to the previous fracture in a regime where it would propagate along the wellbore, it is a possibility that the fracture propagated in a single direction down the interval towards stage 12 rather than equally in each direction. It could also have initiated very close to the edge of the interval. It could have interfered with stage 12.

Stage 14 and 15 exhibit a similar stress pattern to stages 10 and 11. The fracture was assumed to be rotated in order to have a breakdown pressure go from 62 MPa at stage 14 to 40 MPa at stage 15. The results are below.

Table 6-23 Stress at Stage 14 due to Injection at Stage 13

Porosity	Ratio = x_3/x_2					
	0.05	**0.1**	**0.15**	**0.2**	**0.25**	**0.3**
0.001	W > 94 m	W > 94 m	W > 94 m	W > 94 m	W > 94 m	W > 94 m
0.005	W > 94 m	W > 94 m	W > 94 m	-48747.1	-56929.3	-58450.7
0.011	W > 94 m	W > 94 m	-48921.2	-57550.8	-58838.3	-59345.8
0.016	W > 94 m	W > 94 m	-56219.7	-58643.7	-59313.3	-59622.3
0.021	W > 94 m	-23214.4	-57729.3	-59079.3	-59534.9	-59760.9
0.026	W > 94 m	-50191.4	-58385.4	-59316.8	-59665.3	-59845.6
0.031	W > 94 m	-54376.4	-58755	-59467.7	-59752.1	-59903.4
0.036	W > 94 m	-56062.4	-58993.6	-59572.9	-59814.5	-59945.6
0.041	W > 94 m	-56972.9	-59161	-59650.8	-59861.7	-59977.9

There is no exact calculated porosity change and ratio which brings the stress to 40 MPa. However, if the stress at the initiation point of 14 for a ratio of 0.10 is looked at, it can be seen that 40 MPa is achieved around a porosity change of 0.0245.

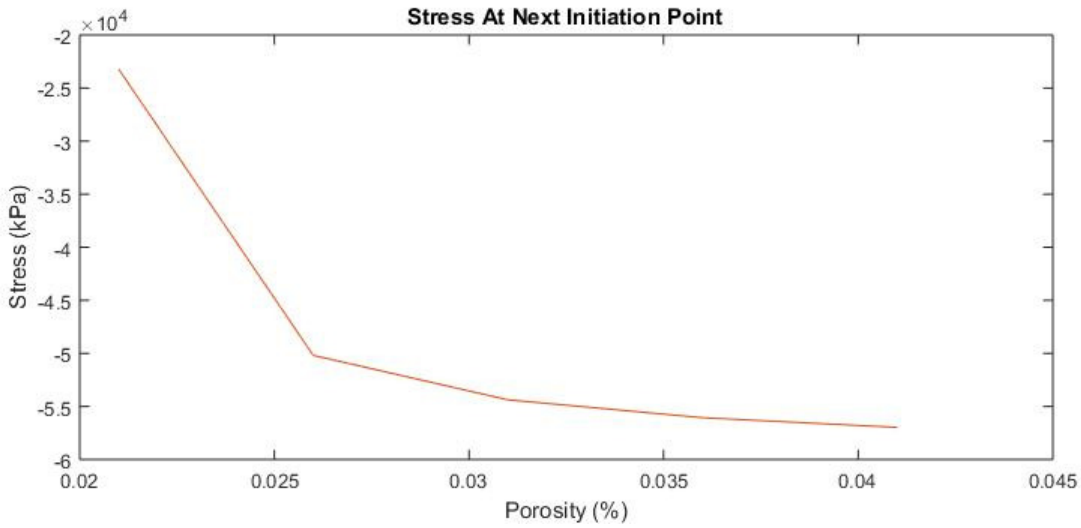

Figure 6-24 Minimum Compressive Stress at Stage 14 due to Injection at Stage 13

The geometry for the fracture is 10.17 m in the z-direction and 101.74 m in the x-direction. This would place the initiation point of stage 14 just 5 m away from the edge of the fracture. This could be unlikely, but if it did occur, the fracture at stage 14 would most likely propagate along the well towards stage 15 if it is in a regime where the minimum compressive stress is aligned with the z-direction.

Looking at the rest of the data, it is very likely that stages 15 and 16 were completed in undisturbed rock, as they both have the same breakdown pressure and have lower injection volumes. The breakdown pressure is significantly lower than that at the toe of the well. It is likely that the stress regime changed at some point near the head of the well. The minimum compressive stress has gone from being somewhere near 55-60 MPa for stages 1 – 13 to around 47 MPa for stages 14-16.

Tests were run using the program to look at the stress changes from stages 14 to 15 and from 15 to 16. It is unlikely that the fracture in stage 15 initiated in an area influenced by the injection at stage 14. No fracture geometry at stage 14 brings about a stress change from 40 MPa to 47 MPa between the two stages.

A diagram of fractures 1 to 13 is presented below along with a table of fracture properties.

Table 6-24 Final Properties of Fractures in Case 2

Stage	Injection Volume (m^3)	Breakdown Pressure (MPa)	Distance From Previous Stage (m)	X Semi-Axis (m)	Y and Z Semi Axis (m)	Porosity	Ratio = x_3/x_2
1	565.8	59		11.21	44.82	0.006	4
2	505.4	58	101	5.19	62.26	0.006	12
3	1050	58	107	7.58	30.31	0.031	4
4	1158.6	55	94	NA	NA	NA	NA
5	134.4	Did Not Break	110	DNB	DNB	DNB	DNB
6	1151.1	57	94	16.25	32.51	0.016	2
7	1230.4	55	106	NA	NA	NA	NA
8	99.5	Did Not Break	94	DNB	DNB	DNB	DNB
9	110.4	Did Not Break	106	DNB	DNB	DNB	DNB
10	1132	65	105	89.66	22.41	0.006	0.25
11	1263.2	40	93	NA	NA	NA	NA
12	254.6	Did Not Break	107	DNB	DNB	DNB	DNB
13	1080.7	62	93	101.74	10.17	0.0245	0.1

*DNB = Interval did not break

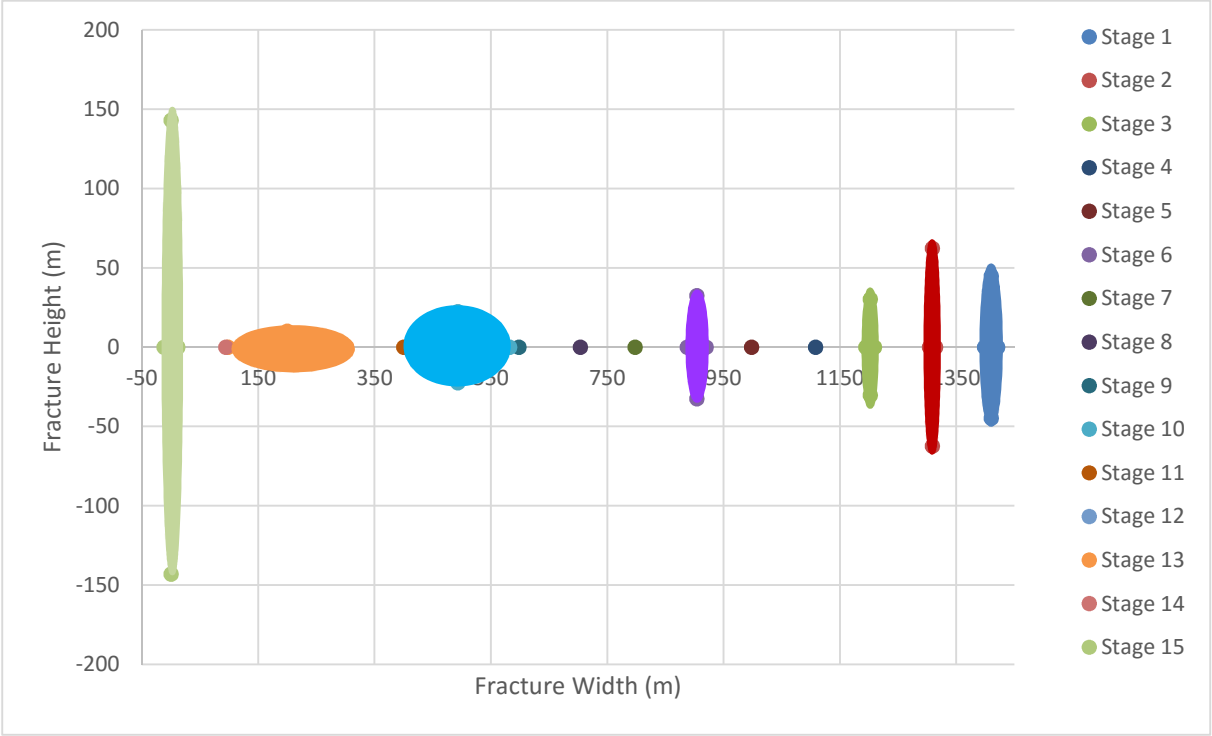

Table 6-25 Final Geometry of Fractures in Stage 2

The figure above makes it clear that there was likely a stress change at some point near the head of the well. The last fracture was predicted to be very long and skinny in order to not interfere with the fracture beside it.

6.2.4 Stress Regimes for Case 2

In order to model the various stages of the well, the *in situ* stresses were assumed to be all equal to the breakdown pressure recorded at the stage that was being modelled. This is not an accurate representation of the physical situation as the Montney Formation is generally anisotropic. The vertical stress direction is also almost always the largest compressive stress in the deep hydraulic fracture jobs; however, it is possible to use the assumption of equal stresses to get a rough idea of what could be occurring.

According to the theory presented in this thesis, breakdown pressure can be used as an approximation of minimum principal compressive stress. Therefore, the other two principal stresses must be greater in magnitude than the breakdown pressure at an interval. It is not possible to know the orientation of the minimum compressive stress, nor is it possible to know the magnitude of σ_2 and σ_3 for this set of data. Due to the set geometry in the program of $x_1 = x_3 \neq x_2$, the stress changes in x_1 direction (y-direction) and x_3 direction (z-direction) will have the same trend even if the initial stress in those directions differs in magnitude. This is evident in all figures in this section where the three stresses along the wellbore are shown.

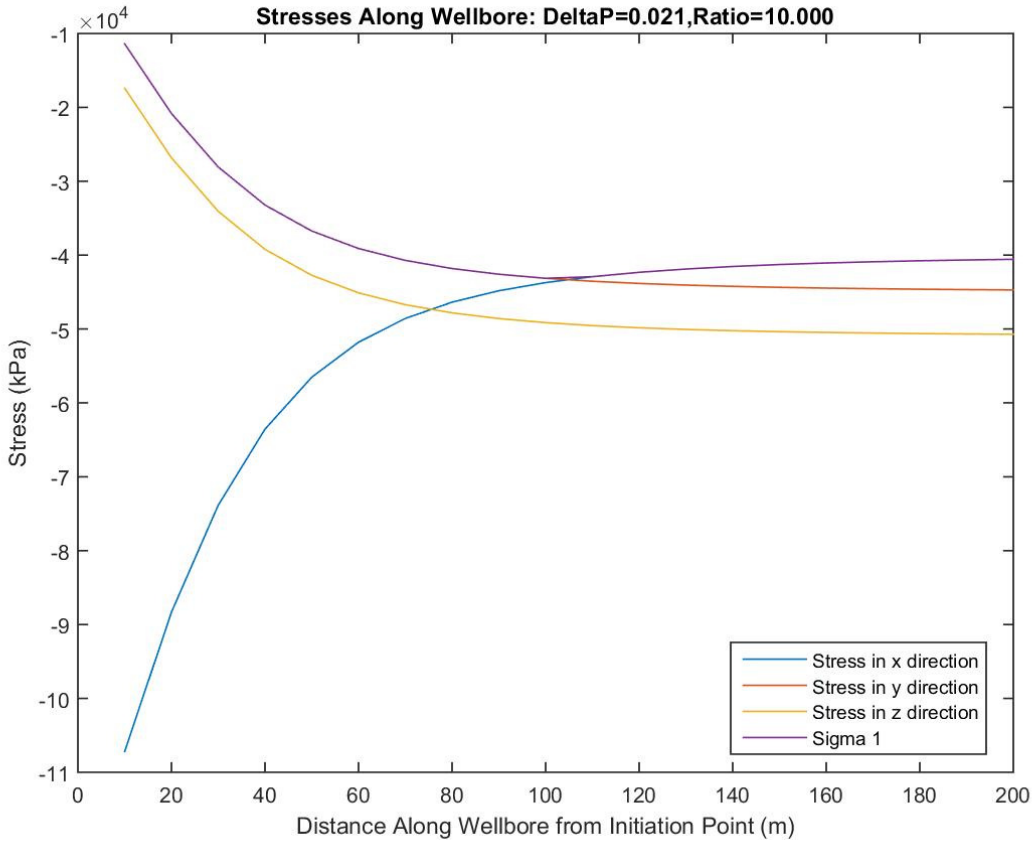

Figure 6-25 Example of Stress Change along the Wellbore ($\sigma_{33} > \sigma_{22} > \sigma_{11}$)

As shown in the modelled data in Figure 6-25, if σ_{33} and σ_{22} (z and y-direction) are greater than σ_{11} (x-direction), there will be an inflection point where σ_1 changes from being aligned with σ_{22} or σ_{33} near the wellbore and will realign with σ_{11}. Several cases were modelled to examine the behaviour of stresses along the wellbore for different stress regimes.

In the case where all stresses are equal to start, the value of σ_{11} is initially high and decreases with distance from the injection point. σ_{33} and σ_{22} are low right outside the stimulated area and then gradually increase, and then increase to the original *in situ* value with distance from the injection point. All stresses approach the original value of their initial *in situ* state as they get further from the wellbore. The minimum compressive stress is always aligned with σ_{33} and σ_{22}. This is shown in the figure below.

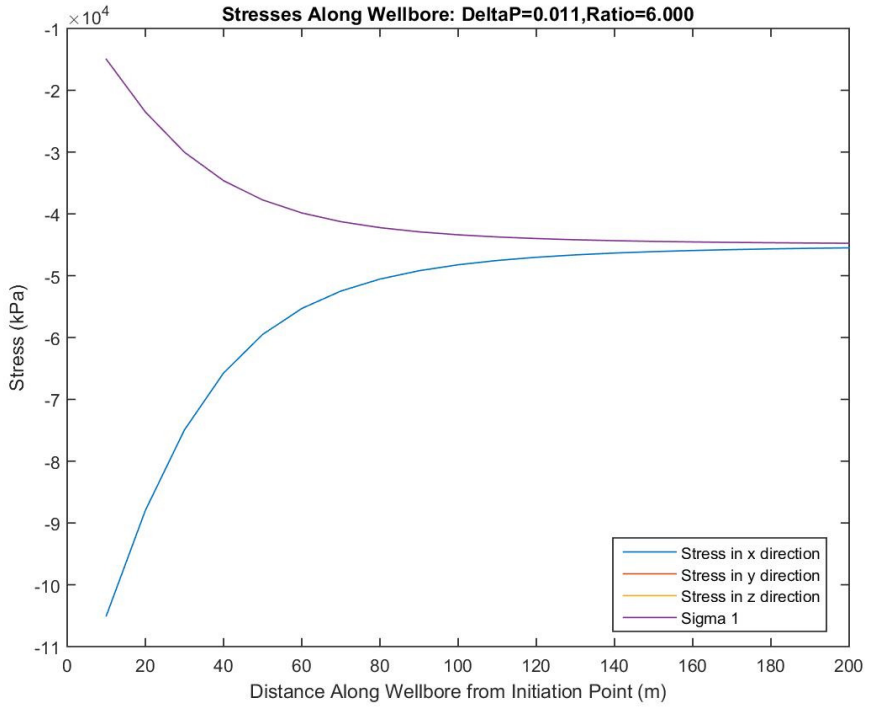

Figure 6-26 Stress along wellbore when $\sigma_{33} = \sigma_{22} = \sigma_{11}$

For the case where $\sigma_{33} = \sigma_{22} > \sigma_{11}$, the trends of the three stresses are still the same as above. However, for this case, the minimum compressive stress is aligned with σ_{33} and σ_{22} initially and then at a crossover point, it becomes aligned with σ_{11}. The same pattern is seen where $\sigma_{33} = \sigma_{22} \gg \sigma_{11}$ however the crossover point is much closer to the injection point. These cases are shown in the figures below.

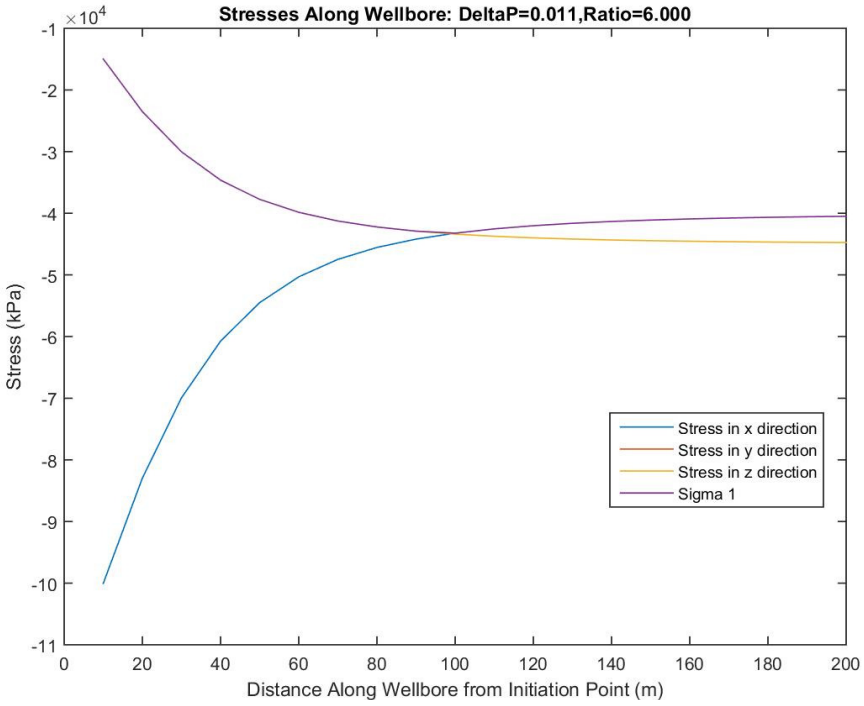

Figure 6-27 Stress along wellbore $\sigma_{33} = \sigma_{22} > \sigma_{11}$

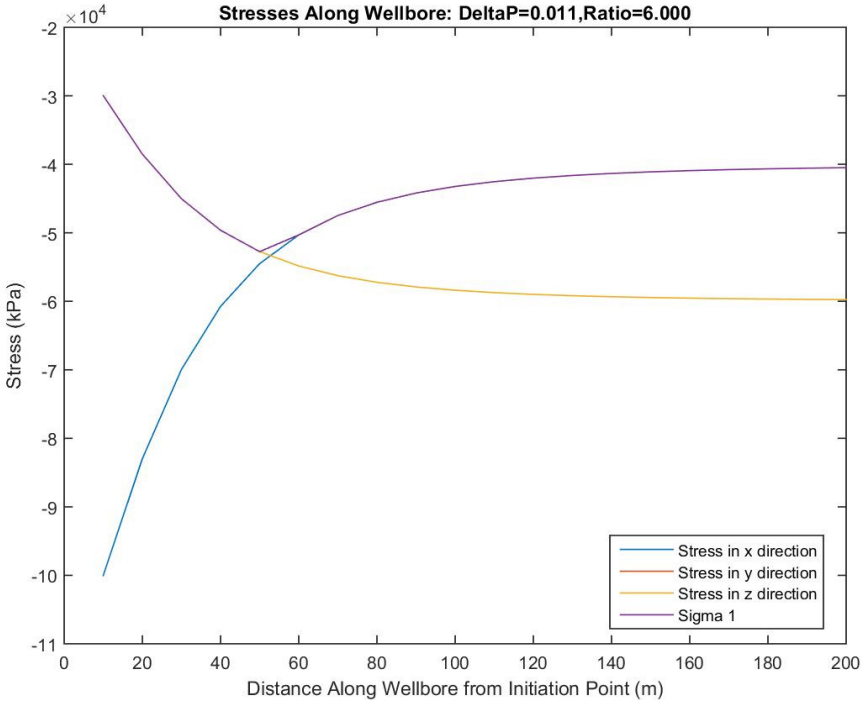

Figure 6-28 Stress along wellbore when $\sigma_{33} = \sigma_{22} \gg \sigma_{11}$

If $\sigma_{33} = \sigma_{22} < \sigma_{11}$, the width of the fracture will likely be greater than the height. No crossover point occurs and the minimum compressive stress stays aligned with σ_{33} and σ_{22}.

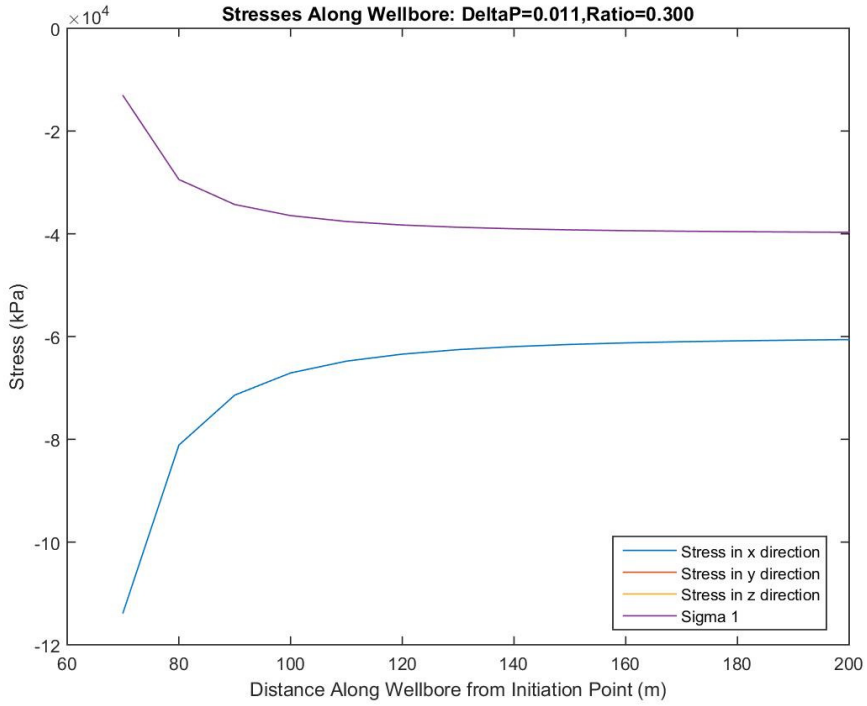

Figure 6-29 Stress along wellbore when $\sigma_{33} = \sigma_{22} < \sigma_{11}$

In the cases where none of the stresses are equal, and σ_{11} is initially the least compressive stress, the stress which is initially smaller in magnitude out of σ_{33} and σ_{22} will be the minimum compressive stress along the wellbore before the cross over point. This can be seen in the figure below.

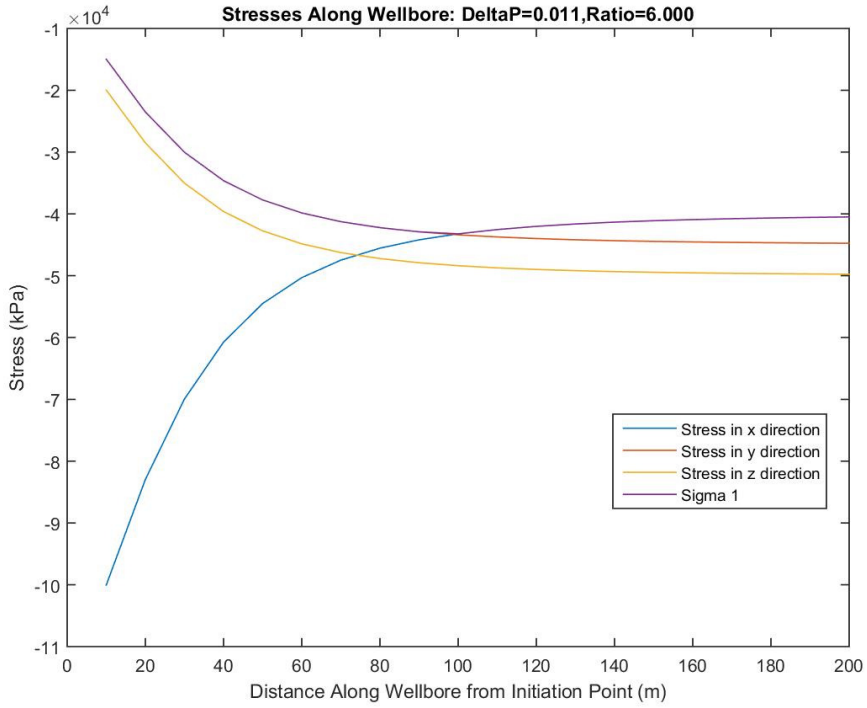

Figure 6-30 Stress along the Wellbore when $\sigma_{33} > \sigma_{22} > \sigma_{11}$

In the case where none of the stresses are equal and σ_{11} is initially the greatest compressive stress, no crossover point occurs. The least compressive stress initially will remain the least compressive stress for the entire length of the well.

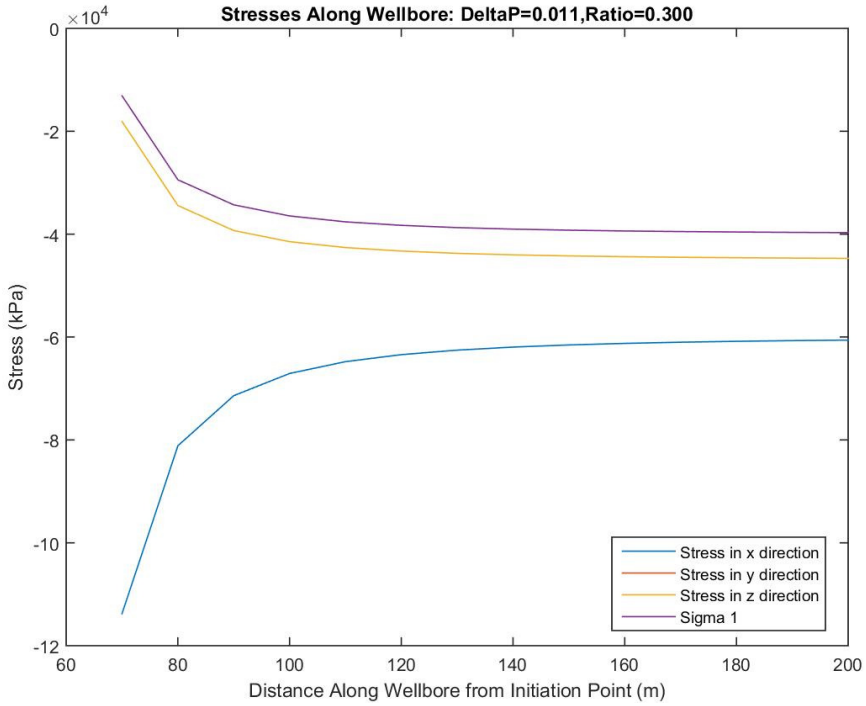

Figure 6-31 Stress along the Wellbore when $\sigma_{11} > \sigma_{33} > \sigma_{22}$

In the cases where none of the stresses are equal and and σ_{11} is initially the intermediate compressive stress, no crossover point for σ_1 will occur. It will remain aligned with the stress which is initially σ_1. The other two stresses will cross each other, but neither will become the least compressive stress. This is seen in the figure below.

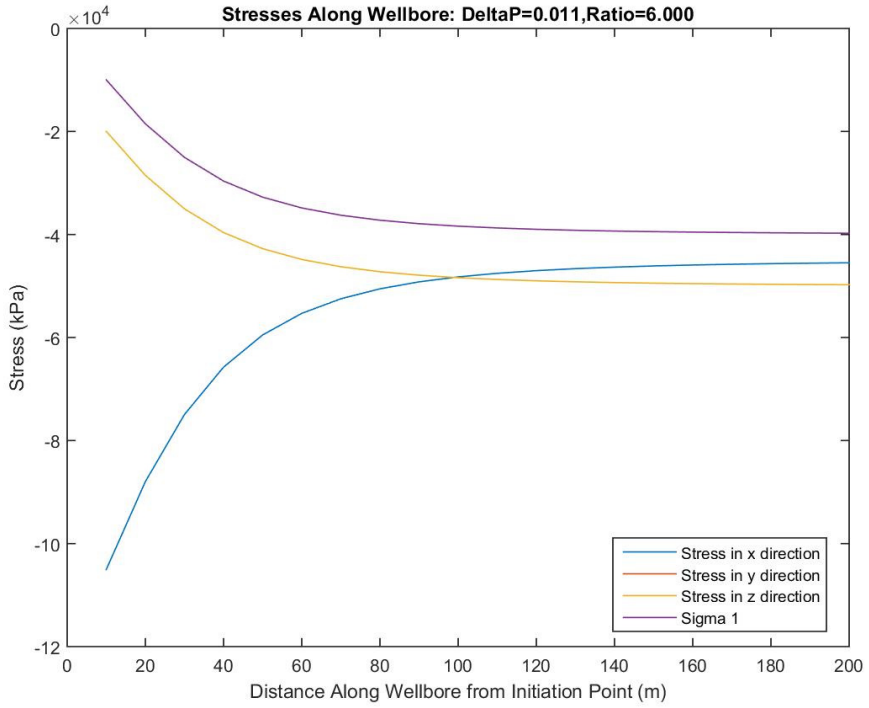

Figure 6-32 Stress along the Wellbore when $\sigma_{33} > \sigma_{11} > \sigma_{22}$

From the analysis above, it can be seen that unless σ_{11} is initially aligned with the least compressive stress, at no point along the wellbore will it become the least compressive stress. Near the wellbore, σ_{11} is never σ_1 as the increase in horizontal stress in the direction of the wellbore is very high. The crossover point (when one occurs) will move based on the difference between the magnitudes of the principal stresses. If the difference between the stresses is large, the crossover point will be found closer to the well than if the difference in stresses was small. The crossover point will only occur between σ_{11} and one other stress due to the way the geometry of the program is set.

There were several reasons that the stresses were all set equal to the breakdown pressure. The figures above helped to visualize the reasoning behind this choice. Assuming σ_1 lines up with one of the three main directions initially, the justification is as follows:

- The only known stress value at each stage comes from the breakdown pressure which, in this thesis, is a proxy for the initial σ_1 (minimum compressive stress).

- The other two principal stresses must be greater than or equal to σ_1
- If σ_1 is aligned with σ_{33} or σ_{22} initially, it will remained aligned with whichever direction it was in line with to start.
- If σ_1 is aligned with σ_{11}, it will be realigned with whichever stress began as σ_2 before realigning with σ_{11} at some distance from the injection point
- No matter the stress regime, σ_1 will always be aligned with the y or z-direction near the well. It will only cross over if the stress in the x direction was $\sigma_1$to begin with. The location of the crossover point is no longer needed when all stresses are equal.
- If all stresses are equal, σ_{22} and σ_{33} will approach σ_{11} at some distance from the well. If the stress value recorded at the next interval falls in an area where the lines are close in value to each other, it likely means that the interval was not affected by stress change (i.e. Figure 6-19 for Stage 3)
- If the stress value recorded at the next interval falls on the σ_{22} or σ_{33} line, and the lines are not close in value, the initiation point is either before the crossover point or σ_{11} is not the minimum compressive stress at any point.
- If the stress value recorded at the next interval is more in line with the σ_{11} value, then the initiation point is likely after the crossover point
- This theory runs into issues when the stresses vary greatly in magnitude. When the stresses are close in value, they all will eventually flatten out at a similar rate and the differences between them become less pronounced along the well. The changes in the trend of σ_1 are larger and occur over a shorter distance when the initial principal stress values are very different in value (~20 MPa).
- This method of equal stresses should only be used to get a rough estimate of what could be occurring underground. It is not suitable for use in predictive practices nor should it be used when better data is available.

6.2.5 Observations and Comments

It could be possible that the fractures in many intervals did not initiate in the middle of the interval. The open hole system allows fractures to begin at any point along the interval as there is no cement casing for the fluid to rupture. The fracture will likely start where the stress is lowest along the interval. This means if a stress shadow has caused an increase in stress, it is possible that the fracture will initiate outside the stress shadow naturally. If the stress shadow has caused a decrease in stress, the fracture is more likely to initiate in the stress affected area.

Stress shadows cause additive changes in stress if they overlap. No accumulation of stress change was considered from one stage to the next in this study. Looking at overlapping stress shadows could give a more accurate representation of the fracture behaviour.

This case study should be reviewed as more as a study in stress behaviour rather than a definitive way to define fracture geometry and porosity changes. Many assumptions were made in order to get an idea of what was happening in the subsurface. It is evident that some fracture rotation was occurring; however, without knowing exactly what the stresses were, this case study is more of a way to see how the program can be used and experimented with rather than an explanation of field data.

6.3 Case Study 3 - Plug and Perforation

Well F was stimulated using the CCPP method. The total vertical depth is 2296 m and slickwater was used for all fractures. Plug and perforation wells have several perforation points per interval which are all theoretically stimulated at the same time and take an equal amount of fluid. The fractures are placed fairly close together which makes the likelihood of stress interference high. Interval 7 of the well is examined as there is evidence in the pressure curve that not all fractures from the four initiation points take equal amounts of fluid. This model will examine what happens to the initiation of the other perforations when all of the fluid is taken by the first perforation, when half is taken, and when the fluid is distributed evenly.

6.3.1 Model Inputs

The inputs for the model can be found in Section 5.4. The initial *in situ* stress conditions are considered to be 52 MPa, 40 MPa, and 36 MPa for $\sigma_v, \sigma_H,$ and σ_h respectively. These numbers were taken from field data. Tables 6-27 through 6-30 summarize the characteristics and outputs of the program.

Table 6-26 Data for Well F

Initiation Point Number	Distance along Wellbore (m)	Distance from Next Perforation (m)
1	3068.0	48
2	3020.0	48
3	2972.0	48
4	2924.0	48

Table 6-27 Minimum Compressive Stress (kPa) at Next Perforation Point if all volume is in first Perforation

Porosity	Ratio = x_3/x_2					
	2	4	6	8	10	12
0.001	-35228	-37487	-38189	-38561	-38404	-38072
0.011	-28018	-31090	-32551	-33501	-34191	-34725
0.021	-26434	-29096	-30501	-31471	-32208	-32797
0.031	-25645	-27995	-29305	-30241	-30970	-31564
0.041	-25154	-27271	-28493	-29385	-30092	-30677

Table 6-28 Minimum Compressive Stress (kPa) at Next Perforation Point if half volume is in first Perforation

Porosity	Ratio = x_3/x_2					
	2	4	6	8	10	12
0.001	-36614	-38034	-38530	-38389	-38028	-37769
0.011	-33166	-34480	-35178	-35662	-36030	-36326
0.021	-32558	-33606	-34213	-34657	-35009	-35300
0.031	-32269	-33158	-33694	-34097	-34424	-34700
0.041	-32095	-32874	-33357	-33728	-34032	-34292

Table 6-29 Minimum Compressive Stress (kPa) at Next Perforation Point volume is distributed evenly

Porosity	Ratio = x_3/x_2					
	2	4	6	8	10	12
0.001	-37760	-38558	-38253	-37881	-37627	-37440
0.011	-36260	-36775	-37074	-37294	-37469	-37614
0.021	-36040	-36426	-36665	-36849	-37000	-37129
0.031	-35940	-36257	-36460	-36618	-36752	-36867
0.041	-35881	-36153	-36331	-36473	-36592	-36697

The average value of minimum compressive stress recorded at a point 48 m away from the initiation point was 31.6 MPa for a volume of 1048 m^3, 34.7 MPa for a volume of 524 m^3 and 36.9 MPa for a volume of 262 m^3. The magnitude of the minimum compressive stress at the next initiation point is higher when the volume in a single fracture is lower. The fractures are very closely spaced, meaning that the initiation point falls before the crossover point. It is beginning in an area where the minimum compressive stress is aligned with the y-direction.

The stress change which occurs when all four initiation points receive equal amounts of volume is very minimal if the stress from just a single perforation is considered. Stresses are additive though, and the stress caused by each equally stimulated area must be considered. The stress at the perforations in the middle will be much greater due to overlapping stress shadows. The extent of a stress shadow from a quarter of the injection fluid in the first point is extensive enough to affect the next two initiation points. It is likely the second initiation point in the stress shadow will be able to grow faster as it is not as affected by a stress shadow. The initiation point in between the other two may not even contribute or initiate due to the overlapping stress shadows.

6.4 Additional Observations on Stress around an Ellipsoid

The location of the crossover point is influenced by several different factors. It was seen in Section 6.2.4 that the crossover point will move closer to the well if the difference in stress magnitudes is very large. If the stresses are all very close in value, the crossover point will occur at quite a far distance from the well. This is independent of fracture ratio, porosity changes, stimulated volume, etc.

Figures 6-3 and 6-4 show how changes in porosity and different ratios affect the location of a crossover point for a general case of σ_1 initially being in the x direction. For a constant ratio of 10 and changing porosity for case 1a, the crossover point is actually fairly consistent in value. For a constant change in porosity of 0.011 and a range in ratios, the crossover point moves by a fair amount. Long, thin fractures (ratio = 8, 10 or 12) produce a crossover point 70 m from the injection point. Medium fractures (ratio = 4 or 6) push the crossover point to 80 m away. A short, wide fracture (ratio = 2) moves the point even

further from the injection point to 90 m away. It is interesting to note that the range in heights of the fractures caused by different changes in porosity is as large as the range in heights caused by the change in ratio. This would suggest that the crossover point is not just dependent on fracture height, but on the overall geometry of the fracture.

Another observation about stress in this program concerns the stress in 2 dimensions rather than just 1. The stress plotted in the program is the stress directly along the wellbore. No shear stress occurs in this location, therefore the principal stresses will align directly with the three principal directions (x, y, and z). If the stress is looked at along the wellbore still, but at different vertical heights, the change in stresses is likely to be vastly different depending on the location of the measurement along the ellipsoid. The width of the ellipsoid has an effect on the stress changes, therefore the stress changes near the top of the ellipsoid will be very different from those directly at the wellbore where the width is the thickest. The stress in the x-direction experiences the largest change in stress at the wellbore which is why it was chosen for modelling purposes. It would be useful though to examine stress contours around an ellipsoid rather than just stress down a single line. The crossover points will be different at different heights along the ellipsoid, meaning that a growing fracture in the next stage might initially start out growing in one direction, and then change based on where the crossover point has been moved to. This will be something to consider in another study.

Chapter 7 Conclusions and Recommendations

The semi-analytical solution for the stress shadow around a hydraulic fracture using the Eshelby solution and energy minimization is an adequate approximation of stress change caused by the inclusion. From the results, it appears that overall fracture geometry has the greatest effect on stress change. Fracture height is the main controlling factor as similar fracture heights will produce similar changes in σ_1 despite total fracture volume or width.

The stress in the x-direction close to the fracture is not usually σ_1. The stress in the y-direction usually becomes σ_1 near the stimulated area as the change in stress in the direction of the wellbore is usually very large close to the initiation point. The point where σ_1 realigns with the x-direciton is called the cross-over point. It should be noted that it is important to determine if the next initiation point is before the cross over point or after it, as the trends in overall stress change will be different depending on which regime the next fracture occurs in.

It is recommended that the model be used as a post-fracture analysis tool rather than one that is used to plan fracture operations. If it is to be used as a predictive tool, the program should be used in conjunction with field data collected during programs in formations similar to future operations and with good engineering judgment. It is clear from the simulation that stress shadowing will effect hydraulic fracture operations, whether it is through the increase in breakdown pressure or through lost intervals due to an inability to break the formation after it has been subjected to a stress change. However, it is impossible to know for certain if the geometry and stimulated volume estimated by the program represent what is truly happening within the subsurface. This model is more useful as a tool to examine potential stress shadow effects and fracture geometry in a formation, rather than an accurate predictive program for stress shadowing during MSHF operations. However, there are several applications for the program as it currently exists.

Standard ball drop open hole wells could use this program as a first order approximation of the optimal distance between stages. This could be done by inputting a given set of geomechanical properties and injection volume for a stage into the program to see the potential stress change at the next injection point. The program would not necessarily predict the exact stress change that will be seen at a point due to an injected volume, but it could output a range of possible stress changes along the well and a range of potential overall stimulated volumes for the fracture. The program could also help confirm propagation direction of fractures and potential overall fracture geometry by showing a set of fractures that are likely to form, considering energy minimization.

Plug and perforation operations could use the program to optimize spacing of injection points in an interval. There are a few ways in which this could be done. The program could be used to estimate the stress at each initiation point considering a variety of injection volumes (assuming all points take equal volume, half volume, etc.). If the stress around an initiation point is high, it is likely that the fracture will have trouble propagating from that point or the width of the fracture will be severely limited. If this is the case, unproductive initiation points could be eliminated from the planned interval.

From the program, it can be seen that two stimulated areas of equal height will produce a similar change in horizontal stress along the wellbore. It appears that the width along the wellbore can vary within the different stimulated areas, but the height will remain fairly consistent in order to produce the desired stress change. This implies that an approximate fracture height of a stage can be estimated using the stress change seen in the field data in the adjacent stage in post fracture analysis. Alternatively if the fracture geometry has been calculated using another method, the program can be used to find the stress change caused by the set height and width.

Another use for the program could be to examine whether or not fracture rotation is likely. There are two ways in which this could be done. The first would be to take a given injection volume and find the inflection points (as shown in Figures 6-4 and 6-5) where σ_1 realigns with the wellbore. The program could show if the next fracture stage is within the area where the minimum compressive stress is no

longer aligned with the wellbore for a given injection volume. The second would be to take a range of injection volumes and see what the maximum amount of fluid is before the adjacent fracture stage is likely to experience rotation.

This study could be improved upon in several ways. Recommendations for expansion of the program and improvement of study are listed below:

- A parameter study should be conducted on the geomechanical inputs (Poisson's ratio, Young's modulus, fracture energy) to see how an increase or decrease in values will affect the stress change along the wellbore and the estimated shape of the stimulated area. The parameter study should have the goal of quantifying which assumptions have a 1st order or 2nd order effect on the outcome of the program.
- The definition of fracture energy should be expanded upon. Right now it assumes values from a lab are applicable to the field. The values obtained in a laboratory setting are for a single, small scale fracture whereas in the subsurface, the stimulated area is likely to have many large and multi-branching fractures which would significantly increase the value of fracture energy.
- Change in porosity should be treated as a variable rather than a constant number in the program. An evolving porosity value would be more representative of a region with a growing fracture.
- More field data should be collected if possible to get a more accurate measure of original *in situ* stress values. Data sets which have ISIP or closure pressure values for every interval would be very useful rather than relying on breakdown pressure, which can be considered a poor representation of minimum compressive horizontal stress.
- A laboratory experiment in which a known rock sample is fractured and measured for stress changes around the fracture would be a useful validation of the Eshelby solution.
- A comparison of potential stimulated area heights and widths of an interval should be compared with microseismic monitoring data for the interval to see if the stimulated volumes are close in

size and shape. Microseismic data can be difficult to interpret, but it could be useful as a first order confirmation of the program's accuracy.

- An entire well, preferably with closure pressures for each interval, should be evaluated using the program with stress becoming additive along the wellbore from each previous interval if applicable. It would be useful to see how fractures behave down the entire length of the well.
- There are several times in the field data when the breakdown pressure drops rather than increases in adjacent intervals. It has been hypothesized that this is due to a lower injection volume in the interval which exists in the stress shadow. The low injection volume does not lead to a stress change in the next interval and therefore the breakdown pressure becomes representative of the initial undisturbed minimum compressive horizontal stress.
- It is recommended that further analysis be done on transverse fractures and the additive effects of their stress shadows.
- In cases of a ball drop, the fracture initiation points should be varied along the well to see the effect on fracture geometry and initiation.
- This program only looks at the stresses directly along the wellbore. The stresses will be different for locations directly above the well as the size of the ellipsoid at that point will be different (width at the top of the ellipse is smaller than at the middle, etc.). Stresses should be examined at different heights of the ellipsoid to see if the stress regimes change.

Some of the outputs require that the geometry or the change in porosity become a value that is not physically likely to occur. The results of the program still need to be evaluated considering the physics of the situation rather than just the output of a mathematical formula. It is more useful as a post-fracture analysis tool than a definitive predictive model.

References

Adachi, J., Siebrits, E., Peirce, A., and Desroches, J. 2007. Computer simulation of hydraulic fractures. International Journal of Rock Mechanics and Mining Sciences, **44**: 739-757.

ALL Consulting, LLC. 2012. The modern practices of hydraulic fracturing: a focus on Canadian resources. Petroleum Technology Alliance Canada and Science and Community Environmental Knowledge Fund, Calgary, Alberta.

Beugelsdijk, L. J. L., de Pater, C. J., and Sato, K. 2000. Experimental hydraulic fracture propagation in a multi-fractured medium. *In* Proceedings of the Society of Petroleum Engineers Asia Pacific Conference on Integrated Modelling for Asset Management, Yokohama, Japan, 25-26 April 2000. Society of Petroleum Engineers. Calgary, Alberta, pp. 177-184.

Biot, M. 1941. General theory of three dimensional consolidation. Journal of Applied Physics, **12**(2): 155-164.

Blanton, E., and Mackenzie, G. 2006. Hydraulic pump-down frac plug and subsequent coiled-tubing removal increases client efficiency in Barnett Shale. *In* Proceedings of the SPE/ICoTA Coiled Tubing and Well Intervention Conference and Exhibition, The Woodlands, Texas, 4-5 April 2006. Society of Petroleum Engineers. Calgary, Alberta.

Bunger, A., Jeffery, R., and Zhang, X. 2013. Constraints on simultaneous growth of hydraulic fractures from multiple perforation clusters in horizontal wells. *In* Proceedings of the SPE Hydraulic Fracturing Technology Conference, The Woodlands, Texas, 4-6 February 2013. Society of Petroleum Engineers. Calgary, Alberta.

Cheng, Y. 2009. Boundary element analysis of the stress distribution around the multiple fracture: implications for the spacing of perforation clusters of hydraulically fractured horizontal wells. *In* Proceedings of the SPE Eastern Regional Meeting, Charleston, West Virginia, 23-25 September 2009. Society of Petroleum Engineers. Calgary, Alberta, pp. 23-25.

Cipolla, C., Lolon, E., and Dzubin, B. 2009. Evaluating stimulation effectiveness in unconventional reservoirs. *In* Proceedings of the SPE Annual technical Conference and Exhibition, New Orleans, Louisiana, 4-7 October 2009. Society of Petroleum Engineers. Calgary, Alberta, pp. 3397-3417.

Cui, A., and Brezovski, R. 2013. Laboratory permeability and diffusivity measurements of unconventional reservoirs: useless or full of Information? A Montney example from the western Canada sedimentary basin. *In* Proceedings of the SPE Unconventional Resources Conference and

Exhibition-Asia Pacific, Brisbane, Australia, 11-13 November 2013. Society of Petroleum Engineers. Calgary, Alberta.

Daneshy, A. 2013. Horizontal well fracturing: a state-of-the-art report. Shale Technology Review.

Dawson, M. 2011. Canadian unconventional resources: energy security and investment opportunities. *In* Proceedings of the Canadian Society for Unconventional Resources at NAPE International Forum, Houston, Texas, 16 February 2010. Canadian Society for Unconventional Gas. Calgary, AB.

Dohmen, T., Zhang, J., Blangy, J., and Corporation, H. 2014. Measurement and analysis of 3D stress shadowing related to the spacing of hydraulic fracturing in unconventional reservoirs. *In* Proceedings of the SPE Annual Technical Conference and Exhibition, Amsterdam, Netherlands, 27-29 October 2014. Society of Petroleum Engineers. Calgary, Alberta.

Dutton, R., Nolte, K., and Smith, M. 1982. Use of the long-spaced-digital-sonic log to determine relationships of fracturing pressure and fracture height for wells in the east Texas cotton valley tight gas play. Houston, Texas. Amoco Production Company.

Dyson, F. 1981. The potentials of ellipsoids of variable densities. Quarterly Journal of Pure and Applied Mathematics, **25**: 259-288.

Eshelby, J. 1957. The determination of the elastic field of an ellipsoidal inclusion, and related problems. Proceedings of the Royal Society of London. Series A, Mathematical and Physical Sciences, **241**(1226): 376-396.

Ferrers, N. 1877. On the potentials of ellipsoids, ellipsoidal shells, elliptic laminae and elliptic rings of variable densities. Quarterly Journal of Pure and Applied Mathematics, **14**: 1-22.

Fischer-Cripps, A. 2007. Introduction to contact mechanics. Springer US.

Fjaer, E., Holt, R., Horsrud, P., Raaen, A., and Risnes, R. 2008. Petroleum related rock mechanics. Elsevier, Oxford, UK.

Geertsma, J., and Klerk, F. 1969. A rapid method of predicting width and extent of hydraulically induced fractures. Journal of Petroleum Technology, **21**(12): 1571-1581.

Goodman, R., Taylor, R., and Brekke, T. 1968. A model for the mechanics of jointed rock. Journal of the Soil Mechanics and Foundations Division **94**(3): 637-660.

Griffith, A. 1921. Phenomena of rupture and flow in solids. Philosophical Transactions of the Royal society of London. Series A, Containing Papers of a mathematical or Physical Character, **221**(582-593): 163-198.

Hack, R., Orlic, B., Ozmutlu, S., Zhu, S., and Rengers, N. 2006. Three and more dimensional modelling in geo-engineering. Bull Eng Geol Env, **65**: 143-153.

Igor, M. 2005. Elliptic Integrals and Functions [online]. Available from MATLAB Central: http://www.mathworks.com/matlabcentral/fileexchange/8805-elliptic-integrals-and-functions. [accessed November 2015].

Inglis, C. 1913. Stresses in a plate due to presence of cracks and sharp corners. Trans. Institution of Naval Architecture, **55**: 219-230.

Jing, L. 2003. A review of techniques, advances, and outstanding issues in numerical modelling for rock mechanics and rock engineering. International Journal of Rock Mechanics & Mining Sciences, **40**: 283-353.

Jing, L., and Hudson, J. A. 2002. Numerical methods in rock mechanics. International Journal of Rock Mechanics & Mining Sciences, **39**: 409-427.

Jones, J., and Britt, L. 2009. Design and appraisal of hydraulic fracture. Society of Petroleum Engineers. Richardson, Texas.

Keneti, S., Park, R., and Wong, R. 2012. Montney shale geomechanical challenges: 2D and 3D FEM/DEM numerical simulations of a layered material fracturing in compression. *In* Proceedings of the 46th US Rock Mechanics/Geomechanics Symposium, Chicago, Illinois 24-27 June 2012. American Rock Mechanics Association. Alexandria, Virginia.

Khristianovitch, S., and Zheltov, Y. 1955. Formation of vertical fractures by means of highly viscous fluids. *In* Proceedings of the 4th World Petroleum Congress, Rome, Italy, 6-15 June 1955. World Petroleum Congress, London, UK, pp. 579-586.

King, G. E. 2010. Thirty years of gas shale fracturing: what have we learned? *In* Proceedings of the Society of Petroleum Engineers Annual Technical Conference and Exhibition, Florence, Italy, 19-22 September 2010. Society of Petroleum Engineers, Calgary, Alberta, pp. 1-50.

McLennan, J., and Roegiers, J. 1982. How instantaneous are instantaneous pressures? *In* Proceedings of the Society of Petroleum Engineers Annual Technical Conference and Exhibition, New Orleans, Louisiana, 29-29 September 1982. Society of Petroleum Engineers, Calgary, Alberta.

Meng, C., Heltsley, W., and Pollard, D. 2011. Evaluation of the Eshelby solution for the ellipsoidal inclusion and heterogeneity. Computers & Geosciences. doi:10.1016/j.cageo.2011.07.008.

Miller, C., Waters, G., and Rylander, E. 2011. Evaluation of production log data from horizontal wells drilled into organic shales. *In* Proceedings of the Society of Petroleum Engineers North American

Unconventional Gas Conference and Exhibition, The Woodlands, Texas, 14-16 June 2011. Society of Petroleum Engineers, Calgary, Alberta.

Mura, T. 1987. Micromechanics of defects in solids: mechanics of elastic and inelastic solids. Springer, Netherlands.

Nagel, N., and Sanchez-Nagel, M. 2011. Stress shadowing and microseismic events: a numerical evaluation. *In* Proceedings of the Society of Petroleum Engineers Annual Technical Conference and Exhibition, Denver, Colorado, 30 October – 2 November 2011. Society of Petroleum Engineers. Calgary, Alberta.

Nagel, N., Sanchez-Nagel, M., Garcia, X., and Lee, B. 2012. A numerical evaluation of the geomechanical interactions between a hydraulic fracture stimulation and a natural fracture system. *In* Proceedings of the 46th US Rock Mechanics/Geomechanics Symposium, Chicago, Illinois, 24-27 June 2012. American Rock Mechanics Association. Alexandria, Virginia.

Nagel, N., Zhang, F., Sanchez-Nagel, M., and Lee, B. 2013. Evaluation of stress changes due to multi-stage hydraulic fracturing - consideration of field results. *In* Rock Mechanics for Resources, Energy and Environment. *Edited by* MarM. Kwansniewski and D. Lydzba. Taylor & Francis Group, London, UK. Pp. 941-946.

National Energy Board. 2013. ARCHIVED - montney formation one of the largest gas resources in the world, report shows. Available from Canada National Energy Board: https://www.neb-one.gc.ca/bts/nws/nr/archive/2013/nr30-eng.html [accessed November 2015].

Nordgren, R. 1972. Propagation of a vertical hydraulic fracture. Journal of Petroleum Technology, **252**: 306-314.

Olson, J. 2008. Multi-fracture propagation and modeling: applications to hydraulic fracturing in shales and tight gas sands. *In* Proceedings of the 42nd US Rock mechanics Symposium and 2nd Canada Rock Mechanics Symposium, San Francisco, California, 29 June-2 July 2008. American Rock Mechanics Association. American Rock Mechanics Association. Alexandria, Virginia.

Ouchterlony, F. 1990. Fracture toughness testing of rock with core based specimens. Engineering Fracture Mechanics, **35**(1-3): 351-366.

Perkins, T., & Kern, L. 1961. Widths of hydraulic fractures. Journal of Petroleum Technology, **13**(90): 937-949.

Rahim, Z., Al-Anazi, H., Al-Kanaan, A., Habbtar, A., and Al-Omair, A. 2012. Improved gas recovery - 2 (conclusion): productivity increase using hydraulic fracturing - expectation vs. reality. Oil and Gas Journal, **110**(5).

Rios, A., Gutierrez, G., Nagel, N., M.A., Z., Sanchez-Nagel, M., and Lee, B. 2013. Stress shadow evaluations for Chicontepec - evaluating new completion options. *In* Proceedings of the 47th US Rock Mechanics/Geomechanics Symposium, San Francisco, California, 23-26 June 2013. American Rock Mechanics Association. Alexandria, Virginia.

Roussel, N., and Sharma, M. 2011. Optimizing fracture spacing and sequencing in horizontal-well fracturing. Society of Petroleum Engineers Production & Operations **26**(2): 173-184.

Roussel, N., Manchanda, R., and Sharma, M. 2012. Implications of fracturing pressure data recorded during a horizontal completion on stage spacing design. *In* Proceedings of the Society of Petroleum Engineers Hydraulic Fracturing Technology Conference, The Woodlands, Texas 6-8 February 2012. Society of Petroleum Engineers, Calgary, Alberta.

M., Smith and Montgomery, C. 2015. Hydraulic Fracturing. Boca Raton, FL: CRC Press.

Suchy, D., and Newelll, K. 2012. Hydraulic fracturing of oil and gas wells in Kansas. Available from the Kansas Geological Survey, Lawrence, Kansas. http://www.kgs.ku.edu/Publications/PIC/pic32.html [cited November 2015].

Terzaghi, K. 1943. Theoretical Soil Mechanics. New York: Wiley.

Warpinski, N., and Teufel, L. 1989. In situ stresses in low-permeability, nonmarine rocks. Journal of Petroleum Technology, **41**(4): 405-414.

Yu, W., Luo, Z., Javadpour, F., Veravei, A., and Sepehrnoori, K. 2013. Sensitivity analysis of hydraulic fracture geometry in shale gas reservoirs. Journal of Petroleum Science and Engineering. **113**(2014): 1-7.

Zienkiewicz, O., Best, B., Dullage, C., and Stagg, K. 1970. Analysis of non-linear problems in rock mechanics with particular reference to jointed rock systems. *In* Proceedings of the Second International Congress on Rock Mechanics, Belgrade, Serbia. International Society of Rock Mechanics, Lisbon, Portugal, pp. 8-14.

Appendix A: Case 1 Figures

Stage 16 to stage 17 stress changes are presented in the following graphs.

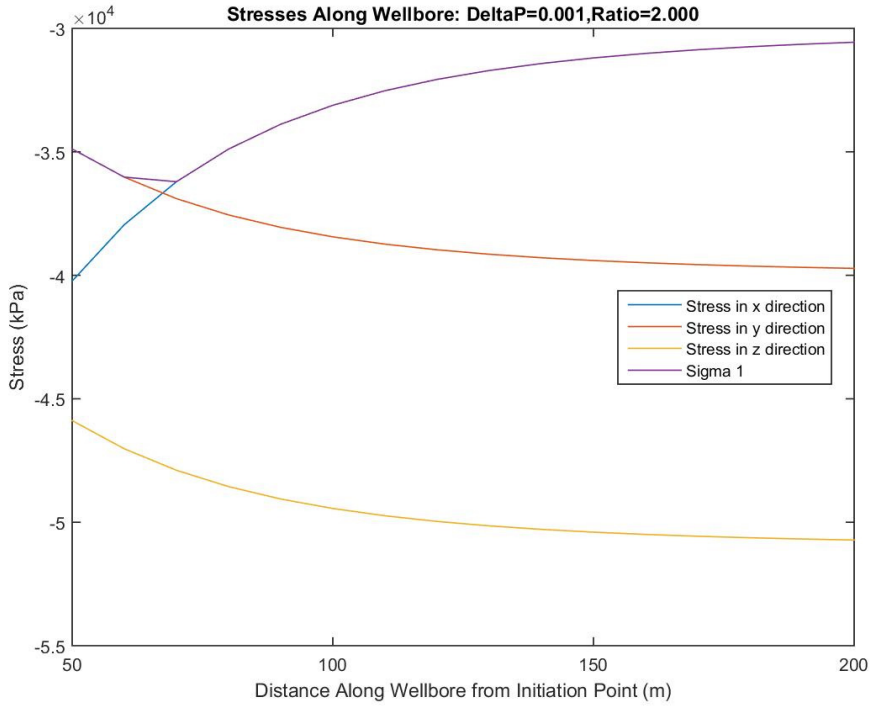

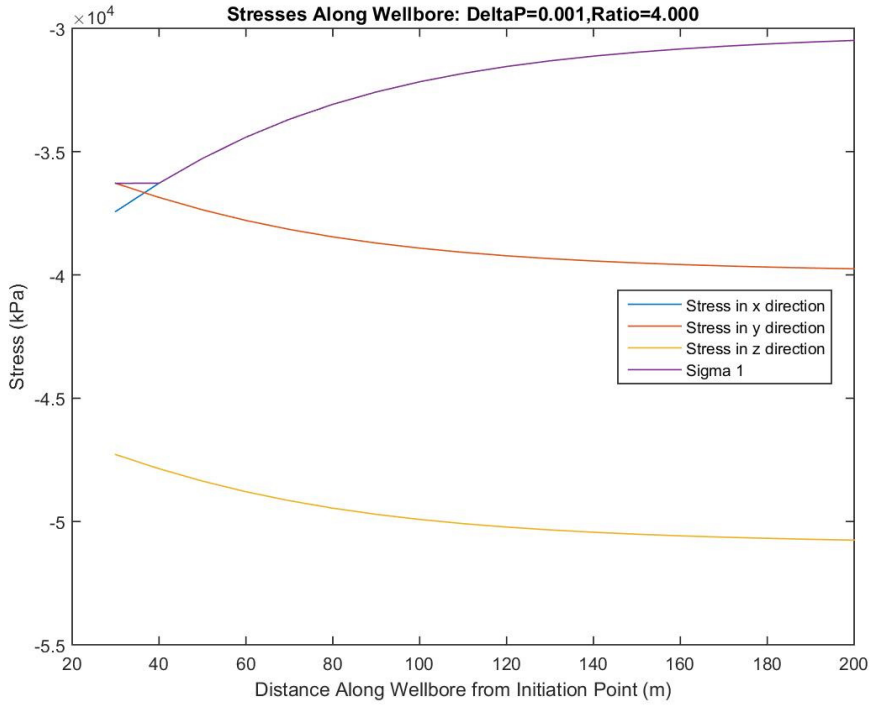

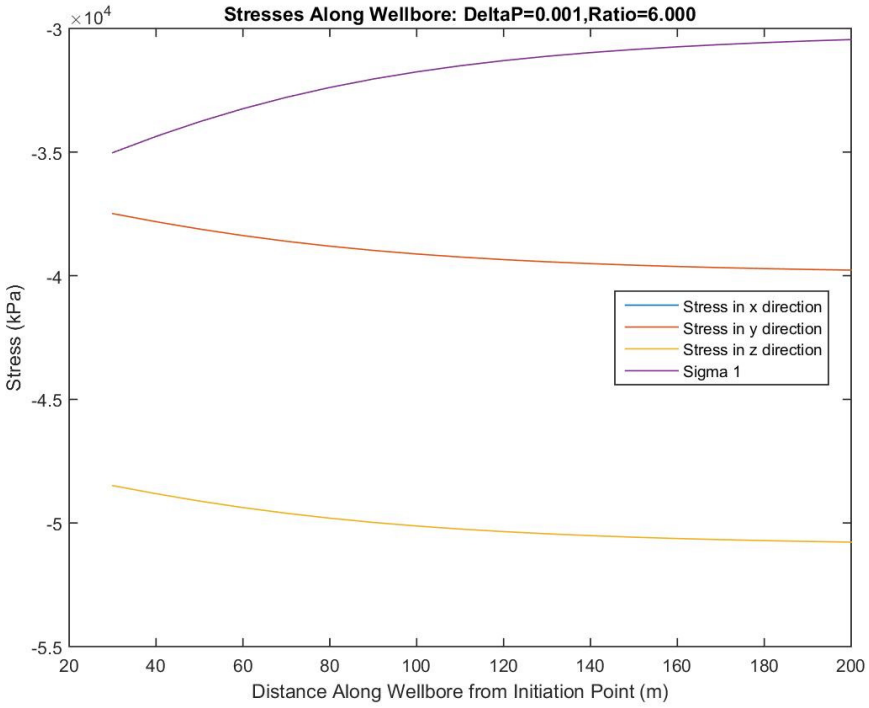
Stresses Along Wellbore: DeltaP=0.001,Ratio=6.000
×10^4
-3
-3.5
-4
-4.5
-5
-5.5
Stress (kPa)
20
40
60
80
100
120
140
160
180
200
Distance Along Wellbore from Initiation Point (m)
Stress in x direction
Stress in y direction
Stress in z direction
Sigma 1

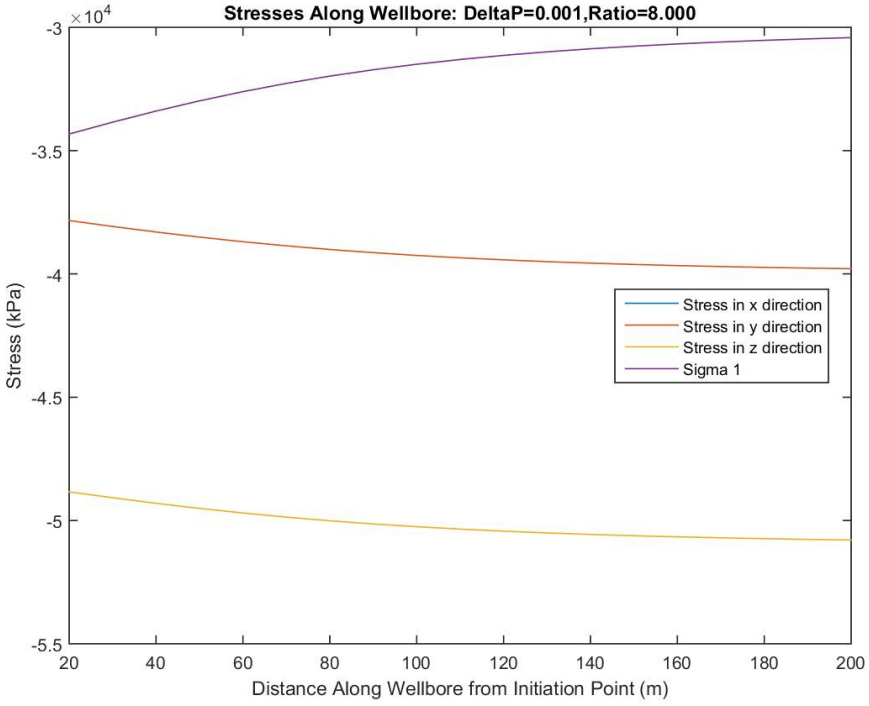
Stresses Along Wellbore: DeltaP=0.001,Ratio=8.000
×10^4
-3
-3.5
-4
-4.5
-5
-5.5
Stress (kPa)
20
40
60
80
100
120
140
160
180
200
Distance Along Wellbore from Initiation Point (m)
Stress in x direction
Stress in y direction
Stress in z direction
Sigma 1

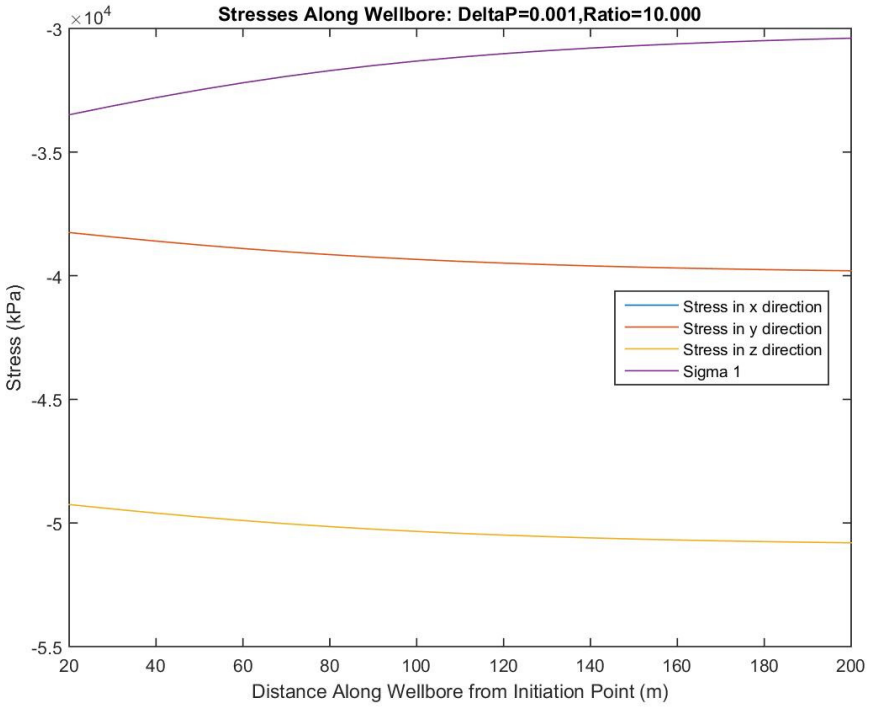
Stresses Along Wellbore: DeltaP=0.001,Ratio=10.000
×10^4
-3
-3.5
-4
-4.5
-5
-5.5
Stress (kPa)
20
40
60
80
100
120
140
160
180
200
Distance Along Wellbore from Initiation Point (m)
Stress in x direction
Stress in y direction
Stress in z direction
Sigma 1

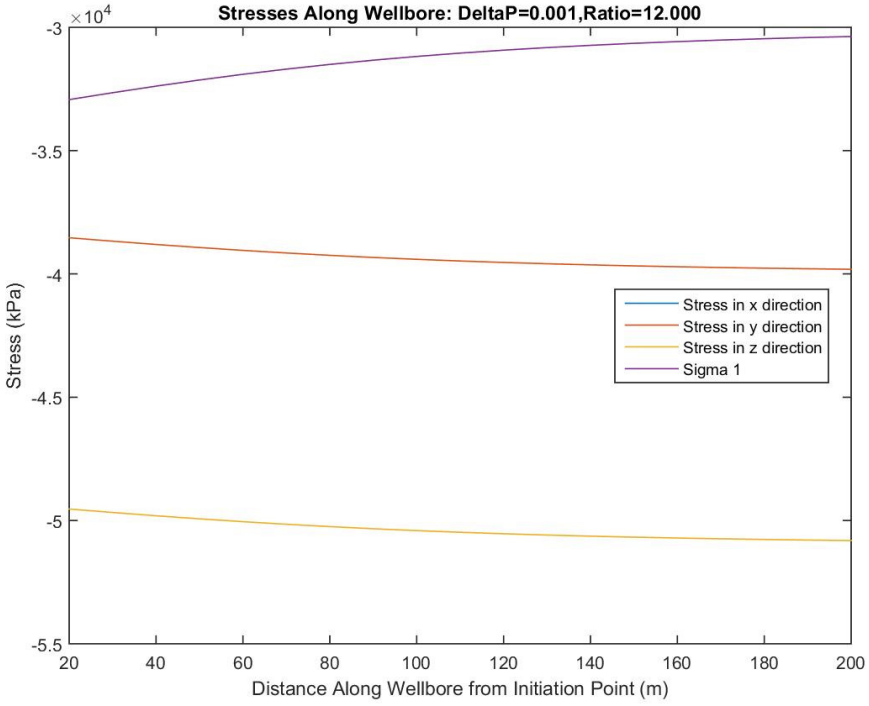
Stresses Along Wellbore: DeltaP=0.001,Ratio=12.000
×10^4
-3
-3.5
-4
-4.5
-5
-5.5
Stress (kPa)
20
40
60
80
100
120
140
160
180
200
Distance Along Wellbore from Initiation Point (m)
Stress in x direction
Stress in y direction
Stress in z direction
Sigma 1

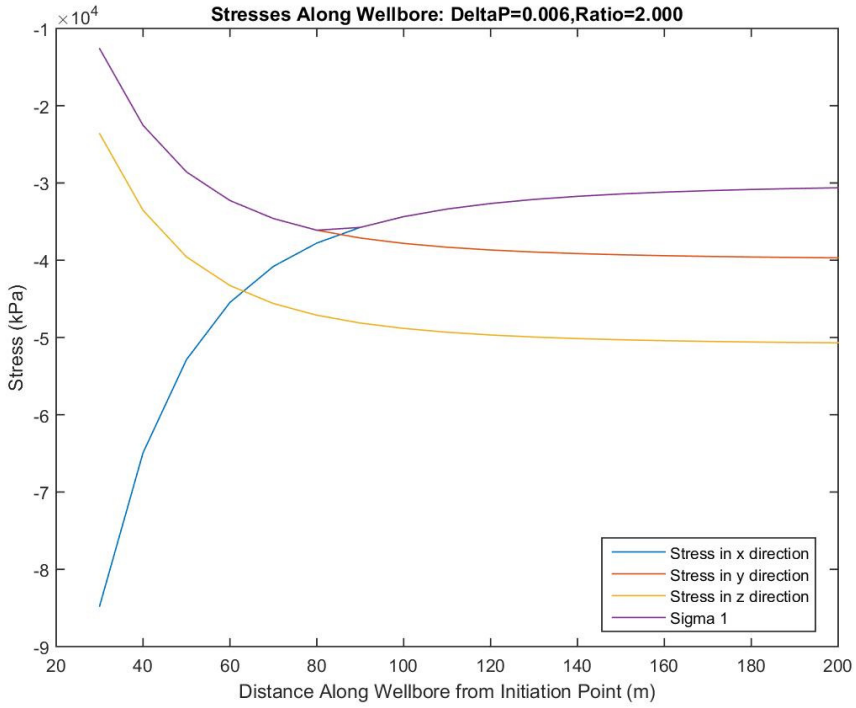
Stresses Along Wellbore: DeltaP=0.006,Ratio=2.000
×10^4
-1
-2
-3
-4
-5
-6
-7
-8
-9
Stress (kPa)
20
40
60
80
100
120
140
160
180
200
Distance Along Wellbore from Initiation Point (m)
Stress in x direction
Stress in y direction
Stress in z direction
Sigma 1

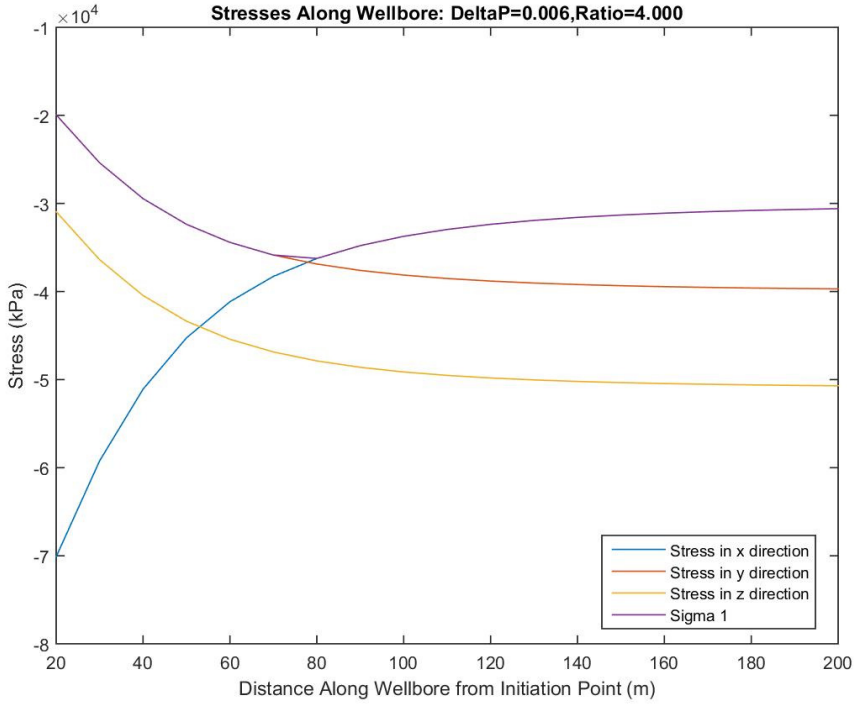
Stresses Along Wellbore: DeltaP=0.006,Ratio=4.000
×10^4
-1
-2
-3
-4
-5
-6
-7
-8
Stress (kPa)
20
40
60
80
100
120
140
160
180
200
Distance Along Wellbore from Initiation Point (m)
Stress in x direction
Stress in y direction
Stress in z direction
Sigma 1

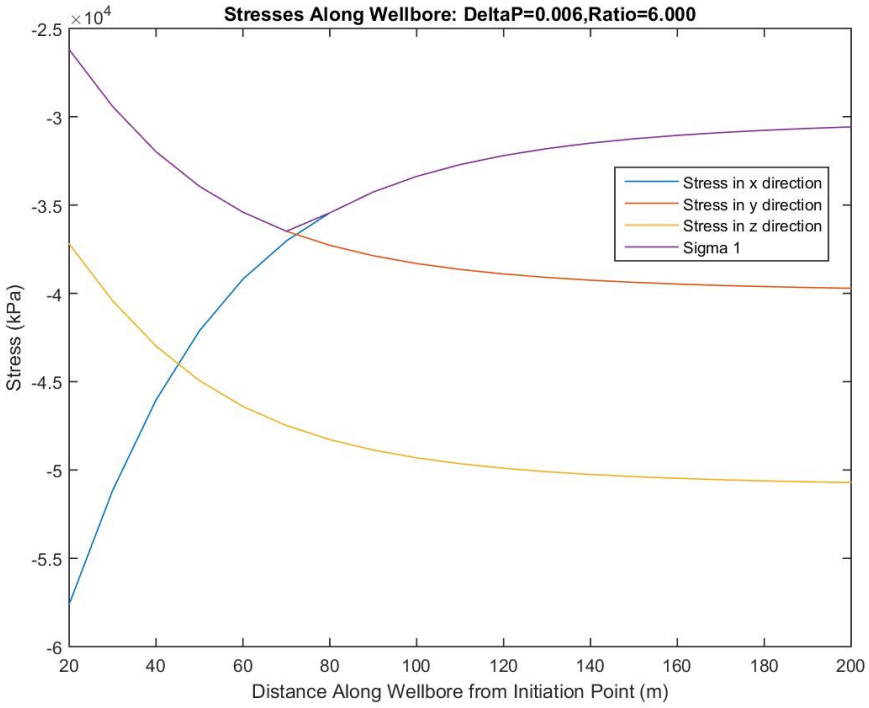
Stresses Along Wellbore: DeltaP=0.006,Ratio=6.000
×10^4
-2.5
-3
-3.5
-4
-4.5
-5
-5.5
-6
Stress (kPa)
20
40
60
80
100
120
140
160
180
200
Distance Along Wellbore from Initiation Point (m)
Stress in x direction
Stress in y direction
Stress in z direction
Sigma 1

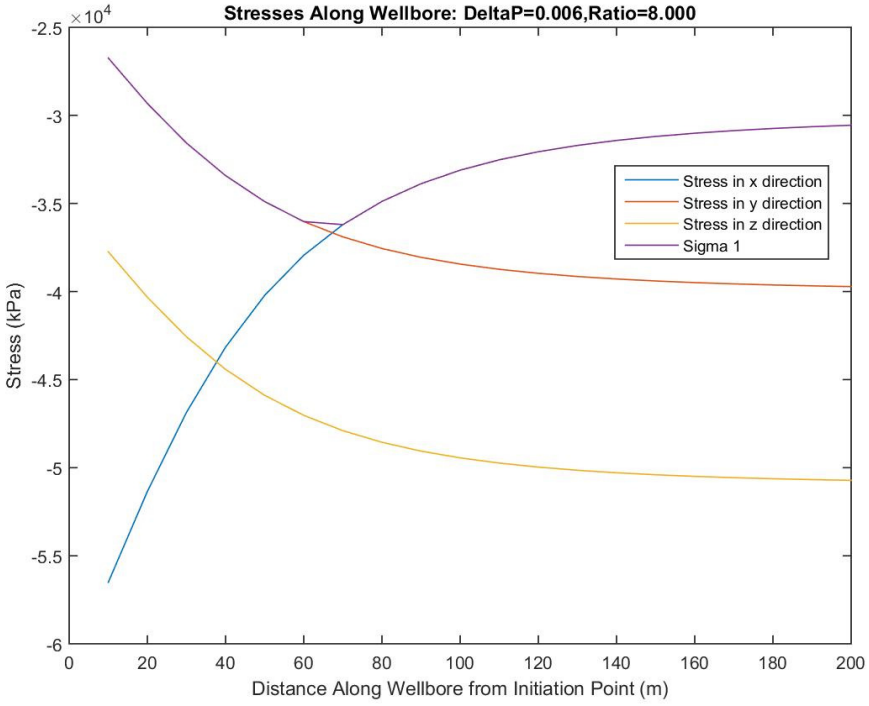
Stresses Along Wellbore: DeltaP=0.006,Ratio=8.000
×10^4
-2.5
-3
-3.5
-4
-4.5
-5
-5.5
-6
Stress (kPa)
0
20
40
60
80
100
120
140
160
180
200
Distance Along Wellbore from Initiation Point (m)
Stress in x direction
Stress in y direction
Stress in z direction
Sigma 1

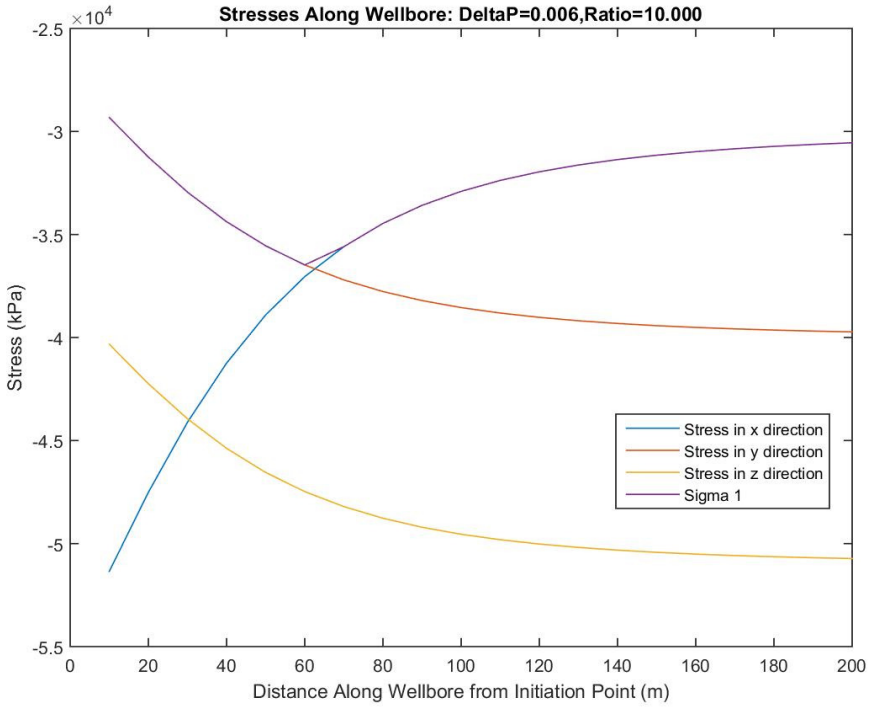
Stresses Along Wellbore: DeltaP=0.006,Ratio=10.000
×10^4
-2.5
-3
-3.5
-4
-4.5
-5
-5.5
Stress (kPa)
0
20
40
60
80
100
120
140
160
180
200
Distance Along Wellbore from Initiation Point (m)
Stress in x direction
Stress in y direction
Stress in z direction
Sigma 1

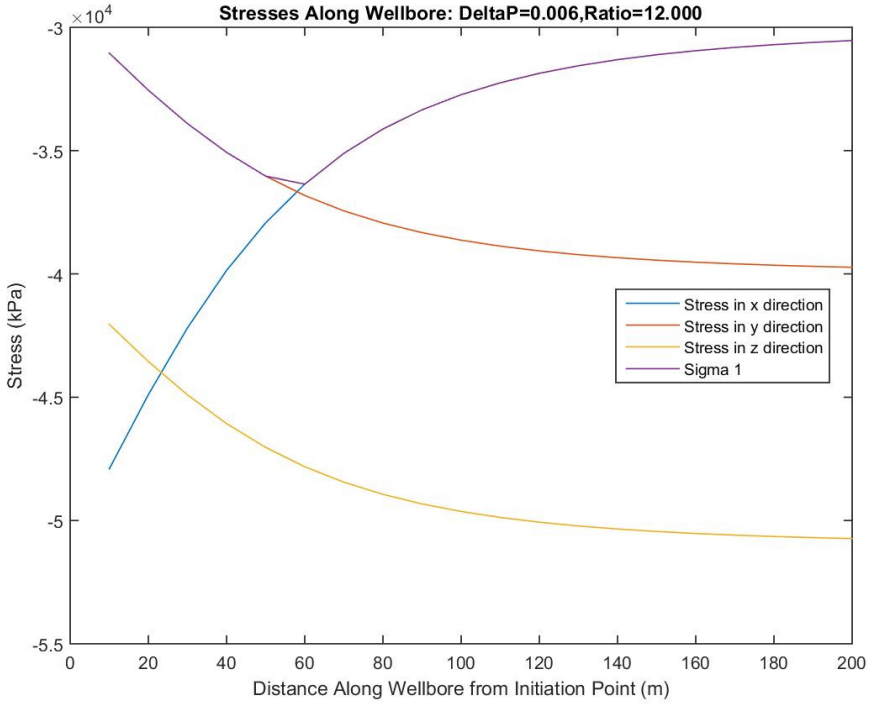
Stresses Along Wellbore: DeltaP=0.006,Ratio=12.000
×10^4
-3
-3.5
-4
-4.5
-5
-5.5
Stress (kPa)
0
20
40
60
80
100
120
140
160
180
200
Distance Along Wellbore from Initiation Point (m)
Stress in x direction
Stress in y direction
Stress in z direction
Sigma 1

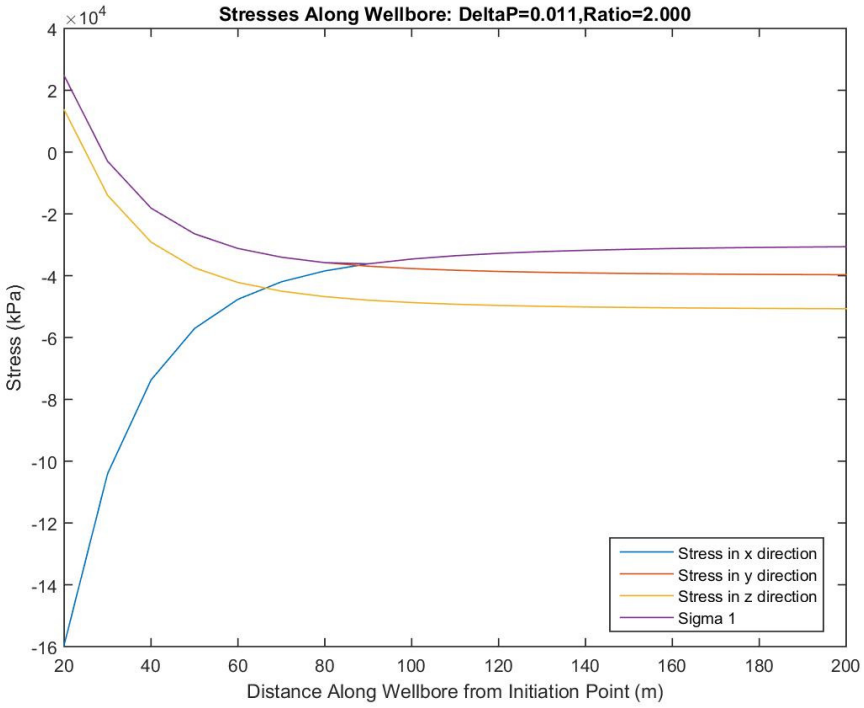
Stresses Along Wellbore: DeltaP=0.011,Ratio=2.000
×10^4
Stress (kPa)
Distance Along Wellbore from Initiation Point (m)
Stress in x direction
Stress in y direction
Stress in z direction
Sigma 1

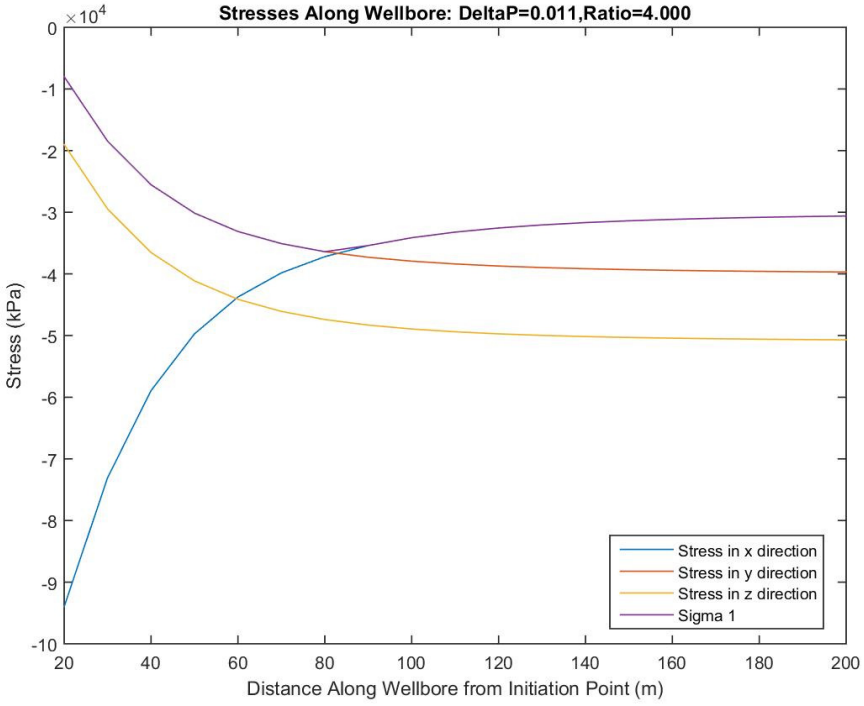
Stresses Along Wellbore: DeltaP=0.011,Ratio=4.000
×10^4
Stress (kPa)
Distance Along Wellbore from Initiation Point (m)
Stress in x direction
Stress in y direction
Stress in z direction
Sigma 1

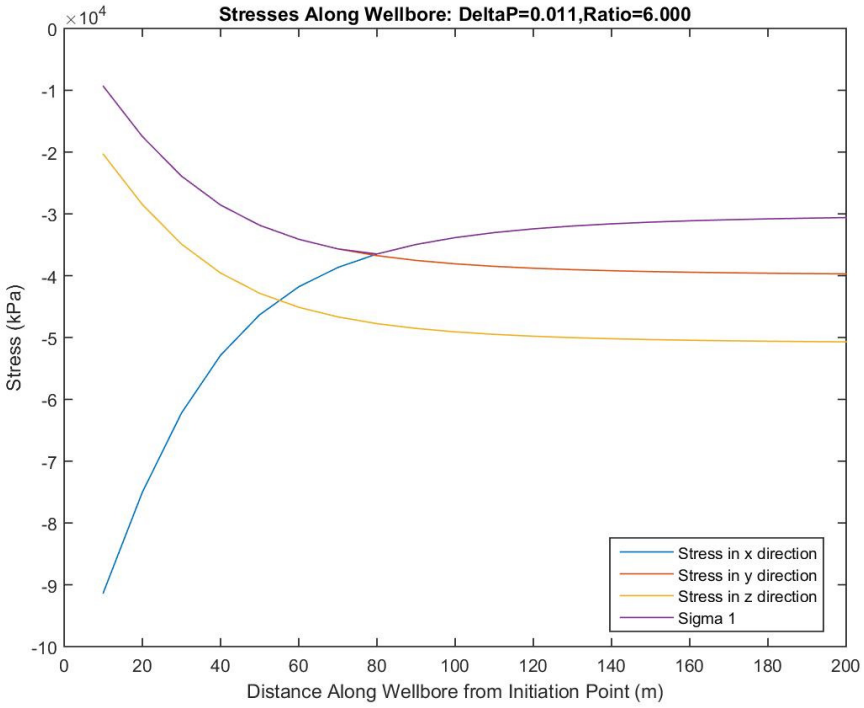
Stresses Along Wellbore: DeltaP=0.011,Ratio=6.000
×10^4
0
-1
-2
-3
-4
-5
-6
-7
-8
-9
-10
Stress (kPa)
0
20
40
60
80
100
120
140
160
180
200
Distance Along Wellbore from Initiation Point (m)
Stress in x direction
Stress in y direction
Stress in z direction
Sigma 1

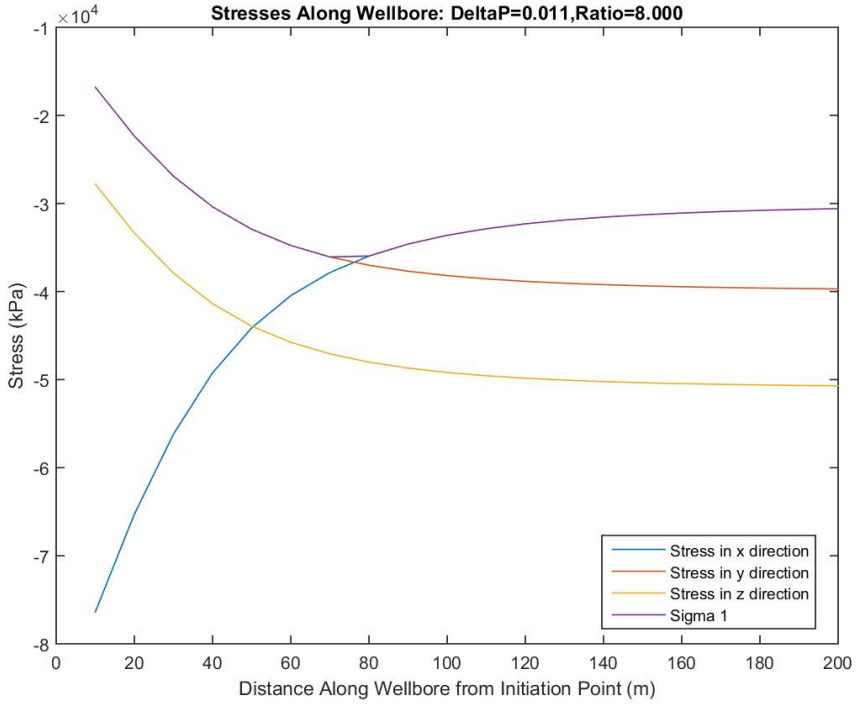
Stresses Along Wellbore: DeltaP=0.011,Ratio=8.000
×10^4
-1
-2
-3
-4
-5
-6
-7
-8
Stress (kPa)
0
20
40
60
80
100
120
140
160
180
200
Distance Along Wellbore from Initiation Point (m)
Stress in x direction
Stress in y direction
Stress in z direction
Sigma 1

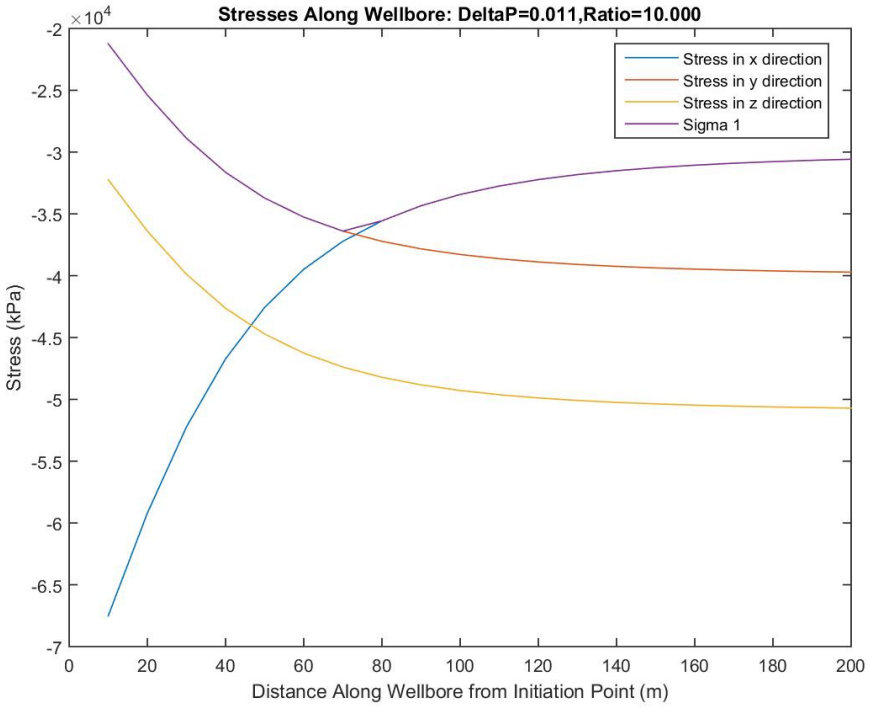
Stresses Along Wellbore: DeltaP=0.011,Ratio=10.000
×10^4
-2
-2.5
-3
-3.5
-4
-4.5
-5
-5.5
-6
-6.5
-7
Stress (kPa)
0
20
40
60
80
100
120
140
160
180
200
Distance Along Wellbore from Initiation Point (m)
Stress in x direction
Stress in y direction
Stress in z direction
Sigma 1

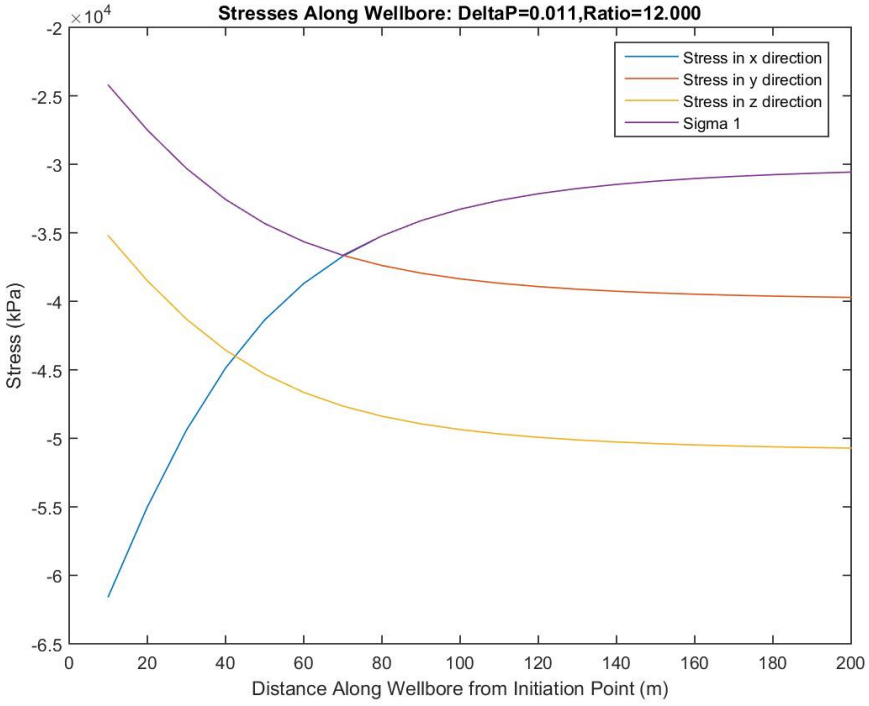
Stresses Along Wellbore: DeltaP=0.011,Ratio=12.000
×10^4
-2
-2.5
-3
-3.5
-4
-4.5
-5
-5.5
-6
-6.5
Stress (kPa)
0
20
40
60
80
100
120
140
160
180
200
Distance Along Wellbore from Initiation Point (m)
Stress in x direction
Stress in y direction
Stress in z direction
Sigma 1

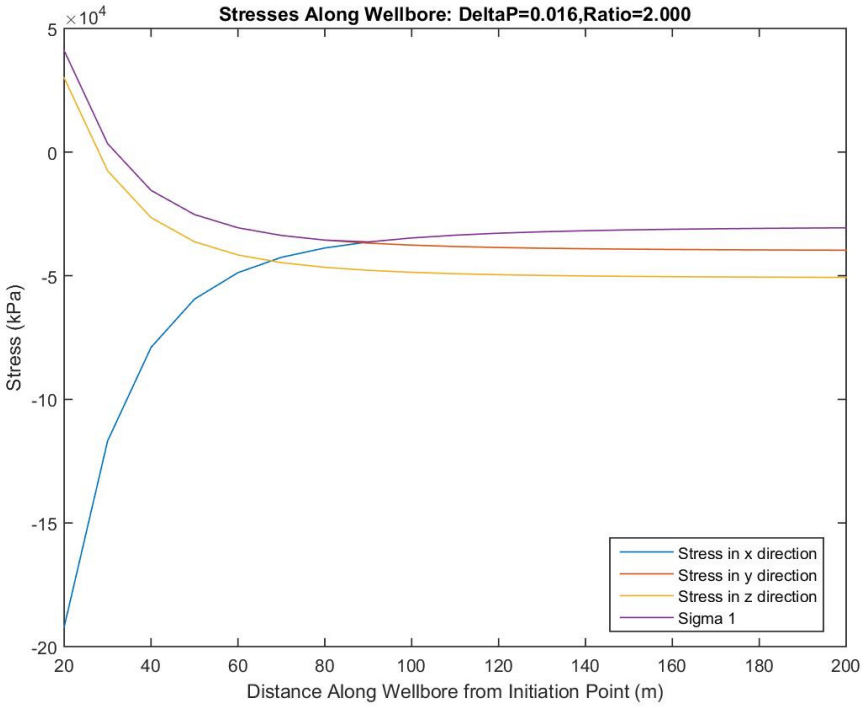
Stresses Along Wellbore: DeltaP=0.016,Ratio=2.000
×10^4
5
0
-5
-10
-15
-20
Stress (kPa)
20
40
60
80
100
120
140
160
180
200
Distance Along Wellbore from Initiation Point (m)
Stress in x direction
Stress in y direction
Stress in z direction
Sigma 1

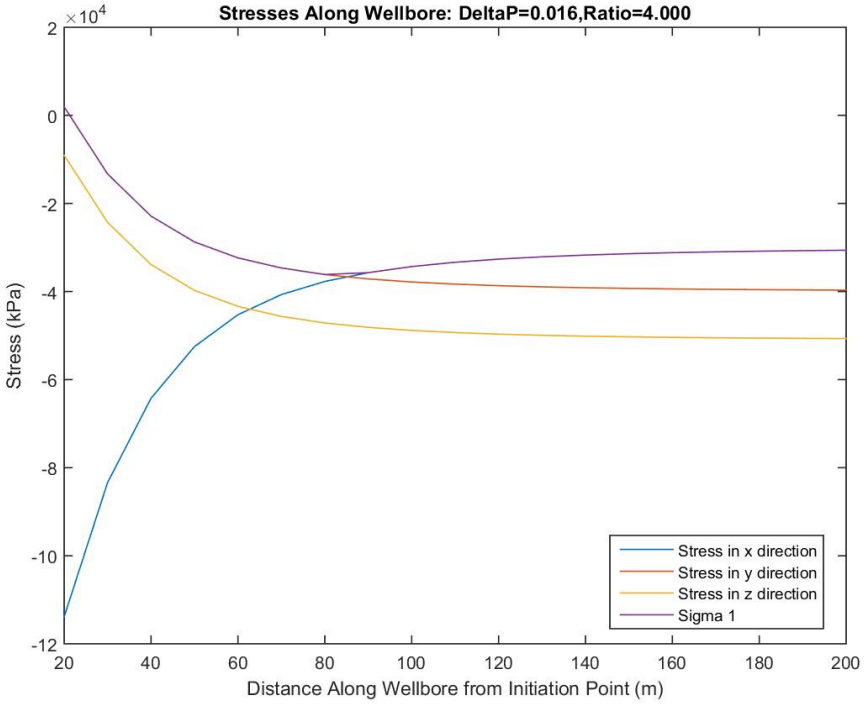
Stresses Along Wellbore: DeltaP=0.016,Ratio=4.000
×10^4
2
0
-2
-4
-6
-8
-10
-12
Stress (kPa)
20
40
60
80
100
120
140
160
180
200
Distance Along Wellbore from Initiation Point (m)
Stress in x direction
Stress in y direction
Stress in z direction
Sigma 1

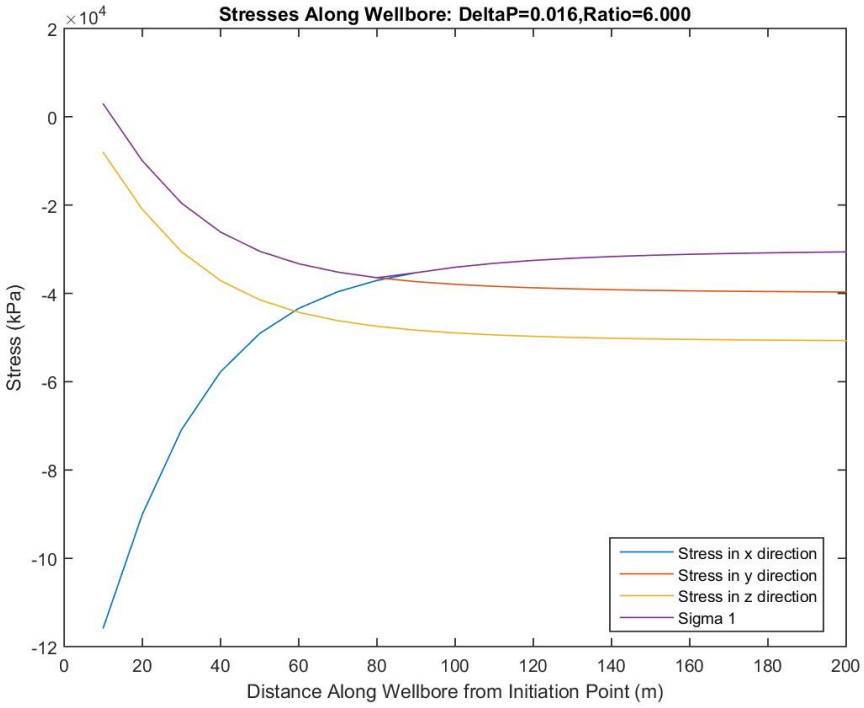
Stresses Along Wellbore: DeltaP=0.016,Ratio=6.000
×10^4
2
0
-2
-4
-6
-8
-10
-12
Stress (kPa)
0
20
40
60
80
100
120
140
160
180
200
Distance Along Wellbore from Initiation Point (m)
Stress in x direction
Stress in y direction
Stress in z direction
Sigma 1

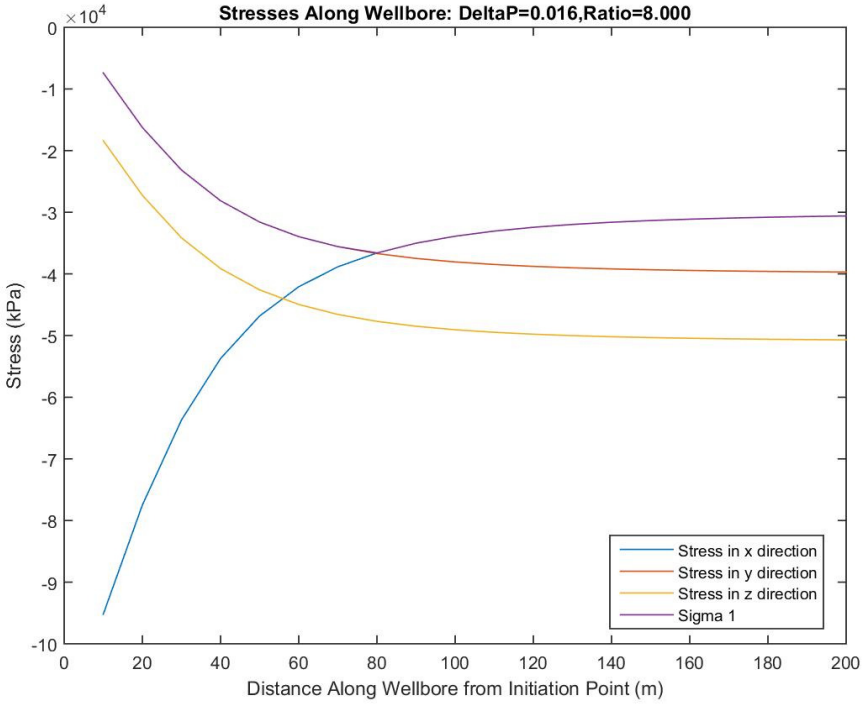
Stresses Along Wellbore: DeltaP=0.016,Ratio=8.000
×10^4
0
-1
-2
-3
-4
-5
-6
-7
-8
-9
-10
Stress (kPa)
0
20
40
60
80
100
120
140
160
180
200
Distance Along Wellbore from Initiation Point (m)
Stress in x direction
Stress in y direction
Stress in z direction
Sigma 1

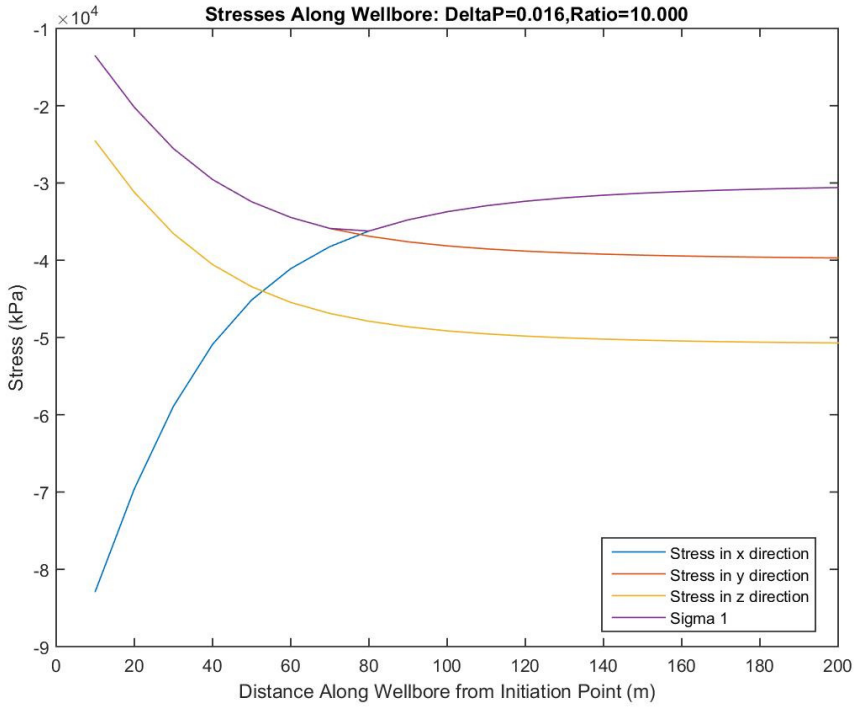
Stresses Along Wellbore: DeltaP=0.016,Ratio=10.000
×10^4
-1
-2
-3
-4
-5
-6
-7
-8
-9
Stress (kPa)
0
20
40
60
80
100
120
140
160
180
200
Distance Along Wellbore from Initiation Point (m)
Stress in x direction
Stress in y direction
Stress in z direction
Sigma 1

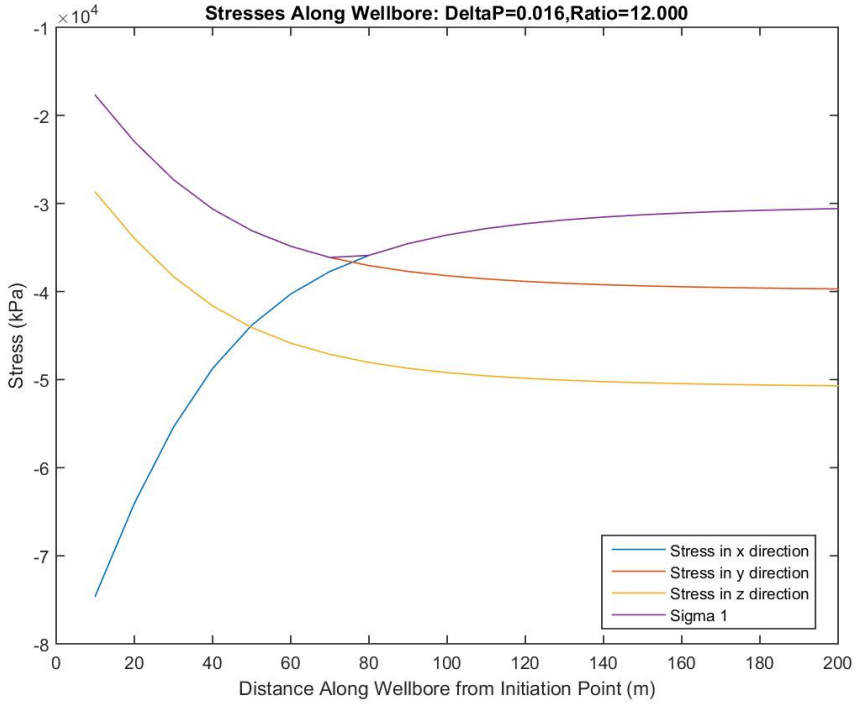
Stresses Along Wellbore: DeltaP=0.016,Ratio=12.000
×10^4
-1
-2
-3
-4
-5
-6
-7
-8
Stress (kPa)
0
20
40
60
80
100
120
140
160
180
200
Distance Along Wellbore from Initiation Point (m)
Stress in x direction
Stress in y direction
Stress in z direction
Sigma 1

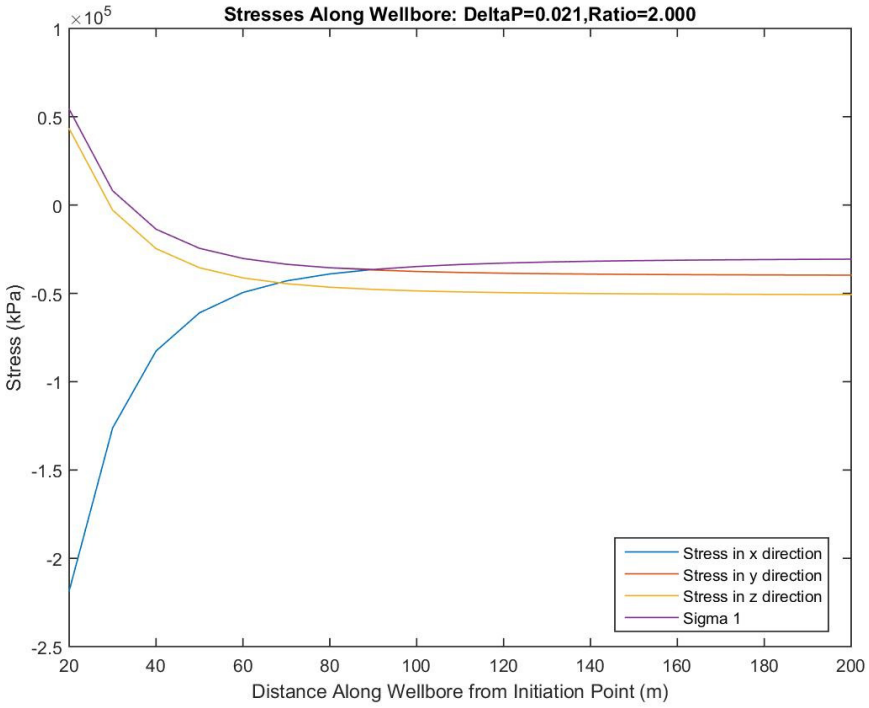
Stresses Along Wellbore: DeltaP=0.021,Ratio=2.000
×10^5
1
0.5
0
-0.5
-1
-1.5
-2
-2.5
Stress (kPa)
20
40
60
80
100
120
140
160
180
200
Distance Along Wellbore from Initiation Point (m)
Stress in x direction
Stress in y direction
Stress in z direction
Sigma 1

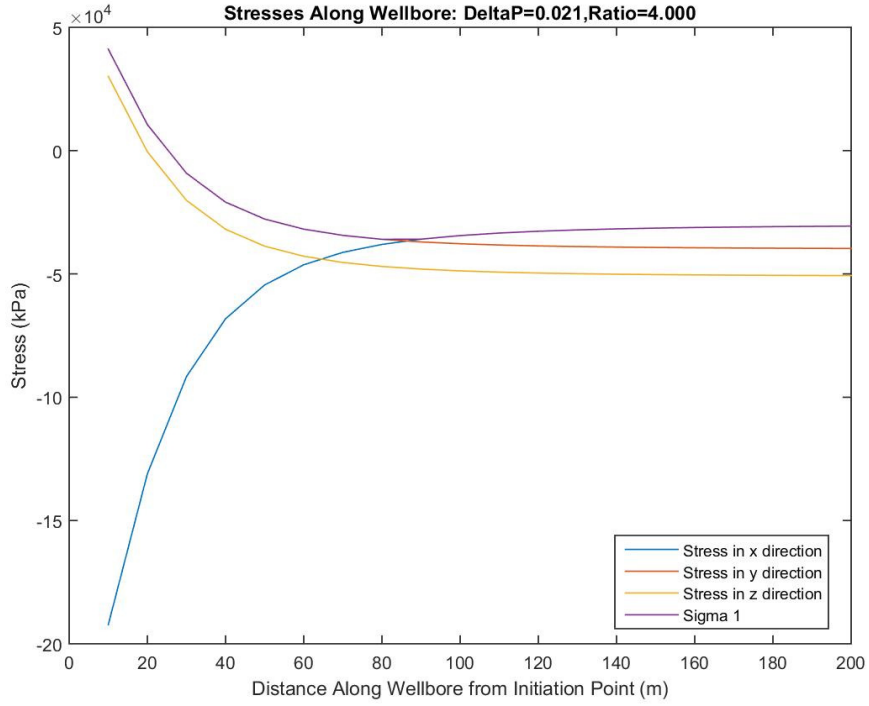
Stresses Along Wellbore: DeltaP=0.021,Ratio=4.000
×10^4
5
0
-5
-10
-15
-20
Stress (kPa)
0
20
40
60
80
100
120
140
160
180
200
Distance Along Wellbore from Initiation Point (m)
Stress in x direction
Stress in y direction
Stress in z direction
Sigma 1

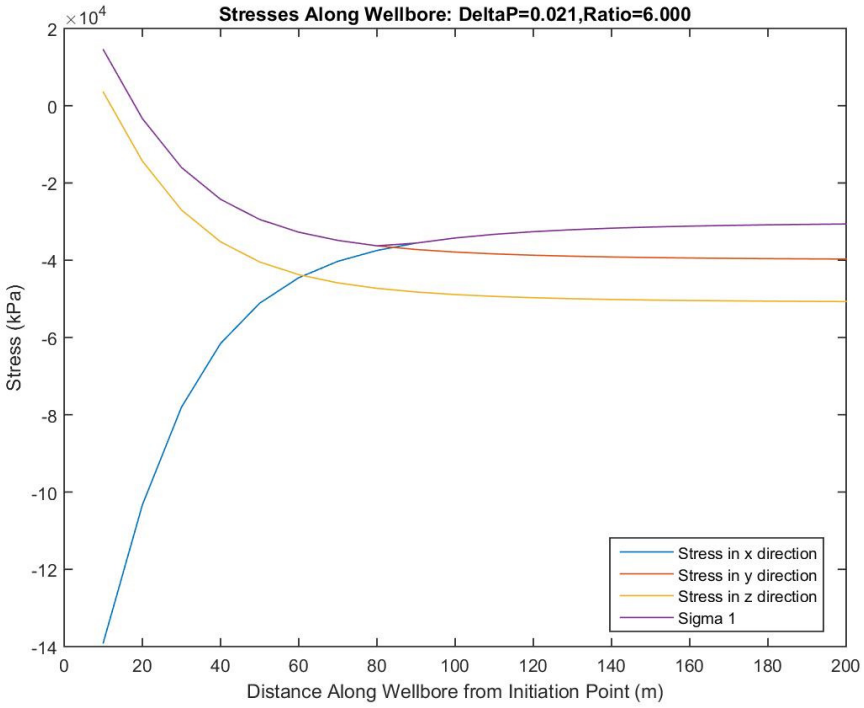
Stresses Along Wellbore: DeltaP=0.021,Ratio=6.000
×10^4
Stress (kPa)
Distance Along Wellbore from Initiation Point (m)
Stress in x direction
Stress in y direction
Stress in z direction
Sigma 1

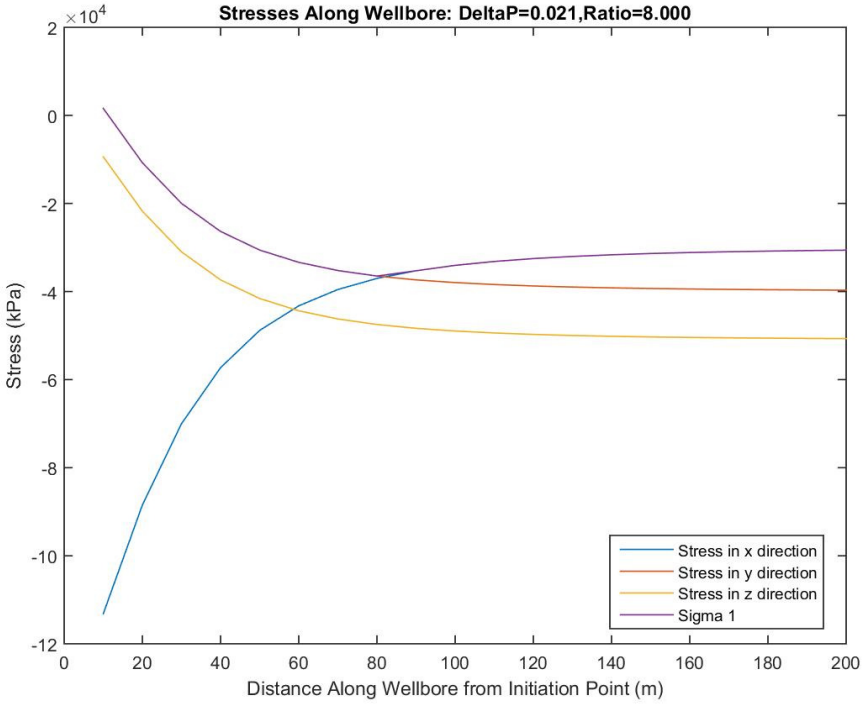
Stresses Along Wellbore: DeltaP=0.021,Ratio=8.000
×10^4
Stress (kPa)
Distance Along Wellbore from Initiation Point (m)
Stress in x direction
Stress in y direction
Stress in z direction
Sigma 1

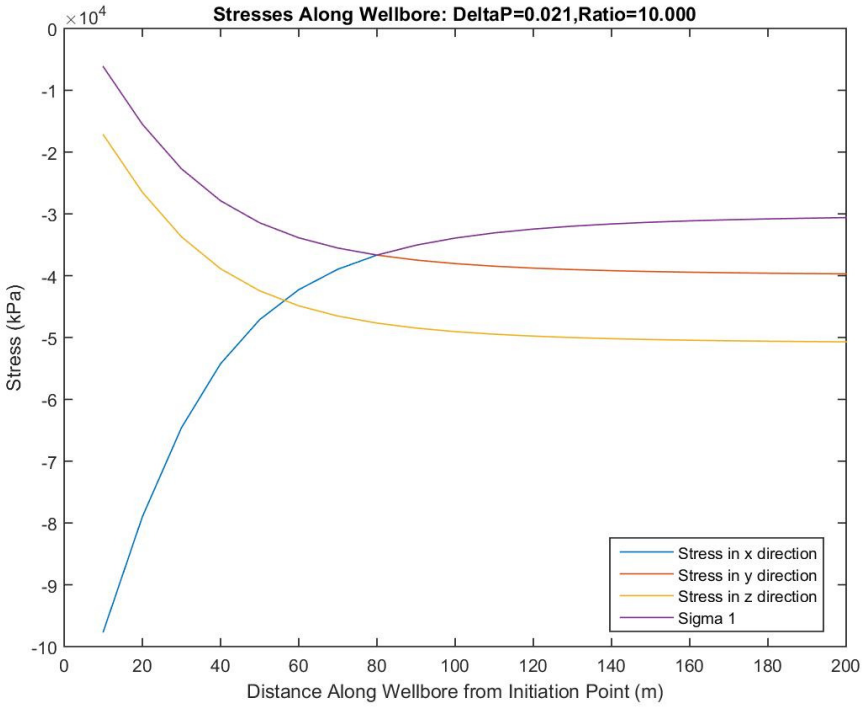
Stresses Along Wellbore: DeltaP=0.021,Ratio=10.000
×10^4
0
-1
-2
-3
-4
-5
-6
-7
-8
-9
-10
Stress (kPa)
0
20
40
60
80
100
120
140
160
180
200
Distance Along Wellbore from Initiation Point (m)
Stress in x direction
Stress in y direction
Stress in z direction
Sigma 1

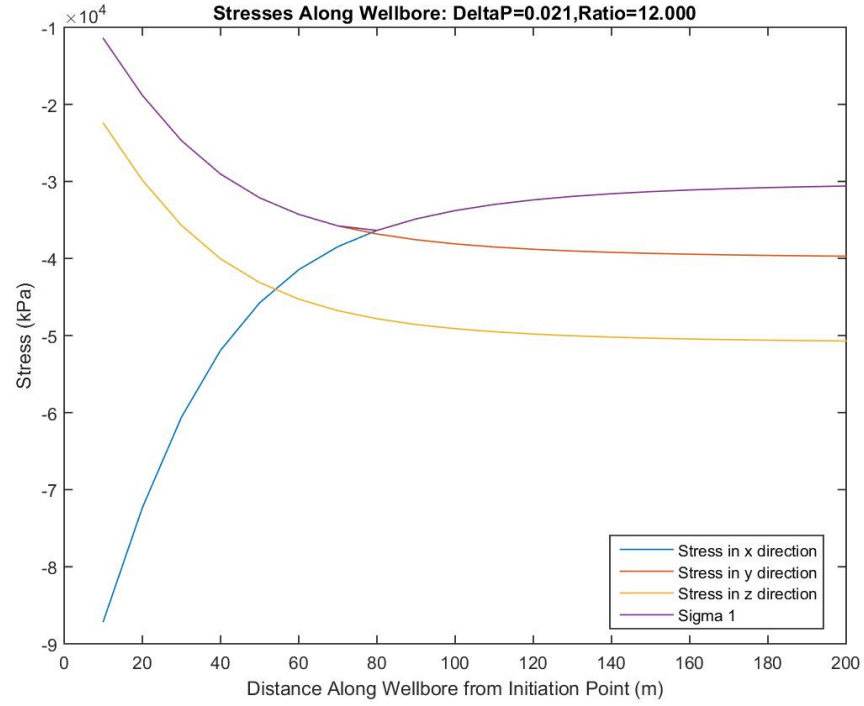
Stresses Along Wellbore: DeltaP=0.021,Ratio=12.000
×10^4
-1
-2
-3
-4
-5
-6
-7
-8
-9
Stress (kPa)
0
20
40
60
80
100
120
140
160
180
200
Distance Along Wellbore from Initiation Point (m)
Stress in x direction
Stress in y direction
Stress in z direction
Sigma 1

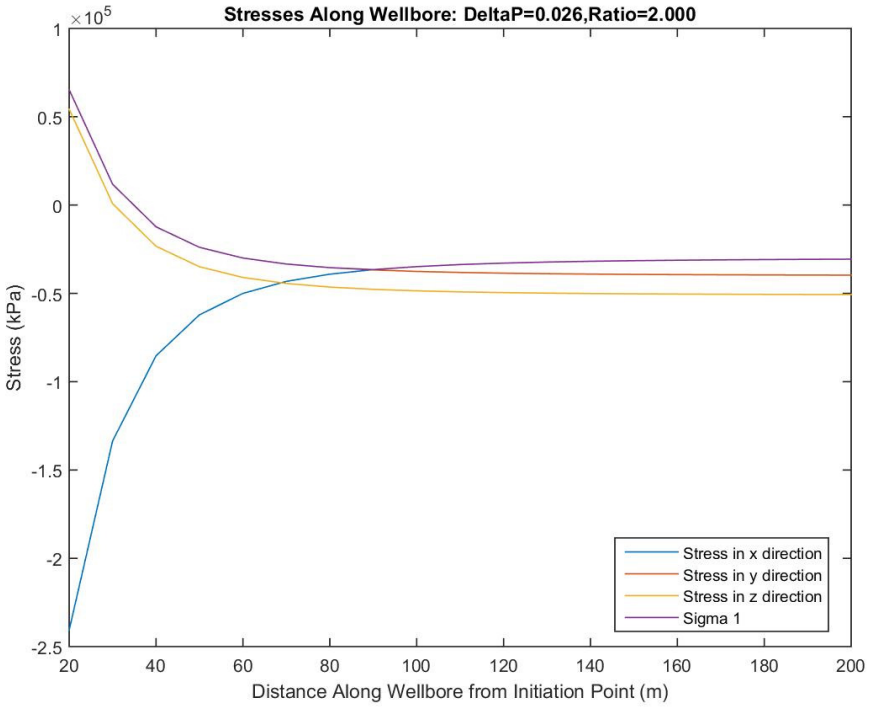
Stresses Along Wellbore: DeltaP=0.026,Ratio=2.000
×10^5
1
0.5
0
-0.5
-1
-1.5
-2
-2.5
Stress (kPa)
20
40
60
80
100
120
140
160
180
200
Distance Along Wellbore from Initiation Point (m)
Stress in x direction
Stress in y direction
Stress in z direction
Sigma 1

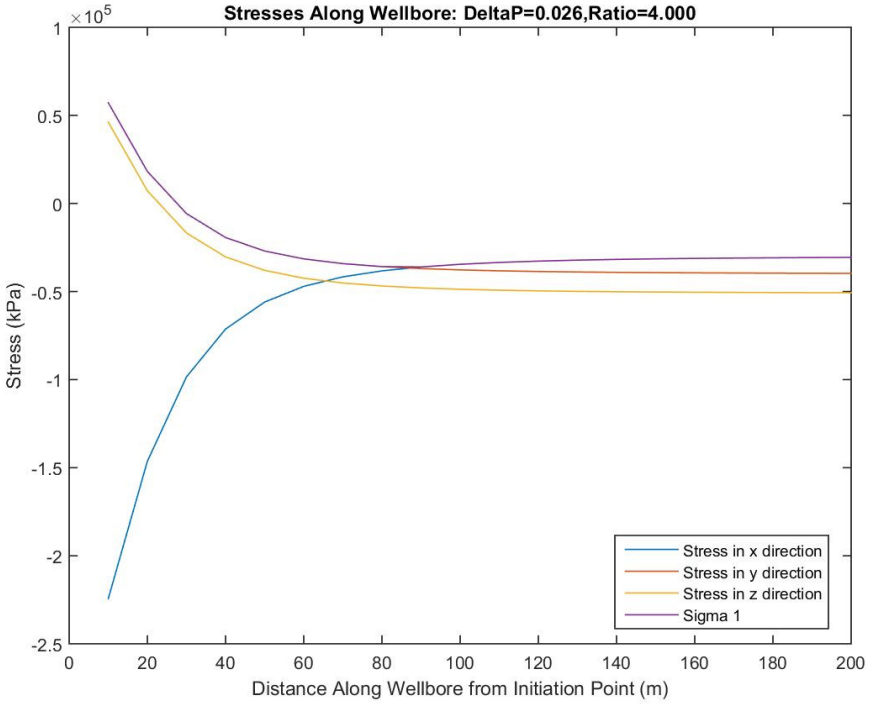
Stresses Along Wellbore: DeltaP=0.026,Ratio=4.000
×10^5
1
0.5
0
-0.5
-1
-1.5
-2
-2.5
Stress (kPa)
0
20
40
60
80
100
120
140
160
180
200
Distance Along Wellbore from Initiation Point (m)
Stress in x direction
Stress in y direction
Stress in z direction
Sigma 1

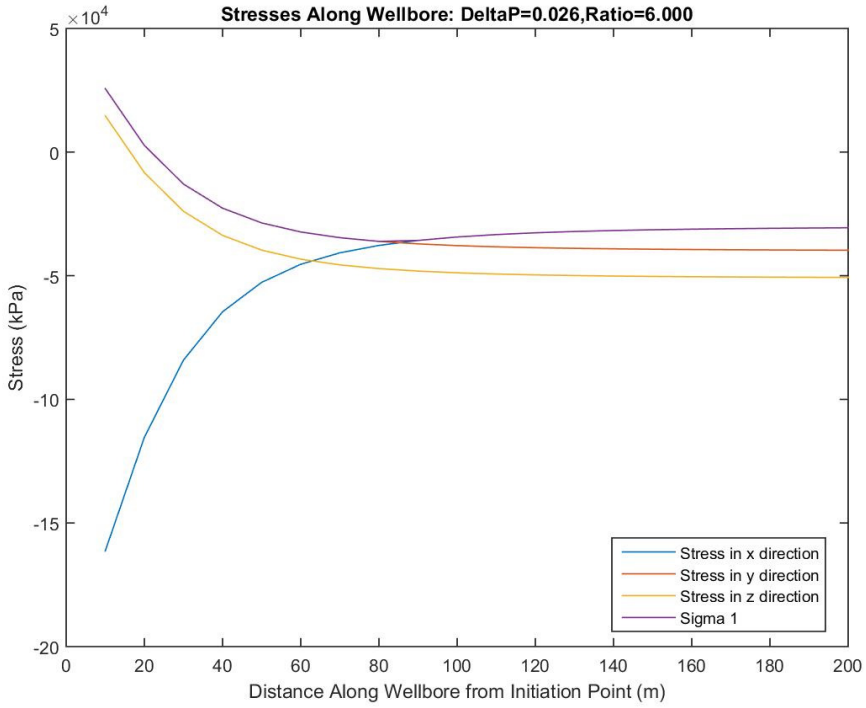
Stresses Along Wellbore: DeltaP=0.026,Ratio=6.000
×10^4
5
0
-5
-10
-15
-20
Stress (kPa)
0
20
40
60
80
100
120
140
160
180
200
Distance Along Wellbore from Initiation Point (m)
Stress in x direction
Stress in y direction
Stress in z direction
Sigma 1

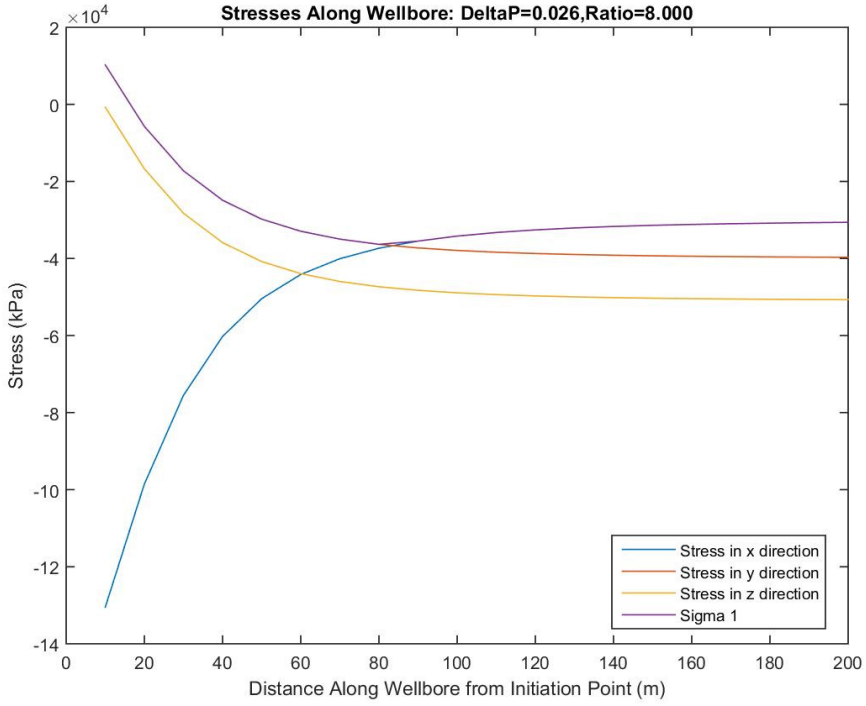
Stresses Along Wellbore: DeltaP=0.026,Ratio=8.000
×10^4
2
0
-2
-4
-6
-8
-10
-12
-14
Stress (kPa)
0
20
40
60
80
100
120
140
160
180
200
Distance Along Wellbore from Initiation Point (m)
Stress in x direction
Stress in y direction
Stress in z direction
Sigma 1

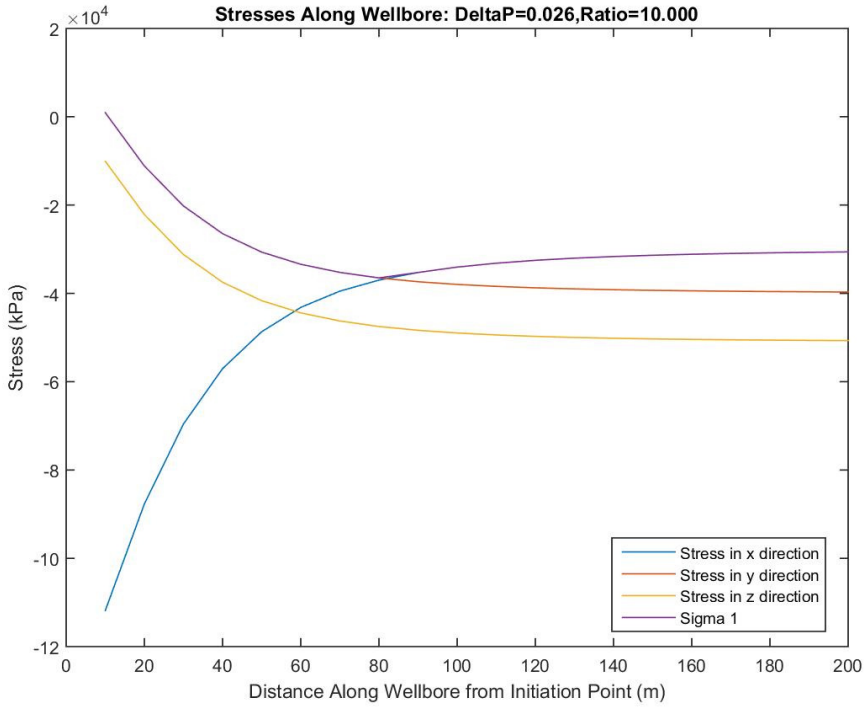
Stresses Along Wellbore: DeltaP=0.026,Ratio=10.000
×10^4
2
0
-2
-4
-6
-8
-10
-12
Stress (kPa)
0
20
40
60
80
100
120
140
160
180
200
Distance Along Wellbore from Initiation Point (m)
Stress in x direction
Stress in y direction
Stress in z direction
Sigma 1

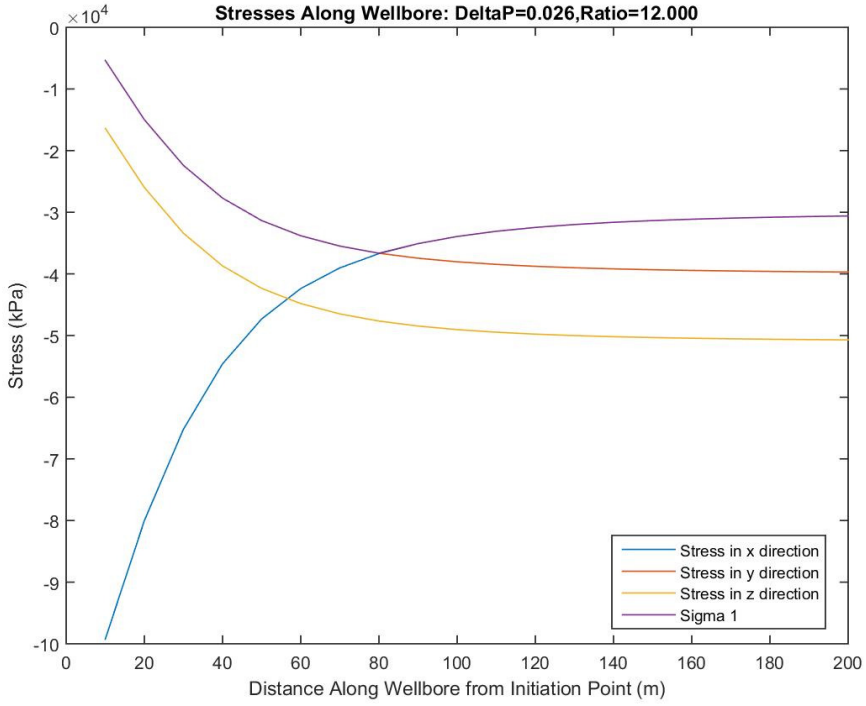
Stresses Along Wellbore: DeltaP=0.026,Ratio=12.000
×10^4
0
-1
-2
-3
-4
-5
-6
-7
-8
-9
-10
Stress (kPa)
0
20
40
60
80
100
120
140
160
180
200
Distance Along Wellbore from Initiation Point (m)
Stress in x direction
Stress in y direction
Stress in z direction
Sigma 1

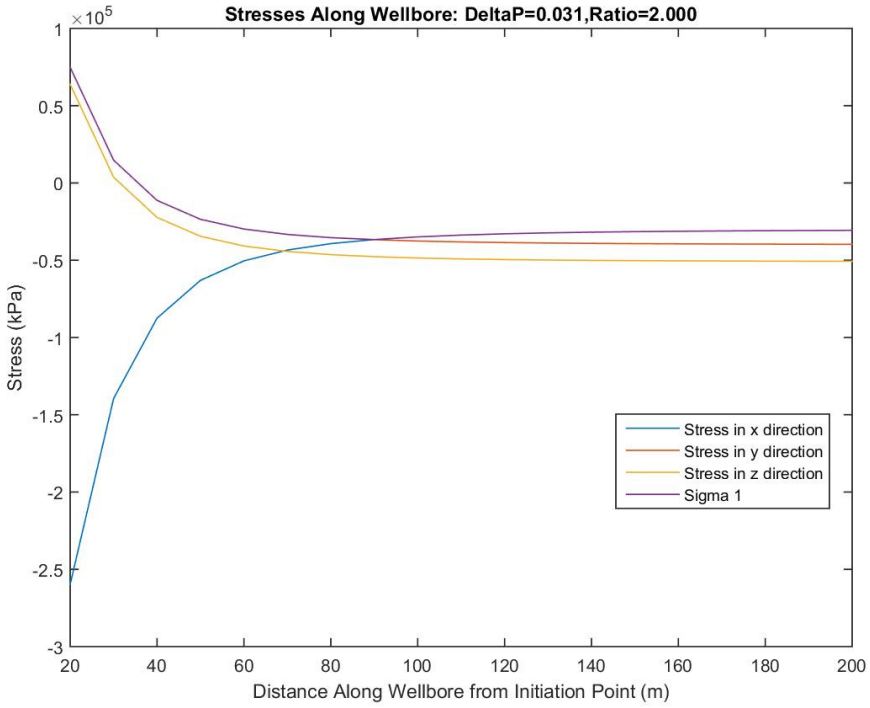
Stresses Along Wellbore: DeltaP=0.031,Ratio=2.000
×10^5
1
0.5
0
-0.5
-1
-1.5
-2
-2.5
-3
Stress (kPa)
20
40
60
80
100
120
140
160
180
200
Distance Along Wellbore from Initiation Point (m)
Stress in x direction
Stress in y direction
Stress in z direction
Sigma 1

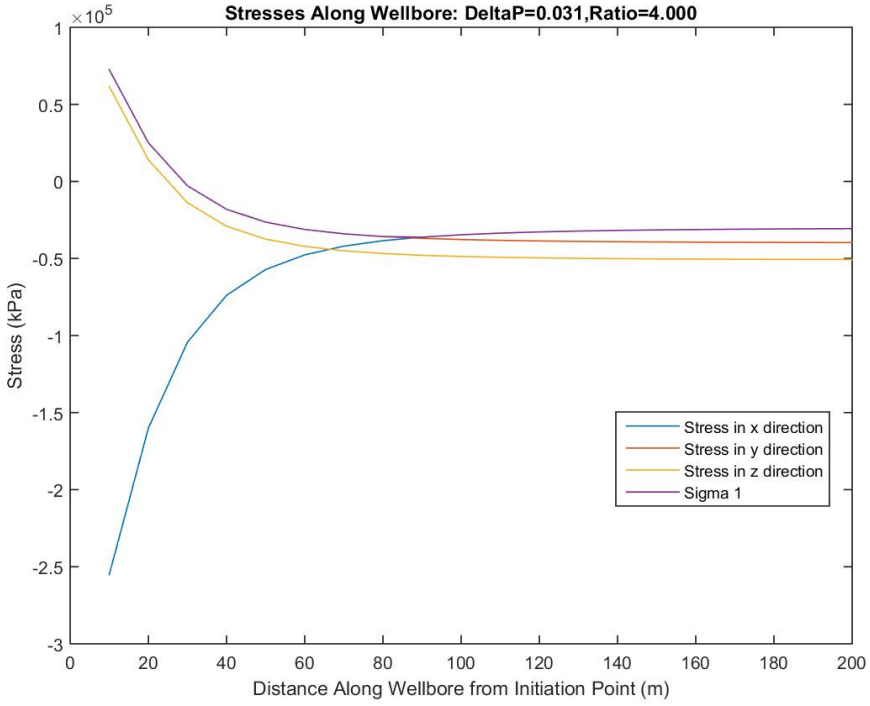
Stresses Along Wellbore: DeltaP=0.031,Ratio=4.000
×10^5
1
0.5
0
-0.5
-1
-1.5
-2
-2.5
-3
Stress (kPa)
0
20
40
60
80
100
120
140
160
180
200
Distance Along Wellbore from Initiation Point (m)
Stress in x direction
Stress in y direction
Stress in z direction
Sigma 1

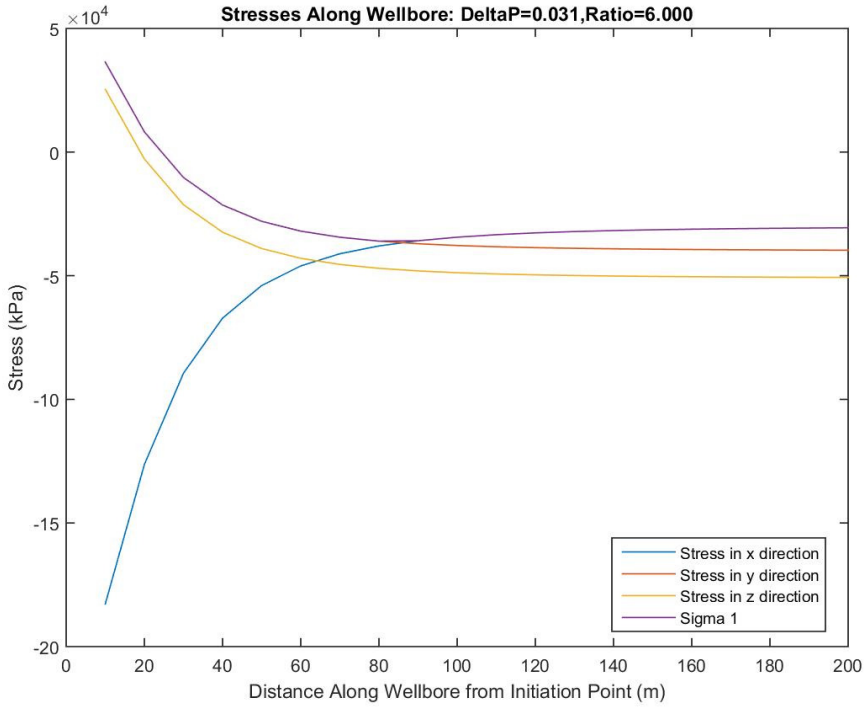
Stresses Along Wellbore: DeltaP=0.031,Ratio=6.000
×10^4
5
0
-5
-10
-15
-20
Stress (kPa)
0
20
40
60
80
100
120
140
160
180
200
Distance Along Wellbore from Initiation Point (m)
Stress in x direction
Stress in y direction
Stress in z direction
Sigma 1

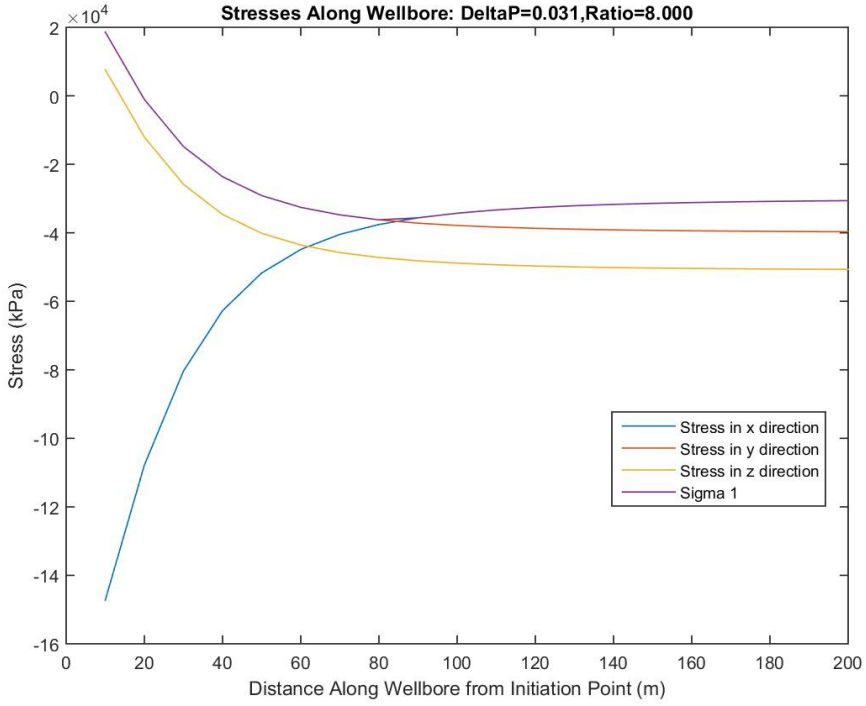
Stresses Along Wellbore: DeltaP=0.031,Ratio=8.000
×10^4
2
0
-2
-4
-6
-8
-10
-12
-14
-16
Stress (kPa)
0
20
40
60
80
100
120
140
160
180
200
Distance Along Wellbore from Initiation Point (m)
Stress in x direction
Stress in y direction
Stress in z direction
Sigma 1

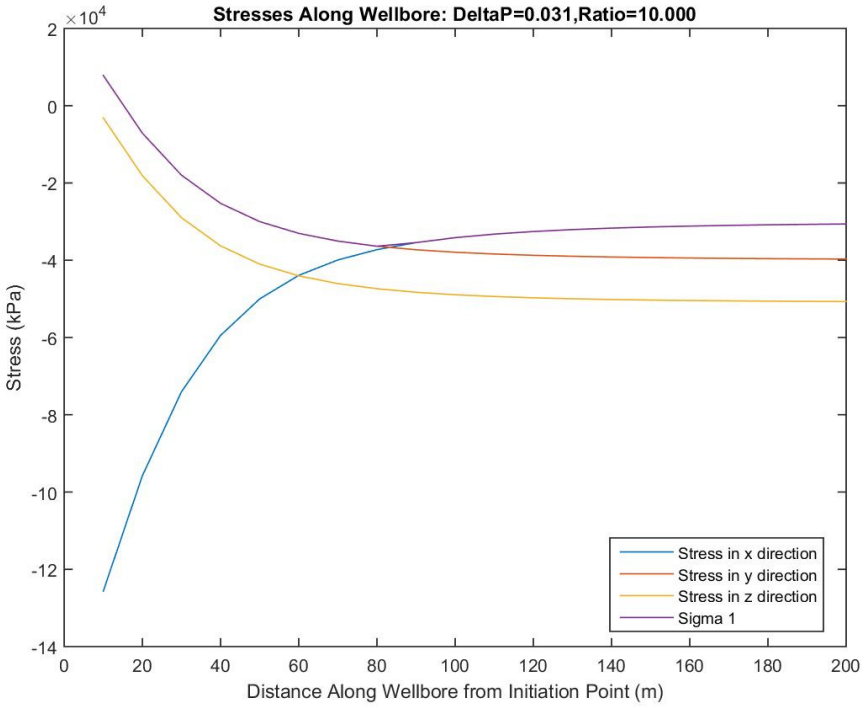
Stresses Along Wellbore: DeltaP=0.031,Ratio=10.000
×10^4
2
0
-2
-4
-6
-8
-10
-12
-14
Stress (kPa)
0
20
40
60
80
100
120
140
160
180
200
Distance Along Wellbore from Initiation Point (m)
Stress in x direction
Stress in y direction
Stress in z direction
Sigma 1

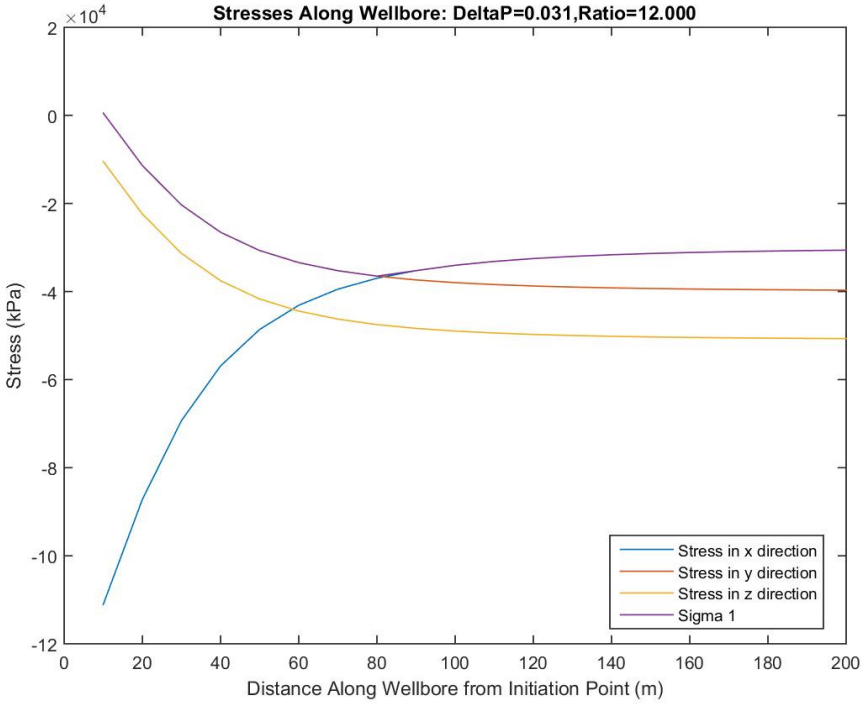
Stresses Along Wellbore: DeltaP=0.031,Ratio=12.000
×10^4
2
0
-2
-4
-6
-8
-10
-12
Stress (kPa)
0
20
40
60
80
100
120
140
160
180
200
Distance Along Wellbore from Initiation Point (m)
Stress in x direction
Stress in y direction
Stress in z direction
Sigma 1

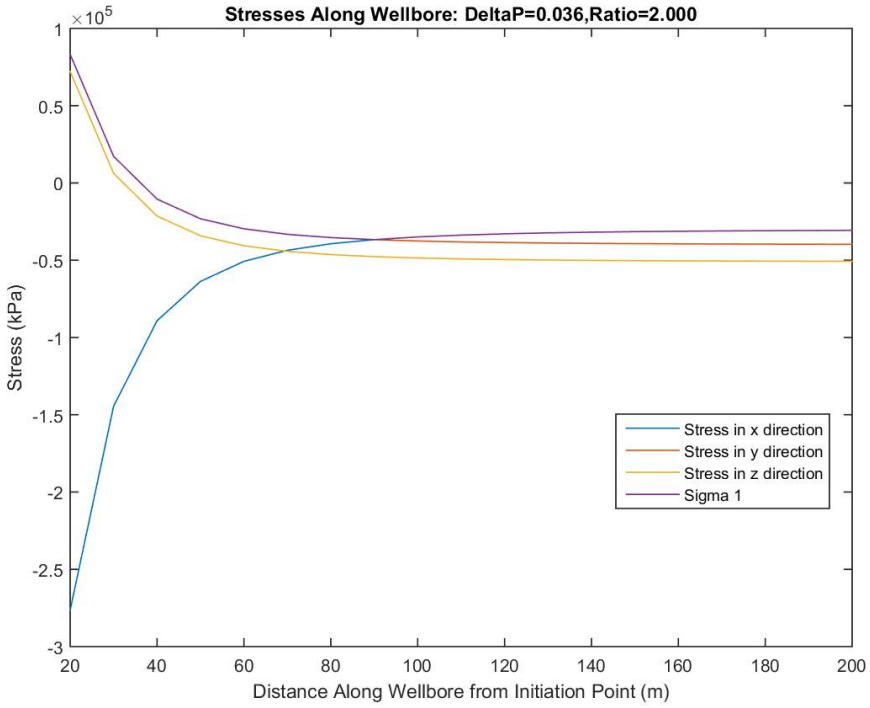
Stresses Along Wellbore: DeltaP=0.036,Ratio=2.000
×10^5
1
0.5
0
-0.5
-1
-1.5
-2
-2.5
-3
Stress (kPa)
20
40
60
80
100
120
140
160
180
200
Distance Along Wellbore from Initiation Point (m)
Stress in x direction
Stress in y direction
Stress in z direction
Sigma 1

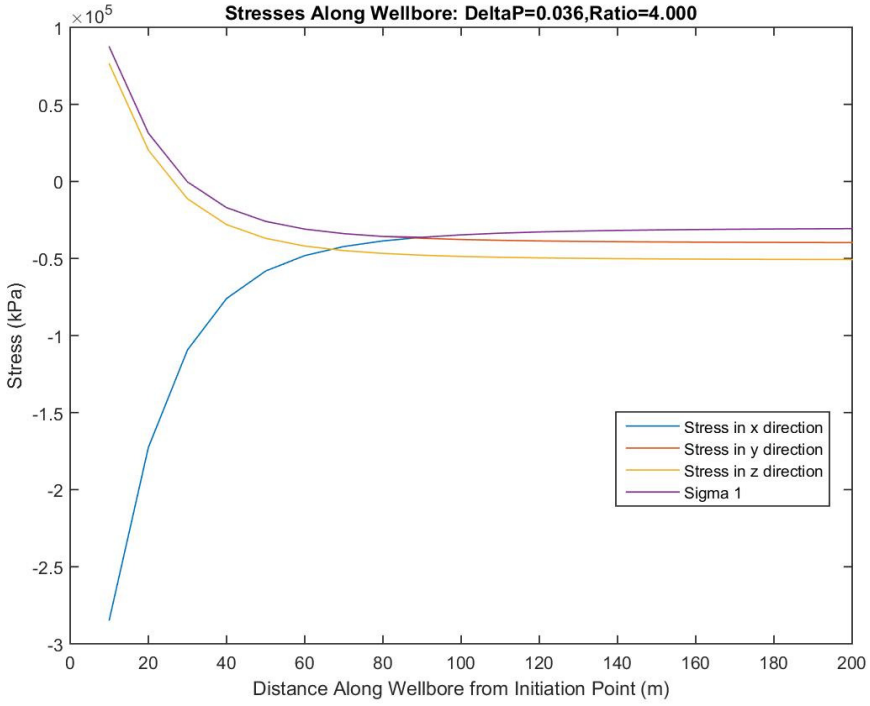
Stresses Along Wellbore: DeltaP=0.036,Ratio=4.000
×10^5
1
0.5
0
-0.5
-1
-1.5
-2
-2.5
-3
Stress (kPa)
0
20
40
60
80
100
120
140
160
180
200
Distance Along Wellbore from Initiation Point (m)
Stress in x direction
Stress in y direction
Stress in z direction
Sigma 1

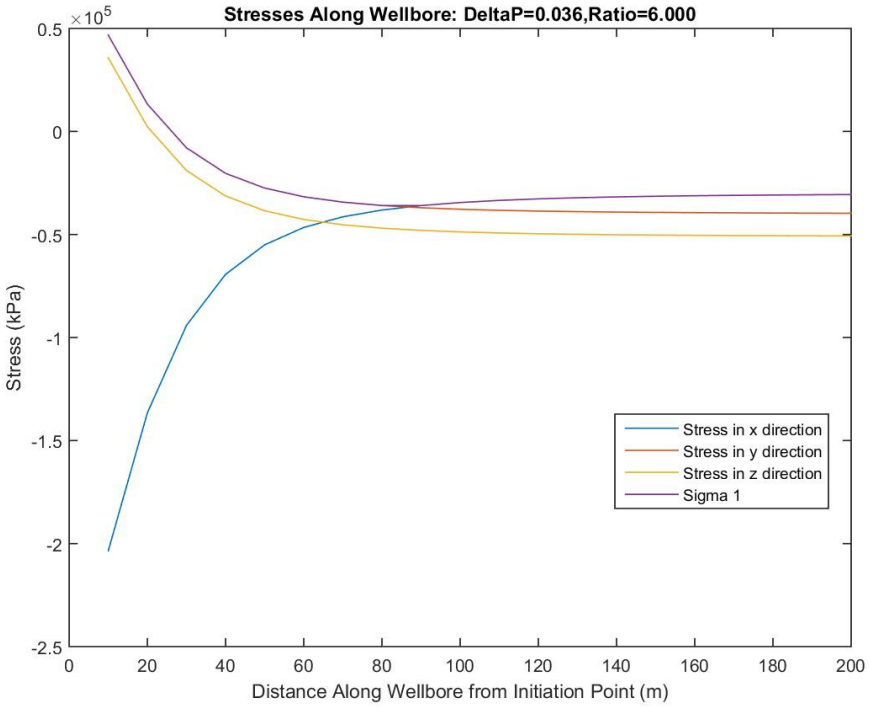
Stresses Along Wellbore: DeltaP=0.036,Ratio=6.000
×10^5
0.5
0
-0.5
-1
-1.5
-2
-2.5
Stress (kPa)
0
20
40
60
80
100
120
140
160
180
200
Distance Along Wellbore from Initiation Point (m)
Stress in x direction
Stress in y direction
Stress in z direction
Sigma 1

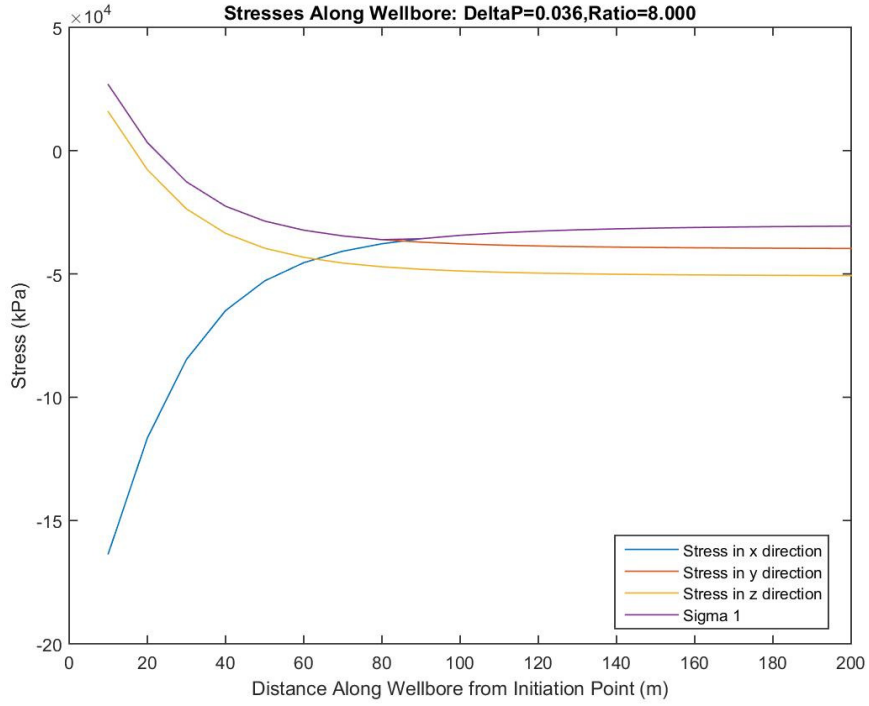
Stresses Along Wellbore: DeltaP=0.036,Ratio=8.000
×10^4
5
0
-5
-10
-15
-20
Stress (kPa)
0
20
40
60
80
100
120
140
160
180
200
Distance Along Wellbore from Initiation Point (m)
Stress in x direction
Stress in y direction
Stress in z direction
Sigma 1

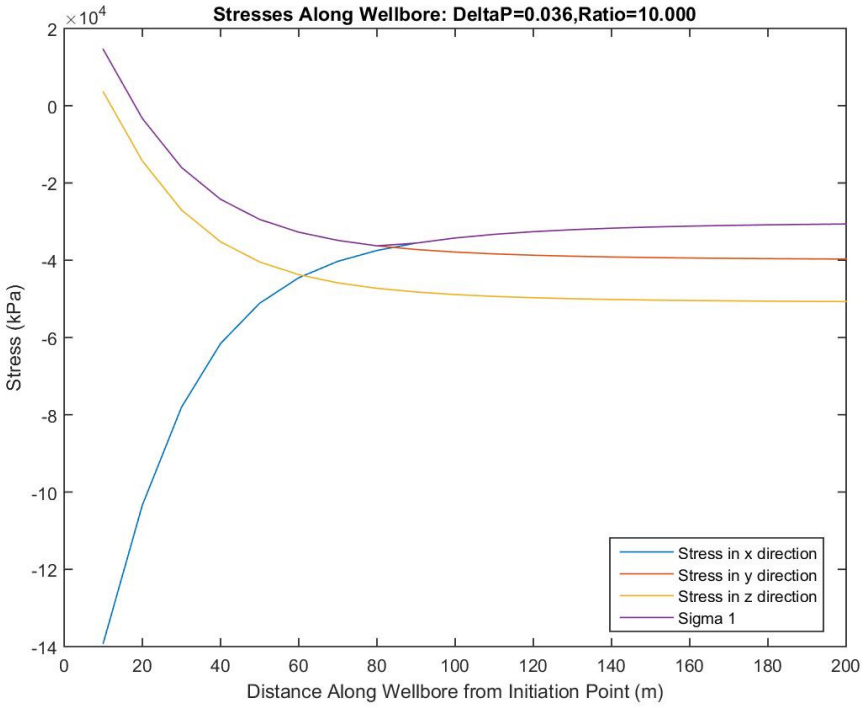
Stresses Along Wellbore: DeltaP=0.036,Ratio=10.000
×10^4
2
0
-2
-4
-6
-8
-10
-12
-14
Stress (kPa)
0
20
40
60
80
100
120
140
160
180
200
Distance Along Wellbore from Initiation Point (m)
Stress in x direction
Stress in y direction
Stress in z direction
Sigma 1

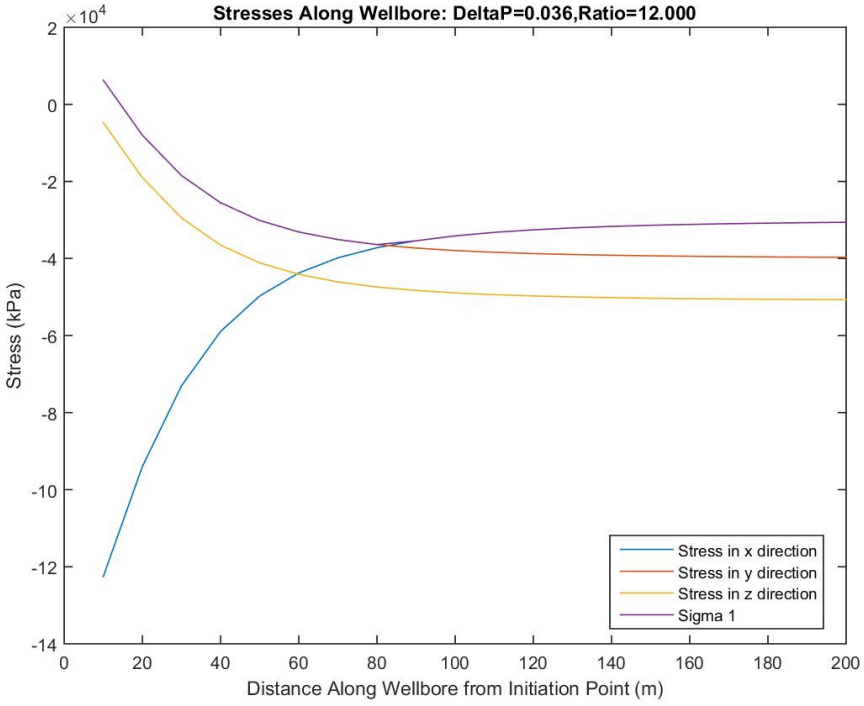
Stresses Along Wellbore: DeltaP=0.036,Ratio=12.000
×10^4
2
0
-2
-4
-6
-8
-10
-12
-14
Stress (kPa)
0
20
40
60
80
100
120
140
160
180
200
Distance Along Wellbore from Initiation Point (m)
Stress in x direction
Stress in y direction
Stress in z direction
Sigma 1

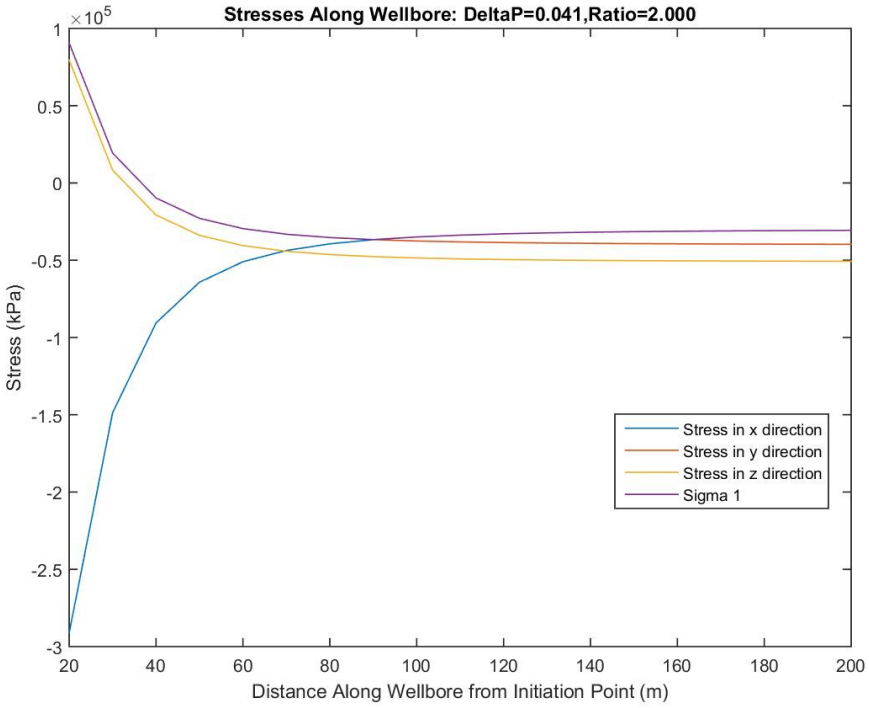
Stresses Along Wellbore: DeltaP=0.041,Ratio=2.000
×10^5
1
0.5
0
-0.5
-1
-1.5
-2
-2.5
-3
Stress (kPa)
20
40
60
80
100
120
140
160
180
200
Distance Along Wellbore from Initiation Point (m)
Stress in x direction
Stress in y direction
Stress in z direction
Sigma 1

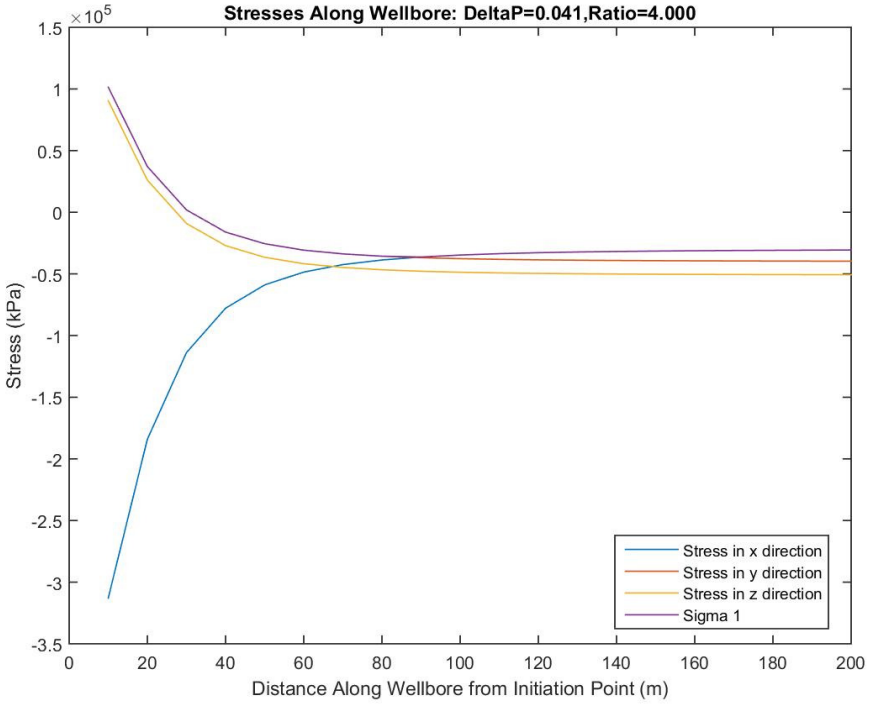
Stresses Along Wellbore: DeltaP=0.041,Ratio=4.000
×10^5
1.5
1
0.5
0
-0.5
-1
-1.5
-2
-2.5
-3
-3.5
Stress (kPa)
0
20
40
60
80
100
120
140
160
180
200
Distance Along Wellbore from Initiation Point (m)
Stress in x direction
Stress in y direction
Stress in z direction
Sigma 1

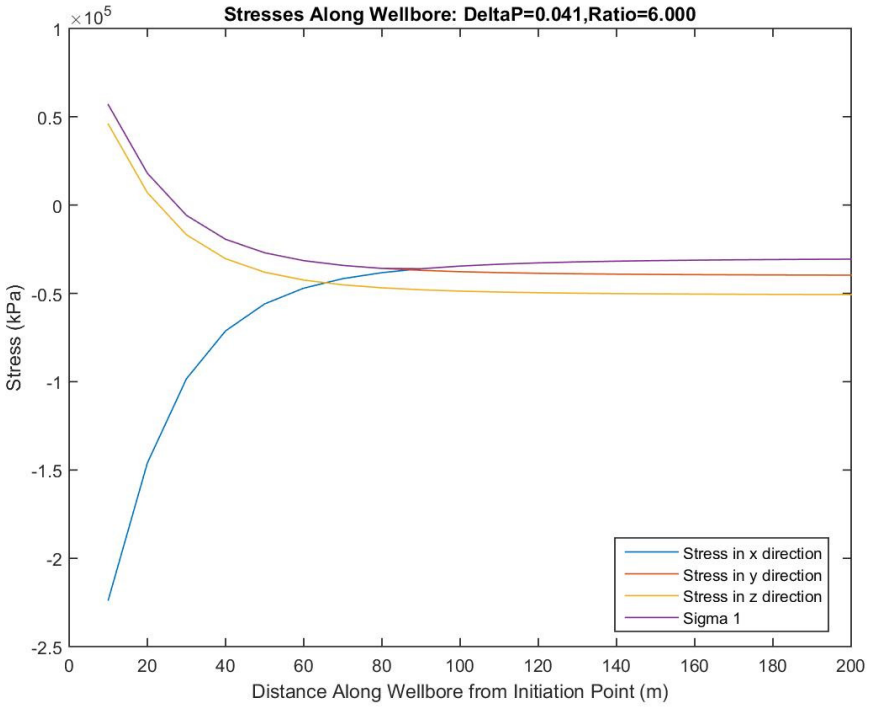
Stresses Along Wellbore: DeltaP=0.041,Ratio=6.000
×10^5
1
0.5
0
-0.5
-1
-1.5
-2
-2.5
Stress (kPa)
0
20
40
60
80
100
120
140
160
180
200
Distance Along Wellbore from Initiation Point (m)
Stress in x direction
Stress in y direction
Stress in z direction
Sigma 1

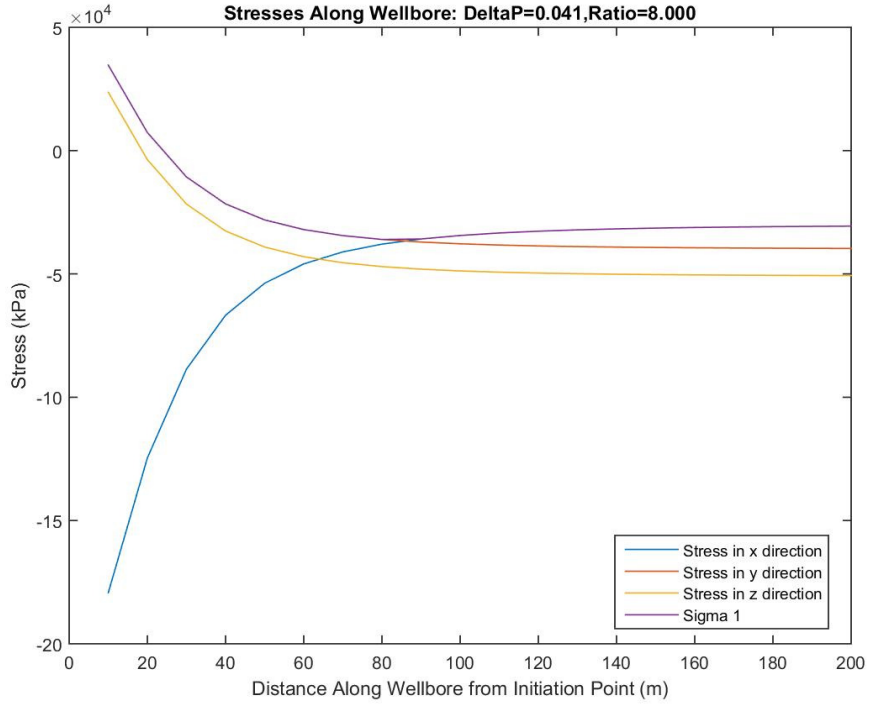
Stresses Along Wellbore: DeltaP=0.041,Ratio=8.000
×10^4
5
0
-5
-10
-15
-20
Stress (kPa)
0
20
40
60
80
100
120
140
160
180
200
Distance Along Wellbore from Initiation Point (m)
Stress in x direction
Stress in y direction
Stress in z direction
Sigma 1

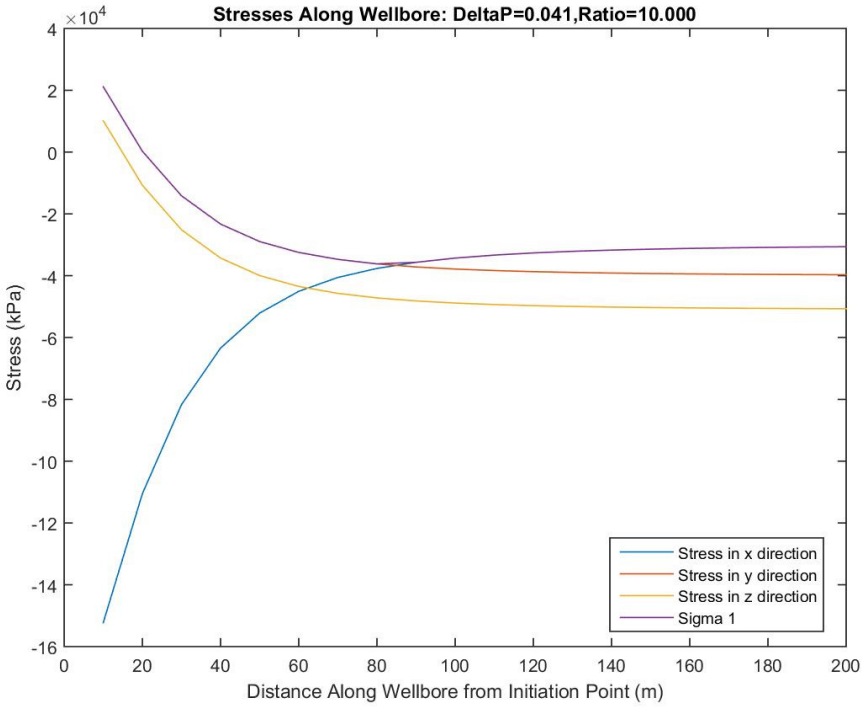
Stresses Along Wellbore: DeltaP=0.041,Ratio=10.000
×10^4
Stress (kPa)
Distance Along Wellbore from Initiation Point (m)
Stress in x direction
Stress in y direction
Stress in z direction
Sigma 1

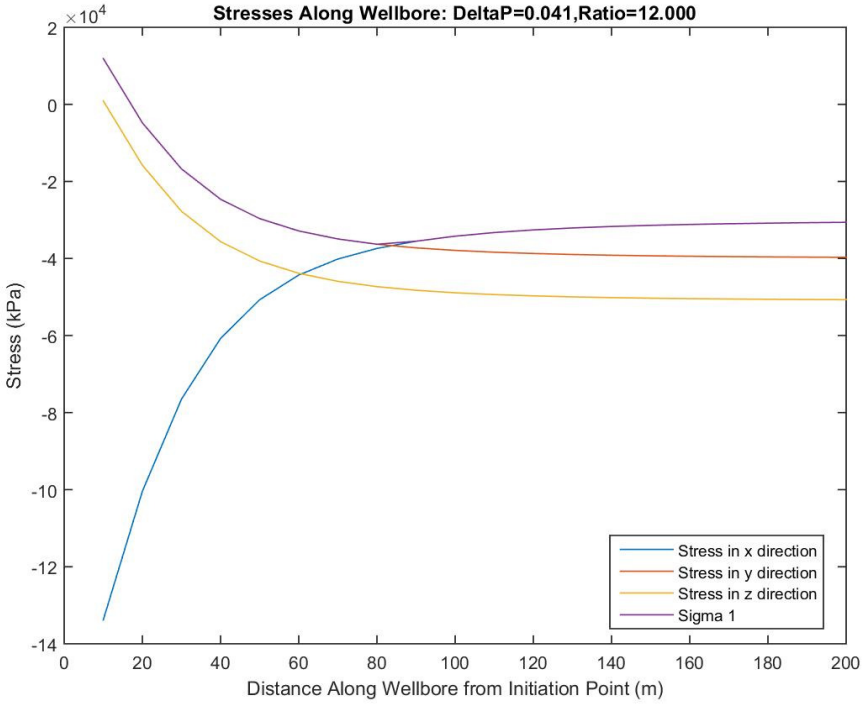
Stresses Along Wellbore: DeltaP=0.041,Ratio=12.000
×10^4
Stress (kPa)
Distance Along Wellbore from Initiation Point (m)
Stress in x direction
Stress in y direction
Stress in z direction
Sigma 1